

Simulations of common-envelope evolution in binary stellar systems: physical models and numerical techniques

Friedrich K. Röpke · Orsola De Marco

Received: date / Accepted: date

Abstract When the primary star in a close binary system evolves into a giant and engulfs its companion, its core and the companion temporarily orbit each other inside a common envelope. Drag forces transfer orbital energy and angular momentum to the envelope material. Depending on the efficiency of this process, the envelope may be ejected leaving behind a tight remnant binary system of two stellar cores, or the cores merge retaining part of the envelope material. The exact outcome of common-envelope evolution is critical for the formation of X-ray binaries, supernova progenitors, the progenitors of compact-object mergers that emit detectable gravitational waves, and many other objects of fundamental astrophysical relevance. The wide ranges of spatial and temporal timescales that characterize common-envelope interactions and the lack of spatial symmetries present a substantial challenge to generating consistent models. Therefore, these critical phases are one of the largest sources for uncertainty in classical treatments of binary stellar evolution. Three-dimensional hydrodynamic simulations of at least part of the common envelope interaction are the key to gain predictive power in modeling common-envelope evolution. We review the development of theoretical concepts and numerical approaches for such three-dimensional hydrodynamic simulations. The inherent multi-physics, multi-scale challenges have resulted in a wide variety of approximations and numerical techniques to be exercised on the problem. We summarize the simulations published to date and their main results. Given the recent rapid progress, a sound understanding of the physics of common-envelope interactions is within reach and thus

F. K. Röpke

Institut für Theoretische Astrophysik, Zentrum für Astronomie, Universität Heidelberg, Philosophenweg 12, 69120 Heidelberg, Germany, and
Heidelberg Institut für Theoretische Studien, Schloss-Wolfsbrunnengasse 35, 69118 Heidelberg, Germany
E-mail: friedrich.roepke@h-its.org

O. De Marco

School of Mathematical and Physical Sciences, Macquarie University, Sydney, NSW 2109, Australia, and
Astronomy, Astrophysics and Astrophotonics Research Centre, Macquarie University, Sydney, NSW 2109, Australia

there is hope that one of the remaining fundamental problems of stellar astrophysics may be solved before long.

Keywords Hydrodynamics · Methods: numerical · Stars: AGB and post-AGB · Stars: evolution · Binaries: close

Contents

1	Introduction	3
1.1	Observations of common-envelope evolution	5
1.2	Terminology of common-envelope modeling	7
1.3	Phases of common-envelope evolution	9
1.4	Structure of this review	10
2	Current theoretical understanding of common envelope interaction	12
2.1	Parametric models: the energy (α_{CE}) and angular momentum (γ) formalisms	12
2.2	One-dimensional inspiral models	16
2.2.1	Analytical approximation of the gravitational drag	16
2.2.2	Parametrized 1D models of dynamical common-envelope inspiral	20
2.3	Three-dimensional hydrodynamic models	22
3	Physical modeling and challenges	23
3.1	The gravo-hydrodynamic model	23
3.2	Why do we need multi-D hydrodynamical simulations?	25
3.3	CE ejection and the end of the dynamical inspiral	27
3.4	Why are common-envelope phases a multi-physics problem?	31
3.4.1	Ionization and recombination effects	31
3.4.2	Magnetic fields	33
3.5	Why are common-envelope phases a multi-scale problem?	34
3.6	The need to simulate the pre-common envelope and post-inspiral phases	36
4	Numerical approaches and limitations	37
4.1	Computational fluid dynamics	38
4.1.1	Eulerian, grid-based methods	39
4.1.2	Lagrangian, smooth particle hydrodynamics	41
4.1.3	Moving-mesh approaches	43
4.2	Implementing the equation of state	45
4.3	Modelling self-gravity	46
4.3.1	Tree methods to calculate self-gravity	46
4.3.2	Alternative methods to calculate self-gravity	47
4.3.3	Gravitational softening	48
4.4	Advantages and drawbacks of hydrodynamic simulation methods	50
4.4.1	Boundary conditions and setup geometries	51
4.4.2	Accuracy, efficiency, and versatility	52
4.4.3	Energy and angular momentum conservation	53
4.4.4	Code speed and scalability	55
4.5	CE phases accessible to 3D hydrodynamic simulations	56
5	Initial conditions and setups of common-envelope simulations	57
5.1	Can the stellar cores be resolved?	57
5.2	Representing the cores of the primaries and the companions	58
5.3	Setting up the primary star in hydrostatic equilibrium	62
5.4	Setting up the binary system	67
6	Multidimensional hydrodynamic simulations	69
6.1	Simulations of the pre-dynamical inspiral phase and the onset of CE interaction	70
6.2	Simulations of the companion–envelope interaction	73
6.3	Global CE simulations	76
6.3.1	Pioneering Eulerian grid-based approaches	76
6.3.2	Modern Eulerian grid-based approaches	79

6.3.3	SPH approaches	84
6.3.4	Moving-mesh simulations of the common-envelope interaction	91
7	Conclusions and future perspectives	96
7.1	Where do we stand?	96
7.2	Missing physical effects	98
7.3	Unresolved numerical problems	99
7.4	Interfacing 3D global simulations with 1D simulations of the common-envelope remnant	100
7.5	Deriving parametric CE prescriptions from 3D simulations	101
7.6	Constraining CE simulations with observations	103
7.6.1	Observations of stars, binaries and PNe that constrain CE simulations	104
7.6.2	Transient events caused by CE interaction	108
7.7	Epilogue	109
	References	110

1 Introduction

The historic detection of gravitational waves from merging black holes ([Abbott et al., 2016](#)) and neutron stars ([Abbott et al., 2017](#)) highlights the importance of understanding the details of binary stellar evolution. What are the physical processes that lead to mergers of these “double-compact objects” ([Kalogera et al., 2007](#))? Reducing the orbit such that a merger commences requires to drain orbital energy and angular momentum from the system. In the last stage before the actual merger, this proceeds due to the emission of gravitational waves—a process that is highly inefficient. Orbital decay is extremely slow. This final phase, driven by gravitational wave emission, must therefore start with a very small orbital separation; otherwise a merger could not occur within a Hubble time.

How is this possible? For some compact objects, a capture of a close companion in a dense stellar environment is conceivable. However, many of the systems that eventually merge are thought to start out as main-sequence star binaries. This, of course, implies an initial separation larger than the sum of the main-sequence star radii, so a mechanism must exist to reduce the orbital separation of the stellar cores¹ sufficiently that eventually they merge via the emission of gravitational waves.

Similar evolutionary mechanisms must be responsible for the formation of interacting binary systems involving one or two compact objects (so-called single- or double-compact binaries). Prominent examples are cataclysmic variables (e.g. [Meyer and Meyer-Hofmeister, 1979](#); [Webbink, 1984](#)), Type Ia supernovae progenitors (e.g. [Wang, 2018](#)), X-ray binaries (e.g. [Tauris and van den Heuvel, 2014](#)), short gamma ray burst progenitors, binary pulsars (e.g. [Chen and Liu, 2013](#)), and close white dwarf binaries (e.g. [Zorotovic et al., 2010](#); [De Marco et al., 2011](#)). Here, the same argument applies: While still on the main sequence, the two stars in the progenitor binary must be sufficiently separated to avoid interaction. The observed phenomena, however, imply an orbital distance significantly smaller than such a relatively large initial separation.

¹ We use the terms “stellar cores” and “core binary” when referring to a system consisting of the core of a giant star and a companion. We note, however, that the companion need not necessarily be a core of a star. It can also be a main sequence star, a planet, or a compact remnant, such as a neutron star or even a black hole.

It is therefore clear that the progenitors of compact binaries were much larger in the past and would not have fitted into the orbits of the systems we observe today. The requirement of sufficient separation of the stellar binary at birth, however, does not need to hold true for the subsequent evolution, where strong interaction and mass transfer is possible, in particular because the radii of stars increase substantially for later evolutionary stages. Paczyński (1976) and others² realized that this is not just another nuisance in the description of the binary system, but rather the key to understanding its evolution towards a close binary: They proposed a phase in which the two stellar cores orbit each other sharing the stellar envelope and coined the name *common envelope* (CE) phase for it. Such an extreme case of binary stellar interaction is the “magic trick” to explain the short orbital separation of single and double-compact systems of various kinds: the orbit of the companion with the core of the “primary” star inside the common envelope causes drag (whether gravitational or hydrodynamical), which transfers orbital energy and angular momentum to the envelope material unbinding it from the system. The stellar cores approach each other, the envelope is ejected and—voilà!—a close binary system emerges.

While critical for the formation of narrow binary systems, the CE phase is also ubiquitous in stellar evolution. A substantial fraction of stars forms in multiples (e.g. Moe and Di Stefano, 2017) and many of them are bound to interact during their evolution. For example, practically all massive stars are born in multiple systems and up to 70% experience binary interaction in their life (Sana et al., 2012). The chances for interaction are not as high for low and intermediate-mass stars, but the consequences are no less impactful for the evolution of these systems (De Marco and Izzard, 2017).

The implications of CE interaction are far-reaching and fundamental for answering questions such as:

- What are the progenitor systems of Type Ia supernovae?
- What defines the rates and parameter distributions of novae and dwarf novae?
- Can planets survive when they are engulfed by their host star?
- How are the source systems of gravitational wave emission formed?

Answers these questions pivotally depend on understanding the post-CE separation distribution. This quantity cannot be determined reliably at the moment because of shortcomings in modeling the inspiral of the companion into the envelope of the primary, orbital tightening of the core binary system, envelope ejection, and potentially other effects in late stages of common-envelope evolution (CEE).

Theoretical modeling of CE phases in binary stellar evolution has a long history. Early attempts used one-dimensional (1D) parametrizations in the framework of classical stellar evolution theory. There are, however, reasonable doubts as to whether their results are physical. Such parametrized models have certain advantages in covering processes that act on longer timescales, but they struggle to capture what is essentially a fast, dynamical phase with no symmetry (Ivanova and Nandez, 2016).

² Paczyński (1976), often cited as the having first formalized the idea of the common envelope interaction, credits aspects of the concept to a number of previous works. As is often the case, a number of separate steps are eventually formalized into a clear hypothesis.

Other models use parametrized prescriptions to follow the evolution of large samples of binary systems or populations. By calibrating the parameters on observational constraints, some of the predictions reach a certain level of confidence. Such population models are used, for instance, to estimate the event rate in gravitational wave detectors (e.g., [Dominik et al., 2012](#); [Belczynski et al., 2014](#)) and to distinguish between different progenitor scenarios for Type Ia supernovae (e.g., [Ruiter et al., 2009](#); [Toonen et al., 2012](#)).

A more direct approach to understanding the physical processes governing CEE is the goal of numerical simulations that we focus on in our review. In addition to the listed examples of astrophysical implications of CE interaction, the process itself is fascinating featuring strong nonlinear dynamical effects. Understanding the underlying physical processes and making reliable predictions for the outcome of CE events cannot be accomplished without complex three-dimensional (3D) hydrodynamics models that cover phases of CEE, because these lack obvious spatial symmetries and proceed on dynamical timescales. The aim of such simulations is to answer specific questions about details of the inspiral and envelope ejection, which then allow for tackling the higher-order questions listed above. Some of these still unanswered, specific questions are:

- How does the system enter CEE?
- How are orbital energy and angular momentum of the core binary transferred to the envelope?
- What physical processes lead to the ejection of the envelope? Which energy reservoirs are tapped for accelerating the envelope material?
- What processes determine the final orbital separation of the remnant core binary?
- Which systems manage to eject the envelope completely?
- What are the conditions under which the process “fails”, i.e. a merger of the core takes place without ejecting the envelope?
- What is the morphology of the ejected envelope in the case of success? Can it explain planetary nebulae?
- What is the role of magnetic fields in CEE?

The ultimate goal is to connect the initial conditions, i.e. the parameters of the system before entering CE interaction, with the properties of the remnant system—most importantly its orbital parameters in the case of successful envelope ejection—but also other quantities that determine its future evolution, such as left-over envelope material or a potentially forming circumbinary disk.

1.1 Observations of common-envelope evolution

The concept of CE was first envisaged by [Paczynski \(1976\)](#) to explain a specific star, V 471 Tau, a detached, compact binary comprising a white dwarf and a K dwarf, rare at the time and presumed to be a direct predecessor of cataclysmic variables. Only through a CE inspiral in the past evolution of the system, could today’s parameters be explained.

Over the years, many more low-mass systems were found that can only be explained with a CE interaction. Low and intermediate-mass star binaries that have

gone through a **CE** interaction are observed as post-red giant branch, sub-dwarf B (sdB) and white dwarf (WD) close binaries, or as post-asymptotic giant branch WD binaries, with either another WD or a main sequence companion. These are the immediate progenitors of cataclysmic variables. In some cases even brown dwarfs or giant planets have been deemed capable of ejecting the **CE** and surviving as binaries with the core of the original giant (e.g., Geier et al., 2011; Schaffenroth et al., 2014, 2019; Vanderburg et al., 2020). Such lower mass, post-**CE** systems are plentiful, and their parameters can be measured with relative precision, thus providing statistical information about the outcome of orbital evolution in the **CE** phase (Iaconi and De Marco, 2019). The direct consequences of envelope ejection can be seen in many planetary nebulae (**PNe**). At least one in five **PNe** is an ejected **CE** (Hillwig et al., 2016; Munday et al., 2020; Jacoby et al., 2021).

After the initial idea of a **CE** inspiral was fleshed out, it became clear how **CE** phases can explain binaries comprising the remnant of massive stars, neutron stars and black holes. Today, this group of binaries is a prime target of multimessenger astronomy. The detection statistics of gravitational-wave induced mergers of double-compact systems is strongly linked to the parameters of the **CE** interaction. There are other massive systems that can be identified as binaries and that must have emerged from a **CE**, such as low and high mass X-ray binaries, but unfortunately the **CE** phase is not the only event that determines the observed parameters of these systems, and therefore they are not ideal to constrain **CE** interaction observationally.

Additionally, thanks to time-resolved astronomical surveys, an increasing number of transient events has been discovered. Supported by pre-outburst observations, several of them have been unequivocally associated with **CE** interactions and stellar mergers (e.g., V1309 Sco, Tylenda et al., 2011). Others have very likely undergone a **CE** inspiral even if there is no definitive proof (e.g., V838 Mon, Bond et al., 2003; Goranskij et al., 2004, but see Tylenda and Soker, 2006 for a discussion of alternative models). By statistical necessity, the majority of objects detected in these brief phases of interaction are the most luminous events, which presumably derive from more massive stars (Kochanek et al., 2014). Examples include NGC 4490-2012OT1 (Smith et al., 2016) and M101-2015OT1 (Blagorodnova et al., 2017) that have been detected in external, sometimes distant galaxies.

A new field of study has emerged from these discoveries, alongside several competing classifications, nomenclatures and preliminary explanations for the observed events. Such transients are commonly known as *gap transients*—observed in the gap between the luminosities of novae and supernovae (Kasliwal, 2012; Pastorello et al., 2019)—or *intermediate-luminosity optical transients* (ILOTs). These include *intermediate-luminosity red transients* (**ILRTs**) (Botticella et al., 2009) and *luminous red novae* (**LRNe**) (Munari et al., 2002) distinguished by their lightcurves and spectral behaviour. The latter are thought to be **CE** interactions between expanding, massive stars and companions that resulted in mergers, although in most cases it is impossible to say for sure if the binary has survived. Interestingly, while **ILRTs** are thought to be electron capture supernovae from super-asymptotic giant branch (**AGB**) stars, there are some cases where the classification is intermediate between **ILRTs** and **LRNe** (Cai et al., 2019). Finally, a distinction between **LRNe** and red novae (**RNe**)

is emerging, where the latter group are a less luminous and possibly less massive counterpart of the former group (Pastorello et al., 2019).

In Sect. 7.6 we will return to these observations and consider how they can constrain the simulations that are the central topic of this review.

1.2 Terminology of common-envelope modeling

Many stars in the Universe form in binaries or higher-order multiples, and a large fraction of these engages in some kind of interaction over their evolution. The nature of such interaction can be manifold; ranging from orbital perturbations mediated by gravitational interaction, irradiation, and hydrodynamical mass-transfer processes to the most violent case: a merger of two stellar objects. CE interaction is very close to this extreme case. In a sense, it classifies as a merger of stars because at least for some period of time two (or perhaps even more³) stellar objects join into a single envelope. Unlike a complete stellar merger, however, this “merged” phase may be a transient phenomenon. After the ejection of the CE, separate stellar cores emerge. Special conditions are required for this to work.

An obvious prerequisite is that one of the interacting stars, which we refer to as “primary”, has to exhibit a clearly separated core–envelope structure. Otherwise, it would not make sense to speak of a *common envelope* in the interaction phase and to define a stellar core that emerges as part of the newly formed binary star system after the envelope ejection. This implies that the primary star has to reach an evolved, giant stage before engaging into the interaction. For a time, the companion resides inside the envelope of the giant primary star. While this companion can be a stellar object of any kind, we encounter a special case if it is another giant star. For this to happen, the initial mass ratio of the binary system has to be very close to unity so that when the primary overfills its Roche lobe as a giant, accretion onto the companion causes it to expand and overfill its Roche lobe, too. A joint CE establishes that consists of material from both stars. Still, during the interaction, two stellar cores orbit each other inside a CE. This case is sometimes (and confusingly) termed *double core evolution*, falling back to the term that was originally used for general CE phases. It is particularly interesting for massive stars (Brown, 1995; Dewi et al., 2006) and may contribute a substantial fraction to the population of double neutron stars (Vigna-Gómez et al., 2018). Despite this ambiguity, a stellar merger with evolved giant stars provides a useful definition of CE interaction and includes the classical case as well as the merger of two giant stars.

Naturally, as the evolution into giant stages is a continuous process, the boundaries between CE interaction and stellar mergers are blurred. For massive stars in the

³ While interaction in a stellar binary system is perhaps the most relevant case, CEE could also proceed in higher-order stellar multiples and involve more than two stellar cores. This case is in itself interesting but has received less attention in simulations (see Glanz and Perets, 2021b, for an exception and references therein for implications of mass transfer in stellar triples). The “traditional” case of a stellar binary is already challenging enough and its processes remain sufficiently unclear to not open Pandora’s box and postpone such complications to future work. Our review will therefore focus on modeling CE interaction in binary systems.

giant stage (so-called *supergiants*), for instance, the separation between core and envelope is less clear than the sharp interface in low-mass red giant (RG) or AGB stars. Another example is the system V1309 Sco (Tylenda et al., 2011). It was modeled as a merger of a $1.5 M_{\odot}$ star expanding into the Hertzsprung gap with a low-mass ($\sim 0.15 M_{\odot}$) main sequence companion. The primary is about 40 times larger than the secondary and the system likely went through a brief common envelope, shortly followed by the disruption of the companion near the core of the primary (Nandez et al., 2014). As a Hertzsprung-gap star, the primary would have had a less clear core-envelope boundary. Therefore, the nature of the physical interaction in the later inspiral is not quite the same as for a system with a more distinguished core.

Another characteristic of CE interaction is the aforementioned interesting possibility that after envelope ejection a tight binary of stellar cores emerges. This case is sometimes referred to as *successful CEE* to distinguish it from the case where the energy available to envelope ejection is insufficient and only parts of it can be removed. The ultimate fate of such a system is a merger of the stellar cores inside the CE, which can also give rise to interesting phenomena: for a high-mass primary star and neutron star companion, such a scenario could lead to the formation of Thorne–Żytkov objects (Thorne and Żytkow, 1975). It has been also suggested that because of the high angular momentum involved, a neutrino-cooled accretion disk forms around a neutron star or a black hole companion when merging with the core of the primary star. This accretion liberates gravitational binding energy, which to a large fraction is carried away by the neutrinos but some part may also be released as mechanical energy—perhaps in form of material accelerated in a disk wind or a jet-like outflow—feeding back on the surrounding envelope material (a scenario originally proposed by Fryer and Woosley, 1998, and Zhang and Fryer, 2001, to explain gamma-ray bursts). The corresponding events have been suggested to resemble some sub-classes of Type II supernovae (such as Type II_n or Type II-P supernovae; e.g. Chevalier, 2012; Soker and Gilkis, 2018; Schröder et al., 2020) and are sometimes called “common-envelope jets supernovae”⁴ (Soker and Gilkis, 2018; Soker et al., 2019). For low-mass stars involved in CE interactions with a white dwarf companion, a thermonuclear explosion resulting from the merger of the degenerate cores has been suggested to explain some peculiar Type Ia supernovae (Sparks and Stecher, 1974; Livio and Riess, 2003). This mechanism is also called the “core degenerate scenario”, e.g. [kashi2011a, ilkov2012a, soker2013a]. While technically for all these events one may speak of a mergers, the term *failed CEE* is commonly used for it, or sometimes, as a compromise, *CE merger*. It highlights the fact that a giant star was involved in the interaction. Also from a practical point of view it makes sense to discuss these cases in conjunction with successful CE interactions because they constitute an interesting limit in the parameter space of such systems.

That said, it may be useful to give examples of cases that do not qualify as CE interaction. A merger of two similarly sized (but not giant) stars, for instance between two white dwarf dwarfs (corresponding 3D simulations were pioneered by Benz et al., 1990; see, e.g., Dan et al., 2009, Dan et al., 2012, Zhu et al., 2015 for

⁴ Events powered by a jet due to accretion onto a neutron star in the envelope instead of the core are termed “common-envelope jets supernova impostors” by Gilkis et al. (2019)

more recent simulations), two neutron stars (e.g. [Rasio and Shapiro, 1992](#), [Ruffert et al., 1996](#), and [Rosswog et al., 1999](#); see also [Faber and Rasio, 2012](#), [Rosswog, 2015](#), [Baiotti and Rezzolla, 2017](#), [Shibata and Hotokezaka, 2019](#), and [Radice et al., 2020](#) for reviews), or two main sequence stars (e.g., [Benz and Hills, 1987](#); [Schneider et al., 2019](#)). Such interactions are distinct from CEE. The initial mass transfer, that invariably commences the interaction, leads to orbital decrease and soon thereafter a tidal disruption of one or both of the stars. We would be hard pressed to state which star is in which star’s envelope.

1.3 Phases of common-envelope evolution

To set the stage for our later discussion, we review some ideas on the temporal evolution of CE interaction proceeds. A classification of stages through which CEE proceeds was given by [Ivanova et al. \(2013\)](#). This classification was largely inspired by concepts of classical stellar evolutionary theory. Here, we focus on the computational modeling of CE interaction. In this context, it is more useful to think of CEE as a three-part interaction, paying attention to the vastly different timescales (to be defined later in our discussion) on which the stages proceed and consequently our ability to model them in numerical simulations:

- (i) The first part starts with mass-transfer triggered by a star growing into its Roche lobe, or from the synchronized orbit becoming Darwin-unstable and leading to a loss of co-rotation. The companion starts to approach the primary. This phase ends when the mass-transfer process assumes a runaway nature.
- (ii) The second part is the inspiral of the companion into the envelope of the primary. It leads to the typical structure in which two stellar cores orbit each other inside a CE. This phase is essentially dynamical.
- (iii) The third phase is a combination of the self-regulating phase (phase III of [Ivanova et al. \(2013\)](#)), its termination (their phase IV) and what comes after (their phase V). This phase starts with the companion–core distance stabilizing and the envelope adjusting thermally to a new equilibrium.

Our classification intentionally leaves out the long-term evolution of the binary system up to CE interaction and the fate of the system after completion of the CE phase. The former is important because it determines the global parameters of the interacting system and sets the initial conditions of the CE interaction. However, we take these as given and focus on the CE phase itself in this review. Likewise, however interesting from an astrophysical point of view, the long-term evolution of the system resulting from CEE is not the subject of our discussion.

There are a lot of subtleties to this picture and to an extent it is a matter of taste how we decide to break down the interaction into different parts. It is also clear that the last ten years of development have refined some of the ideas behind the phases listed by [Ivanova et al. \(2013\)](#). For example, the pre-inspiral phase is more complex than a simple unstable mass-transfer starting out at the time of Roche lobe overflow. If the mass ratio is in the proximity of the analytically-derived threshold for instability ([Tout, 1991](#)), one may expect a longer phase of semi-stable mass-transfer, that

only eventually leads to the formation of a **CE** system. Similarly, the post-inspiral phase may not or not only consist of a self-regulating phase as described in the literature. It is still unclear whether in some setups all envelope material is ejected in the dynamic inspiral phase so that a subsequent self-regulated phase does not establish. The slowing down of the inspiral observed in hydrodynamic simulations is more due to the companion bringing local gas into co-rotation, than an evacuation of the orbit (at least for lower mass stars; Reichardt et al., 2019). And the evolution of the orbit after the end of the dynamical inspiral may have more to do with the distribution and evolution of angular momentum of the gas as the inner envelope contracts. It is also possible that the evolution in late **CE** phases involves phases of mass transfer between the remaining cores or that a circum-binary disk forms.

It is likely not fruitful to complicate the nomenclature while a clearer picture has not yet emerged. So for now we elect to think about these three phases in loose terms as

- (i) the *pre-CE phase*,
- (ii) the *inspiral phase*, and
- (iii) the *post-inspiral phase*.

While the first two proceed largely on dynamical timescales (potentially longer in the pre-**CE** phase), the post-inspiral phase may include dynamical effects as well as processes that take place on longer, thermal timescales. We use this simple subdivisions to provide a reference frame for the discussion that follows. While classical **1D** models of stellar evolution are suitable for addressing processes on longer thermal timescales, the decisive part of **CE** is part (ii) of our classification. Some aspects of parts (i) and (iii) proceed on dynamical timescales, which need to be addressed with the hydrodynamical simulations we focus on in our review.

1.4 Structure of this review

Our review concentrates on advances in the understanding of the common envelope interaction based on multidimensional hydrodynamic simulations. In Sect. 2 we set this discussion into context by reporting the current stance on the common-envelope interaction. It derives from years of modelling using distinct approaches: parametric formalisms (Sect. 2.1) use primarily energy and angular momentum considerations to connect an initial stellar binary system to the outcome of the interaction. One-dimensional “mechanical” models as described in Sect. 2.2 try to determine the drag force experienced by the companion when spiralling into the envelope of the primary star. Integrating a simple equation of motion results in a model for orbital evolution that can be coupled energetically to the envelope whose evolution is then followed with a classical one-dimensional stellar evolution code. Such **CE** models are of interest not only from a historical perspective. They may help to interpret the general behaviour of more complicated hydrodynamic models and to derive a predictive model from them to be used in binary stellar evolution theory. The development of **3D** hydrodynamic models is only briefly mentioned in Sect. 2.3, because they are at the core of the remainder of this review.

In Sect. 3, we discuss the physics that governs CEE and its modeling. This section provides the physical basis of numerical implementations but also points out the modeling challenges caused by physical effects. After introducing the fundamental (but probably insufficient) gravo-hydrodynamic model that describes CE interaction as arising exclusively from hydrodynamic and gravitational interaction in Sect. 3.1, we explain why multidimensional simulations of CE phases are required to properly represent the relevant physical processes in Sect. 3.2. The question of why in such simulations it remains difficult to decide on the most pressing problems—envelope ejection and final orbital separation of the remnant binary system—is discussed in Sect. 3.3. Physical phenomena that should be included in CE simulations are mentioned in Sect. 3.4. We conclude Sect. 3 with pointing out why the dynamic inspiral phase—although demanding to model and decisive for the outcome of CE interaction—is not the full story and the phases preceding and following it have to be taken into account in order to establish a comprehensive model of CEE.

Approaches to numerical implementations of CE models are reviewed in Sect. 4 with a focus on computational fluid dynamics (Sect. 4.1), self-gravity (Sect. 4.3) and problems of energy and angular momentum conservation (Sect. 4.4.3). Different discretization approaches have been used to model CEE and we try to point out advantages and drawbacks of specific methods. Apart from some specific drawbacks of certain schemes, there are general problems arising from the multi-physics and multi-scale nature of the problem that have posed challenges to virtually all CE simulations to date, and we discuss them, too.

A related topic is the setup of 3D hydrodynamic CE simulations. It is sufficiently important, but also delicate in its treatment, to deserve the separate Sect. 5.

The actual 3D hydrodynamic CE simulations published so far are reviewed in Sect. 6. After discussing simulations pertaining to the pre-CE phase (i) of our classification in Sect. 6.1, we give some account of simulations that focus on resolving the details of the interaction between the companion and the gas of the CE in Sect. 6.2. While in these—as a necessary compromise for reaching high spatial resolution—only some part of the system is included in the simulated domain, global CE simulations try to follow the evolution of the entire system through the inspiral phase (ii). As discussed in Sect. 6.3, these have been developed over the past decades, and we give some account for the historical development of ideas and techniques. At the moment, a rapid increase in the quality of such hydrodynamic simulations is observed that originates from a combination of increasing computational power and new numerical modeling techniques.

In Sect. 7 we draw conclusions (Sect. 7.1) and give future perspectives for CE modeling. We discuss physical modeling aspects (such as missing physical effects, Sect. 7.2) as well as numerical issues (e.g. Sect. 7.3 on unresolved numerical problems). The post-inspiral phase (iii) is difficult to capture in 3D hydrodynamic approaches. Therefore, such simulations have to be augmented with 1D classical treatments of stellar evolution as discussed in Sect. 7.4. An ultimate goal of CE modeling is to connect directly to binary evolution calculations (Sect. 7.5) and to astronomical observations (Sect. 7.6).

2 Current theoretical understanding of common envelope interaction

In the previous section, we have introduced the **CE** phase as a necessary model to explain a number of observed systems, and we have emphasized the importance of this phase to explain and connect a number of new observations, such as gravitational wave detections. In this section, we report on the progress that has been made to elucidate the details of this interaction since the days when it first was proposed in the late 1970s. Attempts to model **CEE** can be classified into three categories: parametric formalisms, one-dimensional (**1D**) “mechanical” models and **3D** hydrodynamic simulations. In Sects. 2.1 and 2.2 we discuss the former two categories. This is meant to summarize approaches that can be seen as complimentary to the **3D** hydrodynamic simulations. While potentially useful for the interpretation and—potentially—for casting the results of such simulations into a simpler framework applicable in classical stellar evolution approaches, they lack predictive power and do not require sophisticated computational methods. Arriving at **3D** hydrodynamic simulations of **CEE** in Sect. 2.3 sets the stage for an in-depth discussion of these models in the following sections of our review.

It has to be pointed out, however, that none of the three approaches has, to-date, provided a satisfactory picture of the interaction, nor have they enabled a predictive model of **CEE**. Nevertheless, they have laid a solid foundation for the modern efforts, which will hopefully lead to the next wave of breakthroughs.

2.1 Parametric models: the energy (α_{CE}) and angular momentum (γ) formalisms

Parametric formalisms for modeling **CE** phases are based on general considerations of the energy or angular momentum budget in the interacting systems. They determine the orbital energy and angular momentum required to achieve envelope ejection. This simple estimate allows to determine whether successful **CEE** is possible or a **CE** merger is more likely. From the energy or angular momentum budgets, the formalisms allow to derive the orbital parameters of the surviving binary system. This way, they provide the end stage of **CEE** for a given initial system without attempting to model the dynamical processes linking them. Therefore, such models give little insight into the physics of **CE** phases. Their predictions seem questionable, but they allow us to construct population models to explain observations and they provide guidance for multidimensional simulations of **CEE**.

The *energy formalism* (van den Heuvel, 1976; Webbink, 1984) is the coarsest parametrization of **CEE**. It equates the binding energy of the envelope, E_{bind} , with the loss of orbital energy, ΔE_{orb} , during the inspiral

$$E_{\text{bind}} = \alpha_{\text{CE}} \Delta E_{\text{orb}}, \quad (1)$$

where the efficiency parameter α_{CE} accounts for the fact that only some of the deposited orbital energy may be needed to unbind the entire envelope with the remainder being expended to accelerate all or part of the envelope to speeds in excess of the escape velocity, or being radiated or convected away. This would imply values of α_{CE} in the range from 0 to 1. Accounting for the fact that other energy reservoirs than the

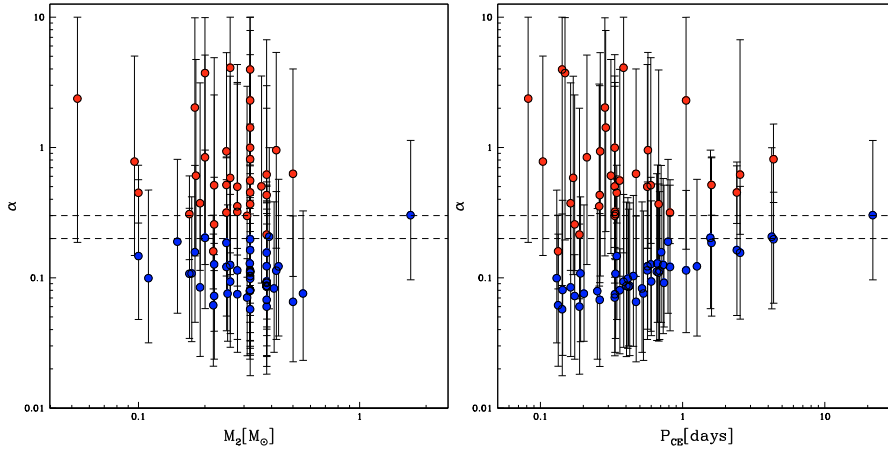


Fig. 1 Values of α_{CE} derived by reconstructing or measuring the binding energy, the initial and the final separations of observed compact single degenerate post-CE binaries. Colors indicate the nature of the primary star in the progenitor system: red dots mark **RG** stars and blue dots **AGB** stars. The results are plotted as a function of companion mass M_2 (left panel) or of the period after the **CE** interaction P_{CE} (right panel). Figure adapted from [Zorotovic et al. \(2010\)](#).

orbital energy of the companion may be tapped to unbind the envelope, $\alpha_{\text{CE}} > 1$ is formally possible.

A reliable determination of α_{CE} is required to turn the energy formalism into a predictive model, but this is difficult to reach. In fact, many questions have been raised about the effectiveness of using this pasteurization to describe the event. What exactly is the value of α_{CE} ? Should be a function of parameters, or of time? [Ivanova et al. \(2013\)](#) point out that α_{CE} being exactly equal to one is an extreme fine-tuning problem. It could be a function of stellar and binary parameters, but has traditionally been set to a constant value for use in population synthesis models that need to predict the final separation of systems given their envelope binding energy (e.g., [Toonen et al., 2018](#)). Some population studies tried to use a functional value of α_{CE} ([Politano and Weiler, 2007](#)), but this has not enlightened the discussion. Observational studies based on close binaries involving white dwarf stars (particularly single-degenerate systems, where the companion is a main sequence star) have attempted a calibration of α_{CE} . Some of these studies proposed a particular constant value for α_{CE} ([Zorotovic et al., 2010](#), see Fig. 1) while others advocated a variable value ([De Marco et al., 2011](#)). In the end, all these approaches are plagued by the large uncertainties introduced in the many steps required to reconstruct the parameters of the white dwarf progenitor star.

The energy formalism involves uncertainties that go beyond the tunable efficiency parameter. They relate to the definition of the binding energy of the envelope. Even if a non-parametric expression can be used, for example by calculating the binding energy from **1D** stellar structure models, according to

$$E_{\text{bind}} = \int_{M_{\text{core}}}^{M_{\star}} \left[-G \frac{M(r)}{r} + \alpha_{\text{th}} u \right] dm \quad (2)$$

(Dewi and Tauris, 2000), there is always the issue of the mass coordinate M_{core} at which the core of the primary star (of total mass M_{\star}) ends and its envelope (of mass M_{env}) begins (e.g. Dewi and Tauris, 2000; De Marco et al., 2011; Kruckow et al., 2016). The choice of this parameter greatly alters the result. For the outcome of CE interaction, the mass coordinate down to which the envelope has to be removed so that the remaining object does not re-expand—sometimes called *bifurcation point*—is of particular interest. It sets the minimum orbital separation that the system has to reach in order to terminate CEE (Tauris and Dewi, 2001; Deloye and Taam, 2010; Ge et al., 2010; Marchant et al., 2021; Vigna-Gómez et al., 2022).

The first term in the integral of Eq. (2) is clear: it is the gravitational binding energy of the envelope gas with G denoting the gravitational constant. The specific⁵ internal energy u in the second term, however, is a bit ambiguous. It should contain all other energies of the envelope that potentially decide on its binding status, such as the thermal energy of the gas, the energy of the radiation field (expressed via the Stefan-Boltzmann law), the ionization energy of the atoms, the dissociation energy of molecules (Dewi and Tauris, 2000). The problem with including these energies is that in order to support envelope ejection, they must be converted into kinetic energy of the gas during CE interaction. Because it is unclear for which of these energies and to which extent this is the case, a fudge factor α_{th} was introduced (Han et al., 1995; Dewi and Tauris, 2000). Unfortunately, the introduction of two tunable parameters, confusingly both called α but with partially different meanings⁶, leads to degeneracies in the formalism. The variation captured in α_{th} could as well enter the global α_{CE} . In order to express the binding energy as a function of the structure of the envelope in a simple way, the structural parameter λ was introduced⁷ by de Kool et al. (1987) via

$$E_{\text{bind}} = -G \frac{M_{\text{env}}(M_{\text{env}} + M_{\text{core}})}{\lambda R}, \quad (3)$$

with the stellar radius R . The structural parameter λ scales the radius of the star to represent its degree of internal concentration. This parameter can be determined by fitting to 1D stellar structure models, or it can remain a free parameter (often used in the combination $\alpha\lambda$, that summarizes both the binding energy and the envelope ejection efficiency). Obviously, the value of λ for a given stellar structure depends on how the binding energy of the envelope is defined—and thus on the uncertainties captured in α_{th} in Eq. (2). For example, using the λ values from the table of Loveridge et al. (2011) requires to adopt their analytical representation for the binding energy, which differs from that of other authors (see the discussion in Iaconi and De Marco, 2019).

Returning to the question of which parts of internal energy can support envelope unbinding (which would justify their inclusion in the second term in the integral of Eq. (2) as counteracting the first gravitational binding energy term), *ionization energy* of the envelope gas seems to be particularly relevant. It has first been argued by Han et al. (1995) that as material in the expanding envelope falls below the ionization

⁵ *Specific* here means per unit mass.

⁶ To add to the confusion the index “th” seems to refer to thermal energy of the envelope gas although it parametrizes also other contributions to its internal energy.

⁷ A similar formalism can be found in Webbink (1984).

threshold, the released recombination energy can be used to expand or even eject the envelope. Its inclusion in the energy budget effectively implies that the binding energy of the envelope is less negative, or indeed even positive, in which case α_{CE} is larger than unity. The exact fraction of recombination energy that is used to do work is in question at the moment because recombined hydrogen is far more transparent to photons than ionized hydrogen, implying that a fraction of the hydrogen recombination energy could escape as radiation instead of being thermalized. Helium recombination energy, in contrast, may be used more efficiently as its release happens deeper in the star, in layers that stay optically thick for longer. Although several treatments of this phenomenon have been presented (e.g., [Ivanova, 2018](#); [Soker et al., 2018](#)), the answer appears to be outside the ability of analytical theory, and gives another reason to recur to simulations that include radiation transport. Additional processes that may be relevant but are not accounted for in the simple energy formalism include nuclear energy generation, tidal heating, energy released by the accretion of material onto the companion star, radiation losses and magnetic field generation ([Ivanova et al., 2013](#)).

Instead of considering energy balance, [Nelemans et al. \(2000\)](#) used the angular momentum balance to relate the pre- and post-CE states of the system. Assuming a linear reduction of angular momentum ΔJ with mass loss ΔM (which could be equated to the envelope mass for full envelope ejection), this gives

$$\frac{\Delta J}{J} = \gamma \frac{\Delta M}{M}, \quad (4)$$

again introducing a tunable parameter γ . The motivation of this *angular momentum*, or *gamma-formalism* was to model the evolution of double helium white dwarfs, which requires $\gamma \approx 1.75$ ([Nelemans et al., 2001b,a](#); [Nelemans and Tout, 2005](#)). The authors argued that explaining these systems with the energy formalism fails, although [Webbink \(2008\)](#) remarks that the reason is that the first of the two mass transfer phases in the systems discussed by [Nelemans and Tout \(2005\)](#) was not a common envelope, but a quasi-conservative mass transfer phase. While this explanation is not perfectly satisfying, as [Webbink \(2008\)](#) also discuss, the main problem with the gamma-formalism stems from its lack of predictive power. The value of γ is in fact constrained to lie in the narrow range between $5/3$ and $5/8$, within which it predicts a wide range of values for the final orbital separation of the post-CE core system.

Parametric models provide a shortcut through the complex CE interaction for population synthesis studies. The validity of the energy and angular momentum formalisms is still to be confirmed with simulations that capture the details of the actual physical interaction. It is therefore important to point out the fundamental differences and the relations between these formalisms and detailed hydrodynamic simulations of CE interaction. The simplified descriptions are based on the global budgets of conserved quantities, but they do not specify where energy is injected and what fraction of it is used for unbinding the envelope. They assume certain initial and end stages without modeling the dynamical processes linking them and therefore give little insight into the physics of CEE. But even within the global view of parametric models, questions arise: Are the efficiency parameters universal? If not, how do they depend on the parameters of the initial models, such as the mass ratio of the

stellar components, the evolutionary state of the primary star, or even the plunge-in time? Consequently, parameters such as α_{CE} or γ by themselves cannot shed much light on the physical processes and they are of little use to constrain 3D hydrodynamic models. Conversely, a goal of more advanced simulations of CEE is to fix or predict parameters like α_{CE} to enable their further use in parametric studies. A full treatment with detailed numerical simulations is ultimately required to validate such parametrizations and—if possible—generate prescriptions for parametrized approaches that supply them with predictive power.

2.2 One-dimensional inspiral models

A more detailed description of CE phases than that provided by the simple parametric formalisms discussed in Sect. 2.1 is obtained from 1D stellar structure models that integrate the change of orbital separation during the inspiral of the companion into the envelope of the primary star as obtained from a parametrized approach to the inspiral (e.g. Alexander et al., 1976; Fragos et al., 2019). These models do not provide a self-consistent description of the drag forces acting on the stellar cores. With an assumed drag force model, they integrate a 1D equation of motion for the inspiral of the companion into the envelope of the primary star. A coarser approach summarizes the inspiral by a bulk mass-loss rate that simply removes the envelope (Xiong et al., 2017; Clayton et al., 2017). Before we can give details of these models, we need to discuss analytical approximations of the gravitational drag force.

2.2.1 Analytical approximation of the gravitational drag

The main energy reservoir driving the CE interaction is the “orbit” of the initial binary system. The mechanism of the transfer of orbital energy to the envelope gas of the primary star is mainly due to the interaction between the companion and the envelope as well as the core of the giant and the envelope.

Quantifying the drag around stellar cores in CEE is a difficult task. Several effects contribute to the total force (Livio and Soker, 1984b): dynamical gravitational braking due to deflection of surrounding gas that transfers momentum onto the companion, drag due to accretion (or evaporation) onto (from) the companion, viscous hydrodynamical or turbulent friction, and tidal forces. In the case of light companions such as massive planets and brown dwarfs, it is easy to see analytically that hydrodynamic friction onto the companion easily competes with gravitational friction, complicating the inspiral (Staff et al., 2016b), but for most other situations, gravitational drag dominates.

When a body moves through gas, gravitational interaction leads to a deflection of the surrounding material into a wake behind the body. Some part of the gas is accreted onto the gravitating object (see Edgar, 2004, for a detailed and pedagogical derivation). This accretion flow was first studied by Hoyle and Lyttleton (1939), who, under the assumption of a sufficiently rarefied gas, considered the problem in terms of a collisionless system. Gas particles around the moving object—modeled as a point mass—are deflected by its gravity and approach the axis of its motion (in this case

the symmetry axis of the problem) downstream of it in a ballistic trajectory. If gas particles are gravitationally bound to the object (i.e. in absolute value their kinetic energy is smaller their gravitational potential energy) they will be accreted with a rate that depends on the distance from the object at which they reach the collimation axis. This, in turn, specifies a critical impact parameter R_a around the moving object inside of which the gravitational deflection directs particles to a point on the axis where they are bound. From this simple picture, an accretion rate is derived:

$$\dot{M}_{\text{HL}} = \pi R_a^2 \rho_\infty v_\infty, \quad (5)$$

where ρ_∞ and v_∞ denote the density and velocity upstream of the gas (Hoyle and Lyttleton, 1939; Edgar, 2004). The subscript ‘ ∞ ’ indicates that the values are measured sufficiently far away from the moving object so that they are not affected by its gravitational attraction. The critical impact parameter is usually called the *accretion radius* and it is given by

$$R_a = \frac{2GM}{v_\infty^2}.$$

Here, G is the gravitational constant and M is the mass of the accreting object. Bondi and Hoyle (1944) extended the analytic treatment of Hoyle and Lyttleton (1939) by relaxing the assumption of a collisionless system. Collimation of the flow to the downstream axis of motion by gravitational deflection increases the density in a collisionless system to infinity, which is unphysical. Instead, a hydrodynamic pressure builds up and a wake of finite density forms behind the object, which Bondi and Hoyle (1944) called an *accretion column*. The finite density of the wake reduces the mass accretion rate to (Bondi and Hoyle, 1944; Edgar, 2004)

$$\dot{M} = \alpha \pi R_a^2 \rho_\infty v_\infty, \quad (6)$$

where, according to Bondi and Hoyle (1944), the factor α ranges between $1/2$ and 1. The setup considered by Hoyle and Lyttleton (1939) applies to highly supersonic velocities of the gravitating object with respect to the gas, but it fails in cases of slow motion. A different setup that avoids dynamical effects was considered as a limiting case by Bondi (1952): a static gravitating object inside a gas that is initially at rest and from which it accretes in a spherically symmetric way. This led Bondi (1952) to introduce a characteristic accretion length scale,

$$R_B = \frac{GM}{c_\infty^2},$$

where c_∞ denotes the sound speed far away from the object. Outside of this *Bondi radius* the accretion flow is subsonic and the density is uniform; inside of it the gas becomes supersonic and accretes onto the object in free fall (Edgar, 2004). The nature of the flow—subsonic or supersonic—is characterized by the *Mach number*,

$$Ma = \frac{v}{c}. \quad (7)$$

The resulting accretion rate onto the static gravitating object is given by (Bondi, 1952)

$$\dot{M} = 4\pi \lambda R_B^2 \rho_\infty c_\infty, \quad (8)$$

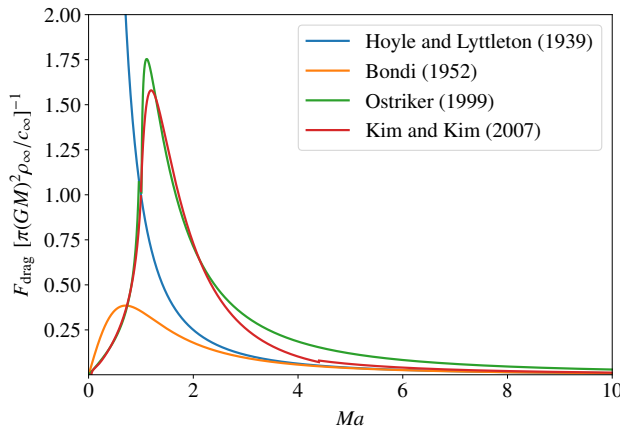


Fig. 2 Drag force as a function of Mach number according to Eqs. (5), (9), (12 – 14) assuming $r_{\max}/r_{\min} = 20$ and the expression given by Kim and Kim (2007) with $r_{\max}/r_{\min} = 10$. Figure modified from L. Thielbeer, Bachelor thesis, Heidelberg 2021.

with an order unity non-dimensional parameter λ . This parameter⁸ plays a role analogous to α in Eq. (6). The similarity of Eq. (8), valid for the limiting case of a Mach number $Ma_{\infty} = 0$, with Eq. (6), that applies to the case of $Ma_{\infty} \gg 1$, led Bondi (1952) to propose the interpolation

$$\dot{M}_{\text{BH}} \sim \frac{\pi(GM)^2 \rho_{\infty}}{(c_{\infty}^2 + v_{\infty}^2)^{3/2}}, \quad (9)$$

often called to as *Bondi–Hoyle accretion rate*. Following Edgar (2004) we will refer to the general framework as the Bondi–Hoyle–Lyttleton (**BHL**) formalism. The considered setups cannot be steady: material is accreted onto the gravitating object, which not only increases its mass, but also leads to a transfer of momentum. The momentum transfer corresponds to a drag force. Dimensional considerations very approximately suggest the relation (Edgar, 2004)

$$F_{\text{drag}} = M\dot{v}_{\infty} \sim \dot{M}v_{\infty}, \quad (10)$$

so that the accretion rates discussed above can be translated into corresponding drag forces that act on a gravitating object moving through gas. It is important to note that the origin of this drag force is not a direct friction of the gas exerted on the moving object—in the model the object is a point mass and does not have a surface—but rather an effect of the material deflected into and accreted from its wake (Edgar, 2004). While, according to Eq. (5), the drag force in the Hoyle-Lyttleton formalism decreases monotonically with the Mach number of the relative motion, the interpolation of Bondi [Eq. (9)] predicts a peak in it at $Ma_{\infty} = \sqrt{1/2}$ (see Fig. 2).

⁸ The notation of the parameters α and λ follows the original references. They are not to be confused with the stellar structure and efficiency parameters of Sect. 2.1.

This, however, has an additional effect: more mass is present on the downstream side of the moving object than upstream of it and this causes a backward-directed gravitational pull on it—an effect that is usually referred to as *dynamical friction* and was first studied by Chandrasekhar (1943) under the assumption of a collisionless system. Dokuchaev (1964) extend the discussion to a collisional fluid dynamical system. For the resulting drag force in the hypersonic case, Ruderman and Spiegel (1971) proposed:

$$F_{\text{drag}} = \dot{M}v_{\infty} \ln\left(\frac{r_{\text{max}}}{r_{\text{min}}}\right). \quad (11)$$

Because of its similarity to the formalism describing Coulomb collisions in plasma physics, the logarithm in this expression is usually called the *Coulomb logarithm*. It introduces two length scales, r_{min} and r_{max} . They result from integration boundaries that represent the minimum and maximum radius of gravitational interaction of the moving object with the gas. Unfortunately, there is no clear definition of what these scales should be and their choice remains somewhat arbitrary. In the hypersonic case, the density asymmetry is a maximum because the material is collimated in the region trailing the moving object. For lower velocities, this is no longer the case and in the subsonic regime the dynamical drag should be smaller. Therefore, the Coulomb logarithm should involve a quantity that characterizes the flow. Rephaeli and Salpeter (1980) suggested a form for the supersonic case that depends on the Mach number of the flow, Ma , but they argued that in the subsonic case the dynamical drag should vanish. Based on a linear perturbation analysis, Ostriker (1999) derived an expression for the drag force

$$F_{\text{drag}} = \frac{\pi R_a^2 \rho_{\infty}}{v_{\infty}^2} I \quad (12)$$

with the Coulomb logarithm

$$I_{\text{subsonic}} = \frac{1}{2} \ln\left(\frac{1+Ma}{1-Ma}\right) - Ma \quad (13)$$

for subsonic relative velocities and

$$I_{\text{supersonic}} = \frac{1}{2} \ln\left(1 - \frac{1}{Ma^2}\right) + \ln\left(\frac{v_{\infty} t}{r_{\text{min}}}\right) \quad (14)$$

for supersonic velocities, where r_{min} is the effective size of the moving object. The resulting drag force is plotted in Fig. 2 as a function of the Mach number.

Still, the specification of the upper integration limit for the gravitational interaction in the supersonic case remains problematic for the application of this formalism to CEE. Ostriker (1999) considered a perturber moving through a uniform gas on a straight line over some finite period of time t and integrate over the path it travels. Kim and Kim (2007) investigated the drag force on a perturber moving on a circular orbit in a uniform gaseous medium. The main effect of this change in geometry is that a trailing tail forms behind the perturber in which the density distribution is asymmetric. Therefore, the drag force has components in lateral as well as radial direction, although Kim and Kim (2007) found that the latter contributes little to the orbital decay. Based on a semi-analytic approach, Kim and Kim (2007) provided fits

for I in Eq. (12) in different flow regimes with a functional dependency on the Mach number that resembles the form of Ostriker (1999), see also Fig. 2.

In addition to shrinking the orbital separation between the stellar cores and transferring angular momentum and orbital energy to the envelope so that it is ejected, drag also affects the eccentricity of the core binary system. Szölgény et al. (2022) argue that while the hydrodynamic drag acting on the companion tends to circularize the orbit, gravitational drag can both enhance or decrease eccentricity, depending on the density structure of the envelope.

The analytic expressions for the drag force discussed here are important to understand the underlying effects and the functional dependencies on characteristic quantities, chiefly the Mach number of the relative velocity between perturber and gas. They are, however, not fully self-consistent because the derived relations are proportional to the drag force up to multiplicative factors, that, at best, are constants. Whether these constants are universal or whether they depend on details of the envelope structure and the inspiral of the companion has to be determined in 3D hydrodynamic simulations. In Sect. 6.2 we discuss further attempts at modelling the gravitational drag using hydrodynamic simulations that do not necessarily comprise the entire CE system but rather simulate objects in “wind tunnels”. In the future, such simulations may join forces with global CE simulations and 1D mechanical models to build a more complete understanding of the entire interaction.

2.2.2 Parametrized 1D models of dynamical common-envelope inspiral

Among the first computational models of CE interaction were approaches that follow the inspiral of the companion into the envelope of the primary and, in most cases, the associated energy deposition into the envelope gas with 1D stellar evolution codes (see Taam et al., 1978; Meyer and Meyer-Hofmeister, 1979). These approaches determine drag forces and energy (and/or angular momentum injection) according to local conditions as encountered in a 1D structure model of the primary star’s envelope. This formulation allows for a simple 1D “mechanical” model of the inspiral phase, i.e. Phase (ii) of our classification in Sect. 1.3. It is based on an equation of motion for the companion under the action of a gravitational force and a drag force,

$$\ddot{\mathbf{r}} = -\frac{G(M_{\star}^* + M_2)}{r^3}\mathbf{r} + \frac{1}{M_2}\mathbf{F}_{\text{drag}}, \quad (15)$$

where \mathbf{r} is the radius vector pointing from the center of the primary star to the companion of mass M_2 (Alexander et al., 1976). The mass of the primary star inside the radius r is denoted as M_{\star}^* .

Obviously, such a model is a gross simplification of the physical processes at work in CEE. It assumes a symmetry of the setup that diverges from reality, where the envelope is deformed by the gravitational interaction. Moreover, for the determination of the orbital shrinkage and the associated energy (and angular momentum) deposition due to drag, it considers only the motion of the companion in the envelope of the primary, whose core is assumed to be fixed in space. This setup thus misses the drag force that acts on the core of the primary star when it orbits the center of mass of the system and thus also moves relative to the envelope gas.

Nonetheless, 1D “mechanical” models extend beyond the simple arguments of energy or angular momentum conservation used in the formalisms discussed in Sect. 2.1. They attempt a physical description of the dynamical interaction between companion and envelope, albeit in a parametric way: The inspiral of the companion into the envelope is followed according to a drag force acting on it. This model raises questions: (i) What exactly is the nature of the interaction between the companion and the envelope gas and how can the drag force F_{drag} perturbing the orbital motion in Eq. (15) be modeled? (ii) How does the envelope react to the injection of energy and angular momentum and what are the consequences of structural changes for the drag force?

As discussed in Sect. 2.2.1, Question (i) has been addressed in analytic treatments in the framework of linear theory, resulting in scaling relations (e.g. Dokuchaev, 1964; Ostriker, 1999). The semi-analytical model of Kim and Kim (2007) extends the original setup of linear motion to the more appropriate case of circular orbits. The omission of nonlinear effects and density gradients in the envelope is accounted for by fudge factors that have to be determined from numerical simulations. We discuss 3D simulations which attempt to quantify the gravitational drag force in Sect. 6.2. They have been calculated either in wind-tunnel type models (where high spatial resolution can be achieved around the point mass that acts as the inspiralling companion, see MacLeod and Ramirez-Ruiz, 2015a; MacLeod et al., 2017b, and De et al., 2020), for massive perturbers on circular orbits in a gaseous medium (Kim, 2010), or in a full CE simulation where the reaction of the envelope to the inspiral can be gauged, but the resolution is inferior (Reichardt et al., 2019; Chamandy et al., 2019). Parametric approaches to the description of the drag force have been used relatively rarely in 1D “mechanical” models. Perhaps the most modern and comprehensive approach was that of Fragos et al. (2019), who used the parametrization of the gravitational drag determined by the 3D hydrodynamic models of MacLeod and Ramirez-Ruiz (2015a).

Question (ii) concerns the expansion and change of structure of the envelope. In the simplest approach, the envelope is treated as static and unperturbed by the inspiral, as assumed, for instance, in the study of MacLeod and Ramirez-Ruiz (2015b). In principle, however, the co-evolution of orbit and envelope can be followed in 1D hydrodynamic stellar evolution models. The idea is to inject the orbital energy and/or angular momentum released by the drag force into the stellar envelope and to model its response in a 1D hydrodynamic stellar evolution code. Different groups have developed recipes for this: Some inject released orbital energy into the thermal energy of the envelope, while others model angular momentum transfer to envelope material that also increases its kinetic energy. The employed 1D parametrizations cannot self-consistently determine what fractions of energy and angular momentum are to be injected into each of these reservoirs. Consequently, the implementations vary, but the general approach has been followed in a number of early CE studies (Taam et al., 1978; Meyer and Meyer-Hofmeister, 1979; Taam, 1979; Delgado, 1980; Livio and Soker, 1984b,a; Soker et al., 1984). In the late 1980s and the 1990s, 1D “mechanical” models were abandoned because of the asymmetries observed in 3D hydrodynamic simulations that called the assumption of spherical symmetry into question. The work of Podsiadlowski (2001), however, revived the method.

The list of deficiencies of 1D “mechanical” CE models’ is long: The assumed spherical symmetry in the parametrized models is a gross simplification. It implies

a local transfer of orbital energy and angular momentum and injects them into a spherical shell. In reality, however, the gravitational perturbation of the envelope is non-local and the energy is not deposited into spherical shells. In fact, the plunge-in of the companion quickly destroys any sphericity of the primary star's envelope. Moreover, the orbit in the **1D** parametrized models remains circular by necessity, with concomitant non-conservation of angular momentum.

Despite all these shortcomings, however, such models have their value and hold promise for capturing effects that would be very difficult to include in **3D** hydrodynamic simulations of **CEE**. Their recent application is therefore motivated by the need to bridge scale gaps that are hard to overcome in **3D** hydrodynamic models.

An example is the inspiral of neutron stars into a massive red supergiant primary star, which pose a strong spatial scale challenge. This was addressed with a **1D** parametrized model by [Fragos et al. \(2019\)](#) generating information about the final product: a binary comprising a $2.6 M_{\odot}$ helium star and a neutron star at a separation of 3.3 to $5.7 R_{\odot}$.

[Clayton et al. \(2017\)](#) explore the evolution of **CE** systems after the inspiral phase (ii) when entering post-inspiral evolution [Phase (iii) of our classification in Sect. 1.3], which poses a time-scale challenge. Generally, during the slower phases, several physical processes such as radiation transfer, convective energy transport, and nuclear burning, can have a substantial effect on the interaction and need to be modelled. These longer phases are themselves needed to understand the interaction as a whole, so the role of **1D** parametrized models could be critical and was advocated as the most important step to further progress by [Ivanova et al. \(2013\)](#).

2.3 Three-dimensional hydrodynamic models

The concept of **CE** interaction is deceptively simple, but the details are complex. As discussed above, finding a trustworthy way to parametrize actual **CEE** turns out to be extremely challenging. Given a set of initial binary parameters, parametric formalisms and **1D** models are still unable to reliably predict the outcome of the interaction.

This is why the first **3D** hydrodynamics attempts started as early as 1987 ([de Kool, 1987](#)). After early works (see also [Livio and Soker, 1988](#); [Terman et al., 1994](#)), efforts with modern codes are those of [Rasio and Livio \(1996\)](#), who used a smoothed particle hydrodynamics (**SPH**) technique and of [Sandquist et al. \(1998\)](#), who used a static nested-grid technique (see Sect. 6.3 for details). These simulations generated a number of useful pieces of information, but they must be considered as being at the toy-model level from today's perspective, mostly because the vast ranges of spatial and temporal scales to be resolved was unmatched by early computational resources.

A second wave of models involved a new suite of codes, both using Eulerian grid and **SPH** techniques ([Ricker and Taam, 2008, 2012](#); [Passy et al., 2012](#)). These modern efforts were fortunately soon followed by a number of additional simulations, which somewhat expanded the considered parameter space, and involved yet more codes and techniques (e.g., [Nandez et al., 2014](#); [Iaconi et al., 2017a](#); [Ohlmann et al., 2016a,b](#); [Chamandy et al., 2018](#); [Prust and Chang, 2019](#); [Reichardt et al., 2019](#)).

The main appeal of 3D hydrodynamic simulations is that they can in principle model the interaction between the stellar cores and the envelope gas in a self-consistent way, although scale problems and resolution issues seriously hinder this prospect. Moreover, 3D simulations of the fast inspiral revealed just how non-spherical the CE interaction is, with outflows relatively close to the equatorial plane, and they revealed the complex flow structures involved in Phase (ii) of CE interaction. They also clearly showed that ejecting the envelope using only orbital energy is very difficult, if not impossible, and paved the way to a deeper understanding of the energy exchange, including the impact of recombination energy on the expanding envelope. While—contrary to initial, perhaps naïve, hopes—3D hydrodynamic CE simulations have not provided a convincing value of α_{CE} for the energy formalism discussed in Sect. 2.1, they do provide a far deeper understanding of the parameter itself. These and other discoveries, which will be described in detail in Sect. 6.3, have convinced many groups to pursue this investigation avenue. Computers and numerical techniques are, after all, advancing rapidly and enable ever more complex simulations. Yet, this enthusiasm also gives way to the realization that, in the end, it might be a clever combination of techniques that will take the podium.

3 Physical modeling and challenges

The system to be modeled consists of (at least) two stellar objects, a giant star and a companion (which can be a star but also a compact object or even a planet). This implies that the objects themselves can be described with a combination of fluid dynamics, thermodynamics, and gravity. The main problem for simulating the evolution of CE systems arises from the discrepancy of scales—most obvious in the required distinction of an extended envelope from a small core in the structure of the giant primary stars (see also Sect. 1.2).

Thus, before turning to the numerical implementation, the physical model for CEE has to be set out. We review it here together with the challenges that arise from the *physical modeling* itself—*numerical* implementation problems often resulting from the chosen physical model will be discussed in Sect. 4.

3.1 The gravo-hydrodynamic model

Astrophysical models are commonly plagued by the different nature the various physical processes at play and the wide ranges of spatial and temporal scales on which they act. Models of CE phases are no exception. In fact, CEE is driven by a complex interaction of physical phenomena combining fluid dynamics, thermodynamics, atomic physics, magnetic fields, radiation, accretion physics, and perhaps other effects. While some of the approaches discussed in Sect. 2 are based on coarse approximations, we are interested here in a modeling basis that rests on fundamental physical principles and avoids approximations.

The most basic model of CEE—which we will refer to as *gravo-hydrodynamic model* in the following—implements the equations of fluid dynamics, most com-

monly the Euler equations⁹, combined with a gravitational source term. The first of them is a scalar equation,

$$\frac{\partial \rho}{\partial t} + \nabla \cdot (\rho \mathbf{v}) = 0, \quad (16)$$

with ρ , t , and \mathbf{v} denoting mass density, time, and velocity, respectively. It expresses *mass conservation*. The second (vector) equation is the *momentum balance*,

$$\rho \frac{\partial \mathbf{v}}{\partial t} + \rho (\mathbf{v} \cdot \nabla) \mathbf{v} + \nabla P = -\rho \nabla \Phi, \quad (17)$$

which accounts for pressure forces ∇P in the momentum flux and includes gravity (with the gravitational potential Φ) as a source term. Finally, *energy balance* is expressed in terms of the specific total energy density,

$$e_{\text{tot}} := \frac{1}{2} |\mathbf{v}|^2 + \frac{\epsilon}{\rho}, \quad (18)$$

where ϵ denotes the density of the internal energy. This gives the last (again scalar) equation

$$\frac{\partial \rho e_{\text{tot}}}{\partial t} + \nabla \cdot (\rho e_{\text{tot}} \mathbf{v}) + \nabla \cdot (P \mathbf{v}) = -\rho \mathbf{v} \cdot \nabla \Phi. \quad (19)$$

Equations (16), (17), and (19) are formulated for a fixed frame of reference. This is called *Eulerian specification*. An alternative is obtained from transforming the system into a frame of reference co-moving with the fluid. This is achieved by introducing the *substantial* (or *Lagrangian*) derivative

$$\frac{D}{Dt} := \frac{\partial}{\partial t} + \mathbf{v} \cdot \nabla. \quad (20)$$

After this transformation, the Euler equations in *Lagrangian specification* read

$$\frac{D\rho}{Dt} + \rho \nabla \cdot \mathbf{v} = 0, \quad (21)$$

$$\rho \frac{D\mathbf{v}}{Dt} + \nabla P = -\rho \nabla \Phi, \quad (22)$$

$$\rho \frac{De_{\text{tot}}}{Dt} + \nabla \cdot P \mathbf{v} = -\rho \mathbf{v} \cdot \nabla \Phi. \quad (23)$$

A special case is encountered for situations where gravity is exactly balanced by the pressure gradient. In this case, the acceleration in Eq. 22 vanishes. This mechanical equilibrium is an excellent approximation for the stratification of stellar envelopes in long-lasting stages of stellar evolution. It is called *hydrostatic equilibrium* (**HSE**):

$$\frac{\nabla P}{\rho} = -\nabla \Phi. \quad (24)$$

⁹ A more general approach could use the Navier–Stokes equations instead, that explicitly account for viscosity. However, because numerical viscosity dominates in implementations, physical viscosity can usually be neglected.

The gravitational potential is determined by Poisson’s equation:

$$\Delta\Phi = 4\pi G\rho, \quad (25)$$

where G is Newton’s gravitational constant.

The Euler equations form a system of hyperbolic partial differential equations and thus pose an initial value problem. For their solution, initial conditions must be supplied. We devote Sect. 5 on how to set up CE simulations. To close the system of Equations (16), (17), and (19), an equation of state is needed that relates pressure, density and internal energy. The equation of state is an essential part of our model system. It accounts for micro-physical interaction between the constituents of matter in the effective macroscopic framework of thermodynamics. In the simplest case, an ideal gas is assumed as a model for stellar material, but radiation pressure can be added via the Stefan–Boltzmann law in a straightforward way.

Obviously, the physical model described by this set of equations is not very specific for the problem at hand—the same set of equations forms the basis for the theoretical treatment of many astrophysical objects ranging from planets to the large-scale structures in the Universe¹⁰. Despite its generic nature, however, the gravo-hydrodynamic model captures the gravitational and hydrodynamic interaction between the orbiting cores and the envelope. Setting up a CE model in this framework, gravitational (and also hydrodynamic) drag is naturally included. The model thus self-consistently accounts for the transfer of orbital energy and angular momentum from the core binary to the envelope gas—one of the most important processes in CEE. In addition, the model also captures convection if it occurs in the stellar envelope.

From a physical point of view, the gravo-hydrodynamic model does not pose particular challenges, but analytic solutions of the system of coupled nonlinear hyperbolic partial differential equations are virtually impossible for complex setups. Therefore, numerical approaches are needed and—as discussed in Sect. 4—neither fluid dynamics nor gravitational interaction are easy to deal with computationally.

3.2 Why do we need multi-D hydrodynamical simulations?

In Sects. 2.1 and 2.2 we have listed the shortcomings of parametric and 1D mechanical models and in Sect. 2.3 we have explained that combining these models with 3D hydrodynamics models can fill in the glaring gaps in our understanding of CEE. This in particular applies to the inspiral of the stellar cores into the CE, i.e. Phase (ii) of our classification in Sect. 1.3: Only 3D hydrodynamic approaches capture the physics of the interaction between the stellar cores and the envelope material consistently. They resolve the flow around the cores and the changes in the structure and morphology of the envelope. Adopting the gravo-hydrodynamical model described in Sect. 3.1, 3D

¹⁰ These equations also form the foundation of classical stellar modeling. Under the simplifying assumptions of spherical symmetry and hydrostatic equilibrium, the first two of the stellar structure equations can directly be derived from them. Energy balance with suitable source terms gives the third of the stellar structure equation. In addition, a prescription of energy transport in stellar material is needed that constitute the fourth equation of the set.

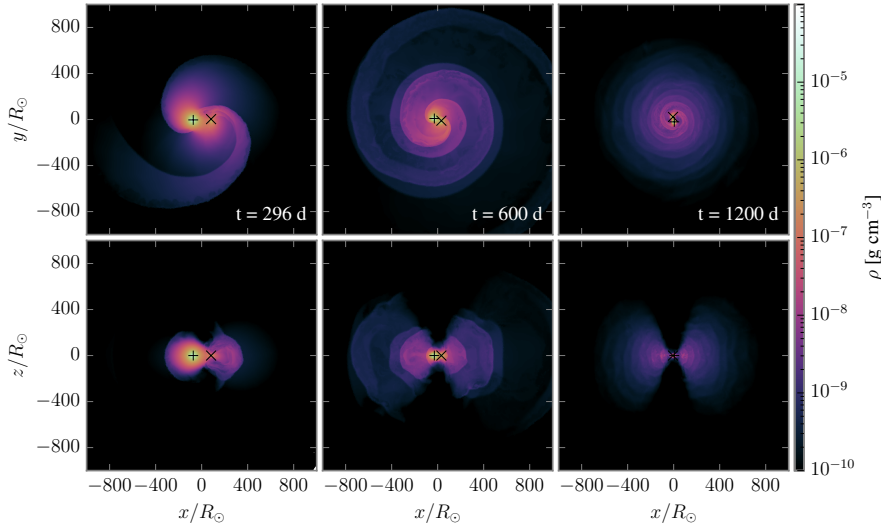


Fig. 3 Density on slices through the orbital plane (top row) and perpendicular to it (bottom row) in a **3D** hydrodynamic simulation of **CE** inspiral of a $0.49 M_{\odot}$ companion (marked with a \times symbol) into a $0.97 M_{\odot}$ early **AGB** star (core marked with a $+$ symbol; Model O.50 of Sand et al., 2020, courtesy of Christian Sand). The times of the snapshots after initiation of the **CE** interaction are indicated in the respective upper panels.

simulations are able to tell where and how the transfer of orbital energy and angular momentum from the core binary onto the envelope material takes place. In this sense, **3D** hydrodynamic simulations are the key to understanding the elusive physics of **CE** interaction.

As **CEE** progresses, the envelope will strongly diverge from spherical symmetry. In an edge-on projection, the density structure of the envelope assumes a toroidal shape (Fig. 3, bottom row). It is immediately clear that perturbations induced to the envelope by the inspiralling core binary system cannot be captured by spherically symmetric models. In addition to the toroidal deformation of the envelope, there is a pronounced spiral shock structure issuing from the core binary that dominates the density structure (Fig 3, top row). In later phases of the evolution, shear-induced hydrodynamic instabilities become visible (Fig. 3, snapshots at 600 d and at 1200 d). While all this does not necessarily mean that the basic results of the interaction such as envelope ejection and orbital decay of the core binary system cannot be represented in **1D** models or parametric formalisms, it seems unlikely that the complex hydrodynamic flows observed in **CEE** would give rise to universal parameters and thus self-consistent predictive prescriptions in such approaches. Full **3D** hydrodynamic models remain indispensable and may be needed to calibrate the simplified models in very fragmented ranges of parameter space.

Moreover, as discussed in Sect. 2.2.1, determining the drag around an obstacle is an extremely challenging problem of **3D** hydrodynamics. A reliable description of accretion and deflection of material around the companion star in **CEE** and the formation of a turbulent wake behind it are of fundamental importance to predict the

envelope ejection efficiency and the orbital shrinkage. In complex setups with non-uniform background densities and circular orbits, 3D hydrodynamic simulations are required to capture the effects in a quantitative way.

Clearly, 3D simulations of the inspiral phase of CEE are a fundamental building block for developing a comprehensive model of this important phase of binary stellar evolution and they are the focus of our review. However, despite their obvious advantages, it is unlikely that they are sufficient. Adopting a fully 3D geometry requires to take a huge leap in the methods and in the computational resources spent on the modeling. Even pushing techniques, algorithm efficiency and computational resources to the limit, there are some inherent difficulties that make it impossible to carry out full 3D hydrodynamic simulations for all the relevant timescales involved in the problem in the foreseeable future—in particular if pre-CE and post-inspiral phases [Phases (i) and (iii) defined in Sect. 1.3] are to be part of the model. So, while in principle the 3D hydro-gravitational model takes into account the interactions between envelope gas and core/companion system, limitations such as resolution may curtail the initial advantages; see also Sect. 7.3.

3.3 CE ejection and the end of the dynamical inspiral

Simulating envelope ejection is a main goal of the numerical modeling of CEE, but it is also one of the most elusive aspects of the interaction. In models, complete envelope removal seems hard to achieve. What are the physical aspects that determine the process and why is it challenging to incorporate them into numerical simulations? The question of envelope ejection is fundamentally related to the question of the final orbital separation of the stellar cores after completing CEE, although, as discussed in Sect. 7.4, it may not be the only process determining it.

The gravo-hydrodynamic model implements the basic mechanism of CEE: orbital shrinkage and unbinding of envelope gas due to transfer of energy and angular momentum from the core binary to the envelope. In its simplest version, it describes the stellar envelope material with an ideal gas equation of state, in some cases adding radiation pressure. This model, however, fails in all 3D simulations that have been carried out so far. The orbital shrinkage stalls or retards when a significant fraction of the envelope is still bound (see Fig. 4 for an example). This leads to the question of how to measure the efficiency of envelope unbinding in a numerical simulation. In a common approach, material is counted as bound if its total energy, determined as the sum of its gravitational potential energy and its kinetic energy is negative. In Sect. 3.4.1, we discuss other forms of energy that could enter this estimate, but here we note that generally arguments based on energy criteria may overestimate the amount of unbound material: Whether or not material is ejected depends not only on its energy but also on its location within the complex perturbed envelope where the total energy is positive. If surrounded by bound material, an unbound fluid element may dissipate its energy without being ejected.

The failure of the basic gravo-hydrodynamic CE model to eject the envelope shows that at some point in the evolution the energy transfer from the cores to the gas becomes inefficient. The fact that the orbital decay ceases (or becomes very slow) in-

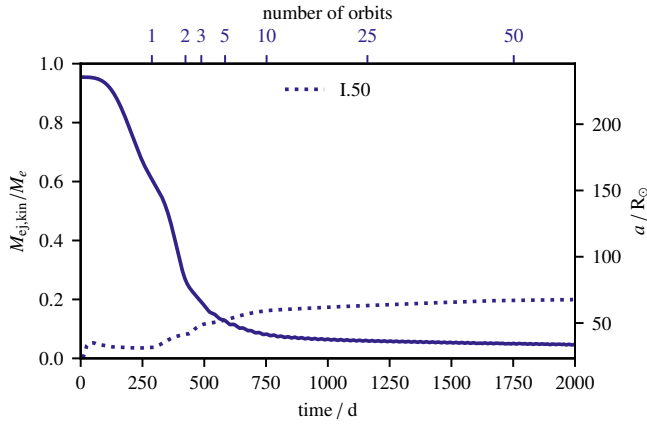


Fig. 4 Simulation of CEE in the gravo-hydrodynamic model for a system with a $1.0 M_\odot$ early-AGB primary star with a companion of mass ratio 0.5. An ideal-gas equation of state was assumed in envelope material (Simulation I.50 of Sand et al. (2020), see Sect. 6.3.4). Shown are the orbital evolution (solid line, right axis) and the fraction of unbound envelope mass (dotted line, left axis) according to the criterion of counting gas in a cell as unbound if its kinetic energy is larger than its gravitational binding energy. Figure courtesy of Christian Sand.

dicates a weaker drag acting on the cores. There are several effects that can potentially contribute to this phenomenon:

- The inspiral of the companion and the associated transfer of orbital energy from the core binary to the surrounding gas perturb the HSE of the envelope such that it expands globally. In the vicinity of the cores, the bow shocks caused by the supersonic orbital motion heat the gas while at the same time the gas is dragged along by the companion and spun up. This injection of energy and angular momentum causes envelope expansion. As a result, the density in the vicinity of the cores decreases with an overall reduction of the drag force. In the analytic treatment of Eqs. (9) and (11), the effect corresponds to $\rho_\infty \rightarrow 0$. Thus, orbital energy release has two counteracting implications: it drives expansion of the envelope and makes its ejection possible in the first place, but, at the same time, dilution of the gas around the stellar cores reduces the efficiency of energy conversion. This makes it hard to predict whether envelope ejection will succeed in the gravo-hydrodynamic model.
- The perturbation of the envelope injecting angular momentum as described above may bring the gas into co-rotation with the core binary. For a vanishing relative velocity between core and gas, $v_\infty \rightarrow 0$ or, equivalently $Ma \rightarrow 0$, the drag force vanishes, see Eqs. (9), (10), (11), and (12). For example, Reichardt et al. (2019) found that establishing co-rotation stalls their inspiral of a $0.6 M_\odot$ point mass companion into the envelope of a $0.88 M_\odot$ RG star. Similarly, Iaconi et al. (2018) analyzed the reason for the halting of the inspiral in two simulations with giants of different masses (0.88 and $2.0 M_\odot$) and a range of companions (from 0.1 to $0.9 M_\odot$). They found that only the heavier companions can evacuate the orbit

and bring gas into co-rotation. The lighter companions struggle to do either (see Fig. 5). They also found that for lighter envelopes (lighter primaries) it takes a more massive companion to evacuate the orbit and/or bring the gas into co-rotation.

- The Mach number of the orbital motion may decrease because the local sound speed increases when the companion reaches the inner, high-temperature parts of the envelope. Except for the Hoyle–Lyttleton formalism [Eq. (5)], all analytic treatments discussed in Sect. 2.2.1 include the subsonic regime, where the drag force decreases. In these models, the drag acquires a maximum value at some finite Mach number and vanishes for $Ma \rightarrow 0$, see Fig. 2. The more elaborate treatments of Ostriker (1999) and Kim and Kim (2007) predict a maximum of the drag force in the range $1 < Ma < 2$. Staff et al. (2016b) showed that a transition through the sonic point may be responsible for the reduction of the gravitational drag in their simulation. This was not observed in the simulations of Iaconi et al. (2018), possibly due to the fact that even their lightest companions were chosen substantially more massive than the planets studied by Staff et al. (2016b).
- Another explanation of why the orbital separation stabilizes, is that the gravitational force between the cores increases as the cores approach each other. Therefore, one needs a larger drag force to noticeably perturb the orbital separation. Thus when the cores approach each other, maintaining the same rate of inspiral requires a larger and larger force, just when in fact orbit evacuation and a reduction of the velocity contrast is reducing the drag.

It is conceivable that all of these effects in combination play a role and conspire to halt the orbital decay. For a better physical understanding, an analysis of the relative contribution and relevance of the processes remains essential and it has to be based on 3D hydrodynamic simulations. This should be possible, because all listed effects are in principle accounted for in the context of the gravo-hydrodynamic base model of CEE.

It is possible, indeed likely, that the dynamics of the envelope would be different if physical effects beyond the simple gravo-hydrodynamic model were accounted for. As discussed in Sect. 2, an important phenomenon is the change in ionization as the envelope expands and cools below the ionization temperatures of hydrogen and helium. The released ionization energy can lead to a substantial increase in envelope unbinding and—for some systems—can even achieve complete envelope ejection (Nandez and Ivanova, 2016; Ohlmann, 2016; Reichardt et al., 2020; Prust and Chang, 2019; Sand et al., 2020; Ondratschek et al., 2022).

While the debate continues on how much of the recombination energy can actually contribute to envelope unbinding (Ivanova, 2018; Soker et al., 2018), we question how the end of the inspiral actually takes place and the extent to which it can be simulated by explicit simulations. It is likely that even if the envelope is not entirely ejected, material may be “lifted” sufficiently to stall the inspiral. Some of this material could, however, fall back rapidly, even dynamically/ballistically and the inspiral could resume.

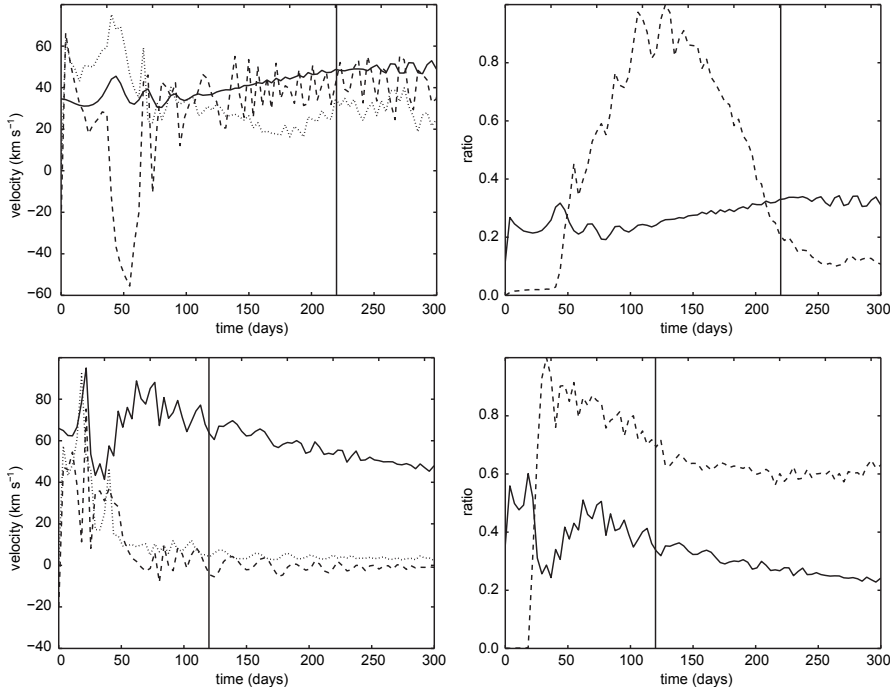


Fig. 5 Parameters playing a role in the gravitational drag in simulations of **CE** interaction of a $0.88 M_{\odot}$, $90 R_{\odot}$ **RGB** primary star (top row) and a $2.0 M_{\odot}$, $66 R_{\odot}$ **RGB** primary star (bottom row) with a $0.6 M_{\odot}$ companion. The vertical lines approximately represent the points where the rapid inspiral terminates. Left column: companion velocity (solid line), local average gas velocity projected on the direction of the companion velocity (dashed line), and local average gas velocity perpendicular to the direction of the companion velocity (dotted line). Right column: companion Mach number (solid line) and normalized average gas density in the companion’s proximity (dashed line). Figure adapted from [Iaconi et al. \(2018\)](#).

As the non-ejected envelope contracts, a “self-regulated inspiral” could be established ([Meyer and Meyer-Hofmeister, 1979](#); [Ivanova et al., 2013](#)): the envelope adjusts such that orbital energy is released at the same rate as convection in the remaining envelope can transport it to the surface where it is radiated away. If the heating becomes too weak, slow contraction revives the interaction of cores and gas, while too strong an interaction leads again to an expansion and dilution of the gas. In this sense, an equilibrium between orbital energy release and energy transport to the stellar surface is established and it is kept stable by self-regulation. This is certainly a slow process and the orbital evolution in the self-regulated inspiral regime is difficult or impossible to follow in **3D** hydrodynamic simulations. Another complication is that the in-falling gas would have substantially more angular momentum, making the final stable configuration difficult to predict. It is possible that instead of a self-regulated envelope, a circumbinary disk could form that interacts with the orbit of the stellar cores and modifies its parameters. Clearly, understanding the end of the inspiral extends beyond the applicability of the basic gravo-hydrodynamic model of **CEE**.

3.4 Why are common-envelope phases a multi-physics problem?

The basic gravo-hydrodynamic description of CEE certainly does not capture all effects associated with this phase of binary stellar evolution. A model extension to account for additional physics must be decided according to its relevance for specific aspects of CEE: some effects may pertain to the dynamical inspiral [Phase (ii)] itself, others to the pre-CE or post-inspiral phases [Phases (i) and (iii)], or even to later phases such as the shaping planetary nebulae expected to form in connection with envelope ejection of some stars. Including additional effects requires to modify the set of model equations (16), (17), and (19).

Even without diverging very far from the basic gravo-hydrodynamic model as discussed in Sect. 3.1, the results of simulated CEE can change dramatically. Modeling the envelope of giant stars and their CE as ideal gas is reasonable and commonly used in simulations for lower mass stars, while for massive stars radiation pressure needs to be taken into account. This can be done with an additive term in the equation of state.

In the following, we discuss changes in the ionization structure of the envelope gas and magnetic fields as important ingredients for model extensions. Other phenomena that are not part of the basic gravo-hydrodynamic model of CEE but still may be relevant include nuclear reactions that may occur in dense accreted material, neutrino cooling in the vicinity of compact object companions, accretion of material, jet formation, evaporation of the companion, and perhaps even relativistic effects. A rigorous assessment of the relevance of these effects for CEE is still missing, but some aspects of accretion onto the stellar cores, the potential formation of a disk and jet-like outflows have been explored in more detail (e.g. MacLeod and Ramirez-Ruiz, 2015a,b; Chamandy et al., 2018; Soker, 2016b; Moreno Méndez et al., 2017; López-Cámara et al., 2019; Shiber et al., 2019; López-Cámara et al., 2020, 2022; Hillel et al., 2022; Zou et al., 2022; Schreier et al., 2019, 2021, 2022).

These examples illustrate that CEE is a pronounced multi-physics problem. Progress in understanding the dynamical evolution of the system cannot only be achieved by improving the numerical methods for simulating it. The extension of the gravo-hydrodynamic base model with additional effects is essential to reach a reliable physical description.

3.4.1 Ionization and recombination effects

Over the past decades it has been realized that ionization effects play an important role in CEE (Ivanova et al., 2015). As the envelope is lifted and starts to expand due to the perturbation by the inspiralling companion, its outer layers may gradually fall below the ionization thresholds of hydrogen and helium and previously ionized material recombines.

This is a micro-physical matter effect leading to a source term in the energy equation of fluid dynamics (19). A simple model assuming local thermodynamic equilibrium is given by the corresponding Saha equation, but a general treatment would be achieved by implementing a detailed network accounting for changes in the ionization states and releasing the corresponding recombination energies. As a conse-

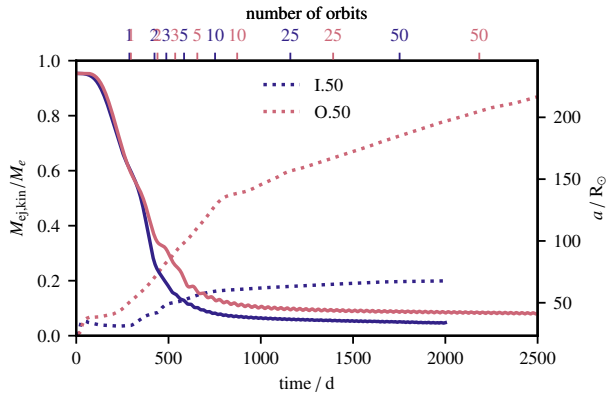


Fig. 6 Fraction of unbound envelope mass (dotted lines, left axis) and orbital evolution of the cores (solid lines, right axis) for Simulation I.50 of Sand et al. (2020) as shown in Fig. 4 (blue color). In addition, in red color we plot the same quantities, but this time for Simulation O.50 of Sand et al. (2020), that accounts for changes in the ionization of envelope material. Figure courtesy of Christian Sand.

quence, temperature and pressure of the gas change and this may cause a transfer into kinetic energy finally supporting envelope ejection. Instead of solving the equations explicitly, the ionization of matter as a micro-physical effect can be absorbed in a suitable equation of state, for instance the *OPAL* equation of state of Rogers et al. (1996) and Rogers and Nayfonov (2002) or its derivative in the *MESA* code (Paxton et al., 2011), see Sect. 4.2. Thus, while formally sticking to the basic gravo-hydrodynamic **CE** model, important physical effects can be incorporated via the equation of state.

The consequence of including ionization effects in **CE** simulations is shown in Fig. 6. Compared with the basic gravo-hydrodynamic model, envelope ejection increases dramatically. Whether or not the released recombination energy can—at least in parts—support envelope ejection depends on its ability to thermalize. Instead of adding to the thermal energy, it may be transported outwards by radiation (Grichener et al., 2018, but see Ivanova, 2018) or convection (Sabach et al., 2017) and lost from surface of the envelope. Wilson and Nordhaus (2019) point out that convection may also remove energy released by the orbital decay directly so that deeper inspiral of the companion is necessary to eject the envelope. While convection is in principle part of the basic gravo-hydrodynamic model (but may not be sufficiently resolved in **3D** hydrodynamic simulations of **CEE**), radiation transport constitutes an extension of the model. Because all simulations that successfully expel the **CE** rely on the contribution of recombination energy to the unbinding of material, it is urgent to include radiation transport into the modeling. Without radiation transport the use of a tabulated equation of state that includes the release of recombination energy may severely overestimate the envelope unbinding, because a (large) fraction of that energy might instead leak out of the star.

This illustrates the ambiguity of defining the unbound fraction of envelope material. Should thermal and ionization energy be counted in into the energy budget? Certainly, the criterion comparing the gravitational binding energy with the kinetic

energy of the gas only is the most conservative choice, although it may still overestimate the effect of released recombination energy if no radiation transfer is included. Counting in the thermal energy of the gas is a widely accepted approximation, while including the ionization energy in addition marks the most optimistic case. The approximation relying on kinetic energy only is illustrated in Fig. 6.

Recombination energy, if it can be fully used to expand the envelope, acts in the immediate post-inspiral phases when the envelope is expanding substantially. During these phases it has been demonstrated that the conditions in the envelope are ideal for dust formation (Glanz and Perets, 2018; Reichardt et al., 2020; Iaconi et al., 2020) which would likely have an impact on the dynamics of the envelope by the increase in opacity. Dust-driven winds are extremely effective in reducing the envelope mass of AGB stars over short timescales with mass-loss rates as high as 10^{-4} to $10^{-3} M_{\odot} \text{ yr}^{-1}$ (Kwok et al. (1978) and these stars are not dissimilar in mass and size to those typical simulated in the context of CEE.

3.4.2 Magnetic fields

A second prominent example of a physical phenomenon that should be considered, are magnetic fields. These can be accounted for by extending to the equations of magneto-hydrodynamics (MHD); see, e.g., Campbell (2018) for a detailed treatment of MHD in binary stars. Apart from the very challenging numerical implementation of MHD, the presence of magnetic fields makes the range of physical phenomena extremely rich and complex. In addition to hydrodynamic flow instabilities, MHD instabilities can play a role. It has been discussed whether the action of magnetic fields can help with envelope ejection. While magnetic fields do not introduce a new energy source—they can only be amplified at the expense of kinetic energy of the gas—they can redistribute energy and angular momentum in the envelope. Based on analytic considerations, Regős and Tout (1995) argued that magnetic fields should be strongly amplified in CE inspirals, while Tocknell et al. (2014) used jet-like features observed in post-CE planetary nebulae as an indication that strong fields must have been present in the late CE stages. The first MHD simulation of CEE was presented by Ohlmann et al. (2016b), see also Sect. 6.3.4. It showed that the accretion flow around the companion star leads to strong amplification of magnetic fields (see left and middle panels of Fig. 7). The reason is proposed to be the magnetorotational instability (MRI; Balbus and Hawley, 1991). In late phases, the amplified magnetic field disperses over the entire CE (Fig. 7, right panel). Despite the strong amplification, however, magnetic fields are not dynamically relevant in the situation modeled by Ohlmann et al. (2016b). Still, they may play a role in transport processes and in shaping the ejected envelope material as shown in the MHD simulations of Ondratschek et al. (2022).

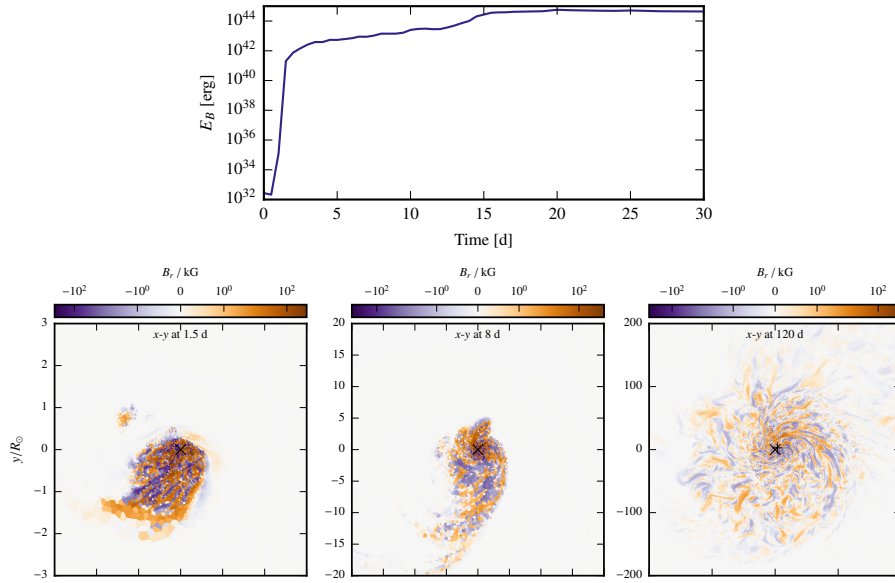


Fig. 7 Magnetic field energy over time (top) and radial magnetic field strength B_r in the orbital plane (bottom) of the high-resolution simulation of Ohlmann et al. (2016b) with a seed field of 10^{-6} G. The times at which the snapshots were taken are indicated in the panels. Note that the left and middle panel show the vicinity of the companion (marked with a \times symbol). The position of the core of the RGB primary star is marked by a $+$ symbol and visible in the right panel. Top figure courtesy of Sebastian Ohlmann. Bottom figures from Ohlmann et al. (2016b).

3.5 Why are common-envelope phases a multi-scale problem?

Like many other problems in astrophysics, CEE is plagued by severe multi-scale challenges. These can be divided into two categories: a spatial and a temporal scale challenge.

The *spatial scale problem* is rather obvious and caused by the discrepancy in sizes between the core of the primary star and the companion on the one side and the total radius of the primary star on the other side. Although typical values vary somewhat, for red giant branch (RGB) and AGB stars core radii, R_{core} , are around $0.03 R_\odot$ while the size of the stars, R_\star , are between $\sim 20 R_\odot$ and $\sim 600 R_\odot$. This gives a range of scales extending over up to four orders of magnitude, which is a lot but not overly impressive in comparison with other astrophysical scale challenges. For red supergiants, the cores have a radius of $\sim 0.07 R_\odot$ and stellar radii are hundreds to thousands of solar radii. Companions can be of various nature, but cases of interest include objects as small as planets, white dwarfs, and neutron stars, thus extending the scale range to eight orders of magnitude. A special case are systems with black hole companions. The orbital separation in the pre-CE stage and the expansion of the envelope in the CE interaction extend the range of relevant spatial scales involved in the problem even more.

The *temporal* scale challenge is usually discussed in terms of the relevant characteristic timescales of the involved objects. One of these is given by the mechanical structure of the envelope. It can be defined as the *free-fall timescale*,

$$\tau_{\text{ff}} \sim \frac{\pi}{2} \frac{R_{\star}^{3/2}}{[2G(M_{\text{core}} + M_{\text{com}})]^{1/2}}, \quad (26)$$

with the gravitational constant, G , the core mass of the primary star, M_{core} and the mass of the companion, M_{com} . Note that τ_{ff} differs from the orbital period of the companion at a distance of R_{\star} ,

$$\tau_{\text{orbit}} = 2\pi \frac{R_{\star}^{3/2}}{[G(M_{\text{core}} + M_{\text{com}})]^{1/2}}, \quad (27)$$

only by a factor of $2^{-5/2}$. Both are due to the gravitational force and estimate the timescale of changes to the system driven by gravitational forces, that has to be captured in simulations of **CEE**. The *dynamical timescale* τ_{dyn} , in contrast, estimates the timescale of changes induced by hydrodynamic pressure effects. It is given by the sound crossing time over the system,

$$\tau_{\text{dyn}} \sim \frac{R}{c_{\text{sound}}}, \quad (28)$$

with the sound speed, c_{sound} . Close to hydrostatic equilibrium, pressure effects should compensate gravity and thus $\tau_{\text{dyn}} \sim \tau_{\text{ff}} \sim \tau_{\text{orbit}}$.

The dynamical timescale of the envelope of **RGB** and **AGB** stars can be estimated to be $\tau_{\text{dyn, envelope}} \sim 50$ d by adopting $R = R_{\star}$ and a typical sound speed of ~ 10 km s $^{-1}$. The cores of **RGB** or **AGB** stars and their envelopes have starkly different thermodynamic properties. The temperature in the cores is about four orders of magnitude higher than in the envelopes and their densities exceed the envelope densities by ~ 10 orders of magnitude. Therefore, the sound speed exceeds 10^3 km s $^{-1}$ in the core of such stars, and the dynamical timescale is as short as $\tau_{\text{dyn, core}} \approx 20$ s.

Some late episodes of **CEE** may rely on thermal readjustment of the envelope which is associated with the much longer *thermal* (Kelvin–Helmholtz) timescale,

$$\tau_{\text{KH}} \sim \frac{GM_{\star}^2}{R_{\star}L_{\star}}, \quad (29)$$

where L_{\star} is the luminosity of the star. For **RGB** and **AGB** stars with $L_{\star} \sim 3000 L_{\odot}$, the thermal timescale $\tau_{\text{KH}} \sim 10^4$ yr, leading to a timescale discrepancy compared with $\tau_{\text{dyn, envelope}}$ of 10^5 . For late **CEE** stages, however, the relevant thermal timescale is that of the remaining envelope when part of the material has already been removed, which may differ significantly from our estimate for unperturbed stars.

3.6 The need to simulate the pre-common envelope and post-inspiral phases

We conclude our summary of the physical challenges to simulating CEE by discussing the phase that leads to the dynamical inspiral—Phase (i), pre-CE evolution—and the phase that follows it—Phase (iii), post-CE evolution. Both of them are likely to take place on thermal, rather than dynamical timescales. This fact alone makes them difficult to treat numerically. The *need* to simulate both of these phases stems from the suspicion that what precedes the inspiral may change the playing field for the inspiral itself and that what follows the inspiral ultimately settles the final orbital separation for the surviving binary or even determines whether a binary survives at all. Here, we quickly set the stage for the physical challenge presented by these phases.

Before engaging into the inspiral phase of CEE, binary interactions may substantially affect the parameters of the system. Pre-CE evolution is likely to involve mass loss from the system, and this effect can be critical in determining whether or not the system enters CEE in the first place (e.g. Ivanova et al., 2013). Moreover, mass loss can change the angular momentum budget of the system and the binding energy of the primary’s envelope. An extreme case of binary interaction preventing CEE is proposed by Soker (2015), who argues that if the companion grazes the envelope of the giant primary star and accretes mass at a sufficiently high rate, it can launch jets that remove material and angular momentum. Additionally, mass and angular momentum can be lost through the second Lagrange point. This way, the envelope is ablated as the companion approaches the core of the primary star without ever entering a CE phase. The orbital decay is very slow and if existing, it is driven by tidal interaction although the companion is never deeply immersed in the envelope. Soker (2015) call this alternative to CEE “grazing envelope evolution” (GEE) and Sabach and Soker (2015) discuss the scenario in the context of triple star systems. Mass loss is also thought to lead to observable features, some of which have been connected to the LRN class of optical transients (see Soker and Tylenda, 2006; Pejcha, 2014; Soker, 2015, 2016a; MacLeod et al., 2017b and Sect. 7.6).

Once the primary star overfills its Roche lobe, mass transfer sets in. Whether or not this leads to the formation of a CE depends on the dynamical stability of this mass transfer, which is determined by the relative readjustments of the Roche lobe to mass transfer and the donor (primary) star’s structure to mass loss: if the donor expands relative to its Roche lobe, mass loss becomes unstable and a runaway in the mass transfer rate sets in. The details involve several complications—for a discussion we refer to Ivanova et al. (2013)—but stability analyses usually determine a critical mass ratio of donor and accretor (i.e. companion) q_{crit} for stability, which itself depends sensitively on the type of donor (Hjellming and Webbink, 1987).

This, however, is not the only criterion determining the events preceding the fast inspiral. Tides dominate the early phases of interaction, even before Roche lobe contact. Giant stars expand and when their companions are located within a distance of some stellar radii (Soker, 1994; Mustill and Villaver, 2012; Madappatt et al., 2016, the exact number is uncertain and can vary), interaction between the two tends to synchronize and circularize the orbit. While the timescales for these processes are reasonably well understood (see Zahn, 1977), the concomitant stellar evolution alters the playing field. In particular, an instability occurs when the angular momentum of

the giant is larger than a certain fraction of the orbital angular momentum (Darwin, 1879). This tends to destabilize a tidally relaxed system leading to a reduction of its orbital separation. All in all, a complex interplay between tidal instability, mass-transfer instability, and stellar evolution set the initial conditions of the subsequent fast inspiral. While not all of these processes take place on the Kelvin–Helmholtz timescale characterizing changes in the thermal structure of the star—tidal interaction for instance is a dynamical process—the timescales of these phenomena are likely still too long to be modelled by global 3D simulations.

After the dynamical inspiral stalls, a number of physical processes (see Table 1 of Soker, 2017, for an overview of some of these) will take hold that operate on lengthening timescales. While some of the current 3D hydrodynamic simulations indicate successful envelope ejection, a general problem seems to be that the orbital separation reached over the simulation time is too large compared with observations of post-CE binaries (e.g. Iaconi et al., 2017b; Kramer et al., 2020). This may be associated with shortcomings in the physical modeling or numerical deficiencies in the simulations, but there is a fair chance that the system parameters are affected by processes that act on timescales longer than the simulation period. Self-regulated inspiral (see Sect. 3.3) is one possibility, but even if most of the envelope was unbound, some returning gas could interfere with the orbit once more, or form a disk around the binary which could alter the orbital parameters. If most of the envelope is still bound, the binary will presumably go through a renewed phase of inspiral. If the new delivery of orbital energy is still not sufficient to unbind the remaining envelope, then a merger of the stellar cores may be the final outcome of the interaction. The newly formed star would then relax on thermal timescales as it radiates the excess energy. However, the orbital angular momentum would have to find a final resting place in the envelope, redistributing itself in some way. Another possibility is that—instead of merging—the companion is destroyed during deep inspiral into the CE. This is in particular possible for low-mass companions such as brown dwarfs or giant planets (Livio and Soker, 1984b; Soker, 1998b; Nelemans and Tauris, 1998; Jia and Spruit, 2018; Kramer et al., 2020)

Modelling the immediate pre- and post-inspiral, i.e. the parts of Phases (i) and (iii) that are closest to Phase (ii), with global 3D simulations is not impossible, as we will discuss in Sects. 6.1 and 7.1, but some simplifications must be incorporated, which may or may not alter the results. The longer timescales likely will need different modelling approaches and, ideally, these will be interfaced with global simulations that best model the dynamical phase (see Sect. 7.4). After discussing the *physical* challenges we face in formulating a full description of CEE, we turn to modelling problems that arise from *numerical* obstacles in the following section.

4 Numerical approaches and limitations

Once the physical model is fixed—which, as discussed above, is highly non-trivial—a valid numerical discretization of the underlying equations is bound to converge to the correct result of that model. In the ideal world of infinite numerical resolution,

any consistent and stable numerical scheme should give the same answer¹¹. This, however, is far from reality: the discrepancy of relevant spatial and temporal scales implies that such a convergence cannot be reached easily. While some effects are treated accurately by numerical approaches, others can only be approximated. Gas flows in the envelope are usually resolved, but effects closer to the cores are increasingly difficult to represent correctly. The challenge is to find appropriate approximations. Various choices are made which may interfere with the original physical modeling so that differences in the numerical results are to be expected. The goal, however, is to reach convergence to the correct results in some key quantities.

Implementing the basic gravo-hydrodynamic model of CEE as defined in Sect. 3.1 requires two ingredients: (i) a solver for the Euler equations of fluid dynamics (16, 17, 19), and (ii) a self-gravity solver that accounts for the Poisson equation (25). Both are in the standard repertoire of computational astrophysics, but also mark some of the more challenging aspects of it. We review methods to obtain solutions to the hydrodynamics in the presence of gravity in Sects. 4.1 and 4.3, but omit implementation details; these can be found in the literature. Instead, we focus on some of the more specific aspects arising from the application of standard techniques to CEE simulations.

It is likely that physical effects beyond the basic gravo-hydrodynamic model become more commonly included in future simulations of CE interaction. These would deserve a dedicated discussion in this section. A prominent example is radiation transfer, which, however, has not yet been established as a standard in the simulations and we therefore refrain from including it at the moment. The same applies to magnetohydrodynamic simulations of CEE, that thus far have only been carried out by a single group (Ohlmann et al., 2016a) with one specific way of treating magnetic field. While we mention these simulations in Sect. 6.3.4, a review of different approaches is not yet called for.

4.1 Computational fluid dynamics

There are numerous approaches to discretize the Euler equations of fluid dynamics. A fundamental distinction is the frame of reference in which the basic equations are formulated. One possibility, where a fixed lab frame of reference is chosen, is given in Eqs. (16, 17, and 19). Discretizing this formulation gives rise to the so-called *Eulerian schemes* for solving the equations of fluid dynamics. Alternatively, discretization of Eqs. (21, 22, and 23) in Lagrangian specification with a co-moving frame of reference results in *Lagrangian schemes* of computational fluid dynamics. Lagrangian approaches are particularly well-suited to simulations of interactions between astrophysical objects—not only in the context of CEE, but in various other setups reaching from the simulation of mergers of compact objects (see Rosswog, 2015, for a review) to mergers and evolution of galaxies in cosmological contexts (e.g., Liu et al., 2016; Croft et al., 2009; Stinson et al., 2013).

¹¹ For linear finite difference equations, this is the Lax–Richtmyer equivalence theorem (Lax and Richtmyer, 1956).

Both the Eulerian and the Lagrangian approaches have their particular strengths and weaknesses. Whether these play out in specific applications depends on the context, the setup, and the research questions to be answered. CEE is in some sense a prototypical “Lagrangian problem”: two main objects orbiting each other and a rotating stellar envelope embedded in vacuum make methods following the fluid flow attractive. The main advantage of Lagrangian methods is that the geometry is adapted to the problem at hand. Following the motion of the fluid, advection errors are minimized. This reduces common problems with angular momentum conservation (see Sect. 4.1.2) and diffusion over the surfaces of the stellar objects. This said, it is not *a priori* clear that Lagrangian schemes perform best in all respects. This is related to the problem that in Lagrangian specification a grid-based discretization approach leads to complicated grid geometries and the danger of tangling if the grid is to be advected along with complex 3D hydrodynamic flows. Therefore, a grid-free Lagrangian approach is commonly chosen (see Sect. 4.1.2), which, however, lacks the precision of grid-based computational fluid dynamics. Eulerian approaches do not face this problem. Their grid-based discretizations are unproblematic and they benefit straightforwardly from the accuracy of Riemann-based hydrodynamics solvers (see Sect. 4.1.1). Therefore, no general statement is justified giving preference to one or the other method and we discuss their application in the context of particular simulations in Sect. 6. CE simulations with moving-mesh codes (see Sect. 4.1.3) combine the advantages of a (nearly) Lagrangian scheme with the accuracy of a grid-based discretization of the equations of fluid dynamics.

4.1.1 Eulerian, grid-based methods

There are various general strategies to discretize and solve the Euler equations in Eulerian specification (Equations 16, 17, 19), once initial conditions are specified. Overviews are given in standard textbooks, such as Ferziger et al. (2020).

In astrophysical applications, finite-volume methods have defined the quasi-standard for the past decades. They discretize space into computational grid cells and assign cell-averages of the conserved hydrodynamic quantities to their centers. Reconstructing these averaged conserved quantities to the cell edges introduces jumps over the interfaces between neighboring cells. Such initial conditions with one discontinuity define *Riemann problems*. In *Godunov schemes* (Godunov, 1959), they are solved to determine the numerical fluxes, which are used to update the cell-averaged conserved quantities.

This discretization of the equations of fluid dynamics in space has to be augmented with a discretization in time. To this end, two main classes of approaches exist: *explicit* and *implicit* time discretization schemes. The former determine the state at the new timestep from the state at the current timestep while the latter solves for the state at the new timestep from the given current and the new state, which requires a numerically expensive matrix inversion. While implicit time discretization can be unconditionally stable, explicit time stepping is restricted by the so-called *Courant–Friedrichs–Lewy (CFL)* condition (Courant et al., 1928). It states that for stability of the scheme, the time step has to be chosen smaller than the crossing time of the fastest wave emerging from the Riemann problem over a grid cell. A rough es-

timate for this would be the sound crossing time over a cell. So far, all hydrodynamic schemes employed for simulations of **CE** interaction use explicit time discretization and their time stepping is therefore subject to the **CFL** condition.

Different methods exist to ensure higher-order accuracy with specific reconstruction and time integration schemes and for enhancing the efficiency with approximate Riemann solvers. For the details of such methods, we refer to textbooks such as that by Toro (2009). The resulting high-resolution shock capturing methods are advantageous for following the spiral shocks in the **CE**. Fundamentally, this property results from the fact that finite-volume methods derive from the *integral form* of the equations of fluid dynamics that in contrast to the differential form as in Eqs. (16–19) allows for discontinuous (so-called *weak*) solutions. Shocks are possible in the solutions of the Riemann problems at the cell interfaces. Depending on the quality of the employed approximate Riemann solver and the numerical dissipation of the scheme, however, shocks are usually smeared out over a few grid cells. In addition to the shock-capturing feature, Godunov methods are known to reproduce phenomena such as hydrodynamic instabilities and turbulence very well.

The orbital motion of the cores and the rotation of the envelope, however, imply that matter will be dragged over the spatially fixed discretization grid. Transforming into a rotating frame of reference can alleviate the problem, but because of the strongly differential motion of the involved matter the problem cannot be completely eliminated. This situation leads to advection errors that can only be mitigated with high spatial resolution, which renders Eulerian grid-based approaches to simulate **CEE** a computationally expensive choice.

Covering the required large domains with equally-sized grid cells for discretization would either lead to low resolution of important parts of the system in case of large grid cells or excessive computational cost when trying to resolve the relevant spatial scales. For this reason, non-uniform grids concentrating resolution in the center around the core binary system or, even better, adaptive mesh refinement (**AMR**) techniques (e.g. Berger and Olinger, 1984; Berger and Colella, 1989) are commonly employed in **CE** simulations. **AMR** methods subdivide grid cells once pre-defined refinement criteria are met and they de-refine when they are no longer fulfilled. Multiple levels of refinement are possible so that very high spatial resolution can be reached in some patches of the domain. In **CE** simulations, mesh refinement is successfully applied around the cores to reduce the advection errors. While not as excessive as global fine resolution, **AMR** still comes at the price of the higher computational effort associated with larger cell numbers and shorter numerical timesteps in smaller cells required by the **CFL** condition plus a significant overhead for the bookkeeping of the complex **AMR** grid structure.

Nonetheless, once the resolution is high enough to ensure reasonable conservation of angular momentum, Eulerian grid-based approaches show excellent reproduction of hydrodynamical effects such as shock waves and instabilities. Moreover, their methodology offers more flexibility for extending the physical modeling base. Magnetohydrodynamics, for instance, is best implemented in grid-based techniques and the formulation of subgrid-scale models for unresolved physical effects is an attractive perspective for the future development of **CE** simulations.

4.1.2 Lagrangian, smooth particle hydrodynamics

The problem of growing complexity of a computational grid with the evolution of the fluid-dynamical system in Lagrangian approaches is avoided in SPH methods (Lucy, 1977, Gingold and Monaghan, 1977; for reviews see Monaghan, 1992, Springel, 2010b, Price, 2012, and Rosswog, 2015). A particle-based discretization of the mass distribution is applied instead of a computational grid. The pressure gradient appearing in Eq. (22), however, raises the question of evaluating the gradients of quantities in a particle representation of matter. To address this problem, the particles are not understood as point masses in SPH schemes, but they rather mark the centers of smoothed-out distributions of the conserved hydrodynamic quantities. The amount of smoothing is quantified by the choice of a *smoothing kernel*, $W(r, h)$, which assigns quantities to a location at a distance of $r = |\mathbf{x} - \mathbf{x}_i|$ from the SPH particle at point \mathbf{x}_i and is characterized by a certain *smoothing length*, h . The mass density at point \mathbf{x} , for instance, is obtained from summing over all N SPH particles:

$$\rho(\mathbf{x}) = \sum_{i=1}^N m_i W(|\mathbf{x} - \mathbf{x}_i|, h). \quad (30)$$

The mathematical form of the smoothing kernel is arbitrary, but has to obey the normalization conditions of giving 1 when integrated over all space and degenerating to Dirac's delta function for $h \rightarrow 0$. An efficient choice are kernels with compact support. They restrict the overlap to nearby particles and thus reduce the terms that have to be evaluated for the sum in Eq. (30). A popular form is the spline kernel of Monaghan and Lattanzio (1985),

$$W(r, h) = \frac{1}{\pi h^3} \begin{cases} 1 - \frac{3}{2} \frac{r}{h} + \frac{3}{4} \frac{r^3}{h^3} & \text{if } 0 \leq \frac{r}{h} \leq 1; \\ \frac{1}{4} (2 - \frac{r}{h})^3 & \text{if } 1 \leq \frac{r}{h} \leq 2; \\ 0 & \text{otherwise,} \end{cases} \quad (31)$$

but there are various alternatives to this choice (e.g. Dehnen and Aly, 2012). At any given point in space, the hydrodynamic quantities thus defined can be determined by summing over contributions with overlapping smoothing kernels. Therefore characteristic size of the kernel determines the spatial resolution in SPH simulations. For all practically useful kernel functions, the standard deviation of the kernel is very similar to the chosen smoothing length. Efficient SPH implementations employ variable smoothing lengths assigning an h_i to each particle such that quantities are determined by summing over similar numbers of neighboring particles independently of the local density. Hence, h_i is an approximate measure of the linear resolution at the location of particle i .

This particle-based discretization leads to a set of ordinary differential equations, the equations of motion of SPH (Lucy, 1977; Gingold and Monaghan, 1977; Monaghan, 1992), that have to be solved numerically. Stability of explicit time integration is again determined by the CFL condition, requiring timesteps smaller than the sound crossing time over a smoothing length (Lucy, 1977; Gingold and Monaghan, 1977).

SPH methods allow to exploit the advantages of Lagrangian schemes in CE simulations and they have been employed extensively for this purpose. Their main benefit

is that they avoid advection errors. This leads to exact conservation of angular momentum (see also Sect. 4.4.3). Reaching an acceptable degree of angular momentum conservation with Eulerian grid-based approaches (which is fundamental for CE simulations) requires high spatial resolution of the rotating objects which often can only be reached with AMR techniques. This makes these schemes computationally more expensive than SPH-based simulations.

Another feature of Lagrangian schemes is Galilean invariance—the solution is not affected by the presence of bulk velocities. Violation of Galilean invariance may suppress hydrodynamic instabilities when altering the background velocity and keeping the spatial resolution fixed. Again, Galilean invariance in Lagrangian schemes results from avoiding advection errors and distinguishes SPH from grid-based approaches.

Conceptually, SPH is very similar to numerical schemes for simulating the evolution of collisionless N -body systems under the action of gravity. The only differences in the underlying equations are the terms involving pressure. For such systems, efficient methods have been developed to calculate self-gravity (see Sect. 4.3) and these are exploited in the SPH-based simulations of CEE, where this effect is fundamental for the dynamics.

Another advantage is that no pseudo-vacuum has to be introduced for embedding the system of interest. SPH particles are placed where the matter of the object of interest is located. The computational domain is arbitrary, free boundary conditions are natural to the scheme and without excessive computational cost the computational domain can be large enough so that no material leaves and conservation of global quantities can be checked. The placement of particles exclusively inside the objects of interest in combination with summing up the contributions to conserved quantities from neighboring particles, however, introduces an imbalance that causes an artificial surface tension in SPH.

Despite these advantages, there is a potential problem with SPH schemes. They are based on a discretization of Eqs. (21–23)—a *differential form* of the equations of fluid dynamics—and therefore allow only for differentiable (so-called *strong*) solutions and not for discontinuities such as shocks. In order to treat shocks in SPH, artificial viscosity has to be introduced to broaden the shock to a numerically resolvable continuous structure (Monaghan and Gingold, 1983). This at the same time allows for the necessary dissipation of energy in the shock. A careful choice of the form of the artificial viscosity is required to avoid undesired effects such as dissipation in non-shocked regions or violation of angular momentum conservation. A correct representation of pre- and post-shock states is possible within the SPH framework, but high resolution (i.e. a local high density of particles) is required to keep the shock structure reasonably thin. In contrast, no artificial viscosity is needed in finite-volume Godunov schemes to represent shocks.

The SPH discretization into particles naturally and necessarily follows the mass distribution of the considered system. As opposed to other astrophysical application examples of SPH, this is a clear disadvantage in CE simulations, where the features in the gas dynamics in a rather dilute envelope may need to be followed.

Still, with limited computational resources, SPH simulations of CEE published so far show better performance than their grid-based Eulerian counterparts. They are able to follow the gross dynamics of the system with a fairly low number of

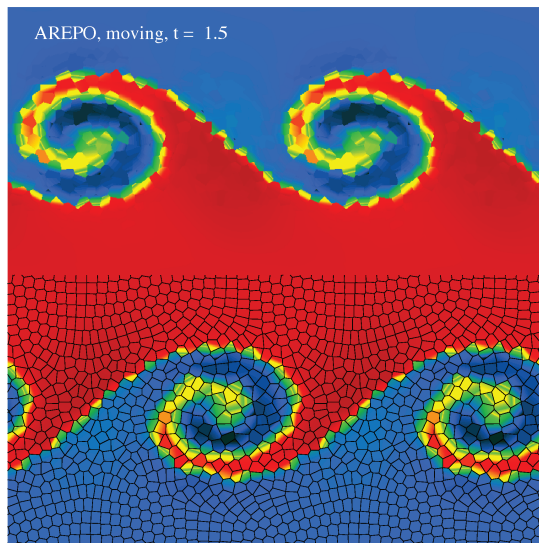


Fig. 8 Simulation of a Kelvin-Helmholtz instability between two shearing fluids with the code `AREPO` in a low-resolution (50×50) to illustrate the Voronoi mesh overlaid in black in the lower half of the box. Figure from [Springel \(2010a\)](#).

particles without sacrificing angular momentum conservation. However, reaching fine resolution in the fluid flows and resolving instabilities requires a drastic increase in the number of particles so that there seems to be some break-even point where grid-based Eulerian techniques become more efficient.

4.1.3 Moving-mesh approaches

A rather recent development is the use of moving-mesh hydrodynamics codes for **CE** simulations. The first of such simulations—based on the `AREPO` code developed by [Springel \(2010a\)](#) for cosmological simulations with the modifications of [Pakmor et al. \(2016\)](#) to ensure second-order accuracy of the scheme—was presented by [Ohlmann et al. \(2016a\)](#). A number of follow-up studies expanded on this including additional physical effects and testing parameters of the setup model ([Ohlmann et al., 2016b](#); [Sand et al., 2020](#); [Kramer et al., 2020](#)). An independent implementation of the moving-mesh technique in the `MANGA` code was used for **CE** simulations by [Prust and Chang \(2019\)](#).

The moving-mesh method can be seen as combining advantages of the Lagrangian particle-based **SPH** technique and Eulerian grid-based approaches. A Voronoi tessellation of space based on a set of discrete points is used to construct a complex unstructured mesh of polyhedral cells, see [Fig. 8](#). As in conventional, finite-volume grid-based codes, numerical flux functions across the thus defined cell boundaries are computed in a Godunov-type approach using Riemann solvers. These provide a scheme to update the cell-averaged values of conserved hydrodynamical quantities. The mesh-generating points can in principle be moved arbitrarily or even kept

fixed—in which case the scheme recovers an Eulerian grid-based approach to numerical fluid dynamics. Advecting the points with the fluid flow, however, yields a nearly Lagrangian method. Its advantages of reducing advection errors, conserving angular momentum, and guaranteeing Galilean invariance¹² are combined with the superior shock capturing capabilities and the improved reproduction of hydrodynamic instabilities of grid-based Godunov-type schemes. For a detailed discussion of the advantages of the moving mesh scheme, we refer to the original publication of the AREPO code (Springel, 2010a).

While moving-mesh methods overcome the notorious problems of grid tangling in grid-based Lagrangian schemes, some measures of correcting stretched cell shapes that would result from complex flows are still required to guarantee numerical benignity (Springel, 2010a). Therefore, the resulting moving-mesh schemes are not exactly Lagrangian but very close to it¹³. The Godunov-type finite-volume scheme for updating the cell values is based on the integral form of the Euler equations of fluid dynamics. It eliminates the need of an artificial viscosity as in SPH schemes. Moreover, it avoids the inherent sampling noise errors in the gradient estimates of SPH (Pakmor et al., 2013).

Based on a finite-volume discretization, moving-mesh schemes retain the versatility of Eulerian approaches with respect to the implementation of additional physical effects. Magnetic fields, for example, can be accounted for (Pakmor et al., 2011; Pakmor and Springel, 2013). The first 3D MHD simulations of dynamical CE interaction were performed by Ohlmann et al. (2016b) with the moving-mesh code AREPO. Unresolved effects can in principle be included via subgrid-scale models. While utilized extensively in cosmological simulations with AREPO (e.g. Vogelsberger et al., 2013), this capability has not been exploited yet in simulations of CEE.

The flexibility of mesh construction can be used to implement AMR capabilities that, in contrast to SPH approaches, are not limited to improving the resolution of high-density regions. This is of particular interest in CE simulations because here the focus is on resolving effects in the rather dilute envelope gas. By adding grid generation points, cells can be split up and the resolution is increased locally; removal of grid generation points reverses this procedure. This spatial adaptivity can be combined with adaptive individual time stepping (as implemented in AREPO and MANGA), which significantly enhances the computational efficiency because it pays attention to the temporal multi-scale nature of the problem as discussed in Sect. 3. A moving, adaptively refined mesh as implemented in AREPO and MANGA is a powerful approach to simulate CEE, where certain parts of the envelope, particularly the regions around the cores, benefit from higher spatial resolution, while other parts of the envelope can be represented with less computational effort.

Another advantage of the currently employed moving-mesh codes is that they were derived from powerful particle-based codes, that had been written for simula-

¹² The failure of Eulerian schemes to obey Galilean invariance is impressively demonstrated in Figure 10 of Springel (2010a), who shows that a background velocity suppresses the development of Kelvin–Helmholtz instabilities on a fixed grid. Robertson et al. (2010), however, argue that Eulerian methods converge may converge to the correct Galilean-invariant solution.

¹³ For this reason, advection errors are minimized but not eliminated, and angular momentum is conserved with high accuracy, but not exactly.

tions of self-gravitating systems. The efficient parallel implementation of the tree-based gravity solver of GADGET-2 (Springel, 2005) carries over to AREPO, and that of CHANGA (Menon et al., 2015) to MANGA.

The origin of the moving-mesh codes from tools to simulate galaxy evolution in a cosmological context required some modifications. Methods for capturing the relevant conditions and effects in stellar matter had to be implemented (Pakmor et al., 2013; Ohlmann et al., 2017; Prust and Chang, 2019), see Sects. 5.3 and 6.3.4.

4.2 Implementing the equation of state

As mentioned in Sect. 3.1, an equation of state relating pressure to density and internal energy (and possibly other quantities such as chemical composition and ionization state) has to be provided in order to close the fluid dynamics equations set.

Realistic treatments of matter require the inclusion of various effects. Already when augmenting an ideal-gas equation of state with radiation pressure, the computational effort increases significantly. The reason is that the equation of state derived from statistical physics and thermodynamics usually provides pressure and internal energy as a function of density and temperature. A fluid-dynamical model, however, follows the conserved hydrodynamic quantities, i.e. density and total energy, from which the kinetic energy can be subtracted to obtain the internal energy of the gas. While an ideal-gas equation of state can still be inverted analytically to give pressure as a function of density and internal energy, this is no longer possible when including radiation pressure and therefore an iteration is required. Since the equation of state is called at least in every hydrodynamic update of each computational cell, the computational expense of this iteration affects the total demand of the simulation significantly.

The situation becomes even more critical when more complex physical effects are included such as degeneracy or ionization. In such cases, modern implementations revert to tabulated data. The look-up of table values and interpolation between them can add substantial computational cost to the hydrodynamics scheme.

As discussed in Sect. 3.4.1, in the context of CE simulations, ionization effects are of particular interest. When envelope gas expands and cools down below the ionization thresholds of hydrogen and helium, the corresponding recombination energies are released into thermal energy. Assuming local thermal equilibrium, the effect can be included into the equation of state as done by virtually all 3D hydrodynamic CE simulations that accounted for these effects. This approach does not provide the detailed ionization structure of the gas, which would require the solution of the Saha equation or a detailed ionization network; however, for CE simulations this is not of immediate interest. As an input, the equation of state is given the local density and the internal energy of the gas (that corresponds to the sum of thermal and ionization energy). From this, temperature and pressure are determined. This can result in a local over-pressure when recombination energy is released, giving rise to expansion and acceleration of material. If no losses due to cooling or radiation are included, all released recombination energy is transferred to kinetic energy of the envelope gas. The processes determining the equation of state are complex and therefore the na-

tive implementation of the `OPAL` equation of state (Rogers et al., 1996; Rogers and Nayfonov, 2002) or its derivative in `MESA` (Paxton et al., 2011) rely on pre-computed tabulated data.

As a side remark, we mention that applying such more elaborate equations of state requires to use suitable exact Riemann solvers (see, e.g., Colella and Glaz, 1985; Chen et al., 2019) or approximate Riemann solvers for Eulerian grid-based methods. This is accounted for in most implementations of modern astrophysical hydrodynamics codes.

4.3 Modelling self-gravity

Gravitational forces define the `CE` interaction. They mediate (1) the binding of the stellar components and the binding of the progenitor binary system, (2) the interaction and orbiting motion of the stellar cores, and (3) the interaction of the cores and the envelope gas giving rise to drag and energy transfer. This highlights the importance of treating gravity accurately and efficiently in `CE` simulations. As a long-range force, gravity enters the modeling as a source term in the momentum [Eqs. (17) and (22)] and energy equations [Eqs. (19) and (23)]. Source terms are often discretized separately from the equations of fluid dynamics in an operator splitting approach. For the case of gravity, there are two basic choices: the gravitational potential can be determined by solving the Poisson equation (25) in the continuum model of matter, or the gravitational forces are computed directly from Newton’s law of gravity between point masses in particle-based discretizations of matter. We note that this choice is independent of the discretization of the equations of fluid dynamics. While `SPH` codes preferably use a particle-based discretization for modeling gravity, mapping to grids in the particle-mesh method is also employed occasionally. Grid-based Poisson solvers seem a natural choice for grid-based discretizations of the equations of fluid dynamics. However, since stellar cores are often modelled as point masses, grid-based schemes are sometimes coupled with particle-based gravity solvers instead.

Approximations, such as a gravitational potential that is constant in time or one that is derived from a low-order multipole expansion of the overall gravitational potential, are inappropriate for capturing `CE` dynamics—a full treatment of self-gravity of the involved envelope gas and stellar cores is inevitable. The Poisson equation of Newtonian gravity (25) poses an elliptic problem and is numerically very challenging. A direct summation of the gravitational forces gives rise to algorithms that scale with the square of the number of cells or particles N quickly leading to prohibitive costs in highly-resolved simulations. In the following, we discuss various approaches employed in `CE` simulations to reduce this $O(N^2)$ operation count to a more modest algorithm complexity, such as $O(N \log N)$.

4.3.1 Tree methods to calculate self-gravity

In particle-based discretizations, a preferred method for calculating self-gravity of astronomical objects is a tree-based approximation (Barnes and Hut, 1986). The method

is based on the fact that the individual contribution of distant particles to the force of a target particle is negligible, so that it is sufficient to treat the collective effect of distant particles in an approximate way, i.e. as a low-order multipole of the gravitational potential. The interaction with close particles, in contrast, is treated accurately. To distinguish close from distant particles, a tessellation of space in a tree hierarchy is constructed. For details, we refer to the literature (e.g. [Appel, 1985](#); [Barnes and Hut, 1986](#)). This method reduces the complexity of the algorithm to the desired $\mathcal{O}(N \log N)$.

Tree-based methods are commonly employed in **CE** simulations. They are a natural choice when particle-based, Lagrangian schemes (**SPH**) are used to solve the equations of fluid dynamics, because they can also help to efficiently search for neighbor particles as required for kernels with compact support (see Sect. 4.1.2). But also in grid-based approaches to fluid dynamics, a particle-based discretization may be used to model the gravitational interaction. This is popular in particular in the context moving-mesh methods. A problem with tree-based methods, however, is that they introduce asymmetries. The approximate treatment of the gravitational interaction of a target particle with distant particles violates Newton's third law (*actio* equals *reactio*). This is in conflict with global momentum conservation and introduces spurious motions. Indeed, many **CE** simulations performed with this methods exhibit a slow drift of the center of mass of the system. There are ways to alleviate this problem. The important notion is that random force errors would cancel during the simulation. The overall drift and momentum conservation violation results from *correlations* between the errors ([Springel et al., 2021](#)). These correlations can be broken, and for this purpose [Springel et al. \(2021\)](#) propose to randomize the relative location of the particles with respect to the computational box.

4.3.2 Alternative methods to calculate self-gravity

An approach that appears as a natural choice in the context of grid-based discretizations, but is also used with a particle-based schemes (see [Taam and Ricker, 2006](#)), are *Fourier methods*. Solving the Poisson equation (25) with a Green's function gives

$$\Phi(\mathbf{r}, t) = -G \int \frac{\rho(\mathbf{r}', t)}{|\mathbf{r} - \mathbf{r}'|} d^3 r', \quad (32)$$

which corresponds to a convolution of the Green's function for the Laplacian with the inhomogeneity of the equation, i.e. the density. In Fourier space, this reduces to a simple multiplication and the required discrete Fourier transforms can efficiently carried out with the Fast Fourier Methods (FFM). Similar to the tree-based methods, this reduces operation count for calculating gravity in an N -body system to $\mathcal{O}(N \log N)$.

A fast grid-based approach that reduces the effort to at least $\mathcal{O}(N \log N)$ is the *multigrid technique* ([Brandt, 1977](#)). It accelerates iterative relaxation methods for solving the Poisson equation ([Press et al., 2007](#)). Changing the elliptic original problem into a pseudo-time dependent expression, a diffusion equation is obtained that—when relaxed to equilibrium where the pseudo-time derivative vanishes—yields the solution of the original problem. Starting from an initial guess for the gravitational potential, the relaxation is achieved in an iteration. The error in the initial guess can be

seen as being distributed over the domain with various modes of different wavelength. Since standard relaxation schemes couple only neighboring cells, short-wavelength errors are quickly eliminated, but damping the long-wavelength error components takes many iteration steps. This is avoided by mapping to a hierarchy of subsequently coarser grids where the original long-wavelength components are short compared to the grid spacing and can be damped out in few relaxation steps. Subsequent projection back to the original fine grid combined with further relaxation steps and cycling through this hierarchy of grids efficiently produces the desired equilibrium solution. The multigrid method is has been used in **CE** simulations by [Ricker and Taam \(2012\)](#).

4.3.3 Gravitational softening

If the Poisson equation (25) is discretized on a grid together with the equations of fluid dynamics, the grid spacing limits the spatial resolution for both the hydrodynamic quantities and the gravitational potential. As discussed above, however, self-gravity can also be solved in a particle-based discretization, independently of the discretization choice for the hydrodynamic part of the model; and even in grid-based approaches the stellar cores are often modeled as point masses. Particles can get arbitrarily close and one may expect an arbitrarily fine spatial resolution in the discretization of gravitational interaction—a potential advantage when combined with a particle-based or moving-mesh discretization of fluid dynamics. As particles approach each other, however, the gravitational forces between them grow without limits requiring the scheme to take ever smaller timesteps. This produces undesirable time sinks in the numerical scheme.

Therefore, a fix is commonly employed: the gravitational potential is unphysically altered to flatten for short distances, so that the force approaches zero instead of scaling with the inverse of the squared distance. Different functional forms are employed in practice, but the simplest *softened* gravitational potential—sometimes called the Plummer form of softening (e.g., [Dehnen, 2001](#); [Price and Monaghan, 2007](#))—reads

$$\Phi_{\text{soft}}(r) := -\frac{Gm}{\sqrt{r^2 + r_{\text{soft}}^2}}, \quad (33)$$

where r denotes the distance to the particle of mass m , and r_{soft} is the parameter altering the physical law—the so-called *softening length*.

In grid-based discretizations of fluid dynamics combined with particle-based gravity solvers, the size of the grid cells δ provides an obvious choice for the scale of the gravitational softening. However, the softening parameter does not necessarily have to be a constant but it may depend on the distance r . [Ruffert \(1993\)](#) suggested the form

$$\Phi_{\text{Ruffert}}(r) := -\frac{Gm}{\sqrt{r^2 + \epsilon^2 \delta^2 \exp[-r^2/(\epsilon\delta)^2]}}, \quad (34)$$

with $\epsilon = 1.5$.

In **SPH** approaches, the only sensible scale for the softening length is the **SPH** smoothing length. This can be implemented by using a general formulation for force

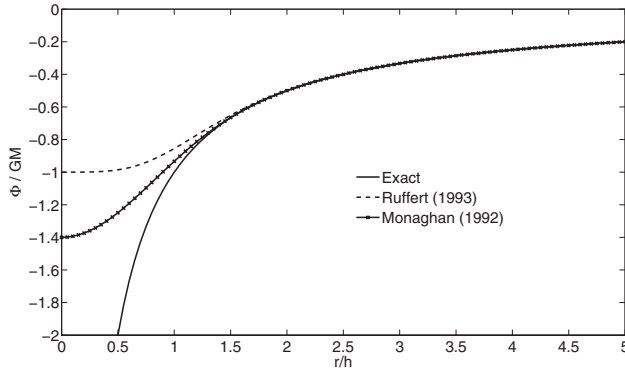


Fig. 9 Exact gravitational potential compared with the softened potential according to Eq. (34), labeled as “Ruffert (1993)” and Eqs. (35,36,31) labeled as “Monaghan (1992)” in arbitrary units with $h = \epsilon\delta = 1$. Figure from [Passy et al. \(2012\)](#).

softening ([Dehnen, 2001](#); [Price and Monaghan, 2007](#)) with the gravitational potential due to all particles $i = 1 \dots N$,

$$\Phi(\mathbf{r}) = -G \sum_{i=1}^N m_b \phi(|\mathbf{r} - \mathbf{r}_i|, h). \quad (35)$$

The *softening potential kernel* ϕ is related to the **SPH** smoothing kernel (31) via the Poisson equation

$$W(r, h) = -\frac{1}{4\pi r^2} \frac{\partial}{\partial r} \left(r^2 \frac{\partial \phi}{\partial r} \right) \quad (36)$$

([Price and Monaghan, 2007](#)). As a consequence, the gravitational potential is softened with a spline function. Such a choice seems preferable because, in contrast to the expressions (33) and (34), splines reproduce the exact gravitational potential outside a finite radius.

While alleviating the time sink problem, a consequence of gravitational softening is that inside r_{soft} the simulated dynamics is altered and less trustworthy. The physical law of gravitational interaction is modified, most strongly at distances shorter than the softening length. This is no fundamental problem for simulating self-gravitating fluids in **SPH** approaches or grid-based methods combined with particle-based discretization of gravity. The scale down to which fluid dynamics is resolved usually corresponds to the scale of the softening; therefore, the gravitational interactions are sufficiently well modeled.

In the context of **CE** simulations, however, the stellar cores are usually represented as point particles (in the case of **SPH** approaches, they are not to be confused with the **SPH** particles; see Sect. 5.2). These core particles are distinct from the envelope gas. They interact via gravitational forces but not via hydrodynamical effects. Since the core particles comprise a substantial fraction of the total mass of the system in two points, the associated gravitational potentials fall off very steeply close to them. Gravitational softening must be applied to the core particles in order to avoid fatal time sinks. For this, a softening length has to be set. Again, depending on the

discretization approach of the hydrodynamics in the envelope gas, assigning r_{soft} to either the grid spacing scale or the smoothing length would be desirable. This, however, requires to follow the very steep gradient of the potential close to the core particle, which makes the numerical representation of mechanical equilibrium configurations (such as required in the setup of **CE** simulations, see Sect. 5.3) challenging. The pressure gradient counteracting gravity has to be resolved in the hydrodynamic part of the simulation and the required fine resolution leads to unacceptably small time steps. In this situation, a softening according to Eq. (34), has a practical advantage over the physically more accurate spline softening: at close distances it is shallower (see Fig. 9) and a shallower gradient can be resolved with fewer discretization elements.

Whatever choice is made for the functional form of the softening, however, setting the gravitational softening to the scale of the hydrodynamic discretization elements does not ensure sufficiently large time steps for currently affordable simulations. Therefore, **CE** simulations usually shy away from a safe choice of gravitational softening parameters—from a computational point of view, the softening length should be large to reduce the computational cost of the time integration. But large r_{soft} implies a large region around the core particles in which the gravo-hydrodynamical interaction is suspicious. The dynamics around the cores are the driver for **CEE** and should be modeled as accurately as possible. In fact, Reichardt et al. (2020) found that smaller softening lengths in their simulations lead to faster interaction and earlier unbinding of the envelope material. Staff et al. (2016a) carried out a similar test using an Eulerian grid-based hydrodynamics code and the interaction seems to be strengthened for smaller softening lengths leading to a slight increase in the final orbital separations of the cores and slightly more unbound mass. In virtually all **CE** simulations softening length for the core particles is set according to computational efficiency considerations at the expense of physical accuracy. Therefore, careful convergence tests are necessary.

4.4 Advantages and drawbacks of hydrodynamic simulation methods

In this section, we summarize some advantages and drawbacks of each of the three main techniques used in **3D** hydrodynamic **CE** simulations: **SPH**, Eulerian grid-based schemes, and moving-mesh approaches. Only few direct comparisons have been carried out (most notably Passy et al., 2012, who compare **SPH** and Eulerian grid-based simulations), and the available results do not point to major systematic discrepancies between simulations employing different numerical methods. It is far more likely that different results are obtained because of individual choices within each method. This, of course, is not a universally true statement but merely an assessment of the current state-of-the-art. As long as the physical models and implementation details of the methods dominate, the specific features of the fundamental schemes may remain hidden.

For future developments, however, it is important to be aware of the different capabilities of the methods. The current status of **CE** simulations, discussed in Sect. 7.1, merely scratches the surface of the problems involved in this complex phase of binary stellar evolution. The basic question of whether envelope ejection is possible under

certain modeling assumptions can be addressed with different numerical schemes. For the current simulations, this choice affects mostly the efficiency of **CE** simulations: The spatial resolution required to capture certain physical processes depends on the discretization method and it differs with its choice. As a consequence, this affects the fidelity of the simulations that can be carried out with given computational resources.

This situation may be regarded as an indication of the immaturity of the field of **CE** simulations: A detailed understanding of **CEE** requires improved simulations and the different features of methods will play out more in the future. Each technique has particular drawbacks that may compromise the fidelity of the simulated parameters of the **CE** interaction. Generally, the important aspects to consider are accuracy, efficiency and parallelizability, boundary conditions and flexibility with the geometry of the setups, conservation properties, and general versatility when it comes to include additional physics.

4.4.1 Boundary conditions and setup geometries

The system to be modeled consists of two stars orbiting each other and engaging into a dynamical interaction. This setup is far from a spherically-symmetric configuration. Because of the lack of spatial symmetries in **CEE**, special grid geometries (such as a spherical grid) do not provide any advantage and there are no obvious boundaries of the domain of interest such as stellar surfaces. Eulerian grid-based **CE** simulations are usually conducted on Cartesian meshes in cubical boxes. This leads to conflicts with the fact that the considered **CE** systems are to a good approximation embedded in vacuum¹⁴. Empty grid cells cause numerical problems and therefore “true” vacuum cannot be represented straightforwardly in grid-based approaches—a problem for both Eulerian and moving-mesh discretizations. Therefore, cells that are located outside of the system are usually filled with a low-density *pseudo-vacuum* in the hope that it does not affect the dynamics of the simulated **CE** interaction. If hot enough, however, this pseudo-vacuum may have a welcome effect on the initial setup: it can reduce the steep pressure gradient at the surface of the primary star and therefore stabilize the stellar model against the dispersion observed in the case of insufficient spatial resolution of the gradient. But this comes at the price that observables cannot be meaningfully be extracted from such simulations (see Galaviz et al., 2017, for a detailed discussion). Moreover, if too hot, pseudo-vacuum cells may reduce the **CFL** timestep. Therefore, it is advisable to keep the pseudo-vacuum as cold as possible. With certain setup procedures (see Sect. 5.3), this is possible.

In grid-based **CE** simulations, the simulated domain has to be finite in its spatial extent and therefore outer boundary conditions at the edges of the computational domain have to be implemented in a way such that they do not interfere with the modeled system. Certainly, no material should flow into the simulation box, but, in principle, outflow of material would be acceptable. A loss of material, however, makes checking for conservation of mass, energy, angular and linear momentum inaccurate

¹⁴ Pre-**CE** stages, however, may lead to mass loss and some circum-binary material may be present in reality.

and thus the simulations cannot be fully validated using these global criteria. For this reason, the domain sizes are usually chosen so large that even with successful envelope ejection no material leaves the domain. This requires to fill large volumes outside of the interacting system with pseudo-vacuum, which can have some unwanted dynamical effects on the simulation (for a discussion see [Chamandy et al., 2019](#); [Iaconi et al., 2018](#)). To minimize such artifacts, the pseudo-vacuum should contain as little mass as possible—i.e. for the desired large domain sizes it should have very low densities.

Representing **CE** systems on a static grid as in the Eulerian approaches causes strong advection errors, implying violation of conservation properties. The only cure to this is an increase in spatial resolution—a common numerical approach to alleviate problems. Because of the spatial scale problem (Sect. 3.5) and in the light of the desire to make the simulation domain as large as possible to avoid interaction with the boundaries, this is only promising if high spatial resolution is only realized certain, temporarily changing parts of the domain. Therefore, as discussed in Sect. 4.1.1, **AMR** techniques are widely used in **CE** simulations.

SPH methods do not require sophisticated outer boundary conditions. Empty spaces between the objects of interest are possible and no pseudo-vacuum is needed. The artificial surface tension mentioned in Sect. 4.1.2 supports the surface of the primary star model and no advection errors disperse the stellar material. These features make **SPH** codes a natural choice for simulations of **CEE** simulations. However, as discussed in Sect. 4.1.2, these have drawbacks when it comes to resolving low-density envelope material and hydrodynamic processes in it.

For this reason, moving-mesh approaches present a favorable compromise. They combine the accuracy of grid-based discretizations with the flexibility of a Lagrangian method. With their spatial discretization based on grid-generating points, adaptive mesh refinement is straightforward and sufficiently large computational domains pose no problem. The need of grid-based methods to fill voids with pseudo-vacuum, however, persists.

4.4.2 Accuracy, efficiency, and versatility

A satisfying flow representation can in principle be achieved with any converging scheme. The key question, however, is the numerical resolution required to reach a certain level of accuracy—and this is where the schemes differ fundamentally. In this context, it has to be pointed out that an often used comparison between the number of particles in an **SPH** simulation and the number of cells in a Godunov-like grid-based simulation is misleading. Whereas **SPH** methods average over the particles within the smoothing kernel, Godunov schemes compute the fluxes of hydrodynamic quantities between cells and reach an effective resolution defined by the grid scale. The effective spatial resolution of **SPH** simulations with the same number of particles is usually lower by a factor of a few.

Generally, finite-volume grid-based discretization techniques are superior over **SPH** methods in resolving hydrodynamic flow features accurately. However, at low resolution, **SPH** methods often have to be given preference. They yield robust results and, in the context of **CE** simulations, are capable of determining global properties

of the evolution with rather little computational cost. While grid-based simulations have to cover vast amounts of pseudo-vacuum with the same effort as the actual stars, **SPH** focuses the resources on modeling the physical objects of interest.

While **AMR** techniques alleviate the problems with grid-based **CE** simulations, they introduce a significant computational overhead and require some implementation effort. Still, Eulerian grid-based simulations reach an accuracy that is very hard to match with **SPH** techniques. These tend to under-resolve low-density regions. Moreover, implementing additional physics such as magnetic fields and other effects seems more natural on a given grid than in the **SPH** approach, although it is not impossible there either (Price, 2012). Subgrid-scale models representing unresolved physical effects require a well-defined grid-scale to connect to.

As mentioned before, moving-mesh techniques combine the best of both worlds: the accuracy and versatility of grid-based finite-volume methods with the geometric flexibility of a Lagrangian method. A drawback is the complex grid-generation procedure that tessellates space in every timestep. This overhead renders moving-mesh approaches computationally more expensive than **SPH** but they are still superior over Eulerian grid-based approaches in terms of efficiency.

4.4.3 Energy and angular momentum conservation

Many hydrodynamics codes guarantee conservation of total (i.e. kinetic plus internal) energy and linear momentum. For finite-volume schemes, cell-averaged conserved quantities are updated via fluxes over the cell edges. What leaves one cell enters its neighbor. This is the reason why finite-volume approaches conserve momentum and energy globally (but not necessarily locally)—inside the domain, net loss or gain in conserved quantities is impossible. In the case of **SPH**, mass and energy are directly ascribed to the discretizing particles and as long as no particle is lost, these quantities are conserved in this scheme, too. Conservation of total energy and linear momentum, however, is not sufficient for reliable **CE** simulations for two main reasons.

The first reason is that for the problem at hand, *angular* momentum conservation is critical. In contrast to linear momentum and energy balance, the Euler equations of fluid dynamics—(16) to (19) or (21) to (23)—do not explicitly include angular momentum balance, but only imply it. Whether or not these quantities are conserved in numerical simulations depends critically on the discretization approach. In grid-based Eulerian schemes, angular momentum conservation is not guaranteed due to the inherent advection errors. These can be decreased by adapting the geometry of the spatial discretization to the expected flow, but this is neither universal nor always possible in complex astrophysical situations. As emphasized above, the flows in **CEE** certainly lack clear symmetries that could be exploited. Therefore, the only way to improve angular momentum conservation in these approaches is a costly increase of numerical resolution. As discussed in Sect 4.1.2, Lagrangian schemes are superior in conserving angular momentum because they avoid advection errors by construction. In fact, a variational derivation of the **SPH** method (e.g. Monaghan and Price, 2001; Springel and Hernquist, 2002) proves this feature: Within the framework of Lagrangian mechanics, the equations of fluid dynamics can be derived from a Lagrangian (Eckart,

1960) via a variational principle. Instead of discretizing the resulting partial differential equations, however, one can discretize the Lagrangian in a particle-based approach and then derive the (discretized) SPH equations directly. Symmetries of the original and discretized Lagrangians give rise to conservation properties: the absence of explicit time dependence implies energy conservation, their translational invariance gives linear momentum conservation, and—most importantly—their rotational invariance leads to angular momentum conservation, not only at the level of the partial differential equations, but also for the discretized equations.

The second problem is that while total energy and linear momentum conservation is—for conservative schemes—guaranteed for the numerical implementation of the equations of fluid dynamics without source terms, they do not generally hold in cases where external forces are discretized in different approaches than the hydrodynamic quantities. This is the case for gravity—which, as for many astrophysical problems, is of fundamental importance for CEE. The basic gravo-hydrodynamic model relies on an exact treatment of the conversion of gravitational binding energy and orbital energy to internal energy and acceleration of the envelope gas. Mismatches between the discretizations of the hydrodynamic variables and the gravitational potential can lead to problems with maintaining the expected mechanical equilibrium in stars (see Sect. 5.3), but they may also lead to accumulating errors in the conserved quantities over long simulation periods modeling the CE interaction. Apart from these more subtle issues, the very treatment of self-gravity already poses challenges to numerical schemes. As argued in Sect. 4.3, an exact direct summation over all contributions of N discrete elements (cells in grid-based approaches, or particles in the corresponding schemes) falls into the rather unacceptable $O(N^2)$ time complexity class. Therefore, approximate algorithms, such as discussed in Sects. 4.3.1 and 4.3.2, are preferred. The employed approximations induce errors that potentially can accumulate over the duration of the simulations—not only in the energy but also in linear angular momentum. The center-of-mass of the considered setup can start to drift. Apart from these numerically and algorithmically caused errors, the softening of the gravitational potential (Sect. 4.3.3) alters the interactions at the fundamental physical modeling level. Still being a central force field, conservation of energy should not be affected, but changes due to adaptive gravitational softening lengths may cause problems because they artificially modify the shape of the gravitational potential in time.

Numerical errors in the conservation of angular momentum and energy are an unavoidable compromise when striving for efficient simulations. It is, however, essential to monitor them. Energy errors are particularly critical in simulations of CEE, because one of the goals is to determine the unbinding of the envelope, which is rather loosely bound in the giant primaries anyway. It has to be ensured that any unbinding of material is physical and not caused by numerical inaccuracies. The question of what level of non-conservation can be tolerated is an important one. Sandquist et al. (1998) published their conservation of energy and angular momentum showing that over their entire simulations they tolerated a change of approximately 10 %, see Fig. 10. There is no strict quantification of an acceptable level and it might affect different output quantities differently. Clearly, if at the end of a numerical simulation the binding energy of remaining envelope gas is of the same order of magnitude as the accumulated energy error, little can be said about the success of envelope ejection.

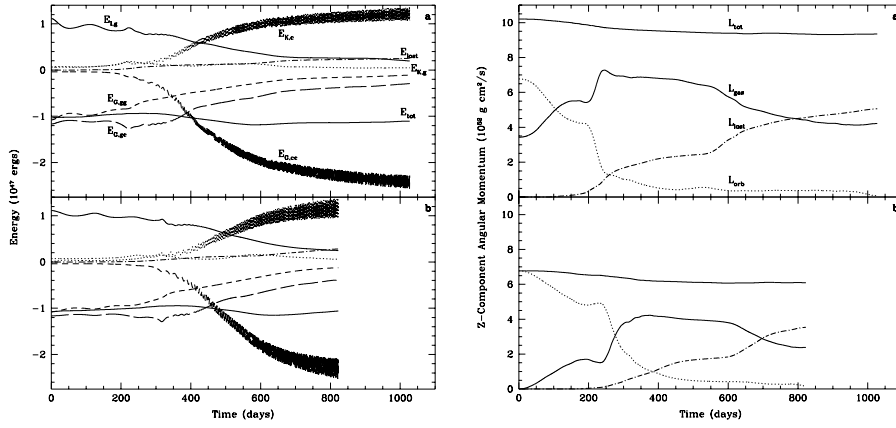


Fig. 10 Evolution of energy and angular momentum in two simulations (panels a and b) of Sandquist et al. (1998) with different initial parameters. Shown are different components: the kinetic energy of the core particles and the gas ($E_{K,c}$ and $E_{K,g}$, respectively), the internal energy of the gas ($E_{I,g}$), energy lost from the simulated domain (E_{lost}), potential energies from gravitational interaction between gas and gas ($E_{G,gg}$), gas and core particles ($E_{G,gc}$), and between the core particles ($E_{G,cc}$), the z -components of the total angular momentum (L_{tot}), the angular momentum of the gas (L_{gas}), and the core system (L_{orb}), and the angular momentum lost from the domain (L_{lost}). By the end of the simulations, conservation of total energy and angular momentum was violated at the $\sim 10\%$ level. Figures from Sandquist et al. (1998).

It is therefore mandatory to track the conservation of energy and angular momentum and the results should be published alongside with the simulations.

Generally, more work is called for to identify and localize the numerical problems that violate energy and momentum conservation. This most likely requires extensive resolution studies.

4.4.4 Code speed and scalability

Performing 3D hydrodynamic simulations of CEE is computationally very challenging. The system has to be followed over long periods of time with high accuracy, i.e. many numerical time integration steps are to be performed and the spatial resolution has to be sufficiently high. Clearly, such simulations require high performance computing (HPC) resources and are only possible when employing parallelization techniques. Therefore, scalability to large numbers of computational cores to be used in parallel is an important criterion when choosing a code for CE simulations.

Parallelization in the spatial domain is standard for the codes currently used for CE simulations. In finite-volume approaches, the hydrodynamics solvers can usually be parallelized on distributed-memory machines with some acceptable communication overhead. Distributed-memory parallelization is more challenging for particle-based discretization approaches as used for modeling self-gravity (see Sect. 4.3.1) or the hydrodynamics itself (see Sect. 4.1.2). For this reason, some of the SPH codes employ shared-memory parallelization (e.g., PHANTOM; Price et al., 2018), which restricts the simulations to a moderate number of computational cores, but there are also SPH implementations with distributed-memory parallelization, e.g. GADGET-2 (Springel,

2005) and SNSPH (Fryer et al., 2006). In moving-mesh approaches, the grid generation poses an additional challenge to efficient parallelization.

For an approximately fixed spatial resolution and a given numerical algorithm, the speed-up that can be reached with parallelization is limited by Amdahl’s law (Amdahl, 1967) or similar considerations. Beyond this limit, an increase of the number of employed compute cores no longer reduces the execution time proportionally. Therefore, it is not only scalability of the employed code that determines the feasibility of a certain CE simulation, but also its overall efficiency, i.e. the required wall-clock time to perform a time integration step for a given number of discretization elements in a fixed parallel setup. A common experience in code development is that these aspects—scalability and overall efficiency—are competing. A higher efficiency often causes load-imbalances and thus comes at the expense of parallel scalability. This does not necessarily imply a disadvantage of the respective code for performing CE simulations. Some of the codes employed for such simulations have been developed originally for extensive cosmological simulations and are highly optimized for efficiency; for example the AREPO code of Springel (2010a) has been used for the groundbreaking *Illustris* project (Vogelsberger et al., 2014).

Ideally each simulation would report the total number of CPU-hours, the number of nodes and cores it was executed on, wall-clock times, and the computer specifications. It is assumed that at least a fraction of the publications would be presenting simulations at the limit of what is feasible. For example the 1 million particle simulation presented by Iaconi et al. (2017b) was at the limit of feasibility for the OpenMP, shared memory code PHANTOM.

4.5 CE phases accessible to 3D hydrodynamic simulations

The numerical methods for 3D hydrodynamic simulations discussed here can be used to follow the dynamical part of CE interaction. This includes the initiation of CEE (perhaps only the last part of Phase (i) of our classification in Sect. 1.3, but not the complete pre-CE evolution) and the plunge in and inspiral of the companion, classified as Phase (ii).

Phase (iii), however, is characterized by different timescales involving the long τ_{KH} , which, as discussed in Sect. 3.5, differs from the dynamical timescale of the envelope of RGB and AGB stars by five orders of magnitude. The discrepancies in relevant timescales are a serious challenge to hydrodynamic simulations and it seems unlikely that the long-term CEE can be followed in 3D hydrodynamic simulations. A reasonable resolution of the objects of interest requires about 10^2 to 10^3 discretization elements (grid cells or softening lengths) per spatial dimension. Taking the dynamical timescale as a proxy for the CFL time step restriction in these discretization elements shows that covering timescales relevant for modeling Phase (iii) requires at least 10^7 to 10^8 time integration steps with hydrodynamic schemes, which makes such simulations unrealistic.

A solution to this problem would be to couple 3D hydrodynamic simulations of the inspiral phase (ii) with classical 1D stellar evolution models to describe the subsequent evolution. While the 3D simulations provide the initial conditions, mapping

them in a useful way to 1D is highly non-trivial. We discuss this problem further in Sect. 7.5.

5 Initial conditions and setups of common-envelope simulations

We now turn to the question of what hydrodynamic simulations of CEE are possible based on the physical foundations discussed in Sect. 3 and the numerical approaches described in Sects. 4.1 and 4.3 with available computational resources. We start with the construction of a sensible initial model for global 3D hydrodynamic simulations of Phase (ii) of CEE according to our classification in Sect. 1.3. This is not only difficult from a technical point of view, but we also have to ensure that such a model represents a reasonable end point of the evolution *preceding* the CE interaction, i.e. at the end of Phase (i).

The high densities in the cores of giant stars are the reason why degeneracy effects play a role in them, which cannot be described by a classical ideal-gas equation of state. Core material must be treated instead as an ideal quantum gas. This is no fundamental problem. The hard limit of what can be accommodated in simulations is set by the scale problems discussed in Sect. 3.5.

5.1 Can the stellar cores be resolved?

At the first glance, the *spatial scale discrepancy* between the radius of the core, R_{core} and the outer envelope of a giant star, R_{\star} , of about four orders of magnitude (see Sect. 3.5)—and for some special cases of early-stage giants perhaps even less—seems challenging but not impossible to represent in numerical treatments. However, a closer look quickly reveals that simulations in which these components are fully resolved are quite unrealistic. A representation of the core structures would require to resolve spatial scales at least a factor of 10 to 100 below R_{core} . Thus, a reasonable resolution of the core leads to a spatial scale difference of about 10^5 between the integral scale of the primary star and the sizes of discrete elements relevant for the CFL condition. Still, this is extremely challenging but not completely hopeless to be resolved in future simulations.

A computational domain that allows to capture the expansion of the envelope during CEE without losing material over its boundaries (which, as discussed in Sect. 4.4.1 would make it hard to track the conservation properties of the simulation) has to extend by several orders of magnitude beyond the radii of the giant stars. Covering such domains uniformly with the finest required resolution requires computational resources far beyond those of the foreseeable future. Adaptive resolution refinement as inherent to SPH methods or included in grid-based approaches via AMR techniques can alleviate the problem somewhat but not sufficiently to render fully resolved simulations a realistic option.

There is yet another, more restrictive reason why CE simulations with resolved cores are unrealistic. It arises from the *timescale problem* mentioned in Sect. 3.5. The dynamical timescale defined in Eq. (28) is the relevant quantity for estimating

the computational cost of the simulation. Generally, hydrodynamic simulations aim to follow the evolution of the modeled system over a duration close to τ_{dyn} , which therefore sets a coarse order-of-magnitude estimate for the required number of time integration steps. This argument, however, can be formalized further. As discussed in Sects. 4.1.1 and 4.1.2, the CFL condition states that numerical stability of hydrodynamic schemes in explicit time discretization necessitates discrete time integration steps smaller than the sound crossing time¹⁵ over a grid cell in grid-based discretizations, or a smoothing length in SPH. As estimated in Sect. 3.5, the dynamical timescale of the envelopes of RGB or AGB stars is about 50 days. In the cores of such stars, $\tau_{\text{dyn,core}}$ is only ≈ 20 s (see Sect. 3.5), i.e. it is lower than $\tau_{\text{dyn,envlope}}$ by five orders of magnitude. When covering the radius of the core with 100 resolution elements (grid cells or SPH smoothing lengths), the CFL condition dictates timesteps that are seven orders of magnitude smaller than the dynamical timescale of the envelope. Global CE simulations striving to resolve the core of the primary star while also following the evolution for a dynamical timescale of the envelope therefore face a temporal scale discrepancy of 10^7 , i.e. ten million numerical time integration steps are necessary to follow the system even over only one $\tau_{\text{dyn,envlope}}$. Even in the most optimistic cases with a low spatial resolution of the stellar core, the timescale difference does not reduce below five orders of magnitude. Therefore, at best for some very favorable configurations fully resolved 3D hydrodynamic simulations of CEE can possibly be attempted with future computational hardware, but this will not become a standard approach anytime soon.

Local time stepping focuses the computational resources on the stellar core—meaning that not the entire domain is evolved in each small time step. Nonetheless, the effort needed to follow the evolution of the envelope remains prohibitive. The CFL condition can be relaxed for unconditionally stable implicit time integration schemes, but such schemes are computationally costly and difficult to implement, so that they have not yet been applied to simulations of CEE. Moreover, although stability is not a concern in time-implicit schemes, accuracy of the solution is still important. If hydrodynamic flows inside the core are to be resolved, a CFL-like condition applies that replaces the sound speed with the flow speed and a substantial gain is only achieved for strongly subsonic flows.

5.2 Representing the cores of the primaries and the companions

As discussed in the previous section, the question of resolving the core of the giant star is not primarily a spatial scale problem; the limiting factor is the timescale problem introduced by the core of the primary star. Depending on its nature, one may hope to resolve the companion. While compact objects such as white dwarfs or neutron stars are too small to achieve sufficient resolution, a main sequence companion may come into reach for future simulations. Still, for a reasonably resolved sun-like companion star, the timescale discrepancy of $\sim 10^5$ remains extremely challenging.

¹⁵ The sound crossing time is sufficient for our estimate, but the actual CFL condition is more specific and refers to the hydrodynamic signal speeds.

When **CE** interactions take place between a primary star that has just initiated its expansion, and a main sequence companion, simulations may be able to represent both stars in their entirety. An example are simulations of the transient V1309 Sco, whose progenitor system is thought to have comprised a slightly enlarged ($\sim 4 R_{\odot}$) $1.5 M_{\odot}$ post-main sequence primary and a $0.15 M_{\odot}$ main sequence companion (Tylenda et al., 2011). Nandez et al. (2014) carried out a number of simulations of this system using, for some of them, a full representation of the two stars. These simulations were conducted with an **SPH** code and extremely low particle numbers of 100 000 to 200 000 for the primary star and 5000 to 20 000 for the companion. Lacking a credible convergence test, caution is required in the interpretation of the results. However, in principle one may attempt such simulations with higher resolution. This setup, however, is already at the rather blurred boundary between **CEE** and stellar mergers and may, because of the lack of a clear core-envelope structure, not completely qualify as **CE** interaction (see our discussion in Sect. 1.2). For completeness we should mention again that stellar interaction simulations with both stars fully represented are also carried out for compact objects such as white dwarfs and neutron stars, as well as for massive main sequence stars, where the two stars have comparable sizes (see Sect. 1.2 for examples). However, these interactions, which result in mergers, do not follow the same path as the **CEE** described here in that one of the stars is usually tidally shredded rather than moving into the envelope of the other.

For more standard **CE** setups, the timescale problem arising from the extremely compact nature of the core of the primary giant star remains an insurmountable obstacle to global, fully resolved simulations of well-defined **CE** interactions in the foreseeable future. There are two ways of dealing with this fundamental problem.

When **CEE** results in the survival of the binary and the ejection of the envelope, simulations should aim to accurately reproduce the core–envelope interaction, the timing and mechanism of envelope ejection and the post-ejection orbital separation of the cores. In this first case, the stellar cores are largely unaffected by the inspiral. Resolving their internal structure is therefore less important than a precise representation of the envelope of the primary star that later becomes the common envelope. It is therefore common practice to replace the cores by a simple model while trying to capture the physics of the envelope on the simulation domain. This is usually achieved by substituting the core of the primary star and also the companion with *point particles* that interact mutually and with the envelope gas only via gravity. In this context, such point masses are often referred to as *core particles*. The main drawback of this approach is that only the gravitational interaction of the cores with the envelope is modeled and any hydrodynamic interaction, such as accretion, expansion, evaporation, and jet formation is ignored. Yet such phenomena may strongly affect the envelope gas. Therefore, subgrid-scale models have been employed to represent them in global **CE** simulations (e.g. Chamandy et al., 2018; Zou et al., 2022).

If, however, the evolution of the large envelope is not the primary interest of the simulation, a second option is to follow inner parts of the system with resolved cores. This may apply to systems where additional simulations capturing the envelope or other considerations lead to the conclusion that envelope ejection fails and a merger of the cores or an evaporation of the companion is the focus.

A clear core–envelope structure of the primary star is a prerequisite for replacing its core by a point particle. But an exact definition of a sharp core–envelope boundary is difficult to give. Depending on the evolutionary stage of the giant and the mass of the star, the boundary may be set according to different parameters. Supergiant stars usually have a less clearly defined core–envelope structure than RGB or AGB stars. From a stellar evolution point of view, chemical composition may provide a useful discrimination: the core may have undergone nuclear burning and the mass fractions of the corresponding “ashes” could be used to indicate the core–envelope boundary. Shell burning, however, leads to ambiguities. For the CE dynamics, it would be more useful to determine the point down to which the envelope material has to be removed so that the remaining bound objects does not re-expand, i.e. the bifurcation point (see Sect. 2.1).

The strategy of a simplified representation of the cores has been implemented in various ways. In SPH simulations, a definition of a core particle is rather straightforward because the envelope material is also discretized as particles.

Grid-based approaches, in contrast, require somewhat more thought. One option here is to plainly ignore the problem when mapping the stellar structure from the initial 1D model to the hydrodynamic computational domain. Such setups do not use core particles. The core of the primary star is simply taken to be part of the central grid cell that comprises the stellar core and some envelope material. In principle, mass flows into and out of this central cell are possible. The density in the central cell containing the core is bound to be high, but its value depends on the spatial resolution. This rather ambiguous and resolution-dependent representation of the stellar core makes convergence studies difficult and must therefore be discarded in modern 3D hydrodynamic simulations of CEE.

The introduction of a core particle alone, however, does not solve the problem satisfactorily straight away. It introduces two ways of treating stellar material—a particle modeling the core and a grid-based discretization of the envelope. These need to be defined and coupled in a physically consistent way. A naïve approach that simply assigns the mass of the stellar core to the particle leaves a resolution-dependent amount of envelope material in the central grid cell. This high-density material is usually not sufficiently resolved to guarantee a correct treatment of core–envelope interaction. Leaving the envelope profile unaltered, as was common practice in many simulations of dynamical inspiral in CEE, leads to perturbations of the HSE in the envelope structure of the primary star and generates spurious velocities. As a resolution-dependent model, numerical convergence of the results of CE simulations is hard to establish with such a setup.

For this reason, Ohlmann et al. (2017) proposed a procedure to cut the original stellar profile (that in practical simulations often results from preceding 1D stellar evolution calculations) at a certain chosen radius into a thus defined “core” and an “envelope”. The “core” is then represented by the core particle and the “envelope” is constructed on the grid in a way that preserves its expected HSE according to Eq. (24) before the onset of CE interaction. The hydrostatic stratification of the gas discretized on the grid is reconstructed with a modified Lane–Emden equation (Ohlmann et al., 2017). In contrast to the original Lane–Emden equation for polytropic stellar models (see, e.g., Kippenhahn et al., 2012), it includes the gravitational force $g_{\text{core}}(r)$ due to

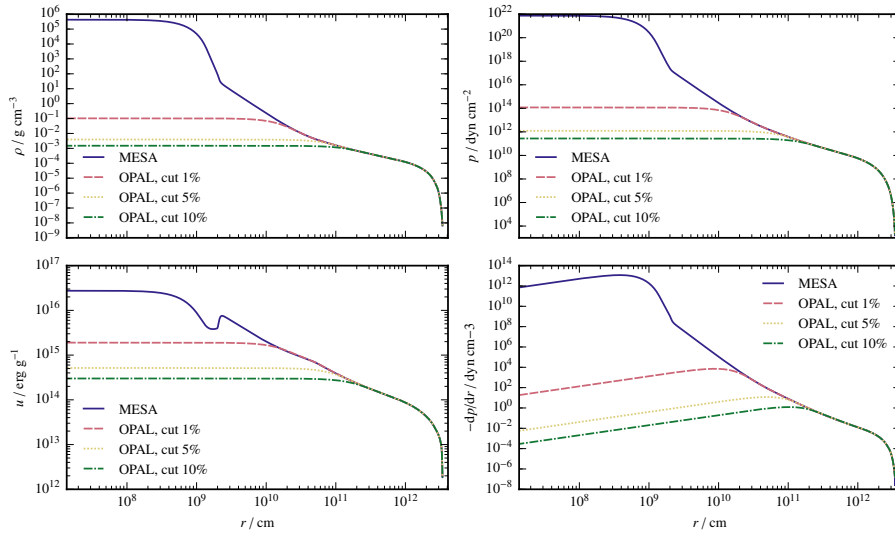


Fig. 11 Radial profiles of density (top left), internal energy (bottom left), pressure (top right), and derivative of pressure (bottom right) of an original MESA model for a $2 M_{\odot}$ RGB star with reconstructed profiles (“OPAL”), in which the cores were cut out at the indicated percentage of the total stellar radius. Figure from [Ohlmann et al. \(2017\)](#).

the core particle as a function of radius r in addition to self-gravity of the envelope gas:

$$\frac{1}{r^2} \frac{d}{dr} \left[\frac{r^2}{4\pi G \rho} \frac{dP}{dr} + \frac{r^2 g_{\text{core}}(r)}{4\pi G} \right] + \rho = 0 \quad (37)$$

This procedure provides a reliable and resolution-independent reconstruction of the envelope profiles (see Fig. 11). The important parameter of this setup model is the cut radius below which material is assigned to the core and represented by a particle. This radius is chosen according to physical considerations and numerical necessities. As discussed in 5.1, a resolved physical core would act as a time sink in numerical simulations and this is also true for the higher-density regions around the core. Resolving the bifurcation point on the grid would be desirable, but it often is located in high-density material. Extending the correct envelope gas representation to this point can result in unacceptable computational costs and compromises are made. According to Eq. (37), the core particle is still embedded in gas within the cut radius, but its density profile does not provide a realistic representation of the envelope close to the core. In fact, depending on the choice of the cut radius, some envelope material is absorbed in the core particle. Despite these deficiencies, the setup procedure of [Ohlmann et al. \(2017\)](#) provides a well-controlled setup with a clearly-defined, if not entirely astrophysical core–envelope boundary. This has not been the case in many other setups employed before.

SPH based setups for CE simulations face a similar problem. The envelope gas represented by SPH particles in the vicinity of the distinct (gravitation-only) core particles and within their gravitational softening radii is not necessarily in HSE when they are placed randomly. To ensure equilibrium, a distribution of SPH particles in

this region can be chosen that represents a density profile according to Eq. (37). Whether or not such a structure captures a realistic core–envelope transition has to be tested and may depend on the number of SPH particles as well as on the value of the softening length (Reichardt et al., 2020).

Although the fluid-dynamical treatment of the core material is discarded for efficiency reasons, it is important to capture the gravitational effects of the cores as precisely as possible. In a fully particle-based implementation in the framework of SPH this is relatively simple; the numerical treatment of self-gravity derives from N -body simulations and is well-suited to deal with the problem. When combining a grid-based discretization of the envelope gas with a particle representation of the cores, however, the treatment of self-gravity is less obvious. One option is to model the gravitational interaction of the gas cells in a particle-based approach, such as using the tree method (see Sect. 4.3.1). To alleviate the inherent asymmetries of tree methods, a direct summation of the contributions to gravitational forces from the core particles is possible. Calculating the gravitational interaction between the core particles and between core particles and gas cells exactly adds a tolerable computational overhead only as long as the gravitational interaction of the many gas cells is treated in an approximate $O(N \log N)$ approach. This is implemented for instance in the moving-mesh CE simulations of Ohlmann et al. (2016a).

A full, grid-based treatment of gravity employing Fast Fourier techniques or multigrid methods (see Sect. 4.3.2), in turn, requires to map the masses of core particles onto the grid, for instance with a cloud-in-cell algorithm (Taam and Ricker, 2006). To avoid force anisotropies, a large number of particles moving rigidly together can be chosen to represent the cores (Ricker and Taam, 2008, use 10^5 particles per core).

The approach of replacing the cores by point masses naturally removes the timescale problem. It seems, however, likely that future generations 3D hydrodynamic CEE simulations will strive to improve the representation of the cores. Even if resolving them spatially remains out of reach, subgrid-scale models may help to refine the implementation of physical properties of the cores and associated effects such as hydrodynamic friction, mass accretion, or evaporation.

5.3 Setting up the primary star in hydrostatic equilibrium

The first step in simulating CEE is to set up a model for the primary star. This step requires some diligence. Although reaching envelope ejection in CE simulations remains a challenge, primary stars are giants and have rather loosely bound envelopes. It is far from trivial to keep them stable over many dynamical timescales in 3D hydrodynamic simulations.

Usually, the initial model for the primary star is obtained from a 1D stellar evolution calculation. Such calculations and their results differ in many aspects from the representations of stars in multidimensional hydrodynamic treatments. Two of them are of particular significance when mapping models of primary stars into CE simulations. (1) Due to their 1D nature, stellar evolution calculations can afford much higher resolutions in spatial or mass coordinates. This is additionally supported by

the common choice of a Lagrangian frame of reference. (2) Classical **1D** models are constructed under the assumption of a mechanical equilibrium in the stellar structure.

Aspect (1) directly links to the question of how to geometrically place the discretization elements in the different **3D** hydrodynamic approaches. Adapting the geometry of the discretization scheme to the shape of the simulated system becomes increasingly important with lower spatial resolution. While observing the overall spherical symmetry of a stellar model, spherical grids are plagued by their axial and central coordinate singularities and are ill-suited for the later simulation of the binary system evolution. In contrast, the geometry of Cartesian meshes is not adapted to the spherical symmetry of the stellar model and their spatial resolution is anisotropic with preferred axis directions. Adaptive mesh refinement techniques can alleviate the geometry problems somewhat.

Particle-based discretizations follow the mass distribution inside the envelope by construction and may therefore provide poor spatial resolution at certain locations (most obviously near the stellar surface). Still, the mesh-free approach of **SPH** and moving-mesh discretizations of hydrodynamics automatically adapt to the geometric properties of the simulated object as it evolves. This advantage, however, comes at a price to pay at the initial setup: unstructured moving meshes and random placements of particles in **SPH** lack any symmetry. Mapping a spherical stellar model onto them introduces noise resulting in spurious velocities in the material. [Ohlmann et al. \(2017\)](#) tested a variety of grid structures for placing the discretization elements in the initial setup—a regular cubic grid, a nested cubic grid, an adaptive cubic grid, and a grid based on a HEALPix tessellation ([Górski et al., 2005](#); [Pakmor et al., 2012](#)). For reasons discussed below, however, they found that the initial grid geometry has little effect on the simulation results.

Aspect (2) is related to the problem of ensuring **HSE** in hydrodynamic simulations. Except for the explosive termination phases, stellar structures remain very close to **HSE** throughout the evolution of the star. This, to good approximation, should hold true for the envelope of the primary star at the onset of **CEE**. Simulations of the dynamic inspiral phase aim to determine the response of the **CE** to the perturbations caused by the orbiting stellar cores. A key requirement for this is that the employed numerical model is able to maintain **HSE** in the unperturbed envelope—any change in the envelope structure should originate from the core inspiral and not from numerical errors. This is challenging because, in contrast to the classical stellar structure calculations providing the initial model for the primary star, **HSE** is not explicit at the level of the fundamental equations in a hydrodynamic model. It rather constitutes a special solution and there is no guarantee that the delicate balance between pressure gradient and gravity in the loosely bound envelope of a giant star is maintained over many dynamical timescales by the approximate numerical schemes. Moreover, the goal is not to force the setup into some arbitrary **HSE** configuration but to reproduce the original stellar model as exactly as possible in the multidimensional hydrodynamic simulation.

To enable the correct **HSE** in the numerical model, the gravitational force as well as counteracting pressure gradient should be reproduced accurately. Since both effects

are discretized independently (see Sects. 4.1 and 4.3), there is little hope for errors to cancel reliably¹⁶.

A minimal requirement for global stability of the stellar model is a sufficiently precise numerical representation of the pressure gradient. To this end, a pressure scale height should be resolved by a certain number of discrete elements (grid cells or particles). Depending on the discretization approach, this can be a difficult task. For finite-volume hydrodynamic schemes, it is possible to estimate the resolution required in order to keep the Mach number of spurious velocities below a certain threshold (Zingale et al., 2002). The result depends on the chosen scheme and the order of reconstruction, but generally a resolution of several cells per pressure scale height is required for reasonably low velocity perturbations. For the solver implemented in the AREPO code, Ohlmann et al. (2017) estimated the Mach number of velocity fluctuations when resolving a pressure scale height H_p with a grid spacing Δ to be

$$Ma = \frac{C_{\text{CFL}}}{12\gamma} \left(\frac{\Delta}{H_p} \right)^3 + \mathcal{O} \left[\left(\frac{\Delta}{H_p} \right)^4 \right], \quad (38)$$

where $C_{\text{CFL}} < 1$ is the fudge factor introduced into the necessary but not sufficient CFL criterion to stabilize the scheme and γ is the adiabatic index of the gas. To stabilize the hydrostatic stratification with this scheme assuming $\gamma = 5/3$ and $C_{\text{CFL}} = 0.4$ down to a Mach number of 10^{-2} , one pressure scale height must be resolved with more than three cells (Ohlmann et al., 2017).

Particular problems arise near the core of the giant star and at its surface, where the pressure gradients are steep. Here, adaptive mesh refinement techniques can help to alleviate the resulting computational costs. Ohlmann et al. (2016a) found that HSE can be maintained only when retaining a certain number of grid cells inside the softening length around the core particle of the primary star model. The rather steep density gradient has to be sufficiently resolved. A universal criterion for the necessary resolution, however, is difficult to establish as it is expected to not only depend on the parameters of the star but also on the numerical methods and their implementation (e.g. the order of spatial reconstruction). Sand et al. (2020), for example, found that a higher resolution is required in the case of AGB primary stars as compared with the RG models of Ohlmann et al. (2016a).

Reaching a sufficient resolution of the pressure gradient near the surface of the star is a harder task because of the even steeper pressure gradient encountered here. It turns out, however, that this is less critical for the overall stability of the modeled stellar envelope than resolving the region around the core. Small departures from equilibrium are often tolerable because they only lead to a slight expansion of the very outer stellar layers that contain little material. Insufficient resolution of the outer layers, and a correspondingly large mass loss over the surface, however, may cause a progressive dilution of the inner parts of the star. Moreover, similar to the problems noted by Galaviz et al. (2017), the lost material may affect the prediction of the color and the lightcurve of the simulated CE event.

¹⁶ There is a special class of numerical schemes—so-called *well-balancing methods*—that aim at ensuring HSE in hydrodynamic codes (see, e.g., Edelmann et al., 2021), but these have not yet been employed to CE simulations.

In low-resolution **CE** simulations with grid codes, a practical way to stabilize the surface of the primary star is to impose a high temperature in the pseudo-vacuum embedding the star such that it is in pressure equilibrium with the surface layers (e.g., Sandquist et al., 1998; Passy et al., 2012; Chamandy et al., 2018). This, however, may lead to problems with predicting observables from **CE** simulations, because the artificially hot pseudo-vacuum prevents a useful estimate of a photospheric temperature (Galaviz et al., 2017). By construction, **SPH** codes have low resolution in the low density regions of the surface. However, they tend to retain the stellar shape without the addition of a hot pseudo-vacuum. In **SPH** schemes, hydrodynamic quantities and their gradients are computed by summing over contributions from a certain set of neighboring particles. At the surface of an object, this leads to a one-sided evaluation of properties that can cause an artificial “surface tension” (e.g. Springel, 2010b). On the one hand, this may help to prevent the slow leakage of low-density material. On the other hand, however, the artificial surface tension may affect the modeling of the phase directly preceding the plunge-in of the companion into the envelope.

A careful preparation of the **3D** stellar model involves not only the mapping from the original **1D** structure but in addition it requires a damping to ensure initial **HSE** in the discretized structure. In particular, the arbitrary initial placement of the grid-generating points in moving-mesh hydrodynamics schemes and of the particles in **SPH** requires care to not disturb local **HSE** conditions, which would lead to spurious velocities in the envelope of the primary star. But also Eulerian grid-based simulations should be damped to **HSE** because of the change in resolution in the mapping process. The damping can be implemented as an artificial friction term (Rosswog et al., 2004; Pakmor et al., 2012) proportional to

$$\dot{\mathbf{v}} = -\frac{1}{\tau}\mathbf{v}, \quad (39)$$

where τ is the timescale over which the velocities are damped. Following Pakmor et al. (2012), Ohlmann et al. (2017) perform the damping with a constant τ over several dynamical timescales of the object, reduce the damping over a certain period and then follow the undamped evolution over some dynamical timescales to ensure stability of the obtained configurations, see Fig. 12. The necessary damping step is the reason why the choice of the initial grid geometry is unimportant as long as it provides a reasonable representation of the structure: The adaptive moving mesh or the positions of the **SPH** particles adjust themselves in the damping process and attain a structure that is largely independent of the initial choice. The purpose of the relaxation step is to approach the lower limit for the Mach numbers of spurious motions implied by criteria such as Eq. (38). Similar damping procedures have been applied successfully for many years, starting with (Ricker and Taam, 2008) and they are used time and again from Passy et al. (2012) to Ohlmann et al. (2017), Chamandy et al. (2018), and Prust and Chang (2019).

An additional problem arises when a correct representation of the thermal structure of the **1D** stellar model in the hydrodynamic simulation setup is intended. This usually implies the need to use exactly the same equation of state in both the stellar evolution code providing the **1D** model and in the hydrodynamic code. With minimal

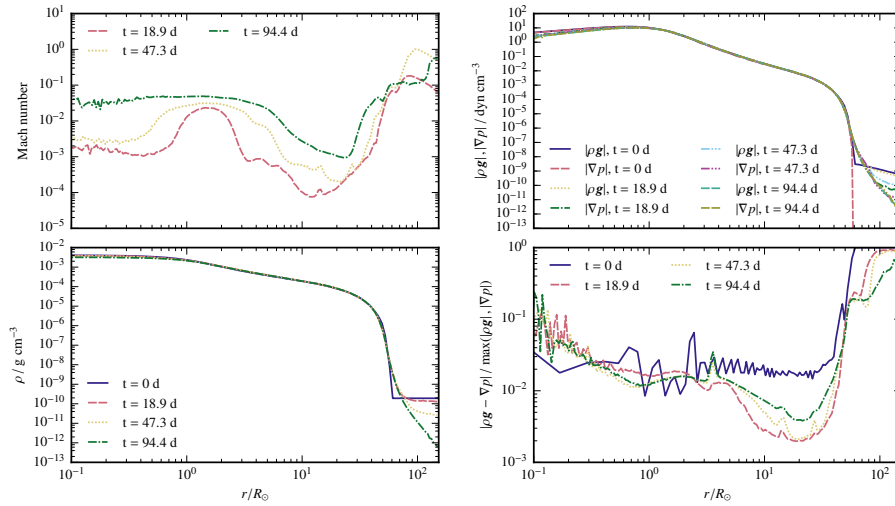


Fig. 12 Relaxation of the setup model shown in Fig. 11. Shown are the radial profiles of the Mach number (top left), the density (bottom left), the two terms in the equation of HSE (24) (top right) and the relative error in HSE for different times during the relaxation procedure. The density profile is well-preserved and the deviation from HSE is at the percent level within the stellar structure (but not in the pseudo-vacuum embedding it). The Mach number increases but stays reasonably low inside the stellar envelope. Figures from Ohlmann et al. (2017).

changes in the hydrodynamical structure, however, it is possible to preserve the correct convective properties of the envelope when using the setup procedure proposed by Ohlmann et al. (2017) based on Edelmann et al. (2017).

Ohlmann et al. (2017) list five quality criteria for the representation of primary stars in 3D hydrodynamic CE simulations:

1. Correct representation of the mechanical structure: deviations from the original 1D model in the pressure and density profiles should be small.
2. Correct representation of the HSE: the difference between both sides of Eq. (24) should be small.
3. The Mach numbers in the envelope of the primary star model should be small compared to the Mach numbers expected in the later CE evolution.
4. Correct thermal structure of the envelope: if the convective structure of the primary star is retained in the mapping and relaxation procedures, a stationary state of convection should be reached in the model.
5. Stability against large-scale oscillations: If the original primary star is not pulsating, the potential energy of the model should be constant.

These criteria should be checked carefully before adding a companion and starting the actual CE simulation. Again, we advocate to perform such tests as a standard procedure when performing CE simulations and to document the results in the related publications.

5.4 Setting up the binary system

After setting up a primary star model and checking its stability, a companion is added. This requires to choose the parameters of the progenitor system, such as the initial orbital separation, the spin of the two stars, and the eccentricity of the orbit. Physically, these parameters are determined by the evolution of the progenitor binary system and set by choosing the time at which the simulation of this system is started. From this point of view, initializing the actual CE simulation as early as possible seems advisable in order to capture the formation of the CE correctly. The pre-CE evolution, however, takes place on timescales that are not easily accessible to 3D hydrodynamic models (see Sects. 3.6 and 4.5). Therefore, an initial condition for the binary evolution must be constructed that reproduces an expected structure at a certain stage of the pre-CE evolution. Starting at the onset of Roche lobe overflow appears to be a natural choice: The initial system is set up at the time when the primary, with radius R_\star , just fills its Roche lobe, whose radius, r_\star^{Roche} , can be approximated by

$$R_\star = r_\star^{\text{Roche}} = a \frac{0.49 q^{2/3}}{0.6 q^{2/3} + \ln(1 + q^{1/3})}, \quad (40)$$

where $q = M_\star/M_{\text{comp}}$ is the mass ratio of the primary star to the companion (Eggleton, 1983). This determines the initial orbital separation, a .

We could ask whether starting the simulation at onset of Roche lobe overflow, as, e.g., in Rasio and Livio (1996) and Nandez et al. (2014), is actually necessary. After all, we do not know whether the simulations capture correctly the transition between stable Roche lobe overflow and the onset of instability and inspiral. Following this argument, the choice for the starting point of 3D hydrodynamic CE simulations is often made according to practical considerations. A too large initial separation makes the simulations very expensive. Many orbits of the binary have to be followed from before the onset of mass transfer until the actual plunge-in of the companion into the envelope of the primary. This is possible provided that the employed hydrodynamics scheme preserves angular momentum well, which, of course, is desirable. With this, we face the paradoxical situation that the better the codes reproduce physical conservation laws, the more expensive the simulations become. As a compromise, many simulations position the companion near the surface of the primary (e.g., Sandquist et al., 1998; Ohlmann et al., 2016a). The companion could even be initially placed inside the envelope—a choice motivated with the argument that there is very little binding energy in the outer layers (Law-Smith et al., 2020). The danger with this approach is that a simple binding energy argument is insufficient. The inspiral is a dynamical process driven by the drag force. Therefore, an extreme choice may select an orbital separation of the initial core binary system that seems energetically plausible but is never reached in the actual dynamical evolution because the envelope is lifted earlier and the drag force vanishes.

Placing the companion close to the primary star—be it at Roche lobe filling distance or closer—raises the question of how to define a consistent setup configuration. It implies that early tidal effects are missed. For a late initiation of the simulation, the primary star cannot be assumed to be spherical, but many simulations start out with

exactly this assumption. From a practical point of view, a spherical setup of the primary star has the advantage that sufficient stability of its envelope can be guaranteed, e.g. by the procedures described in Sect. 5.3. This allows to separate physical effects during the CE evolution from numerical artifacts, which would be more difficult to ensure in a binary setup. Therefore, the assumption of a spherical primary star gives rise to numerically well-defined initial conditions for CE simulations. Still, concerns remain as to whether this is a physically valid approach.

There are methods that allow to initiate the binary with a separation larger than Roche lobe contact and to follow the evolution in a numerically efficient way. After creating a stable model of a spherical primary star as in Sect. 5.3, another step is taken before simulating the plunge-in of the companion. This intermediate step aims at relaxing the envelope of the primary star into the potential of the binary system close to the onset of mass transfer. For white dwarf merger simulations, such a procedure has been suggested by Dan et al. (2011). The idea is to place the spherical stellar models in orbit with a companion at an orbital separation large enough that the tidal interaction is negligible. The computational cost of following the slow inspiral due to gravitational wave emission is prohibitive. To speed up the orbital evolution, the distance is artificially decreased on a timescale that is substantially longer than the dynamical timescale of the stars. This allows the stellar structures to adapt to the changing potential. Such initial models, however, are not common in CE simulations yet. Retaining force balance in the loosely bound envelopes of giant stars is more challenging than in the compact structures of white dwarfs.

Even agreeing to start all simulations at the time of Roche lobe overflow, we next would need to decide on the rotation of the interacting stellar objects. Since the companion and the core of the primary star have to be treated as point particles (see Sect. 5.2), this question boils down to the rotation of the envelope of the primary. The general idea of the onset of CEE is a loss of co-rotation between the orbit of the binary companion and the envelope of the primary. This triggers the inspiral, because for the drag force to act, a non-vanishing relative velocity between the companion and the envelope material is necessary. It remains unclear, however, how much co-rotation is to be expected in the epoch the simulation is initialized (provided, of course, that this initialization reflects a physical evolution stage in the first place). Moreover, not all progenitor systems may reach full co-rotation before entering CEE. In simulations, anything between full co-rotation and a non-rotating primary star has been used. It may be surprising that even full co-rotation leads to inspiral, but this is due to non-relaxed initial conditions in the binary potential which quickly re-arrange the density distributions so that tidal forces can act.

The issue of primary-star rotation and the extent of primary–orbit co-rotation goes hand in hand with the issue of stabilization of the binary in a certain rotating configuration. While the primary is always stabilized as a single star in the inertial frame (see Sect. 5.3), some simulations also stabilize the binary in the rotating frame (Rasio and Livio, 1996). Nandez et al. (2014) and following papers stabilize the binary in the corotating frame using the method of Lombardi et al. (2011), but such a method is not universally adopted by all simulations. Reichardt et al. (2019) evolved a Roche lobe contact system in the rotating frame, but like Sandquist et al. (1998), they did not

stabilize the binary in that frame, effectively spinning up a star that was in equilibrium only when non-rotating.

An additional, dynamically important but poorly constrained parameter is the initial eccentricity of the system. Many simulations assume circularization of the orbit prior to the onset of CEE, and this is also supported by simulations (MacLeod et al., 2022), but cases with eccentric initial orbits have also been considered in numerical simulations (Staff et al., 2016a; Glanz and Perets, 2021a). Eccentric post-CE binaries are observed and may result from pre-existing eccentricity or generation of eccentricity during the CE interaction. In simulations with the companion initialized in a spherical orbit close to the edge of the primary star, the generation of substantial eccentricity in the plunge-in is indeed observed.

Our discussion in the previous sections indicates that the setup of CE simulations is a very delicate issue. Unlike the inspiral phase of CE interaction, the prospects for 3D hydrodynamic simulations of large parts of the pre-CE evolution are discouraging, leaving us with rather arbitrary choices of initial system parameters. This unsatisfactory situation calls for careful testing of the impact these parameters have on the results. The studies carried out thus far indicate some, but surprisingly little impact of the initial separation and even the rotation of the primary star on the final orbital separation (Sandquist et al., 1998; Iaconi et al., 2017b; Prust and Chang, 2019). This, however, may depend on secondary parameters, such as the mass and evolutionary stage of the giant star and the mass of the companion. More extended parameter studies are required to settle the impact of the choice of initial parameters on the final orbital separation, but also on the mass and morphology of ejected envelope material.

6 Multidimensional hydrodynamic simulations

For reasons given in Sects. 3, 4 and 5, only certain stages of CEE are accessible to 3D hydrodynamic modeling. Although all phases are methodologically challenging, the dynamical inspiral, Phase (ii) of our classification in Sect. 1.3, is out of reach for classical approaches to stellar evolution modeling. Yet, it is perhaps the most critical phase for the fate of the system. Progress in binary stellar evolution fundamentally depends on a detailed understanding of this phase. We argue that only 3D hydrodynamic simulations provide the required realism and predictive power to solve this problem.

In this section, we review simulations pertaining to parts of the pre-CE evolution of the progenitor system, the dynamical CE interaction in the plunge-in phase, and a few tens to hundreds of orbits afterwards. These have been carried out over the past decades by several groups. In contrast to the previous sections, where we discussed general aspects of CE simulations and expressed our own view on the approaches taken, we here summarize the findings reported by the respective authors of the studies. The interpretations and conclusions drawn are often complementary, but occasionally also contradictory. This is an unavoidable consequence of the historical development of the field, which we intend to convey from a neutral perspective. We therefore try to hold back our own views.

6.1 Simulations of the pre-dynamical inspiral phase and the onset of CE interaction

Until recently, work on the pre-CE evolution was mostly carried out based on analytical models, stellar evolution calculations or binary population synthesis tools. We have briefly discussed some important aspects of the pre-CE interaction in Sect. 3.6 and refer the reader to Chapter 6 of [Ivanova et al. \(2013\)](#) for a more comprehensive review. A broader scope of modeling binary interactions, both with 1D stellar evolution approaches and with multidimensional hydrodynamic methods, is covered in the review of [De Marco and Izzard \(2017\)](#). Here, we restrict our discussion to the few available multidimensional, hydrodynamic models that pertain to the onset of CEE.

There is no doubt that the physical parameters of the binary system together with the nature and evolutionary stage of the primary star and the companion determine its fate in and after the CE phase. But still we lack a comprehensive understanding of which systems achieve successful envelope ejections leaving behind a compact binary and which of them end up in a merger of the cores. It is expected that this is determined by the physical initial conditions and the many resulting processes that lead to the onset of CEE discussed in Sect. 3.6. As mentioned there, there is little hope to capture this complex phase comprehensively in 3D hydrodynamic simulations, but a few attempts exist.

[Pejcha et al. \(2016b\)](#) and [Pejcha et al. \(2016a\)](#) carried out 3D, SPH-based radiation-hydrodynamic simulations aimed at understanding the pre-merger phase of the transient V1309 Sco ([Tylenda et al., 2011](#)). This is now established to have been the merger of a slightly enlarged, $\sim 1.5 M_{\odot}$ main sequence or sub-giant primary star and its much less massive main sequence companion. As discussed in Sect. 1.2, this configuration does not qualify as a show-case example of a CE system, but is rather at the blurry interface between CEE and classical stellar mergers. Nonetheless, the similarity of this system and the less extreme spatial scale challenges render it a suitable example to test some models with numerical simulations and comparisons to observations. The simulations of [Pejcha et al. \(2016b\)](#) and [Pejcha et al. \(2016a\)](#) modelled a very specific process: the mass loss of the interacting binary system from the outer Lagrange point L_2 and its observational consequences.

SPH was coupled to a simplified treatment of radiation that splits the process into flux-limited diffusion of radiation energy, radiative cooling in the direction perpendicular to the orbital plane, and—only in [Pejcha et al. \(2016b\)](#)—irradiation of the gas from the central binary. A suitable equation of state was used to account for the ionization structure of the gas. The setup of [Pejcha et al. \(2016b\)](#) consisted of a central binary with a mass ratio between 0.06 and 0.8, modeled only including the mutual gravitational force of the stars, but with no back-reaction of the gas flow on the binary orbit. The SPH particles representing the gas component were injected directly at the L_2 Lagrange point of the binary system allowing one to follow the structure of the outflow, which was not self-consistently modeled in the hydrodynamic simulation but assumed in the setup. The spiral arms generated by the outflow overlapped and merged at a certain distance from the binary, which is of interest for observing the corresponding system. Shock waves thermalized and about 10% to 20% of the radial kinetic energy of the outflow was converted to thermal energy. Depending on

the system parameters, some of this energy was radiated away, diffused or generated adiabatic expansion of the gas and dominated the resulting luminosity. Conditions for dust formation were found to prevail in the ejected material. The temperatures and luminosities detected in the simulations of Pejcha et al. (2016b) matched observations of LRN in order of magnitude, but because the model did not follow the dynamical evolution of the binary itself, lightcurves could not be reproduced.

Pejcha et al. (2016a) extended the study to other mass ratios of the binary system and found outflows of unbound material from L_2 if the thermal content of the ejecta was sufficiently high, i.e., the ratio between the sound speed and the orbital velocity at the injection point was large. On the other hand, cold outflows outside the mass ratio range determined in Pejcha et al. (2016b) remained marginally bound. A rich phenomenology was observed in the simulations. Again, the expected optical emission from the implied processes was found to explain prolonged activity of systems due to L_2 mass loss before the peak of the emission was reached in the actual merger event. Informed by the radiation-SPH simulations of Pejcha et al. (2016a,b), Metzger and Pejcha (2017) proposed that the interaction of material ejected in the dynamical stellar merger or CE event with the previous outflow generates a shock that contributes to powering the lightcurves of LRNe. This was suggested to explain typically observed double peaks.

Pejcha et al. (2016b,a) assumed an outflow over an outer Lagrange point and studied its implications in their simulations, but they did not model the dynamics of the binary system itself. Although they focused on the pre-CE evolution, they did not attempt to model how the system enters CEE, nor the impact of the simulated phase on the following inspiral.

This was addressed for the first time by MacLeod et al. (2018b)¹⁷, who studied the evolution from the onset of mass transfer towards the formation of a CE in a system comprising an evolved primary star and a lower-mass companion. Their choice of parameters ensured that mass transfer reduces the binary separation initiating unstable mass transfer. To simulate the hydrodynamic evolution in 3D, MacLeod et al. (2018b) employed the Eulerian MHD code ATHENA++ (Stone et al., 2020), but without accounting for the evolution of magnetic fields. The spherical polar mesh was uniformly spaced in angular directions, with the spacing growing logarithmically with radius. Two nested levels of static grid refinement were prescribed around the binary orbital plane. The giant star’s envelope was constructed as a polytrope. Both the core of the primary star and the companion were modeled as point masses. Following the details of mass transfer required meticulous preparation of the initial model for the 3D hydrodynamic simulation. The envelope of the primary was relaxed damping out spurious velocities to ensure numerical HSE. The gravitational force of the companion was slowly turned on to allow the structure to adapt to its presence. At Roche-radius separation, mass transfer commenced in an unstable mode with an increasing rate so that the orbit of the binary core system eventually experienced runaway decay. A fit to the loss rates of mass and angular momentum was provided that allows for an analytic description of the orbital evolution. The morphology of the gas outflow was

¹⁷ Stellar mergers in other contexts have been studied in numerical simulations before. Motl et al. (2017) give an overview and discuss differences in the evolution when simulating mass transfer and mergers between white dwarf stars in different approaches.

observed to change during the evolution: initially a thin stream of high-entropy gas was launched from the L_2 and L_3 Lagrange points, which later developed into a broad fan of gas ejected on ballistic trajectories. The origin of the transition between the two modes was identified as desynchronization of the orbital motion with the rotation of the donor star’s envelope. [MacLeod et al. \(2018a\)](#) interpreted their results in terms of observational features with particular emphasis on the formation of bipolar structures observed in remnants of stellar coalescences. While it is not the only path to binary coalescence and systems with mass ratios close to unity may evolve differently, their simulation captured an important case for the formation of a **CE**.

The case of “grazing envelope evolution” impeding or even preventing the onset of **CEE** (see Sect. 3.6) was simulated by [Shiber et al. \(2017\)](#) and [Shiber and Soker \(2018\)](#) who prepared a model of a $3.4 M_{\odot}$ **AGB** star of radius $\sim 215 R_{\odot}$ in the **MESA** code and mapped it into the **FLASH** code ([Fryxell et al., 2000](#)) on a uniform Cartesian grid and assumed an ideal gas equation of state. The inner third of the radius was replaced with a constant density sphere. Gravity was modeled as constant, temporal evolution of the gravitational field and the effect of the companion star were ignored. A low-mass main sequence companion star was initialized on a Keplerian orbit at various radii. This radius was kept constant by [Shiber et al. \(2017\)](#) while [Shiber and Soker \(2018\)](#) allowed for inspiral to a two thirds of the initial radius of the primary star at a prescribed rate inspired by **CE** simulations. At the location of the companion, a bipolar jet was put in perpendicular to the orbital plane with a mass injection rate motivated by a **BHL** formalism and a prescribed opening angle and velocity. [Shiber et al. \(2017\)](#) observed a complicated flow morphology and an efficient removal of material due to jet action. [Shiber and Soker \(2018\)](#) concluded that the grazing envelope evolution may substantially delay or even prevent an inspiralling of the companion.

Simulations trying to model the processes leading to the formation of a **CE** system have to be distinguished from the conditions in which multidimensional hydrodynamic simulations are initialized, which are often chosen for practical and numerical reasons instead of a stringent physical motivation (see Sect. 5.4). Is this a fundamental problem for the credibility of current **CE** simulations? A look into the currently available simulations and even semi-analytical descriptions suggests that the ability of the system to eject the envelope ultimately deciding between the formation of a compact binary remnant or a merger of the cores is less sensitive than one might expect to the initial conditions of the simulation, such as the degree of co-rotation and the initial distance of the companion from the primary star when setting up global simulations of **CEE**. Some impact of these parameters, however, is recorded. For example, the exact value of the final orbital separation ([Iaconi et al., 2017b](#)) and the rate of orbital decay, do depend on the degree of co-rotation and the initial orbital angular momentum. The extent of these dependencies and whether there are large differences for different systems is not yet established.

Following [Iaconi et al. \(2018\)](#), [Reichardt et al. \(2019\)](#) carried out full **CE** interaction simulations starting at the time of Roche lobe overflow¹⁸. They tested the sensitivity of the outcome of the simulations to the conditions at the start of the inter-

¹⁸ Simulations of the early **CE** phases starting out with unstable mass transfer were already conducted by [Rasio and Livio \(1996\)](#), see Sect. 6.3.3.

action. The mass transfer (though Lagrange point L_1) and mass loss (though L_2 and L_3) rates were found to be lower for higher resolution and for simulations that were carried out in the corotating frame, while the time before inspiral was longer. As a result, the mass lost before the inspiral was relatively insensitive to numerical conditions. The outcome of the simulations compared to similar ones that did not model the pre-CE inspiral led to the conclusion that the clearest difference is the shape of the expanded and ejected CE, which was found to be more symmetric in simulations that model the pre-inspiral thanks to the interaction with the disk of material formed during the early mass loss. However, it is likely that these conclusions only pertain to the chosen parameter set and cannot be generalized. This leaves us with the question of Sect. 5.4: how should we setup the simulation? Clearly, more work has to be devoted to the onset of CEE and its impact on the processes in the inspiral phase.

6.2 Simulations of the companion–envelope interaction

One of the fundamental questions of CEE is how the companion star interacts with the envelope gas as it passes through it. This question was already addressed in the earliest models of CE phases in binary stellar evolution, that were carried out in 1D in the framework of classical stellar evolution calculations, see Sect. 2.2. The inspiral of the companion was attributed to the action of a hydrodynamical or tidal drag force and analytic approximations (see Sect. 2.2.1) were employed to implement this interaction into CE simulations (Sect. 2.2.2).

The simplistic approximate 1D view on the interaction in CEE, however, diminishes the predictive power of the simulations. Effects that are not or only approximately captured in the basic formalism include density gradients in the envelope, asymmetries, nonlinearities, and the simple fact that not only the companion moves through the envelope gas but both stellar cores orbit each other inside it. To test some of these effects and to improve the accuracy of 1D models, multidimensional hydrodynamic simulations were used to study the interaction of objects with the stream of envelope gas—because of their similarity to technical setups they are sometimes called *wind tunnel simulations*. In terms of the physics modeling, they are quite similar to the “global” CE simulations in the framework of the basic gravo-hydrodynamic model, that are discussed in Sect. 6.3. There are, however, two important differences: the advantage of “local” wind tunnel simulations is that they potentially can resolve the stellar core and the flow in its immediate vicinity—a region that often remains under-resolved in global simulations because they have to accommodate the entire structure of the giant primary star. Their drawback, however, is that they do not account for the global geometry, the full gravitational potential of the primary, the eccentricity of the orbit, large-scale distortions of the flow of envelope gas, instabilities, and microphysical effects such as the recombination of ions (MacLeod and Ramirez-Ruiz, 2015a). Nonetheless, wind tunnel simulations may capture main effects and with their superior spatial resolution they constitute an important complimentary approach to global CEE simulations.

The astrophysical problem of a compact body moving through gas while accreting material and being subject to drag forces is rather ubiquitous. Not all simulations of

this type were performed in the context of **CE** studies. Despite the differences in the setups, however, their results often carry over to the problem at hand. A review of such studies can be found in [Edgar \(2004\)](#). In their Section 3.1, [MacLeod and Ramirez-Ruiz \(2015a\)](#) summarize some of the findings.

Early wind tunnel simulations were carried out by [Shima et al. \(1985\)](#) with a finite-volume discretization of fluid dynamics based on the Riemann solver of Osher ([Osher and Chakravarthy, 1983](#)) under the assumption of axisymmetry. They tested the analytic prescriptions discussed in Sect. 2.2.1 and studied the details of the flow configurations relaxing the collisionless assumption. Overall, in the case of high-Mach number flows, the gas was found to converge behind the object. A bow shock forms slightly upstream of the body and it encloses the region where gas converges and flows towards the gravitating object, where it is accreted. This confirms the basic picture of **BHL** accretion. Consequently, [Shima et al. \(1985\)](#) cast their results in the corresponding form of the drag force,

$$F_{\text{drag}} = C_d \frac{1}{2} \pi R_a^2 \rho_\infty v_\infty^2, \quad (41)$$

i.e. a variant of Eq. (6), and determined the drag coefficients C_d from their simulations with varying Mach numbers of the flows and specific heat ratios of the gas.

3D hydrodynamic simulations including a density gradient in the gas were carried out by [Soker et al. \(1986\)](#) and [Livio et al. \(1986\)](#) with a hybrid particle-grid based scheme, and by [Fryxell and Taam \(1988\)](#) and [Ruffert \(1997, 1999\)](#) with the piecewise-parabolic finite-volume method ([Colella and Woodward, 1984](#)). These studies were motivated by other astrophysical scenarios and therefore considered shallower density gradients than those expected in **CEE**. Additional simulations focused on flow instabilities that may occur in the Mach cone behind the moving object (e.g. [Ruffert, 1994, 1995, 1996](#); [Foglizzo et al., 2005](#)). [Armitage and Livio \(2000\)](#) performed two-dimensional (**2D**) simulations with the finite-volume code **ZEUS** ([Stone and Norman, 1992](#)) to model the accretion during **CEE** in the context of the formation of black holes.

The treatment of drag forces discussed in Sect. 2.2.1 is based on linear perturbation theory and applies to low-mass perturbers. In **CEE**, the companion mass is sufficiently large so that we expect the density wakes to be in the nonlinear regime. Following up on their semi-analytical approach ([Kim and Kim, 2007](#)), [Kim \(2010\)](#) performed **3D** hydrodynamic simulations with the **ZEUS** code ([Stone and Norman, 1992](#)) for a massive perturber moving through gas on circular orbits. They found that for supersonic motion a bow shock develops upstream of the perturber through which the flow becomes subsonic. In its immediate vicinity, the perturber was surrounded by a near-hydrostatic spherical envelope, which reduced the drag force below the estimates from linear perturbation analysis, and an extended low-density region trailed the object.

The **3D** wind tunnel simulations by [MacLeod and Ramirez-Ruiz \(2015a\)](#) were specifically aimed at **CE** interaction. They used the **FLASH** code ([Fryxell et al., 2000](#)) to model a gravitating object (which one can think of as the companion in a **CE** interaction) represented by a point particle with a softened gravitational potential. The

point mass was surrounded by an absorbing boundary so that gravitational softening did not affect the flow. Block-wise AMR was employed and between six and nine levels of refinement were used based on the second derivative of pressure, but still centered at the gravitating object. MacLeod and Ramirez-Ruiz (2015a) pointed out that typical Bondi–Hoyle accretion radii in CE dynamics are much larger than the companions and extend over a substantial density gradient in the envelope. This breaks the symmetry of the flow and leads to an angular momentum barrier impeding accretion onto the companion (with consequences for a potential growth of neutron star masses in CE interaction), while the drag force is only mildly affected. MacLeod and Ramirez-Ruiz (2015a) pointed out that the drag forces observed in their simulations are not dominated by hydrodynamic friction but are of dynamical origin, i.e., they are caused by envelope gas piling up due to gravitational interaction with the companion. They fitted their results to the formalism of Bondi and Hoyle (1944), see Eq. (6). Contrary to the 2D simulations of Armitage and Livio (2000), the 3D simulations of MacLeod and Ramirez-Ruiz (2015a) showed no formation of a persistent disk around the companion. The study of MacLeod et al. (2017a) included the gravitational potentials of both the primary (assuming a planar geometry in the wind tunnel setup) and the companion and extended the parameter range in a systematic way. Different Mach numbers of the flow, density gradients, and mass ratios between primary and companion were tested. Again, the accretion rate was found to be reduced by the angular momentum barrier due to the density gradient.

The universality of the drag forces determined in wind tunnel simulations remains an open question. Are they sufficient to calibrate semi-analytic 1D simulations so that they gain predictive power? A detailed discussion on the question of which quantities and phases in CEE can be captured this way was presented by Everson et al. (2020). Chamandy et al. (2019) compared the drag calculated using the analytical formalism of MacLeod et al. (2017a) with the drag measured in their 3D global CE simulations of a $\sim 2 M_{\odot}$ RGB primary star and a $\sim 1 M_{\odot}$ companion. They found that the two quantities match well only up to mid-inspiral. Afterwards, the analytical fit over-predicts the force experienced by the companion in the simulation by up to an order of magnitude. Other 3D simulations compared the measured gravitational drag with different variants of the analytical drag formalism (Sect. 2.2.1) to find reasonable agreement (Staff et al., 2016b; Reichardt et al., 2019). This said, there has never been a comprehensive parameter study nor a systematic comparison between drag estimates and therefore, for the time being, it is impossible to conclude on the extent to which the drag in 3D global simulation matches predictions from analytic formalisms.

In addition to simulations aiming at determining the drag force acting on the companion, studies have been performed that explore the effects of accretion and jet formation. In a series of publications, López-Cámara et al. (2019), López-Cámara et al. (2020), and López-Cámara et al. (2022) report on modeling jets launched from a compact object in a common envelope environment with the MEZCAL code (De Colle et al., 2012). The compact object is represented by a point particle and a self-regulated jet is injected through an inner boundary. It is powered by a fraction of the mass accretion rate onto the compact object as measured at that boundary. Different parameters (efficiency of jet launching, inclination angle of the jet) are explored. In some cases, a neutron-star could drive a jet that breaks through the material piled up

around it (López-Cámara et al., 2019, 2020). A white dwarf companion star, however needs a very high efficiency to successfully launch a jet and for main sequence stars accretion is found to be too weak so that the jet does not break out of a RG star envelope but is choked (López-Cámara et al., 2022).

6.3 Global CE simulations

Global CE simulations have a history dating back to the 1980s. Much of the early work was published in a series of papers on what was called back then “double-core evolution” by different groups of authors with various numerical methods (Bodenheimer and Taam, 1984; Taam and Bodenheimer, 1989, 1991; Terman et al., 1994; Taam et al., 1994; Terman et al., 1995; Yorke et al., 1995; Terman and Taam, 1996; Sandquist et al., 1998).

The different approaches to numerical fluid dynamics that have been employed reflect the development of similar simulation techniques in other branches of computational astrophysics. CE simulations have benefited substantially from the rapid evolution of computational resources over the past decades, which enabled significant refinement in the physical and numerical modeling. Each of the approaches has its strengths and drawbacks and we gave an account of this in Sect. 4.4.

6.3.1 Pioneering Eulerian grid-based approaches

At a first glance, Eulerian approaches discretizing the equations of fluid dynamics on a static spatial grid may seem little appealing for simulating CEE. Missing obvious symmetries, the grid geometry cannot easily be adapted to the CE dynamics. Moreover, as detailed in Sect. 4.1, such schemes are not Galilean invariant and therefore the representation of physical phenomena, such as hydrodynamic instabilities, may depend on whether the simulations are conducted on a static or rotating frame of reference. Notorious advection errors tend to destabilize orbiting stellar objects and angular momentum conservation is problematic. Nonetheless, some Eulerian grid-based methods have been employed to studying CEE early on, motivated as natural extensions of 1D CE simulations in the drag force formalism. The primary goal was to alleviate a fundamental problem of the 1D models, where gravitational drag luminosity is injected into a spherical layer instead of a local energy deposition as expected to operate around the companion in reality.

To give proper credit to early attempts to simulate CEE in multidimensional hydrodynamic approaches, we start out our treatise with *pioneering* grid-based simulations. Some of their value lies in the discussion of fundamental processes, that remains valid until today. Many of the employed methods, however, no longer meet modern standards. We therefore refrain from discussing them in detail; they are of historical interest rather than a guide for future developments.

The first 2D simulation of CEE was conducted by Bodenheimer and Taam (1984), who used a “fluid-in-cell” approach to discretize the equations of fluid dynamics and assumed axisymmetry. Their setup system consisted of a $16 M_{\odot}$ supergiant star, of which only a part of the envelope was modeled, and a $1 M_{\odot}$ companion representing a

neutron star. Interestingly, this early multidimensional model already addressed a situation that—as a progenitor system of a gravitational-wave emitting merger event—is of utmost interest today, but still challenges numerical simulations. The transfer of angular momentum and orbital energy from the companion to the envelope gas was not self-consistently followed, but instead an analytic expression for frictional heating in the Bondi–Hoyle–Lyttleton formalism was applied following Taam et al. (1978); see also Sect. 2.2.1. The gravitational interaction of the cores with the envelope gas was not included in this model. This simulation approach can be seen as a multidimensional generalization of earlier attempts to follow the inspiral of a companion into a giant star in classical 1D stellar evolution codes, such as discussed in Sect. 2.2.2. Bodenheimer and Taam (1984) found that about $1 M_{\odot}$ of material is ejected in the evolution, preferentially in the direction of the orbital plane. Based on the multidimensional structure of the outflow, they argued that modeling CE events based on energy conservation arguments alone is insufficient. Applying the same numerical method, Taam and Bodenheimer (1989) explored CEE in a system with a $5 M_{\odot}$ RG primary star, whose core is replaced by a point mass to reduce the associated time-scale problem, and a $1 M_{\odot}$ companion. They report a significant mass ejection.

The study of Taam et al. (1994) was performed with the hydrodynamical code of Różyczka and Spruit (1989) and changed the model of the interaction between the companion and the envelope gas. The orbital decay of the core binary was explicitly prescribed according to angular momentum conservation: The angular momentum of the envelope gas was approximated in a 2D setup that modeled the dynamics in the orbital plane. Its temporal change was equated to the change in angular momentum of the core binary thus providing the evolution of the orbital separation. The in-fall of the companion was not followed completely. Instead, the focus was on simulating the gravitational torques in late stages of CEE of a $3 M_{\odot}$ RG star, whose core was replaced by a point mass, and a companion, whose mass was slowly increased to $1 M_{\odot}$ in a relaxation step. In agreement with the results of the SPH simulation conducted by Terman et al. (1994) (see Sect. 6.3.3), these torques were found to establish co-rotation of the envelope material close to the companion. Taam et al. (1994) suggested this effect to be responsible for the termination of the inspiral phase.

Yorke et al. (1995) used an axisymmetric setup of a $0.7 M_{\odot}$ main sequence star immersed into the envelope of a $3 M_{\odot}$ AGB primary to follow later stages of CEE in this system. In contrast to previous simulations, both cores were allowed to move and a nested-grid technique afforded a higher spatial resolution in the inner regions of the CE: eight levels of cylindrical polar grids were used, each smaller by a factor of two in the radial extent than the next higher level grid. The treatment of angular momentum loss of the cores followed that of Taam and Bodenheimer (1991), with some modifications. Yorke et al. (1995) found that in their simulation the entire envelope was likely to be ejected without the cores merging. Orbital decay terminated at a separation of $15 R_{\odot}$ due to a spin-up to near co-rotation of envelope gas in the vicinity of the cores. Owing to the nested grid approach, the expansion of the ejected material could be followed to relatively large distances and Yorke et al. (1995) commented on the shaping the emerging planetary nebula.

A leap forward in the quality of Eulerian grid-based **CE** simulations was taken with the **3D** hydrodynamic simulations of Sandquist et al. (1998)—reported in the last paper of the series on “double-core evolution”. By abandoning analytic models for the drag force or the orbital decay, the modeling fidelity of physical processes drew level with the **SPH** simulations conducted slightly earlier by Terman et al. (1994, 1995), Terman and Taam (1996) and Rasio and Livio (1996), (see Sect. 6.3.3). Therefore, the simulations of Sandquist et al. (1998) were the first to model **CE** self-consistently in a **3D** Eulerian grid-based approach. With their nested-grid approach similar to Yorke et al. (1995), but extended to three spatial dimensions in Cartesian geometry, Sandquist et al. (1998) claimed to reach higher spatial resolution than the **SPH** simulations. The nested-grid hydrodynamics code was based on that of Burkert and Bodenheimer (1993) and employed a second-order finite-difference method to solve the equations of fluid dynamics. To determine the gravitational potential of the gas, the Poisson equation was solved on the coarsest grid with a particle-mesh algorithm. Two collisionless particles were used to model the core of the primary star and the companion. Their mutual gravitational interactions and their interactions with the gas were softened according to Ruffert (1993), with an adaptive reduction of the softening length as the core particles approached each other. The envelope was modeled with an ideal-gas equation of state in combination with radiation pressure. The setups followed the interactions of **AGB** primary stars of 3 and 5 M_{\odot} with main sequence companions of 0.4 and 0.6 M_{\odot} .

Sandquist et al. (1998) found that about 20% to 30% of the envelope gas was ejected at the end of the simulations, but most of the mass, although largely removed from the volume of the original giants, remained marginally bound at larger distances. Because of limited spatial resolution, the core orbit did not completely settle to a final separation, and extrapolating to the further evolution, Sandquist et al. (1998) predicted full envelope removal for their setups with the 3 M_{\odot} primary, while for the more massive **AGB** star they concluded that a merger of the cores may be possible. The most important result of Sandquist et al. (1998) is perhaps the first detailed description of the dynamical change in the envelope structure due to flows that are clearly not axisymmetric. Their resolution of the coupling between the core particles and the envelope gas allowed to identify for the first time spiral density waves that were generated in front of both stellar cores. Sandquist et al. (1998) concluded that these spiral shock waves were the primary mechanism for transporting the angular momentum released in the core inspiral outwards through the envelope (but see also Rasio and Livio, 1996).

With the same numerical approach, Sandquist et al. (2000) performed a systematic exploration of **CEE** with **RG** primaries of different total and core masses with companions of various masses. They found that such low-mass binary systems can survive **CEE** provided that the total mass of the **RG** primary is below 2 M_{\odot} and its degenerate helium core exceeds about 0.25 M_{\odot} . The remnants of these interactions are associated with observed helium double degenerate systems, pre-cataclysmic variables and subdwarf B stars. With the same code, De Marco et al. (2003a,b) simulated the **CE** phase between an **AGB** primary star and companions of 0.1 and 0.2 M_{\odot} as a potential origin of Wolf-Rayet central stars of planetary nebulae.

6.3.2 Modern Eulerian grid-based approaches

Up to this point in the history of Eulerian grid-based CE simulations, the treatment of fluid mechanics followed fluid-in-cell or finite-difference methods that are not commonly in use in modern astrophysical simulations any longer. The advantages of finite-volume techniques and high-resolution shock capturing schemes (see Sect. 4.1.1) were introduced into the field of CE simulations only relatively late compared with other astrophysical applications. This is surprising given the fact that conservation properties and resolution of shock waves are essential ingredients for capturing the dynamics of such events. Simulations performed after Sandquist et al. (2000) can be considered *modern efforts*: Eulerian approaches stepped up using techniques such as finite-volume methods, Godunov schemes and AMR. As such, they started to flank SPH techniques in addressing the complications of the CE interaction.

The work of Ricker and Taam (2008, already hinted at in Taam and Ricker 2006, who discussed some of the technical advantages) introduced the first modern Eulerian grid-based framework for numerical fluid dynamics to CE simulations. The FLASH code (Fryxell et al., 2000) features the piecewise-parabolic reconstruction method of Colella and Woodward (1984). The use of AMR techniques significantly improves flexibility in spatial resolution over fixed nested grids. This allows one to refine at shock fronts and in the vicinity of the stellar cores. As discussed in Sect. 4.1.1, it is this technique, that ultimately renders Eulerian grid-based approaches to simulating CEE competitive to alternative SPH and moving mesh techniques that we discuss in Sects. 6.3.3 and 6.3.4. However, even with AMR it is impossible to resolve the $0.36 M_{\odot}$ core of the $1.05 M_{\odot}$ RG primary star modeled by Ricker and Taam (2008)—in particular in the view of the small time steps required by the CFL condition (see Sect. 5.1). They therefore represented the core of the primary as well as the $0.6 M_{\odot}$ companion by clouds of 2×10^5 particles each occupying a volume given by a length scale that exceeds the finest grid spacing by a factor of three. The particles are moved rigidly with their centers of mass. Their gravitational coupling is modeled with a cloud-in-cell interpolation and Ricker and Taam (2008) argued that particle clouds avoid force anisotropy problems that would arise from using single particles in this approach.

With their 8-level AMR setup, Ricker and Taam (2008) reached an effective resolution of 2048^3 cells over the domain size. Transient motions in the setup of the primary star were damped for one dynamical timescale before the companion was added and the primary was set spinning with an angular velocity of 95% of co-rotation with the orbit (that, if not previously stabilized, would have induced expansion). The simulation of Ricker and Taam (2008) covered only a very short initial phase of CE interaction—less than one orbit of the binary system is followed—but it confirmed the earlier finding of Sandquist et al. (1998) that the orbital decay was dominated by non-axisymmetric gravitational drag, which is one to two orders of magnitude larger than hydrodynamic drag. Moreover, Ricker and Taam (2008) found a much faster orbital decay than predicted from the BHL formalism. This was explained by the fact that within the BHL framework, the predicted gravitational drag is similar to the hydrodynamic counterpart because it is only affected by the local formation of a wake. In CEs, however, this drag is increased by the gravitational forces over a

larger volume of the entire envelope. Although [Ricker and Taam \(2008\)](#) emphasized the shortcomings of their model in capturing accretion onto the companion caused by the lack of an inner boundary around it, they argued that the accretion rate onto the companion should be significantly smaller than expected from [BHL](#) accretion arguments.

[Ricker and Taam \(2012\)](#) presented an update of their previous work, again employing the `FLASH` code, following the same system for somewhat longer times of the evolution, now covering five orbits. They explicitly mentioned the treatment of self-gravity in this simulation: the Poisson equation was solved with a multigrid method (see Sect. 4.3.2). The number of particles used to represent the stellar cores was increased to 2×10^5 for each cloud and 9 levels of [AMR](#) were used. [Ricker and Taam \(2012\)](#) reported an ejection of 25% of the envelope’s mass over the simulated time, higher than reported by [Sandquist et al. \(2000\)](#), and possibly caused by a larger mass ratio between primary star and companion in their system. They further noted a rapid decrease of the eccentricity of the orbit and identified imprints of spiral shocks on the morphology of the envelope gas that was expelled preferentially close to the orbital plane. Again, they confirmed that gravitational drag dominates over hydrodynamic drag and emphasized that the [BHL](#) prescription overestimates the accretion rate onto the companion.

Recently, the same group, still using `FLASH`, has been attempting the simulation of [CEE](#) in more massive systems. There is so far only one brief publication ([Ricker et al., 2019b](#)) presenting a simulation of [CE](#) interaction with an $82 M_{\odot}$ red supergiant primary star of radius of $2891 R_{\odot}$ at low metallicity, deriving from an $88 M_{\odot}$ main sequence star. The companion was a $35 M_{\odot}$ point particle, supposed to represent a black hole. This simulation included for the first time both the effects of partial ionization, via a suitable equation of state (see Sect. 4.2) and the effects of radiation, via a single-group, flux-limited diffusion approximation. Interestingly, [Ricker et al. \(2019b\)](#) concluded that envelope unbinding is not benefiting from recombination energy. Clearly, these simulations are critical to answer the question of whether double black hole binaries that merge under the emission of detectable gravitational waves can be formed via an isolated binary channel ([Belczynski et al., 2016](#)), but more work is needed to confirm the still very preliminary results of [Ricker et al. \(2019b\)](#).

The next grid-based code to be exercised on the [CE](#) problem was `ENZO` ([Bryan et al., 1995](#)). This code was originally developed for cosmological simulations and [Passy et al. \(2012\)](#) adapted it to the stellar problem. Core and companion were modelled as point masses with the usual softening of the gravitational potentials (see Sect. 4.3.3). Self-gravity was implemented with a fast Fourier transform technique (see Sect. 4.3.2), while the gravity of the two point masses was treated analytically by adding the (softened) potential to that calculated for the gas. Starting out from a [1D](#) stellar model, [Passy et al. \(2012\)](#) mapped a $0.88 R_{\odot}$, $100 R_{\odot}$ [RGB](#) star with a core of $0.392 M_{\odot}$ onto a grid without any additional levels of refinement. Two resolutions with $[128]^3$ and $[256]^3$ cells were used. They carried out five [CE](#) simulations for each resolution with companion masses of 0.1, 0.15, 0.3, 0.6 and $0.9 M_{\odot}$ and two additional low-resolution simulations to test the effects of the initial orbital separation and ec-

centricity. The companions were initialized on the stellar surface¹⁹. One finding of these simulations was the—perhaps expected—realization, that in none of them the entire CE became unbound²⁰. The range of final separations was ~ 6 to $30 R_{\odot}$, with wider final separations for more massive companions. The most important achievement of this study, however, was a direct comparison between Eulerian grid-based and SPH (see Sect. 6.3.3) approaches to CE simulations, which used the SNSPH code of Fryer et al. (2006). This paper also raised some questions which remain unanswered to this day. The most pressing of them is whether the final separation of the stellar cores measured in the simulations is the actual post-CE separation. The values determined from the simulations appeared to be on the high side of observations and it was therefore concluded that in post-dynamic inspiral phase the companion would migrate inwards.

The ENZO code was the basis for a number of follow-up papers, which, as an upgrade, used its AMR capability and the adaptive particle-mesh solver of Passy and Bryan (2014). Iaconi et al. (2017b, 2018) modelled the same primary as Passy et al. (2012), but this time fully investigated the effect of initial orbital separation. They concluded that starting the simulation at a wider separation (approximately that of the start of Roche lobe overflow) does result in a somewhat wider orbital separation due to the giant expanding before the fast inspiral rather than spinning up. They too carried out a comparison with an SPH simulation (see Sect. 6.3.3), this time with the PHANTOM code (Price et al., 2018). In a subsequent paper, Iaconi et al. (2018) compared results from setups identical to those of Passy et al. (2012) with simulations in which the primary was a more massive ($\sim 2 M_{\odot}$) AGB star. The reasoning was that if the envelope was more massive it would expand more reluctantly and allow the companion to sink deeper. This was expected to cause an increased transfer of orbital energy to the envelope. While companions did spiral in deeper, no substantial increase in unbound mass was observed: in both the original setup and in the simulations involving an AGB primary star, the unbound mass fractions ranged between a few and about 15 percent.

Staff et al. (2016b) carried out ENZO-based CE simulations involving a $\sim 3 M_{\odot}$ AGB star and companions between 0.6 and $3.0 M_{\odot}$ with a range of eccentricities. Their aim was to understand systems such as the protoplanetary nebula OH 231.8+4.2. These had been suggested to result from a CE interaction in an eccentric binary. On the one hand, these simulations were used primarily as platforms for a series of analytical discussions on the ability of the companion to launch a jet *before* the actual CE interaction, that would result in the observed nebular energetics. On the other hand, these simulations were among the few that started out with high eccentricities in the initial system, AGB primary stars, and stellar masses above the common $\sim 1 M_{\odot}$. With the relatively low resolution achieved in these simulations, however, it remained difficult to put the results appropriately into context. Most of the envelope mass remained bound (again, between a few and about 15 percent of the material was unbound) and the separation still ranged on the wide side compared to observa-

¹⁹ For one simulation, an initial eccentricity was imposed by increasing slightly the initial separation of the two core particles.

²⁰ Passy et al. (2012) do not list the fraction of envelope that is unbound but these values are very similar to those of their comparison simulations carried out with an SPH code and presented in Sect. 6.3.3

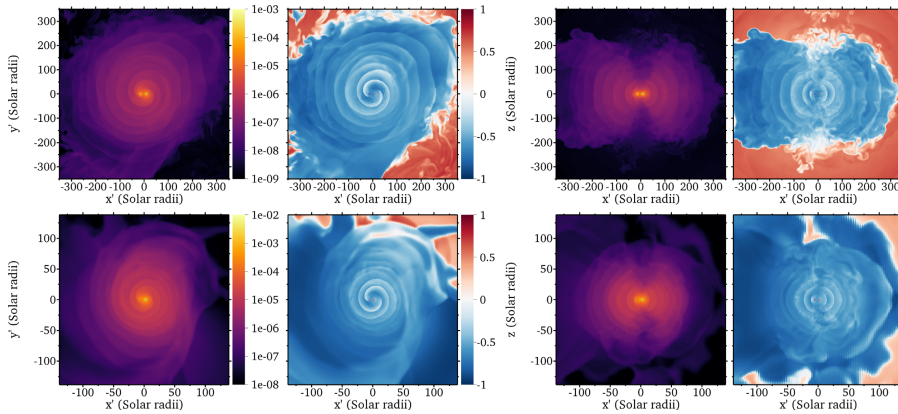


Fig. 13 CEE simulations with an AGB (top panels) and an RGB (bottom panels) primary star. Shown are slices after ten orbits of the core binary system through the orbital plane (left) and perpendicular to it in density (left panels) and total energy (right panels, where blue is bound gas while red is unbound). Figure from Chamandy et al. (2020)

tions. Moreover, the study concluded that if mass transfer takes place at periastron passage, the orbital elements are altered and it is likely that these orbital changes lead to a CE within a short period of time. This means that it is unlikely that objects like OH231.8+4.2 could be formed by repeated jet episodes that take place during periastron passage.

In a companion paper, (Staff et al., 2016a) used the same $3 M_{\odot}$ AGB primary star as well as an RGB star of similar mass to determine the outcome of planetary intrusions into the envelopes of giants. Somewhat unsurprisingly the conclusion was that planets would inspiral and merge with the core within a decade (RGB star) to a century (AGB star). Considerable angular momentum would be added to the envelopes of the giants which would expand somewhat and spin up to values commensurate with the fastest rotating giant stars observed by de Medeiros et al. (1996).

Also using the version of ENZO adapted by Passy et al. (2012), Shiber et al. (2019) carried out a simulation using the same star used by Passy et al. (2012). This time, however, the effect of jets was explored, that are potentially launched by the companion throughout the inspiral. In particular, the focus was on whether such jets enhance envelope unbinding. The jets were not self-consistently simulated, but were instead launched according to analytically derived quantities such as mass loss rate, launch speed and opening angle. The outcome of the simulation was not dramatically different from the equivalent simulation without jets: the final separation was somewhat wider and additional envelope gas was unbound (the unbound mass increased from $\sim 10\%$ without jets to $\sim 30\%$ with jets). This indicated that while jets may aid envelope ejection, it seems unlikely that they can fully explain it.

Schreier et al. (2019) explore the effect of jets in CEE of a triple system: a tight binary system is placed into the envelope of a $4 M_{\odot}$ AGB star with $100 R_{\odot}$. The inner $5 R_{\odot}$ are replaced with a sphere of constant density, pressure, and temperature. The binary system is not resolved; one of its stars is assumed to accrete material and to launch two jets in opposite directions with an inclination relative to the orbital plane

of the binary and the core of the **AGB** star. In the simulation, the jets are injected with an inclination angle of 45° at the location of the binary system. The simulation is carried out with the **PLUTO** code (Mignone et al., 2012) on a cubical domain with $400 R_\odot$ side length covered with 48 cells and three to four levels of **AMR**. Self-gravity is not accounted for in the setup: gravitational effects of the tight binary system and of the deformed envelope are ignored. Schreier et al. (2019) observe vortices and associated density fluctuations perturbing the envelope structure and discuss implications for dust formation and the shaping of “messy” **PNe**. The follow-up studies of Schreier et al. (2021) and Schreier et al. (2022) were carried out with the **FLASH** code (Fryxell et al., 2000) in similar setups but with a more massive primary star of a zero-age main sequence mass of $15 M_\odot$ evolved to a red supergiant stage ($M = 12.5 M_\odot$, $R = 881 R_\odot$). To avoid prohibitively small time steps in the simulation, the inner 20% of the stellar radius are replaced by an inert core. The **AMR** capabilities of the **FLASH** code are used. Schreier et al. (2021) assume a neutron star companion that passes through the envelope of the giant on a highly eccentric orbit—an event Gilkis et al. (2019) call a “common-envelope jets supernova impostor”. The neutron star is modeled as a point particle and the jets are launched artificially “by hand”. Again, neither gravity of the neutron star nor self-gravity of the envelope are included in the model such that no gravitational drag acts on the companion. Only one orbit of it is simulated. A complicated clumpy outflow morphology is detected and the luminosity of the event is estimated to place it into the regime of “gap transients” between classical novae and supernovae. Schreier et al. (2022) explore the deposition of angular momentum into the envelope due to jets that are launched perpendicular to the orbit and due to tilted jets (motivated by the triple scenario where the companion neutron star or black hole is part of a tight binary system).

Another set of grid-based **CE** simulations was carried out with the **AMR** code **ASTROBEAR** (Carroll-Nellenback et al., 2013). A few studies have been published so far, concentrating on the analysis of two primary stellar structures and a range of companions. The two structures are an **RGB** and an **AGB** star deriving from a $2 M_\odot$ main sequence star, with radii of $49 R_\odot$ and $122 R_\odot$, respectively (Chamandy et al., 2018, 2020). All simulations initialized the companion approximately at the stellar surfaces.

Chamandy et al. (2018) benchmarked **ASTROBEAR** against a similar simulation carried out with the moving mesh code **AREPO** (Ohlmann et al., 2016a, see Sect. 6.3.4). They also investigated the amount of accretion that would likely take place onto the companion—a very important topic, particularly in the massive-star regime when massive companions may generate large amounts of feedback energy. They concluded that the amount of accretion cannot be estimated just using control surfaces around the companion because a high-pressure pseudo-atmosphere that settles around the point mass companion and reduces the accretion. Chamandy et al. (2018) suggested that the introduction of mass “disappearance” likely results in a more realistic outcome and that high accretion rates ($\sim 1 M_\odot \text{ yr}^{-1}$) could exist during the short-lived inspiral phase. In the simulation, this was implemented with a subgrid-scale accretion model. Following Krumholz et al. (2004), the companion was represented by a sink particle in one of the runs. The simulations were also used to draw a comparison between the gravitational drag force measured in the simulation and what would be

derived using the analytical approximations of MacLeod et al. (2017a). Chamandy et al. (2018) concluded that the simulated force was similar to the analytical prescription only early on and until mid inspiral, but diverges later with the simulated force being much smaller than the analytical approximation.

Chamandy et al. (2020) were first to model CEE of a low-mass AGB star with a $\sim 1 M_{\odot}$ companion. The conclusions that they could draw from a comparison of their RGB and AGB simulations was that the two were remarkably similar (see Fig. 13). However, both simulations were started with the companion at the surface, not accounting for the redistribution of gas that takes place when the simulation is started at the time of Roche lobe overflow. Only a fraction of the envelope mass was unbound during the simulated time, but Chamandy et al. (2020) estimated a full envelope ejection over 10 years if the rate of mass unbinding measured in the simulations stayed constant.

Zou et al. (2022) modified the setup of Chamandy et al. (2018) that, with a $2 M_{\odot}$ RG primary star and a $1 M_{\odot}$ or $0.5 M_{\odot}$ companion, was similar in the parameters and the treatment of the RG core to that of Ohlmann et al. (2016a) but used the AstroBEAR code. They included a jet launched via a subgrid model from the companion. This model injects mass at a chosen constant rate with a certain velocity perpendicular to the orbital plane into a prescribed opening angle. Comparing this model to simulations without jets, the influence of a potential jet on orbital evolution and the morphology and unbinding of the envelope is explored and the parameters of the jet model are tested. The jets were found to be choked in the envelope and transferred additional energy onto it so that the unbound mass was increased by 10% over the ten simulated orbits compared to simulations without jets. Based on this result, Zou et al. (2022) expect that jets launched from main sequence or white dwarf companions are unlikely to dominate envelope unbinding.

Except for the study of Ricker et al. (2019b), none of “modern” Eulerian grid-based simulations of CEE accounted for ionization effects in the envelope material. None of them achieved a successful envelope ejection over the simulated time; the unbound mass fraction typically stayed below $\sim 20\%$.

6.3.3 SPH approaches

In logical continuation of previous 1D models, early Eulerian grid-based approaches to simulating CEE (see Sect. 6.3.1) modeled the interaction of the companion with the envelope by explicitly imposing a drag force on it. SPH simulations, in contrast, from the start relied on a self-consistent treatment of this interaction by implementing self-gravity. Although with their limited resolution simulations carried out in the 1980s and 1990s failed to converge in reproducing the effect, with increasing computer power this approach became gradually more realistic. In this sense, the development of SPH methods for CE simulations was not subject to breaks and breakthroughs in the modeling technique itself—although an efficient parallelization of the SPH framework to distributed memory machines is not trivial and was achieved only in the early-to-mid 2000s (e.g. Springel et al., 2001; Springel, 2005; Fryer et al., 2006). It paved the way to increasing the resolution of the simulations, but still today not all SPH-based CE simulations are carried out with MPI parallelization.

The application of **SPH** for simulating the onset of **CEE** was pioneered by [de Kool \(1987\)](#). He modelled the interaction of a $11 M_{\odot}$ giant with a $4 M_{\odot}$ companion star. Only 600 particles were used to represent the envelope of the primary star assuming a polytropic equation of state while its core and the companion were modeled by single particles. The setup was obtained from relaxing the stellar envelope to hydrostatic equilibrium and—for the initial binary setup—by slowly reducing the separation between the interacting stars. This setup procedure is largely followed in **SPH**-based **CE** simulations to this day. [Livio and Soker \(1988\)](#) simulated **CEE** in a hybrid “particles in cell” (PIC) discretization of the equations of fluid dynamics, which combines a pseudo-particle approach with an Eulerian grid and thus differs from the **SPH** formalism.

The increase of computational power and improvements in numerical methods—most notably the introduction of a hierarchical tree algorithm for calculating self-gravity—allowed to conduct more detailed **3D CE** simulations with **SPH**. For the first time, and in contrast to contemporary grid-based Eulerian simulations (see Sect. 6.3.1), such simulations were able to follow the inspiral of the companion into a giant primary with the gravitational interaction between the cores and the envelope gas captured by the model instead of using an analytic prescription for a drag force.

[Terman et al. \(1994\)](#) discretized the co-rotating envelope of a $4.67 M_{\odot}$ **RG** primary mapped from a polytropic model using 10 000 **SPH**-particles. After random initial placement of the particles, frictional damping established **HSE**. The core of the primary star as well as the $0.94 M_{\odot}$ companion were represented by single massive collisionless particles. A fictitious drag force was applied only initially to bring the binary system into the **CE** stage—the actual **CEE** was followed self-consistently with the drag force resulting from the modeled interaction. With this setup, [Terman et al. \(1994\)](#) demonstrated that gravitational tidal torques cause rapid orbital decay of the core binary after the onset of **CEE**. The evolution of the system was followed for 0.6 yr when the orbital separation settles to about $6 R_{\odot}$ because of a spin-up of the gas in the vicinity of the cores approaching co-rotation. This simulation exploited the capability of **SPH**-based approaches to follow the inspiral phase over many orbits. It was eventually terminated because the gravitational softening of the core particles became larger than their separation rendering the model nonphysical. Only about 13% of **RG** envelope mass was ejected to this point. Based on their simulations, [Terman et al. \(1994\)](#) discussed the importance of the **3D** response of the envelope to the motion of the binary composed of the giant’s core and the companion, pointing out deficiencies of models that assumed an inspiral of a companion star into a fixed core–envelope primary structure.

[Terman et al. \(1995\)](#) extended their numerical approach to simulating the inspiral of a $1.4 M_{\odot}$ neutron star into massive primaries of 16 and $24 M_{\odot}$ in various evolutionary stages. These simulations exploited the efficiency of the **SPH** approach to simulate **CEE**, although the achieved resolution was insufficient to accurately separate the core–envelope structure of the primary stars, which, with the given parameters, remains a challenge even for current simulations. For some of the considered systems, a mass ejection efficiency of $\sim 30\%$ – 40% was reported. [Terman et al. \(1995\)](#) pointed out that the survival of the core binary, as opposed to a merger of the neutron star with

the primary’s core potentially forming a Thorne–Żytkov object (Thorne and Zytkov, 1975), depends on the structure and evolutionary stage of the non-compact star.

Terman and Taam (1996) relaxed their assumption of a polytropic equation of state to include both gas and radiation pressure in simulations of systems with a $5 M_{\odot}$ RG and companions with 0.5 and $1.0 M_{\odot}$. Again, 10 000 SPH-particles were used for modeling the RG envelope, which, in this suite of simulations, was set up as spherical and non-rotating. The size of the cores was reduced with respect to the simulations of Terman et al. (1994), allowing the simulations to follow the inspiral for longer, which resulted in the ejection of up to 70% of the envelope gas.

Rasio and Livio (1996) used up to 50 000 particles to follow the onset of the unstable mass transfer and initial inspiral of a $0.7 M_{\odot}$ main sequence star into a RG of $4 M_{\odot}$ until a quasi-static CE had formed. They pioneered the construction of a rotationally synchronized binary system in HSE by means of a relaxation and damping procedure—in contrast to Terman and Taam (1996) and without the need of applying an initial fictitious drag force as in Terman et al. (1994). The core of the primary star and the secondary were modeled as point particles and their gravitational potentials were softened over a length comparable to the SPH smoothing length of the innermost particles, typically a hundredth of the radius of the RG primary (which is similar to what Terman and Taam, 1996, used). Under this assumption, the core of the primary star is much larger than in reality. In their simulation, Rasio and Livio (1996) identified a co-rotating region of gas around the central binary and found indication for the onset of convection in the envelope in agreement with the predictions of Meyer and Meyer-Hofmeister (1979). Only about 10% of the envelope material was unbound—most likely because of the establishment of co-rotation in late stages of the evolution as opposed to the findings of Terman and Taam (1996) whose models eject a substantial fraction of the envelope. Rasio and Livio (1996) attributed this discrepancy to differences in the spatial resolution, but as neither the numbers of particles nor the sizes of the core models differ significantly, this interpretation appears questionable.

In their paper comparing CE simulations carried out with a grid-based Eulerian code (see Sect. 6.3.2) and SPH, Passy et al. (2012) employed the SNSPH code of Fryer et al. (2006). It adopts a distributed-memory parallelization (Fryer et al., 2006) and therefore allowed to conduct simulations with enhanced resolution. SNSPH uses a special tree-based method (a parallel hashed oct-tree, Warren and Salmon, 1993) to calculate gravitational accelerations. As in their grid-based counterpart simulations, Passy et al. (2012) followed the interaction of a non-rotating $0.88 M_{\odot}$ RG primary star of $83 R_{\odot}$ with companions of masses between 0.9 and $0.1 M_{\odot}$ that were initially placed at the primary’s surface in a circular orbit and were modeled as collisionless particles. These simulations were set up as close as possible to the counterpart grid-based ENZO simulations (see Sect. 6.3.2). The envelope, modeled with an ideal-gas equation of state, was represented by an unprecedented number of 500 000 SPH-particles, that were initially placed with a weighted Voronoi tessellation. In contrast to other setups, the core of the giant primary star was treated as a massive SPH particle of $0.392 M_{\odot}$ and not as a collisionless particle, such that its pressure stabilized the envelope against gravitational collapse. It was placed at the center, embedded in a region with SPH-particles, such that the profile of density connected smoothly at the

core-envelope boundary, which was located at twice the smoothing length of the core particle, i.e. $0.2 R_{\odot}$. Therefore, the interaction of the core with the envelope gas was better resolved than in any of the previous SPH simulations of CEE. The simulations of Passy et al. (2012) followed the evolution until the orbital separation and the mass of the unbound envelope gas saturated. The amount of envelope gas ejected during the simulation varied with the mass ratio and was expelled mostly close to the orbital plane. It remained below 10% in all cases and the final orbital separations between the core particles were systematically larger than those found in observations of post-CE systems. Passy et al. (2012) discussed additional physical effects that may increase the envelope ejection efficiency. They emphasized the capability of the SPH method to model the accumulation of gas around the companion star—a direct implication of the Lagrangian nature of the scheme in which the spatial resolution automatically adapts to the mass distribution.

The next group to simulate CEE with SPH codes were Nandez et al. (2014), who modelled the interaction in system V1309 Sco (a $1.5 M_{\odot}$ subgiant and a $\sim 0.15 M_{\odot}$ main sequence star; Tylenda et al., 2011), using the SPH code STARSMAHER (Lombardi et al., 2011). In this simulation, the two stars were spatially resolved because of their relatively similar sizes (with particle numbers ranging from 20 000 to 200 000 for the primary star and from 2000 to 19 000 for the companion), and the interaction lead to a merger.

V1309 Sco is a particular system and perhaps not a clear CE case (see Sect. 1.2). A more traditional CE interaction was later simulated by the same group (Nandez et al., 2015) with the goal of modeling the double white dwarf system WD 1001+364. For this purpose, the core of the RG primary was selected to be $0.32 M_{\odot}$ (slightly larger than the value of the original 1D stellar profile in order to match the envelope structure) and represented by a point mass interacting only gravitationally. The $0.36 M_{\odot}$ companion was also modeled as a point particle. Various masses between 0.668 and $1.481 M_{\odot}$ were assumed for the RG envelope and resolved with 100 000 particles; one run was carried out with twice this resolution. Nandez et al. (2015) were the first to model the effect of recombination processes in a 3D CE simulation. For that purpose, they adapted the MESA equation of state (Paxton et al., 2011), that accounts for changes in the ionization structure by implementing the OPAL tables, see Sect. 4.2. They found that while simulations of the basic gravo-hydrodynamic model removed only about 50% of the envelope mass, complete envelope ejection could be achieved when assuming the released recombination energy to thermalize locally.

The same approach was used by Nandez and Ivanova (2016) for a range of primary RG stars with masses of 1.2 to $1.8 M_{\odot}$ and companions with masses of 0.32 to $0.40 M_{\odot}$ meant to be white dwarfs and modelled as point particles that interact only gravitationally, as did the cores of the RG primaries. The resolution of 100 000 SPH particles was similar to the production runs in Nandez et al. (2014). Almost complete mass ejection was obtained thanks to their use of the tabulated equation of state that includes recombination energy. Their simulations were then used by Ivanova and Nandez (2016) to infer a number of parametrizations to be used, e.g., in population synthesis studies.

Iaconi et al. (2017b) carried out a simulation of CE interaction using the same setup as Passy et al. (2012), but with a wider initial separation between the pri-

primary star and the $0.6 M_{\odot}$ companion. They used the shared-memory (OpenMP) parallelized SPH code PHANTOM of Price et al. (2018). This time, both the core of the primary and the companion were modeled as collisionless massive single particles. For gravitational softening, the prescription of Ruffert (1993) was applied instead of the previously used formulation of Monaghan (1992). The envelope was represented by one million particles. Both the obtained post-CE orbital separation and the amount of unbound gas ($\sim 16\%$ of the initial envelope material) were found to be slightly larger than those of Passy et al. (2012).

Reichardt et al. (2019) followed up on these studies and simulated CEE with the PHANTOM code again in a system similar to that of Passy et al. (2012). Their resolution varied between 8×10^4 and 1.1×10^6 SPH particles representing the envelope of the RG primary star, which for one of their simulations was set up to co-rotate with the binary system. In contrast to previous simulations, the initial binary separation was chosen such that the RG primary star just filled its Roche lobe and mass transfer started immediately. This way, Reichardt et al. (2019) extended the simulation to the time before the inspiral, which was possible thanks to the excellent angular momentum conservation of SPH-based simulations (see Sect. 4.4.3). While the duration of the pre-inspiral evolution was found to be resolution-dependent, this simulation paves the way for the study of the impact of the initial conditions on the CEE. Moreover, mass lost over the L_2 and L_3 Lagrange points of the system before the inspiral was found to remain bound and to potentially form a circumbinary disk. This disk was destroyed in the subsequent CE ejection, but the authors speculated about its survival for other system parameters. The measured drag force in the CE inspiral phase was consistent with analytical models, but only a small fraction of the envelope material (about 10% to 30%) was ejected—confirming previous simulations that indicated less unbound mass for increasing numerical resolution.

Reichardt et al. (2020) equipped the PHANTOM SPH code with an equation of state that can account for changes of the ionization structure of the envelope material. With this modification and assuming local thermalization of the released recombination energy, they carried out two simulations with RG primary stars of $0.88 M_{\odot}$ and $1.8 M_{\odot}$ and companions of $0.6 M_{\odot}$ and $0.36 M_{\odot}$, respectively. The latter configuration was the same as one of Nandez and Ivanova (2016), who claim complete envelope ejection for this case. In agreement with Nandez and Ivanova (2016), Reichardt et al. (2020) found that including recombination effects leads to a dramatic increase in envelope ejection. The system with the less massive primary star achieved complete envelope ejection, promoted by the release of both helium and hydrogen recombination energy. The model with the more massive primary, unbound more mass, seemingly at the hand of helium recombination energy (see Fig. 14), but the system did not achieve complete envelope ejection, contrary to Nandez and Ivanova (2016). The cause for this discrepancy is the definition of unbound gas (see also Sect. 3.4.1): When including recombination energy in the definition, effectively the entire envelope becomes unbound. If instead only the thermal energy is accounted for, the conclusion is that no more than 37% of the envelope are unbound. Moreover, Reichardt et al. (2020) discussed that while the hydrogen recombination energy may be more readily lost into space, helium recombination energy is much less prone to be radiated away, because it takes place deeper in the envelope, and it is therefore more likely to par-

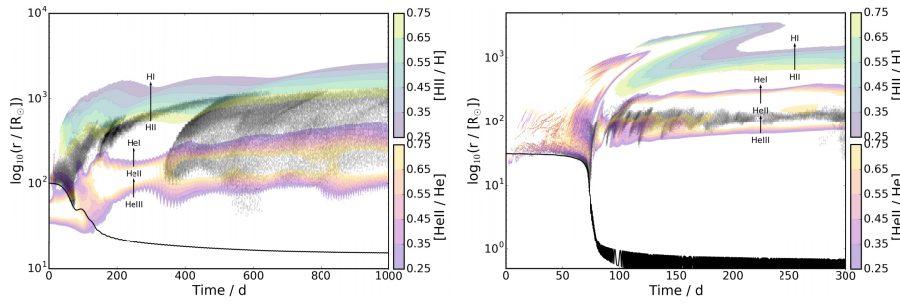


Fig. 14 Correlation between unbinding of gas and recombination zones in the simulations of Reichardt et al. (2020) with a $0.88 M_{\odot}$ (left) and a $1.8 M_{\odot}$ RGB (right). The locations and times at which SPH particles became permanently unbound are plotted in black. The coloured zones represent the partially ionized regions of H and He gas. The black line indicates the distance between the stellar cores. Figure from Reichardt et al. (2020)

take in the envelope ejection. Finally, they pointed out that the formation of dust in the expanded envelope is extremely likely. This could change the game-plan for the interaction. Reichardt et al. (2020) compared their simulations accounting for recombination energy release and assuming its local thermalization to counterparts carried out with an ideal-gas equation of state (that do not account for these effects). They found that the final orbital separation was almost unaffected by the equation of state and by the success of envelope ejection.

An efficient SPH code with parallelization on distributed memory architectures is GADGET2 of Springel (2005). It was originally developed for cosmological simulations and has been applied to simulating CE interaction. Glanz and Perets (2018) pointed out the potential importance of dust formation for CEE based on a simulation with GADGET2. They set up a solar-like star and evolved it to the RG stage ($R_{\star} = 83 R_{\odot}$, core mass $M_{\text{core}} = 0.39 M_{\odot}$) with the MESA code. The CEE with a main sequence companion was then simulated with GADGET2, but Glanz and Perets (2018) give little details about the setup and the numerical treatment. The structure resulting from the CE simulation was compared to the structure of an AGB star and it was concluded that large parts of the envelope meet the conditions for dust condensation.

A similar approach was taken by Glanz and Perets (2021a) to model CEE in binaries with eccentricities of $0 \leq e \leq 0.95$. Primary stars of $1 M_{\odot}$, $4 M_{\odot}$, and $8 M_{\odot}$ were evolved to the RGB stage with MESA (core masses of $0.39 M_{\odot}$, $0.48 M_{\odot}$ and $1.03 M_{\odot}$, respectively), the intermediate-mass model was in addition followed to the AGB stage. The stellar envelopes were mapped to distributions of 250 000 SPH-particles assuming an ideal-gas equation of state, while the cores were represented by point particles. For the mapping, the AMUSE framework of Portegies Zwart et al. (2009) was used and the obtained configuration was relaxed in a damping procedure (Glanz and Perets, 2021b). Companions of $0.6 M_{\odot}$ were added with varying eccentricities to the two lower mass primary star models, while for the high mass model a companion of $2 M_{\odot}$ was chosen. These were modeled as point particles interacting only via gravity. In their simulations, Glanz and Perets (2021a) found that that the initial eccentricities only partially circularize. Because of the closer initial approach

of the cores, more mass was unbound in highly eccentric systems compared to circular setups. However, no matter what setup was used the unbound mass was between $\sim 5\%$ to $\sim 25\%$, typical values for all simulations that use an ideal-gas equation of state.

Glanz and Perets (2021b) later used similar tools to simulate CEE in a triple system in the “circumstellar” case, where a compact binary system (corresponding to the inner binary in a hierarchical triple) orbits in the envelope of a giant. In addition to the construction of the primary star models with MESA and the mapping and relaxation in the GADGET2 computational domain, however, they modeled the dynamics of the binary companion system inside the potential of the primary giant star with the N-body code HUAYNO (Pelupessy et al., 2012), likewise integrated in the AMUSE framework of Portegies Zwart et al. (2009). As models for primary stars, a $2 M_{\odot}$ and an $8 M_{\odot}$ star were evolved to the RG stage (core masses of $0.36 M_{\odot}$ and $1.03 M_{\odot}$, respectively). For mapping these models into the SPH code GADGET2, resolution tests were carried out with 100 000, 250 000, and 500 000 SPH-particles representing the envelope of the giant primary star. For the production runs, Glanz and Perets (2021b) settled to a resolution of 250 000 particles. The masses of the objects in the close binary companion system were set to $0.6 M_{\odot}$ and $0.4 M_{\odot}$ for the lower mass primary star and to $1 M_{\odot}$ for both objects when interacting with the more massive primary star. For the fate of this compact binary system, two cases were observed: a merger inside the envelope of the primary star and a disruption which—together with the core of the primary star—leads to chaotic triple dynamics. In the latter case, typically one of the former close-binary components was found to eventually merge with the core of the primary star, while the second component is ejected or continues “classical” binary CEE. The effect of a compact binary companion system in the case of triple-CE interaction was a slower inspiral and an increased mass ejection—attributed to the extraction of energy and momentum from the compact binary companion. Whereas comparison simulations with classical binary CE setups resulted in ejecting about 10% of the envelope mass (a typical value for simulations assuming an ideal-gas equation of state and not considering ionization effects), the triple systems unbound 11% to 28% of the envelope mass. Glanz and Perets (2021b) commented about the imprints of the altered triple dynamics on the morphology of the ejected material.

Recently, Lau et al. (2022a) carried out an SPH simulation using PHANTOM of a $12 M_{\odot}$ star and companions of $3.0 M_{\odot}$ and $1.26 M_{\odot}$, located at an orbital separation such that the primary just filled its Roche lobe (for their lower-resolved simulations with 50 000 and 500 000 SPH particles) or overfilled the Roche lobe by 25% (for their higher-resolution simulations, two million particles, which would have been unfeasibly long if started farther apart). These simulations were among the first modern attempts to model CE interaction with a massive primary star. Comparisons were carried out using three equations of state: an ideal gas, an ideal gas plus radiation, and a “full” equation of state that included the effects of recombination. The final separation of the binary was of the order of $30\text{--}44 R_{\odot}$ (for the $3.0 M_{\odot}$ companion; the other companion sinks below the sum of the softening lengths of the core and companion, where the interaction is not reliable). Compared to simulations with a simple ideal-gas equation of state, including radiation pressure resulted in separations larger by about 10% and accounting for recombination energy enlarged the final separations

by another $\sim 20\%$. The highest-resolution simulations with the $3.0 M_{\odot}$ companion unbound 18%, 28% and 60% of the envelope for the ideal gas, ideal gas plus radiation, and full equations of state, respectively (using a criterion that accounts for mechanical and thermal energy, see Sects. 3.3 and 3.4.1). The measurement of the unbound mass was taken at a particular point after the inspiral, not at the end of the simulation. The additional unbound gas in the case of the a full equation of state derived from the thermalization of the helium recombination energy, which, even if radiation transport were included, was released in the deep layers and is unlikely to escape. For the full equation of state, three quarters of the envelope were unbound by the end of the simulation and mass unbinding still continued at $0.2 M_{\odot} \text{ yr}^{-1}$, demonstrating that the envelope was likely to become completely unbound.

Finally, Lau et al. (2022b) studied the effects of hydrogen, helium and molecular hydrogen recombination energy on the same structure as that investigated by Lau et al. (2022a). They concluded that helium recombination energy alone, already unbinds 30% more gas than an ideal-gas equation of state and that the delivery of that energy is so deep in the envelope that it is highly likely that the entire payload can be thermalized and eventually converted to work. Somewhat more surprisingly, this is also so for hydrogen recombination energy. Only a fraction of the hydrogen recombination energy is needed to unbind the envelope and the delivery depth is such that, once again, we would conclude that it would be mostly thermalized locally and not escape. For a $12 M_{\odot}$ common envelope it is therefore to be concluded that recombination energy may well help unbind effectively the entire envelope.

6.3.4 Moving-mesh simulations of the common-envelope interaction

In Sect. 4.1.3 we have described the moving-mesh approach to hydrodynamical simulations. Based on its implementation in the AREPO code of Springel (2010a), Ohlmann et al. (2016a) simulated the dynamical inspiral of a $1 M_{\odot}$ companion into a RGB primary star of $2 M_{\odot}$ with a $0.4 M_{\odot}$ core. This rather standard setup was chosen because the scale problems discussed in Sect. 3 are less pronounced with a RG primary than, e.g., with an AGB star. The simulation is illustrated in Fig. 15. It demonstrated the advantages of using a moving mesh approach. The method allowed to follow the evolution for many orbits extending over the initial plunge-in phase into a regime where the orbital separation of the cores changed only very slightly. This was not only enabled by the efficiency of the method but also by its excellent conservation of angular momentum and energy lending credibility to the results even in late stages of the evolution. As discussed in see Sect. 4.4.3, this advantage derived from the almost Lagrangian nature of the scheme. At the same time, the Godunov approach to compute fluxes in the underlying finite-volume discretization facilitated high spatial resolution and captured hydrodynamical instabilities better than SPH methods. This allowed the authors to detect large-scale flow instabilities between adjacent layers of the spiral shock after about 20 orbits that were not noticed in earlier simulations. This effect ultimately lead to turbulent convection in the envelope. The simulation of Ohlmann et al. (2016a), however, failed to unbind the envelope. Only about 8% of the material was ejected. This failure of the gravo-hydrodynamic model triggered the inclusion of additional effects into moving-mesh CE simulations.

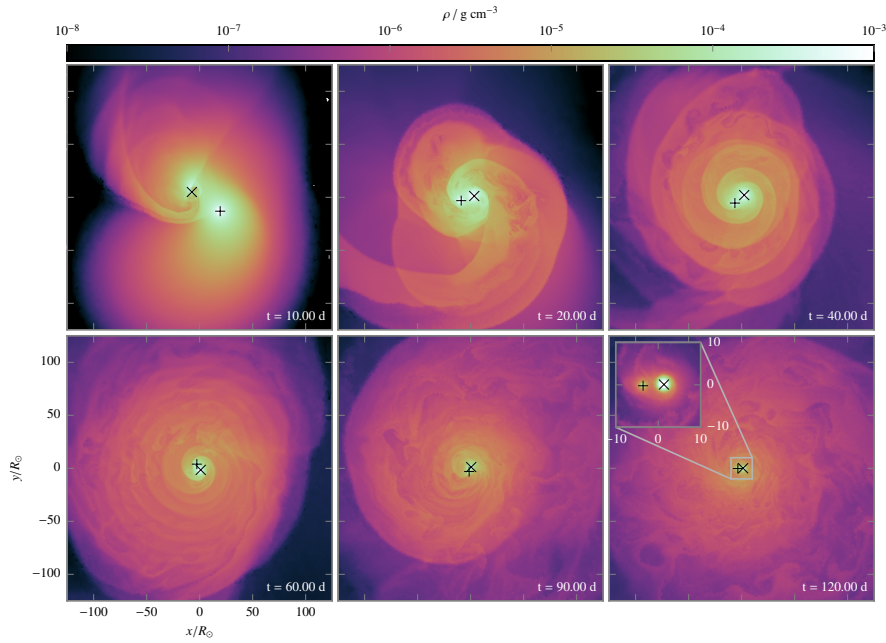


Fig. 15 Time series of density cuts through the orbital plane during the inspiral simulated with the moving-mesh code AREPO. The positions of the core of the **RG** primary star and the companion are marked by a “+” and a “x”, respectively. The inset in the last panel shows the central region with a diameter of about $20 R_{\odot}$. Again, density is color-coded and ranges from 10^{-6} to $10^{-3} \text{ g cm}^{-3}$. Figure from [Ohlmann et al. \(2016a\)](#).

The first **MHD** simulation of **CEE** was carried out by [Ohlmann et al. \(2016a\)](#). It showed that tiny initial magnetic fields are strongly amplified in the evolution. While previous studies speculated about dynamo processes in the differentially rotating envelope ([Regős and Tout, 1995](#)), magnetic field generation in an accretion disk formed from a tidally disrupted companion ([Nordhaus et al., 2011](#)), or in the outer layers of the degenerate core ([Wickramasinghe et al., 2014](#)), the simulation of [Ohlmann et al. \(2016a\)](#) allowed to settle the issue by a direct simulation of the entire **CE** structure. Three stages of magnetic field amplification could be distinguished (see [Fig. 16](#)):

- (i) In the initial plunge-in of the companion into the primary’s envelope, a fast amplification of the magnetic field in the forming accretion stream around the companion was observed.
- (ii) Once this accretion stream had been established, the amplification slowed down.
- (iii) Eventually, the magnetic field saturated and was dispersed over the envelope.

The magnetic field amplification in the accretion flow was found to be consistent with the action of the magnetorotational instability (MRI, [Balbus and Hawley, 1991](#), [Balbus, 1995](#)). The observed generation of strong magnetic fields during the dynamical **CE** phase is an interesting effect and may contribute to shaping the expected formation of a planetary nebula. However, the resulting fields are too weak to have a dynamical impact on the **CEE** itself or to alter the transport of angular momentum

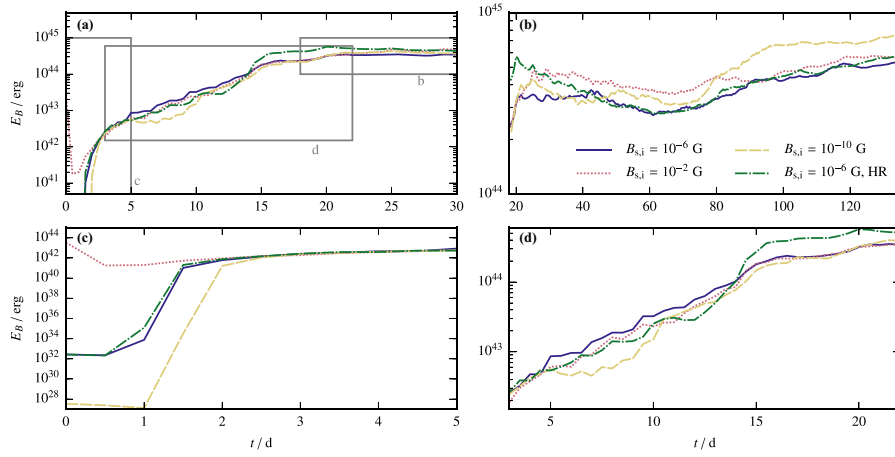


Fig. 16 Magnetic field energy in the **CE** simulation of [Ohlmann et al. \(2016b\)](#). The three stages of the amplification process are marked in panel (a). Panel (c) zooms in on the fast amplification phase (i), the slow amplification phase (ii) is shown in panel (d) and the phase of saturation (iii) is shown in panel (b), where the initial surface fields are given. Figure from [Ohlmann et al. \(2016b\)](#)

significantly. In the setup of [Ohlmann et al. \(2016b\)](#), the envelope-mass loss exceeded that in non-MHD simulations with identical parameters only by a few percent.

As discussed before, additional physical processes have to be considered to achieve envelope ejection. One of the most promising effects for unbinding envelope material that is ignored in the basic gravo-(magneto)hydrodynamic **CE** model is the release of ionization energy when the envelope gas expands and recombines ([Nandez et al., 2015](#); [Nandez and Ivanova, 2016](#)). This effect has been implemented in **CE** simulations with moving mesh codes ([Ohlmann, 2016](#); [Prust and Chang, 2019](#)).

[Prust and Chang \(2019\)](#) used the moving-mesh hydrodynamics code MANGA to simulate **CEE** in setups similar to that of [Ohlmann et al. \(2016a\)](#). In one of their models, 95% initial co-rotation of the primary star’s envelope with the companion was assumed while a second simulation was started with a non-rotating primary star. Instead of assuming an ideal-gas equation of state, they used the MESA equation of state ([Paxton et al., 2011](#)) to include ionization effects (see Sect. 4.2). Compared with the simulations of [Ohlmann et al. \(2016a\)](#), a significant increase in unbound envelope material ($\gtrsim 60\%$) was observed.

An interesting new feature in modeling methods was introduced by [Prust \(2020\)](#). Moving-mesh hydrodynamics codes allow for moving boundaries inside the simulated domain ([Springel, 2010a](#)). As a proof-of-concept, [Prust \(2020\)](#) embedded the companion in a **CE** simulation in a sphere of $4R_{\odot}$ surrounded by a reflective moving boundary condition. This paves the way to an improved modeling of accretion or mass outflow around the companion object.

[Sand et al. \(2020\)](#) followed **CEE** in systems with a $1.0 M_{\odot}$ early-AGB primary star and companions of different masses. This was a step towards a computationally more challenging scenario, because the spatial scale range widens compared with systems involving **RG** primaries. Moreover, stabilizing the more loosely bound **AGB**

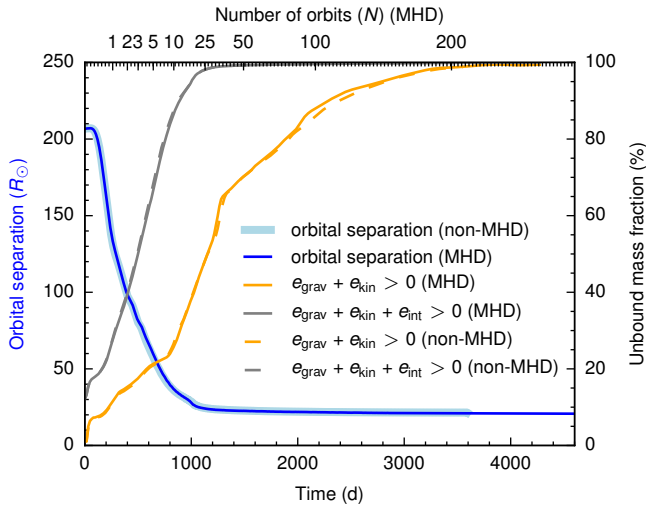


Fig. 17 Orbital separation and unbound mass fraction measured according to the criteria given in the legend for CE simulations with a $0.970 M_{\odot}$ AGB primary star and a $0.243 M_{\odot}$ companion. Magnetohydrodynamic simulations are labeled with “MHD” while “non-MHD” indicates pure hydrodynamical models. Figure from Ondratschek et al. (2022).

envelope required an increased spatial resolution of the region around the core of the star. Despite the less tightly bound AGB envelope, Sand et al. (2020) found that envelope ejection in the basic gravo-hydrodynamic model fails, but the inclusion of recombination effects render a complete envelope ejection likely—at least under the assumption of local thermalization of the recombination energy.

The efficiency of moving mesh approaches to simulate CEE has been exploited to explore the parameter space of models and we give two examples here. Sand et al. (2020) tested the effect of different ratios between the mass of an AGB primary star and that of the companion on the mass loss rate and the final orbital separation. Less massive companions were found to spiral deeper into the CE and Sand et al. (2020) proposed a linear relation between the mass ratio and the orbital separation at the end of dynamical inspiral. Envelope ejection was found likely to be complete under the above-mentioned assumption of local thermalization of recombination energy. Kramer et al. (2020) addressed the question of whether hot sub-luminous B-type (sdB) stars can form from CE interaction of primaries close to the tip of the RG branch with light companions as suggested by observations (e.g. Geier et al., 2011; Schaffenroth et al., 2014, 2015). They conjectured that down to the regime of brown dwarfs such a formation scenario is likely to work; whether or not envelope ejection can be triggered by a much less massive companion, such as a planet, remains to be explored in more detail although the simulations of Kramer et al. (2020) indicated that this may be hard.

A shortcoming of all recent CE simulations that include ionization effects—whatever method was used for modeling the fluid dynamics—was that the evolution could only be followed for a rather short period of time. At termination, not all of the

ionization energy was released by recombination effects. Therefore, while including the ionization energy in the energy budget to determine unbound material indicated successful envelope ejection in the case studied by Sand et al. (2020), it remained to be proven that recombination indeed releases this energy so that it is converted into kinetic energy. This was achieved by Ondratschek et al. (2022), who were able to follow one of the systems modeled by Sand et al. (2020) to a stage where the energy conversion was completed. They found that—under the assumption of local thermalization of recombination energy and no radiative losses—complete envelope ejection was indeed reached, see Fig. 17. In contrast to Sand et al. (2020), however, the simulations of Ondratschek et al. (2022) included magnetic fields. Confirming the results of Ohlmann et al. (2016a), and as illustrated in Fig. 17, they found that although a weak initial field is strongly amplified during plunge-in of the companion, the magnetic field strength remains dynamically unimportant for envelope ejection. In the very late stages of CEE a new phenomenon was observed. As the stellar cores came very close, mass transfer between them initiated and the resulting structure resembled a contact binary system. This led to a second phase of strong magnetic field amplification. In the resulting structure, a high-velocity jet-like outflow was launched. This magnetically-driven outflow was directed in polar direction of the orbital system and low-density, high-velocity material propagated along the chimney-like hole in the ejected CE material perpendicular to the orbital plane. While this material had velocities of $\sim 10 \text{ km s}^{-1}$, the polar outflow reached $\sim 100 \text{ km s}^{-1}$. The resulting structures and the two velocity components of the gas resemble observations of bipolar PNe (see Sect. 7.6.1).

The first moving-mesh 3D magneto-hydrodynamic simulations of CEE of objects with masses typical for neutron stars or black holes with a massive star were presented by Moreno et al. (2021). For the primary star model, a $10 M_{\odot}$ star was evolved with MESA to the red supergiant stage. The choice of this mass was motivated by the numerical challenges introduced by massive stars when represented in CE simulations. Therefore, a massive star at the lower end of the range of masses still capable of producing a neutron star at the end of its evolution was chosen. Moreno et al. (2021) demonstrated that with the setup procedure of Ohlmann et al. (2017) it is possible to construct a sufficiently stable model for a primary star in CE simulations. CEE was followed with the AREPO code and the stellar cores were represented by point masses. Assuming local thermalization of the released recombination energy, nearly complete envelope ejection seemed possible for the considered systems. The orbital separation at the end of the simulations, however, was too large to allow for a gravitational-wave induced merger of the eventually resulting double compact system. Moreno et al. (2021) argued that for a favorable alignment of the expected supernova kicks, some of the systems may still qualify as progenitors of gravitational-wave emitting mergers of double neutron stars.

7 Conclusions and future perspectives

7.1 Where do we stand?

3D hydrodynamic simulations of CEE have seen a rapid improvement over the past decade. But still, these simulations are insufficient to answer fundamental questions and thus they only mark the beginning of a deeper physical understanding of CE interaction.

What can potentially be learned from 3D hydrodynamic CE simulations? For given initial parameters of the pre-CE binary systems, the ultimate questions to CE modeling are:

- (1) How much of the envelope gas is ejected?
- (2) What is the final separation of the core binary in case it has not merged?

If the stellar cores merge or the companion is destroyed, the long-term evolution of the remnant object poses an additional question. Certainly, 3D hydrodynamic approaches are a prerequisite to finding answers, but can we settle the questions with the currently available simulations?

Regarding Question (1) the situation seems rather optimistic. As discussed in Sects. 3.3 and 6, when including the ionization energy released in recombination processes and assuming that it thermalizes locally, envelope ejection seems plausible for many of the studied systems. It also seems likely, however, that in certain regions of the parameter space, envelope ejection still fails. Even if all of the recombination energy can be used to support envelope ejection, there may be cases where this energy is still insufficient to unbind the entire CE—especially for high-mass primary stars (Kruckow et al., 2016). Moreover, Sabach et al. (2017), Grichener et al. (2018) and Soker et al. (2018) questioned the validity of the assumption of local thermalization and argued that instead recombination energy may be transported away by convection (Wilson and Nordhaus, 2019, 2020) or radiation. However, Ivanova (2018) estimated that the amount of hydrogen recombination energy lost by these processes was negligible. Convection is in principle part of the basic gravo-hydrodynamic model of CEE. The question is whether it is sufficiently resolved in the simulations. At least moving-mesh hydrodynamics schemes (Ohlmann et al., 2016a; Ohlmann, 2016; Prust and Chang, 2019; Sand et al., 2020) seem capable of reproducing convective flows. However, radiation transport is usually not accounted for. Sand et al. (2020) estimated that in their setup, most of the ionized material remains well inside the photosphere for most parts of the CEE, but ultimately the question of how much of the recombination energy can be used to eject the envelope material has to be answered by simulations that model radiation transfer. In summary, the answer to Question (1) is challenged by potentially missing physical effects and not primarily by numerical problems or deficiencies in the model setups, although Reichardt et al. (2020) show that a smaller softening length of the potentials around the stellar cores alters the rate at which mass is unbound.

The effects determining the orbital evolution of the system during the rapid inspiral phase—Phase (ii) of our classification, but not in the later CEE in Phase (iii)—are also implemented in current models. Some part of the pre-CE evolution, the ac-

tual plunge-in phase of CEE and several hundred orbits of the inner core binary following it are accessible to 3D hydrodynamic simulations. However, we suspect that the period of time immediately after these 3D simulations—perhaps up to the thermal timescale—may be critical to the parameters characterizing the binary (or the merged object) later. Iaconi et al. (2017b) summarized final orbital separations obtained global hydrodynamic simulations of CEE and found that they are commonly too wide compared with observations of post-CE binary systems. This points to additional physical processes (see Sect. 3.3) that follow the simulated dynamical inspiral of the companion into the primary star and the first few hundred orbits, i.e. in Phase (iii) of our classification. Bound gas in the outer parts of the envelope may re-contract on thermal timescales leading to an increase of the drag force, further inspiral, and more unbound envelope material. This could proceed in cycles or as a slow process that is regulated by the energy transport rate through the remaining envelope material (see Sect. 3.3). On the other hand, returning envelope gas has high specific angular momentum, which could change the orbital separations in Phase (iii) drastically (Kurwita et al., 2016). It is also possible that once a certain orbital separation is reached, one or both of the cores start to overflow their Roche lobes. These additional mass transfer episodes would again alter the orbital separations. It therefore seems likely that the final orbital separation is not only set by the dynamics in Phase (ii) but also affected by Phase (iii) of our classification in Sect. 1.3. *But-hic sunt dracones*—this is territory that is difficult or impossible to access with multidimensional hydrodynamic simulations (see Sect. 3.3). In Sect. 7.4, we discuss how 3D hydrodynamic simulations need to be interfaced with simulations able to model longer timescales, including the future evolution of the star(s). As for answering Question (1), we again encounter the problem that not all physics deciding about Question (2) may be included in 3D hydrodynamic CE simulation.

Before extending our models, however, we need to have confidence in the parameters at the end of the 3D hydrodynamic simulations. It has to be determined why the plunge-in phase ceases in 3D simulations, giving rise to the subsequent phase that takes place on longer timescales. Regardless of whether or not the separation at the end of Phase (ii) is the actual final separation, we need to understand whether the slow-down of the inspiral, temporary as it might be, is in fact physical. A simplified view is to assume complete envelope ejection so that there is no matter left behind and the drag forces acting on the cores cease. But the 3D hydrodynamic simulations discussed in Sect. 6.3 show a different picture (e.g. Iaconi et al., 2018): Envelope ejection—if successful—happens rather late in the evolution, when the expansion of the envelope leads to the release of recombination energy that ultimately unbinds the material (Nandez et al., 2015). At this stage, however, the orbital evolution has already slowed down. But still, the orbital volume is usually not completely devoid of gas, though the density has decreased. It is therefore not the evacuation of the orbit that slackens the inspiral. As discussed in Sect. 3.3, other effects may contribute to reduce the drag: towards the end of the inspiral, the relative motion between cores and gas becomes very subsonic, for which the formalisms of Bondi (1952), Ostriker (1999), and Kim and Kim (2007) predict a drastic reduction of the drag force. Ultimately, co-rotation may be re-established between the core binary and the surrounding envelope gas, particularly for the more massive companions. This would

decrease the drag force dramatically. But for tighter orbits, stronger drag is needed to change the orbit appreciably: As the cores approach each other, their mutual gravitational attraction becomes stronger. This force is what sets the orbital separation and only a drag force on the same order of magnitude would lead to a change in orbital separation. This becomes ever more unlikely in the late stages of the evolution.

While these reasons plausibly justify the end of the inspiral, there is still the concern that the representation of the stellar cores as point particles and the softening of the gravitational potentials impact the simulated orbital separation. We could assume that, while the core region is undisturbed, the simulation of the central part of the star is reasonable. Even so, we do worry that once the envelope has expanded and the core and companion are near one another, the structure of the flows may be non-physical. The mass adopted for the particle representing the core of the primary star is somewhat arbitrary. Even with the rather controlled approach suggested by [Ohlmann et al. \(2017\)](#), a certain cut radius has to be defined, that is often chosen to be equal to the gravitational softening length of the core particle. Towards the end of the simulations, the stellar cores may have come so close that the softened regions overlap and this may compound any specific problem. Moreover, the physical modeling of cores as point masses raises other concerns. For example, they accumulate material in their vicinity which travels with the point masses. This material could in reality be accreted onto the cores under the release of energy. Certainly, the effects that these choices have on the final orbital separation call for further study.

7.2 Missing physical effects

As discussed in Sect. 3.1, simulations carried out thus far show that the CE can only be ejected if recombination energy is utilized to do mechanical work, i.e. expand the envelope as opposed to being convected and radiated away. Thus, one of the most urgent questions to CE modeling is to test whether this assumption is justified. Estimates based on 1D stellar structure models ([Ivanova, 2018](#)) and on the optical depth at which recombination energy is released in 3D hydrodynamic CEE simulations ([Reichardt et al., 2020](#); [Sand et al., 2020](#); [Lau et al., 2022a](#)) seem to support this mechanism to aid CE ejection. But for a solid conclusion, radiation transport in the envelope gas has to be modeled. The other mechanism to drain energy from its location of release by recombination—convection—is part of the fundamental gravo-hydrodynamic model and therefore readily included provided a careful preparation of the setup. While its proper representation is a challenge to the numerical methods and the spatical resolution reached in the simulations, radiation is an additional physical process that has to be modeled explicitly. Introducing a radiation transfer model into CE simulations would not only help to determine the contribution to envelope ejection by recombination effects, but it would also allow a more accurate localization of the photosphere and therefore improve predictions of optical observables from CE events. Moreover, for simulations of CEE with very massive primaries, the setup requires to include radiation in order to properly represent the structure of these stars ([Ricker et al., 2019a](#)).

The energy transport by radiation depends critically on the opacity of the material it passes through. Here, effects can play a role that extend beyond the ionization structure which is usually followed in simulations accounting for recombination energy release. Dust potentially forming in outer layers of the ejecta (Clayton et al., 2017, Glanz and Perets, 2018, Reichardt et al., 2020, Iaconi and De Marco, 2019, and Iaconi et al., 2020) would increase the opacities dramatically. Therefore, models of dust formation are another important ingredient to reaching a comprehensive physical modeling basis for CE simulations.

Magnetic fields have been introduced into CE simulations, where strong field amplification is observed (Ohlmann et al., 2016a). Their dynamical effect remains negligible, but they potentially contribute to the shaping of planetary nebulae (e.g. García-Segura et al., 2020; Ondratschek et al., 2022). It is also possible that magnetic activity favors dust formation as has been suggested for AGB stars (Soker, 1998c; Rapoport et al., 2021).

Additional physical effects concern the vicinity of the companion and the primary core, as well as their structure. Related processes include accretion to or perhaps mass loss from the bound cores, accumulation of material in their vicinity, and mass transfer episodes between the remaining cores following the initial dynamical CE phase. Some low-mass companions such as planets may dissolve in the envelope gas (e.g., Staff et al., 2016b). If the companion star is very compact, for example a neutron star, densities close to it may reach values where nuclear burning and neutrino processes become important; in the case of black holes potentially even effects of general relativity.

7.3 Unresolved numerical problems

The future challenge to improvements of the numerical approaches is the same as today: dealing with the scale problems in both time and space will persist as the main difficulty for CE simulations. The timescale challenge applies in particular to Phases (i) and (iii) of our classification. As discussed in Sect. 3.5, processes in these phases may take place on longer timescales than those accessible to 3D hydrodynamic simulations. This may pertain to some restructuring of gas remaining bound to the cores that involves radiation processes and acts on the thermal timescale, but it may also be caused by minute changes on dynamical timescales whose cumulative effects after very many orbits may determine, e.g., the onset of CEE or the final orbital separation of the remnant core binary.

The spatial scale problem mainly concerns the region around the cores and the cores themselves. While for special progenitor systems a (marginal) resolution of companions may be possible, this problem prevents a direct modeling of the detailed effects in the vicinity of the cores. Yet, for reaching the next level of numerical modeling, the details of the evolution of the cores and their interaction with the immediate surroundings are of primary interest, see Sect. 7.2. These processes, however, are out of reach for common numerical techniques and available computational resources (see Sect. 5.1). Resolving the core of the primary spatially may become possible if the timescale problem is alleviated. For this, a parallelization in the time domain,

i.e. in the time level hierarchy instead of a spatial domain decomposition, is a potential future direction. For the time being, however, the barrier towards resolving the cores cannot be overcome, and thus the advantage gained from a modest increase in spatial resolution of the envelope remains limited. The focus of current simulations lies instead on determining the main “global” quantities, such as orbital separation between core and companion and mass ejection. For these, numerical convergence can typically be established at a moderate number of discretization elements (some 10^6 grid cells or particles). There is, however, the prospect of using subgrid-scale models to capture at least some of the missing effects. Accretion, for instance, can be represented by sink particles similar to those used in star formation simulations (e.g. [Krumholz et al., 2004](#); [Chamandy et al., 2018](#)).

In current and in future models, establishing the convergence of the simulation results is an important issue. While for the setup, hydrostatic equilibrium provides a well-understood reference to compare with, it is less clear what resolution is needed in later phases of the evolution at different locations. Due to the exploding computational costs, a global increase of the spatial resolution seems little promising and may not be necessary. Adaptive mesh refinement techniques can concentrate resolution to regions where it is needed for reaching convergence. The task in the near and mid-term future is to figure out what regions matter and what resolution needs to be reached in them for convergence.

Another potential problem for **CE** simulations are conservation properties. In principle, the applied finite-volume and **SPH** schemes conserve energy. In addition, **SPH** conserves angular momentum by construction. Moving-mesh codes are nearly-Lagrangian and inherit this property to good accuracy. For Eulerian codes, **AMR** provides the required resolution for reaching acceptable conservation of angular momentum. Still, simulations of global **CEE** require to follow hundreds of orbits and errors may accumulate.

A fundamental problem for all numerical approaches arises from the coupling between hydrodynamics and gravity as an external force which enters the equations as a source term. Even with the approximate schemes discussed in Sect. 4.3 gravity itself can be calculated to any desired precision, so it does not by itself constitute an unavoidable error source. But it is discretized in a different approach than the hydrodynamic quantities and tiny mismatches lead to accumulating energy errors. After a large number of orbits this error may be on the same order of magnitude as the binding energy of the non-expelled gas and it is therefore difficult to judge the success of envelope ejection. As mentioned in Sect. 5.3, in setups close to hydrostatic equilibrium, well-balancing methods improve on this issue (e.g. [Edelmann et al., 2021](#)), but the lack of a clear reference state renders such approaches less promising in the context of the dynamical core–envelope interaction.

7.4 Interfacing 3D global simulations with 1D simulations of the common-envelope remnant

A promising avenue to understand what happens *after* the dynamical **CE** inspiral phase is interfacing **3D** hydrodynamic simulations to **1D** hydrostatic or hydrody-

dynamic time-implicit codes that can evolve the remnant much further in time. This is not an easy project for a number of reasons. The first is that the post-CE object may be non-spherical and deciding how to map it into a 1D configuration is non-trivial. The second problem is that the dynamic and thermodynamic structure of the object may not be a good fit for the 1D code. Nonetheless, the work of Munson et al. (2021) provides some guidance in this direction.

In a thoughtful paper, Ivanova and Nandez (2016) compared a 1D model of the inspiral with a 3D model. While the goal was to determine how to interface a 3D inspiral model to a 1D, longer-timescale post-inspiral model, the paper actually also discusses 1D simulations of the *entire* common envelope. They encountered a number of problems which they catalogued, together with recommendations for further efforts of this type. For example, the structure of the envelope during inspiral is quite different, as shown in Fig. 18, where the difference between the potential of the 1D and 3D inspirals is plotted as a function of time and location. They recommend that if the fast inspiral phase is to be modelled in 1D, kinetic energy should be injected instead of heat into the 1D model envelope to simulate the deposition of energy and angular momentum due to orbital decay. This is preferable because injecting released orbital energy into heat alters which layers of material release ionization energy in recombination processes, which has a strong effect on the envelope dynamics. An important point made by Ivanova and Nandez (2016) is that while modelling the inspiral in 1D is difficult at best, modelling the inspiral in 3D and then mapping to 1D for the post-inspiral phase also presents some serious problems when trying to interface the two simulations. This said, interfacing 3D and 1D models is an active research area with some success for the cases of main-sequence star mergers (Schneider et al., 2019, 2020) and mergers between white dwarfs (Munson et al., 2021). While the future will no doubt see sophisticated 3D hydro simulations, it is likely that short- and intermediate-term progress will have to rely on the ingenuity of the researchers in combining different computational tools.

If the binary is definitely going to survive and the envelope is mostly or fully ejected by the end of the simulation, then mapping the ejected envelope gas into a 1D code may pose additional challenges. Disks may form with certain properties that may contribute to change the orbital parameters towards the “final” orbital separation. It would be difficult to have a thorough self-consistent simulation of this phase, but it is possible that its parts may be addressed separately. For example if the parameters of the disk could be extracted, then it might be possible to determine its impact on the inner binary (Kashi and Soker, 2011).

7.5 Deriving parametric CE prescriptions from 3D simulations

A practical goal of simulating the CE interaction is to derive simple analytic parametrizations that can be used in population synthesis studies. Classical approaches are the α_{CE} and the γ formalisms discussed in Sect. 2.1. The values of the involved parameters, or—in more sophisticated approaches—the functional dependence of their values on stellar and system characteristics, has been investigated extensively with a range of techniques. How can 3D hydrodynamic simulations improve on this?

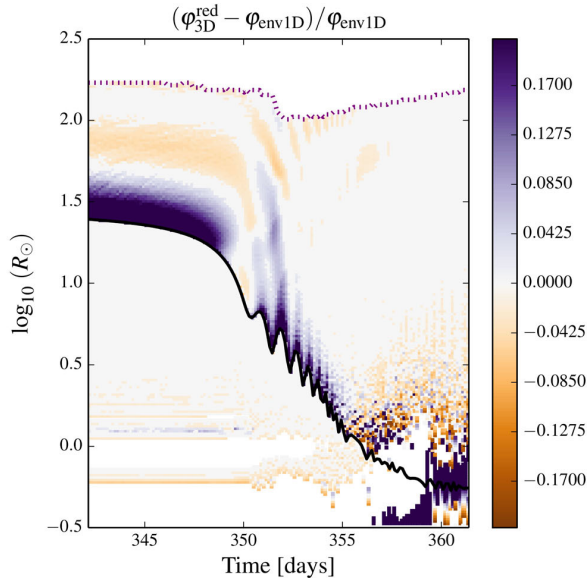


Fig. 18 Comparison of the gravitational potentials in the 1D (φ_{env1D}) and 3D ($\varphi_{3\text{D}}^{\text{red}}$) approaches. The difference is color-coded and shown as a function of radius and time. The solid black line indicates the location of the companion and the dashed purple line marks the surface of the envelope intended as the outer boundary of bound gas. Figure adapted from [Ivanova and Nandez \(2016\)](#).

If we are to use global 3D hydrodynamic simulations to derive parametric descriptions of successful CEE, three requirements must be met:

- (1) The 3D hydrodynamic simulations must be converged and include all effects that determine the quantities to be parametrized.
- (2) Arguably, the envelope must be mostly or even fully unbound.
- (3) A suitable parametric model has to be identified that is able to capture the functional dependencies that determine the quantities.

None of these issues is resolved yet. Determining whether convergence has been reached is difficult. Even if the envelope was fully unbound and requirement (2) is met, one wonders whether the recombination energy, which ultimately unbound the envelope should be fully thermalized, or whether some of it should have escaped into space. Fulfilling requirement (1) is even more challenging. Changes to the orbital parameters take place in the post-CE phase on longer timescales and modeling such effects is outside of the capabilities of 3D time-explicit hydrodynamic approaches. Also requirement (3) poses questions: In the context of the parametrization given by Eqs. (1)–(3), should the orbital energy term on the right hand side of Eq. (1) be accompanied by a recombination energy term, and should there be more than one efficiency parameter to accompany these two energy sources? Or should the recombination energy, together with thermal energy be included in the envelope’s internal energy, and used on the other side of Eq. (1), that quantifies the binding energy of the envelope? In any choice and consideration, there are many approximations and caveats.

An early attempt to derive the parameter α_{CE} defined in Eq. (1) from 3D hydrodynamic simulations of CEE was made by Sandquist et al. (1998, 2000), despite the fact that their models failed to unbind the envelope and therefore violated requirement (2). In order to circumvent this problem, they only considered the *change* in binding energy defined as the initial binding energy of the giant minus the value at the end of their simulation. In doing so, they presumably included potential and thermal energy in their binding energy calculation.

Ivanova and Nandez (2016) carried out a similar calculation using some of the first 3D global simulations to successfully eject the envelope and meeting requirement (2). They derived values for $\alpha\lambda$ according to Eqs. (1) and (3) from their simulations of CEE with RGB primary stars. Sand et al. (2020) carried out a similar analysis, but they differentiated the two cases where only potential energy is included in the value of the binding energy, and the case where the full internal energy (including recombination energy) is accounted for. This way, they chose an agnostic approach with respect to requirement (3) and calculated the values of λ and α separately for the two cases. When only considering gravitational potential energy in the binding energy of the envelope, they found $\alpha_{\text{CE}} > 1$ which—rather unsurprisingly—implies more than the orbital energy has been used to unbind the envelope.

Lau et al. (2022a) carried out an additional exercise. They took advantage of the fact that they had carried out a CE simulation between a $12 M_{\odot}$ red supergiant and a companion using three different equations of state: ideal gas, ideal gas plus radiation and an equation of state that additionally accounts for ionization energy. From these they could calculate three different α , one to quantify the fraction of orbital energy used to unbind the envelope, the second to quantify the fraction of thermal energy used to unbind the envelope and the last to quantify the fraction of recombination energy used to unbind the envelope. It is still to be seen whether these considerations have any universal significance.

Iaconi and De Marco (2019) attempted to reconcile information from all simulations known at the time with observation of single-degenerate binaries, just to demonstrate how very complex the topic is. As discussed in Sect. 7.1, the uncertainty of the final orbital separation determined from 3D hydrodynamic CE simulations hampers these efforts.

7.6 Constraining CE simulations with observations

How can the results of 3D hydrodynamic simulations be connected to astronomical observations? What can we learn from such a connection? Is it possible to constrain models of CEE from observations? To discuss these questions, we distinguish between observations of stars, binary systems, and PNe, whose parameters can directly or indirectly be compared with CE simulations, and observations of transient events that are associated with systems in the act of undergoing a CE interactions.

7.6.1 Observations of stars, binaries and PNe that constrain CE simulations

We know of a number of close binary classes that must be post-CE systems because one or both of the objects in the binary must have been much larger in the past than the orbit is today. The simplest objects of this type are those where the companion is a low mass main sequence star, while the primary is usually a white dwarf remnant of the giant star or a helium-burning, horizontal branch star. There are two types of giant producing the observed remnants: RGB and AGB stars. In the first case, the post-CE remnant tends to be a core-helium burning, horizontal-branch star, almost always classified as a subdwarf B or O (sdB or sdO) or it can be a helium white dwarf, often of lower mass. In the second case the remnant is a carbon-oxygen white dwarf. In most cases, it is not known whether the primary of the CE event was an RGB or an AGB star; however, if the binary is in the middle of a planetary nebula, we can be *almost* certain that the giant was recently on the AGB (there is only a handful of planetary nebulae for which the central star can be shown to be a post-RGB star; see Jones, 2016).

These post-CE binaries are used to constrain the post-CE separation of the remnant core system if we assume that today's separation is the same as that at the end of the CE interaction. In some cases one can compensate for the fact that the binary may have suffered additional orbital reduction due to magnetic braking or gravitational wave radiation (e.g., Schreiber and Gänsicke, 2003). If the mass of the primary is known, one can derive the mass and the radius of the giant at the beginning of the CE phase, with some assumptions and moderate uncertainties (e.g., Zorotovic et al., 2010; De Marco et al., 2011). This reconstruction allows one to estimate the parameters of the pre-CE system, which, together with the observed post-CE systems parameters, gives a value for α_{CE} in the energy formalism described in Sect. 2.1. In practice, this method is fraught with uncertainties and assumptions, and there is a rich literature of what can and what cannot be derived from it (see Iaconi and De Marco, 2019, for a review).

Another type of post-CE binary that recently gained increased attention are sdB or white dwarf stars orbited by very low mass companions, most often brown dwarfs, but possibly even massive planets. There are approximately a dozen systems with companions in the mass range of $0.027\text{--}0.07 M_{\odot}$ (Schaffenroth et al., 2014; Casewell et al., 2018). The primary question arising from these observations is how such low mass companions can have escaped merging with the primary in the CE interaction. As discussed in Sect. 6.3.4, Kramer et al. (2020) performed 3D hydrodynamic CE simulations of such systems. They concluded that if the companion is more massive than $\sim 0.05 M_{\odot}$, it can successfully eject the envelope of a primary star with a main sequence mass of $1 M_{\odot}$ evolved to the tip of its RGB. If the mass of the companion is between 0.03 and $0.05 M_{\odot}$, partial ejection may take place, while below $0.03 M_{\odot}$, only a small fraction of the envelope is ejected. This is consistent with the observations of sdB stars, but the final orbital separations measured at the end of the simulations of Kramer et al. (2020) are too large compared with the observations.

Iaconi and De Marco (2019) compared a number of CE simulations to observations of post-CE binaries such as the ones just described, where the companion is a main sequence star and the primary is either an sdO, sdB (O and B, post-RGB,

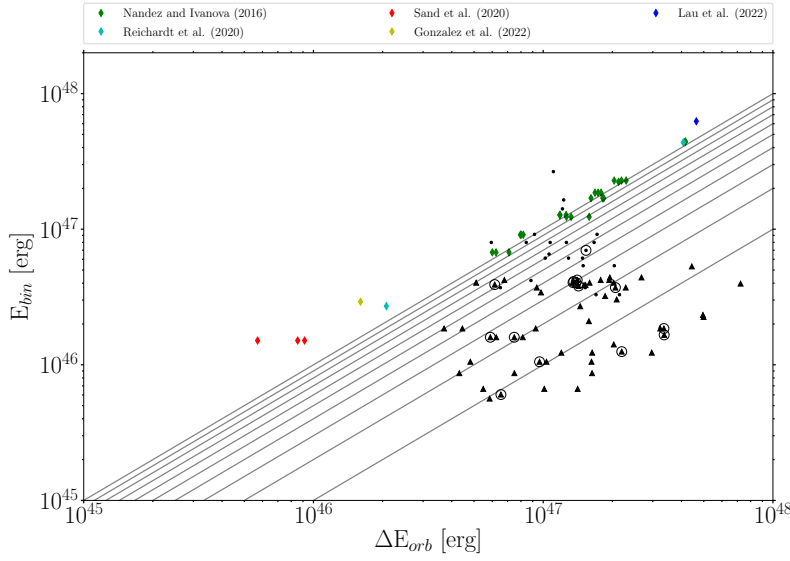


Fig. 19 A comparison of simulations (coloured symbols) and observations (black symbols; dots: post-**RGB** post-**CE** binaries; triangles: post-**AGB** post-**CE** binaries; with circles: a planetary nebula surrounds the binary), in the delivered orbital energy vs. binding energy plane. The binding energy is that of the giant star at the time of the **CE** interaction and includes potential and thermal energy. The solid lines denote α values from 1 to 0.1 (top to bottom).

core helium burning stars) or a white dwarf. They analyzed post-**CE** separations as a function of pre-**CE** system parameters, such as the mass ratio between primary star and companion and the binding energy of the envelope of the pre-**CE** giant. Unfortunately most of the simulations available at that time did not unbind the envelope, making the simulated final separations upper limits. In Fig. 19 we show an updated figure mimicking what was presented by [Iaconi and De Marco \(2019\)](#) in their Figure 3. Here we only use simulations that eject the entire **CE**. The simulations by [Sand et al. \(2020\)](#) and by [Gonzalez-Bolivar et al. \(2022\)](#) used an **AGB** primary, those of [Lau et al. \(2022a\)](#) used a massive red supergiant, while the other adopted low mass **RGB** stars.

Figure 19 shows that the α parameters derived from simulations are approximately unity (most simulations are even in the $\alpha > 1$ region, throwing some doubt on the virtue of the formalism itself; for a discussion see [Lau et al., 2022a](#)). Moreover, as also observed by [Iaconi and De Marco \(2019\)](#), there seems to be a systematic difference between post-**RGB** and post-**AGB** observations, but the simulations, in particular those with **AGB** primaries, have far wider separations than the observations. With the exception of the **RGB** simulations of [Nandez and Ivanova \(2016\)](#) that fall on the same region as the post-**RGB** observations, the post-**AGB**, post-**CE** binaries with their extremely compact orbits, are not reproduced by simulations.

Other post-**CE** systems, such as close white dwarf binaries—sometimes referred to as *double degenerate systems*, or high- and low-mass X-ray binaries are too com-

plex to provide useful constraints: Double degenerate systems went through two episodes of mass transfer, that could have been two common envelopes. [Nelemans and Tout \(2005\)](#) wrote extensively about the ambiguity of the evolutionary path in these cases. X-ray binaries consist of a low- or high-mass giant that transfers mass to a neutron star or a black hole, hence an object that derives from a core-collapse supernova whose effect on the binary is very difficult to predict. These systems must have gone through a **CE** but the uncertainties in their evolution leave us with constraints that are even weaker than those obtained from lower-mass systems discussed above.

An alternative approach to constraining **CE** simulations is given by the analysis of the **PNe** around post-**CE** binaries. At least one in five **PNe** is formed in **CE** interaction; possibly quite a bit more ([Miszalski et al., 2009](#); [Jacoby et al., 2021](#)). The shape of the nebula is likely not only carrying the blue print of the interaction, but also guarantees that the **CE** interaction took place in the immediate past of the object, or else the nebula would have dispersed (**PNe** cannot be seen for much longer than 50 000 years after ejection, and usually are quite a bit younger than that). The shapes of **PNe** around post-**CE** systems were already studied in the 1990s ([Bond et al., 1992](#)), and [De Marco \(2009\)](#) showed that there is a diversity of morphologies even around relatively similar binaries. The immediate conclusion is that there must be a diversity of interactions. Elongated or bipolar morphologies are often observed in remnants of interacting systems such as V838 Mon or Nova 1670 (CK Vul; [Kamiński et al., 2021](#)) and can possibly interpreted as a result of jets or collimated outflows. Such mechanisms potentially contribute to the shaping of **PNe** (e.g. [Corradi and Schwarz, 1995](#); [Soker, 1998a, 2004b,a](#)). It is suggestive that shapes of post-**CE** remnants are a sensitive probe of the details of the interaction.

Pre-**CE** interaction and potentially also jets around the companion in the early inspiral phase may be important for the morphology of **PNe** (e.g. [Akashi and Soker, 2021](#)). The spaping of bipolar **PNe** and proto-**PNe** by jets or collimated outflow from a companion in a binary system was simulated by, e.g., [Lee and Sahai \(2003, 2004\)](#), [García-Arredondo and Frank \(2004\)](#), [Akashi et al. \(2008\)](#), [Akashi and Soker \(2008\)](#), [Dennis et al. \(2008\)](#), [Huarte-Espinosa et al. \(2012\)](#), [Velázquez et al. \(2012\)](#), [Akashi and Soker \(2016, 2017, 2018\)](#), and [Akashi et al. \(2018\)](#). These simulations assumed the interaction to take place in an isotropic wind issued from an **AGB** star or inside the envelope of such a star but did not explicitly account for **CE** interaction.

[García-Segura et al. \(2018\)](#), [Frank et al. \(2018\)](#), [Zou et al. \(2020\)](#), [García-Segura et al. \(2020\)](#), and [García-Segura et al. \(2021\)](#) modelled the formation of **PNe** using, as starting point, the circumstellar gas distribution generated by a **CE** simulation. [García-Segura et al. \(2018\)](#) employed the Eulerian grid-based **CE** simulation of [Ricker and Taam \(2012\)](#) under the assumption that the **CE** gas represents the circumbinary environment into which the post-**AGB** primary blows its low-density, spherical, fast wind, generating the visible **PN** (the origin of fast wind is not under debate, although there are scenarios in which this wind is not spherical at the origin, but already collimated; [Balick and Frank, 2002](#)). [García-Segura et al. \(2018\)](#) carried out axisymmetric simulations of the long-term evolution for (10 000 years—typical **PNe** have maximum lifetimes of 50 000 to 100 000 years—accounting for ionization effects. The symmetry of their simulated **PNe** is not a surprise given the dimensional-

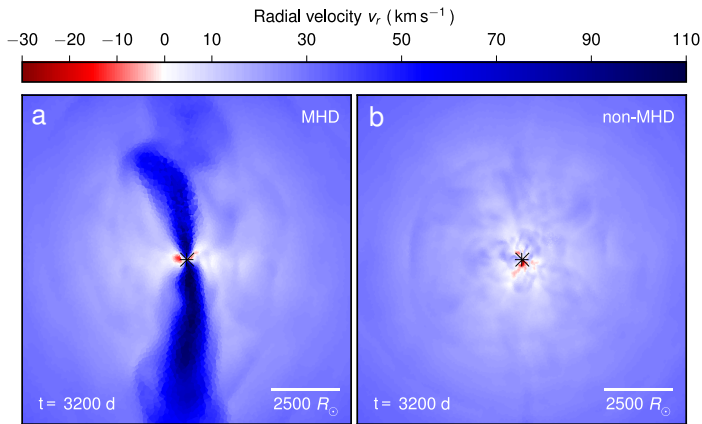


Fig. 20 Radial velocity (a) in the **MHD CE** simulation of Ondratschek et al. (2022) compared with that in a pure hydrodynamics model (b). Figure from Ondratschek et al. (2022).

ity of their simulation, but it already gives an idea that the nebula has a bipolar shape because of the typical equatorial concentration of the expanding **CE**.

Frank et al. (2018) and Zou et al. (2020) carried out **3D** simulations of **PN** formation using as starting point the **SPH CE** interaction model of Reichardt et al. (2019) taken several years after the end of the inspiral. As was the case for the work of García-Segura et al. (2018), they launched a spherical wind of a certain strength. However, the simulation covered only a shorter timescale of three years. Interestingly, they observed pronounced inertial collimation, but noticed that strong **3D** effects do not guarantee a symmetric **PN**.

García-Segura et al. (2020) continued the work started by García-Segura et al. (2018) investigating different types of magnetized fast winds blown into the **CE** ejecta. They also commented that the collimation observed by Zou et al. (2020) was due to the pronounced evacuated polar funnels in the **CE** ejecta which, they remarked, must be due to the adiabatic nature of the **CE** simulation. Only additional simulations will be able to tell just how much collimation is expected.

Ondratschek et al. (2022) took a different approach to the problem of **PN** formation. Their **CE** simulation, which included magnetic fields and extended to a later phase of **CE** interaction, where the envelope is completely unbound even according to the conservative estimate involving the kinetic energy of the gas only, results in a collimated jet, magneto-centrifugally launched towards the end of the inspiral. Similar jet-like outflows were also reported by García-Segura et al. (2021). The resulting bipolar morphology is certainly different from that of simulated ejected **CEs** that do not include magnetic fields, see Fig. 20 for a comparison. The shaping of the **PN** deriving from such configuration will still be affected by whatever fast wind is launched next due to the heating central star and, as is the case for the other post-**CE PN** simulations, by the ionization front propagating through the material. Clearly this line of comparison between **PNe** and **CE** ejecta is in its early days, but it promises to yield very convincing results.

7.6.2 Transient events caused by CE interaction

The dynamical part of the CE interaction is short-lived and it is therefore expected to be observed only rarely. With the advent of time-domain astrophysical observations, e.g., Palomar Transient Factory (Law et al., 2009), the Catalina Real Time Transient Survey (Drake et al., 2009), SkyMapper (Murphy et al., 2009), and The Zwicky Transient Factory (Bellm et al., 2019), we have now realized that a number of luminous outbursts, or transients, were actually CE interactions, demonstrated beyond doubt for at least some objects (such as V 1309 Sco, Tylenda et al., 2011). In the near future, the Legacy Survey of Space and Time at the Rubin Observatory (Ivezić et al., 2019) will undoubtedly make great progress thanks to the discovery of a large amount of the fainter events (according to Howitt et al., 2020, about 20 to 750 detections are expected).

The current thinking is that the class of objects known as gap transients—which we have mentioned in Sect. 1.1—are actually deriving from a number of physical phenomena, only some of which are likely CE interactions. While the terminology has been slightly confusing in the earlier literature, with the benefit of more observations, Pastorello et al. (2019) have proposed that the terms *red nova* (RN) and *luminous red nova* (LRN) are reserved for binary coalescence events of a CE nature for lower and higher mass primary stars, respectively.

The best examples of RNe and LRNe to date are V1309 Sco, with an inferred primary star mass of $\sim 1.5 M_{\odot}$ and a mass ratio (companion star mass over primary star mass) of the interacting stars of $q = 0.1$ (Tylenda et al., 2011), V838 Mon with a progenitor mass of $5\text{--}10 M_{\odot}$ (Tylenda et al., 2005), M31-LRN2015 with a progenitor mass of $3\text{--}5.5 M_{\odot}$ (MacLeod et al., 2017b) and M101 OT2015-1 with a progenitor mass $\sim 18 M_{\odot}$ (Blagorodnova et al., 2017), with more massive examples being NGC4490-OT ($20\text{--}30 M_{\odot}$ Smith et al., 2016) and possibly, η Carinae (Smith et al., 2016; Rest et al., 2012). For most of these objects, which—again confusing the terminology—may not all be standard CE events but belong to the broader class of stellar interactions, we have only partial lightcurves. Occasionally, progenitor photometry is identified with the best case being the V1309 Sco system which had complete photometry for three years prior to outburst (Tylenda et al., 2011).

Due to the rarity of CE events, we tend to observe the brightest cases, usually deriving from more massive objects and/or less evolved donor stars (Kochanek et al., 2014; De Marco and Izzard, 2017). Another observational bias is that we currently have no compelling evidence that in any of the observed cases a close binary has survived. This may indicate that the observed systems failed CE ejection and resulted in a merger of the cores. On the other hand, Howitt et al. (2020) argued that the brightest events may betray the presence of a surviving binary. In truth, we do not know. Not having observed the post-CE binary is no proof of the CE having resulted in a merger, as in some cases a binary could have survived that either has not been detected yet due to a lack of data or simply because it is still embedded in considerable circumstellar material. As the number of observed RNe and LRNe increases, the interpretation will become more robust. Further monitoring of past transients will also, hopefully, determine whether there is a *binary remnant*, in which case we would be able to connect the event with post-CE binary classes. The connection between RN

and **LRN** transients and post-**CE** binaries needs to be established if we are to use these observations as constraints of simulations. They may also hold an answer to why, as discussed in Sect. 3.3, simulations struggle to unbind the **CE** material—a prerequisite to the survival of the binary.

Lightcurves of **RN** and **LRN** (for a one-dimensional model see, e.g., [Matsumoto and Metzger, 2022](#)), whether they eventually prove to be **CE** events where the core binary has survived or where it has merged, should be able to provide some constraints on simulations, if only simulated lightcurves could be calculated. These, however are not yet available ([Galaviz et al., 2017](#)). For their “common-envelope jets supernova impostor” scenario, [Schreier et al. \(2021\)](#) give an estimate for optical observations. For the “grazing envelope evolution” scenario, [Soker \(2015, 2016a\)](#) argue that a fraction of the energy carried away by the jets may be converted to radiation. Consequently, a bright object may be observable as an intermediate-luminosity optical transient (perhaps a **LRN**). Besides the lightcurves, other observables of mergers that can constrain simulations are parameters such as the photospheric size [MacLeod et al. \(2017b\)](#) or the initial ejection velocities, which could be measured if early spectroscopy of the event were available.

For **CE** mergers with massive primary stars and neutron stars or black holes as companions, supernova-like events have been suggested in the scenario of “common-envelope jets supernovae” (e.g. [Chevalier, 2012](#); [Soker and Gilkis, 2018](#); [Schröder et al., 2020](#)). It is still to be determined how to distinguish this scenario from other explanations for Type II_n or Type II-P supernovae. Interaction with **CE** material may lead to a different shaping of the light curve than what is expected from other circumstellar material [Soker et al. \(2019\)](#). **CE** mergers of low-mass stars with white dwarf companions may give rise to thermonuclear explosions. In this “core-degenerate” scenario ([Kashi and Soker, 2011](#); [Ilkov and Soker, 2012](#), e.g.), the merger dynamics is essentially that of the usual double degenerate scenario for Type Ia supernova explosions. The difference is in the rate and delay time of the expected events, because inspiral of the degenerate cores in a **CE** is driven efficiently by drag whereas without the envelope material it is determined by gravitational wave emission. For the appearance of the event, however, the **CE** material is important: hydrogen lines may be present in the spectra in contrast to the typical Type Ia supernovae ([Livio and Riess, 2003](#); [Soker et al., 2013](#)).

While comparing **CE** models with optical observations seems promising, there are alternatives. Gravitational waves have been detected from mergers of compact objects and this naturally implies the question of whether **CE** events would be detectable with upcoming observatories, such as the Laser Interferometer Space Antenna (LISA, [Baker et al., 2019](#)). Analytic and semi-analytic studies ([Holgado et al., 2018](#); [Ginat et al., 2020](#); [Renzo et al., 2021](#)) have looked into this question, but settling it requires a treatment in the framework of full **3D** hydrodynamic simulations of **CEE**.

7.7 Epilogue

Shortly after the **CE** phase in binary stellar systems had been proposed by [Paczynski \(1976\)](#), the first numerical simulations of this binary interaction were presented. How-

ever, the spatial and temporal timescale challenges in combination with lacking spatial symmetries required coarse approximations and parametrizations of effects that could not be resolved by the simulations in the 1980a and 1990s. For this reason, early simulations failed to be predictive about the success of envelope ejection and the final orbital separation of the remnant core binary system.

The key to understanding CE phases are 3D hydrodynamic simulations of the inspiral of the companion into the envelope of the giant primary star. Thanks to increasing computational power and sophisticated numerical techniques, modeling these processes with sufficient accuracy is now within reach. This has motivated different groups using different hydrodynamics codes to join the search for a full description of the interaction and substantial progress was made recently.

In our review, we discussed the basic physical modeling approaches and numerical methods used in 3D hydrodynamic simulations of CEE. On this basis, we provided an overview of the simulations performed to date, which has allowed us to emphasize where the computational frontier currently stands. We hope that this provides a guide to concentrate efforts on some of the critical problems of modelling approaches, such as for example the need to interface different modelling methodologies. By doing so we will be able to carry out increasingly sophisticated, direct comparisons of CE simulations with astronomical observables, which are themselves proliferating with the detection of large numbers of transient phenomena.

The rapid development in modeling CE interaction has the potential to solve one of the last remaining fundamental problems of stellar astrophysics. It can complete our understanding of the evolution of the progenitors of gravitational-wave emitting mergers of double-compact objects, supernovae, planetary nebulae, gamma-ray bursts, X-ray binaries, radio-millisecond pulsars in binaries, and cataclysmic variables, among others.

Acknowledgements This review would have been impossible without the help of many of our colleagues. We are grateful for their input and their permissions to reproduce figures from their publications. FKR acknowledges support from the Klaus Tschira Foundation. OD acknowledges support from the Australian Research Council's Discovery Project award DP210101094.

Conflict of interest The authors declare that they have no conflict of interest.

References

- Abbott BP, Abbott R, Abbott TD, et al. (2016) Observation of Gravitational Waves from a Binary Black Hole Merger. *Phys. Rev. Lett.* 116(6):061102. <https://doi.org/10.1103/PhysRevLett.116.061102>. [arXiv:1602.03837](https://arxiv.org/abs/1602.03837) [gr-qc]
- Abbott BP, Abbott R, Abbott TD, et al. (2017) Multi-messenger Observations of a Binary Neutron Star Merger. *ApJ* 848:L12. <https://doi.org/10.3847/2041-8213/aa91c9>. [arXiv:1710.05833](https://arxiv.org/abs/1710.05833) [astro-ph.HE]
- Akashi M, Soker N (2008) Shaping planetary nebulae by light jets. *MNRAS* 391(3):1063–1074. <https://doi.org/10.1111/j.1365-2966.2008.13935.x>. [arXiv:0805.2332](https://arxiv.org/abs/0805.2332) [astro-ph]

- Akashi M, Soker N (2016) Bipolar rings from jet-inflated bubbles around evolved binary stars. *MNRAS* 462(1):206–216. <https://doi.org/10.1093/mnras/stw1683>. [arXiv:1605.02574](https://arxiv.org/abs/1605.02574) [astro-ph.SR]
- Akashi M, Soker N (2017) Shaping planetary nebulae with jets in inclined triple stellar systems. *MNRAS* 469(3):3296–3306. <https://doi.org/10.1093/mnras/stx1058>. [arXiv:1701.05460](https://arxiv.org/abs/1701.05460) [astro-ph.SR]
- Akashi M, Soker N (2018) The formation of ‘columns crowns’ by jets interacting with a circumstellar dense shell. *MNRAS* 481(2):2754–2765. <https://doi.org/10.1093/mnras/sty2479>. [arXiv:1808.00276](https://arxiv.org/abs/1808.00276) [astro-ph.SR]
- Akashi M, Soker N (2021) Shaping “Ears” in Planetary Nebulae by Early Jets. *ApJ* 913(2):91. <https://doi.org/10.3847/1538-4357/abf7bb>. [arXiv:2012.08917](https://arxiv.org/abs/2012.08917) [astro-ph.GA]
- Akashi M, Meiron Y, Soker N (2008) X-ray emission from jet wind interaction in planetary nebulae. *New Astronomy* 13(8):563–568. <https://doi.org/10.1016/j.newast.2008.03.002>. [arXiv:0711.3265](https://arxiv.org/abs/0711.3265) [astro-ph]
- Akashi M, Bear E, Soker N (2018) Forming h-shaped and barrel-shaped nebulae with interacting jets. *MNRAS* 475(4):4794–4808. <https://doi.org/10.1093/mnras/sty029>. [arXiv:1712.07156](https://arxiv.org/abs/1712.07156) [astro-ph.SR]
- Alexander ME, Chau WY, Henriksen RN (1976) Orbital evolution of a singly condensed, close binary, by mass loss from the primary and by accretion drag on the condensed member. *ApJ* 204:879–888. <https://doi.org/10.1086/154236>
- Amdahl GM (1967) Validity of the single processor approach to achieving large scale computing capabilities. In: Proceedings of the April 18-20, 1967, Spring Joint Computer Conference. AFIPS '67 (Spring). Association for Computing Machinery, New York, NY, USA, p 483–485. <https://doi.org/10.1145/1465482.1465560>, URL <https://doi.org/10.1145/1465482.1465560>
- Appel AW (1985) An Efficient Program for Many-Body Simulation. *SIAM Journal on Scientific and Statistical Computing* 6(1):85–103
- Armitage PJ, Livio M (2000) Black Hole Formation via Hypercritical Accretion during Common-Envelope Evolution. *ApJ* 532(1):540–547. <https://doi.org/10.1086/308548>. [arXiv:astro-ph/9906028](https://arxiv.org/abs/astro-ph/9906028) [astro-ph]
- Baiotti L, Rezzolla L (2017) Binary neutron star mergers: a review of einstein’s richest laboratory. *Reports on Progress in Physics* 80(9):096901. <https://doi.org/10.1088/1361-6633/aa67bb>. [arXiv:1607.03540](https://arxiv.org/abs/1607.03540) [gr-qc]
- Baker J, Bellovary J, Bender PL, et al. (2019) The laser interferometer space antenna: Unveiling the millihertz gravitational wave sky. *arXiv e-prints* arXiv:1907.06482. [arXiv:1907.06482](https://arxiv.org/abs/1907.06482) [astro-ph.IM]
- Balbus SA (1995) General Local Stability Criteria for Stratified, Weakly Magnetized Rotating Systems. *ApJ* 453:380. <https://doi.org/10.1086/176397>
- Balbus SA, Hawley JF (1991) A powerful local shear instability in weakly magnetized disks. I - Linear analysis. II - Nonlinear evolution. *ApJ* 376:214–233. <https://doi.org/10.1086/170270>
- Balick B, Frank A (2002) Shapes and shaping of planetary nebulae. *ARA&A* 40:439–486. <https://doi.org/10.1146/annurev.astro.40.060401.093849>
- Barnes J, Hut P (1986) A hierarchical $O(n \log n)$ force-calculation algorithm. *Nature* 324(6096):446–449. <https://doi.org/10.1038/324446a0>

- Belczynski K, Buonanno A, Cantiello M, et al. (2014) The formation and gravitational-wave detection of massive stellar black hole binaries. *ApJ* 789(2):120. <https://doi.org/10.1088/0004-637X/789/2/120>. [arXiv:1403.0677](https://arxiv.org/abs/1403.0677) [astro-ph.HE]
- Belczynski K, Holz DE, Bulik T, O’Shaughnessy R (2016) The first gravitational-wave source from the isolated evolution of two stars in the 40-100 solar mass range. *Nature* 534(7608):512–515. <https://doi.org/10.1038/nature18322>. [arXiv:1602.04531](https://arxiv.org/abs/1602.04531) [astro-ph.HE]
- Bellm EC, Kulkarni SR, Graham MJ, et al. (2019) The Zwicky Transient Facility: System Overview, Performance, and First Results. *PASP* 131(995):018002. <https://doi.org/10.1088/1538-3873/aacbe>. [arXiv:1902.01932](https://arxiv.org/abs/1902.01932) [astro-ph.IM]
- Benz W, Hills JG (1987) Three-dimensional hydrodynamical simulations of stellar collisions. I - Equal-mass main-sequence stars. *ApJ* 323:614–628. <https://doi.org/10.1086/165857>
- Benz W, Bowers RL, Cameron AGW, Press WH (1990) Dynamic Mass Exchange in Doubly Degenerate Binaries. I. 0.9 and 1.2 M_{sun} Stars. *ApJ* 348:647. <https://doi.org/10.1086/168273>
- Berger MJ, Colella P (1989) Local adaptive mesh refinement for shock hydrodynamics. *Journal of Computational Physics* 82(1):64–84. [https://doi.org/10.1016/0021-9991\(89\)90035-1](https://doi.org/10.1016/0021-9991(89)90035-1)
- Berger MJ, Oliger J (1984) Adaptive Mesh Refinement for Hyperbolic Partial Differential Equations. *Journal of Computational Physics* 53(3):484–512. [https://doi.org/10.1016/0021-9991\(84\)90073-1](https://doi.org/10.1016/0021-9991(84)90073-1)
- Blagorodnova N, Kotak R, Polshaw J, et al. (2017) Common Envelope Ejection for a Luminous Red Nova in M101. *ApJ* 834(2):107. <https://doi.org/10.3847/1538-4357/834/2/107>. [arXiv:1607.08248](https://arxiv.org/abs/1607.08248) [astro-ph.SR]
- Bodenheimer P, Taam RE (1984) Double-core evolution. II - Two-dimensional hydrodynamic effects. *ApJ* 280:771–779. <https://doi.org/10.1086/162049>
- Bond HE, Ciardullo R, Meakes MG (1992) Close binary nuclei of planetary nebulae. In: Kondo Y, Sistero R, Polidan RS (eds) *Evolutionary Processes in Interacting Binary Stars*. vol 151. p 517
- Bond HE, Henden A, Levay ZG, et al. (2003) An energetic stellar outburst accompanied by circumstellar light echoes. *Nature* 422:405–408. <https://doi.org/10.1038/nature01508>. [astro-ph/0303513](https://arxiv.org/abs/astro-ph/0303513)
- Bondi H (1952) On spherically symmetrical accretion. *MNRAS* 112:195. <https://doi.org/10.1093/mnras/112.2.195>
- Bondi H, Hoyle F (1944) On the mechanism of accretion by stars. *MNRAS* 104:273. <https://doi.org/10.1093/mnras/104.5.273>
- Botticella MT, Pastorello A, Smartt SJ, et al. (2009) SN 2008S: an electron-capture SN from a super-AGB progenitor? *MNRAS* 398(3):1041–1068. <https://doi.org/10.1111/j.1365-2966.2009.15082.x>. [arXiv:0903.1286](https://arxiv.org/abs/0903.1286) [astro-ph.SR]
- Brandt A (1977) Multi-level adaptive solutions to boundary-value problems. *Mathematics of Computation* 39:333–390
- Brown GE (1995) Neutron star accretion and binary pulsar formation. *ApJ* 440:270–279. <https://doi.org/10.1086/175268>

- Bryan GL, Norman ML, Stone JM, Cen R, Ostriker JP (1995) A piecewise parabolic method for cosmological hydrodynamics. *Computer Physics Communications* 89(1-3):149–168. [https://doi.org/10.1016/0010-4655\(94\)00191-4](https://doi.org/10.1016/0010-4655(94)00191-4)
- Burkert A, Bodenheimer P (1993) Multiple fragmentation in collapsing protostars. *MNRAS* 264:798. <https://doi.org/10.1093/mnras/264.4.798>
- Cai YZ, Pastorello A, Fraser M, et al. (2019) The transitional gap transient AT 2018hso: new insights into the luminous red nova phenomenon. *A&A* 632:L6. <https://doi.org/10.1051/0004-6361/201936749>. [arXiv:1909.13147](https://arxiv.org/abs/1909.13147) [astro-ph.HE]
- Campbell CG (2018) *Magneto-hydrodynamics in binary stars*, 2nd edn. Springer Nature, Switzerland
- Carroll-Nellenback JJ, Shroyer B, Frank A, Ding C (2013) Efficient parallelization for AMR MHD multiphysics calculations; implementation in AstroBEAR. *Journal of Computational Physics* 236:461–476. <https://doi.org/10.1016/j.jcp.2012.10.004>
- Casewell SL, Braker IP, Parsons SG, et al. (2018) The first sub-70 min non-interacting WD-BD system: EPIC212235321. *MNRAS* 476(1):1405–1411. <https://doi.org/10.1093/mnras/sty245>. [arXiv:1801.07773](https://arxiv.org/abs/1801.07773) [astro-ph.SR]
- Chamandy L, Frank A, Blackman EG, et al. (2018) Accretion in common envelope evolution. *MNRAS* 480(2):1898–1911. <https://doi.org/10.1093/mnras/sty1950>. [arXiv:1805.03607](https://arxiv.org/abs/1805.03607) [astro-ph.SR]
- Chamandy L, Blackman EG, Frank A, et al. (2019) How drag force evolves in global common envelope simulations. *MNRAS* 490(3):3727–3739. <https://doi.org/10.1093/mnras/stz2813>. [arXiv:1908.06195](https://arxiv.org/abs/1908.06195) [astro-ph.SR]
- Chamandy L, Blackman EG, Frank A, Carroll-Nellenback J, Tu Y (2020) Common Envelope Evolution on the Asymptotic Giant Branch: Unbinding within a Decade? *MNRAS* <https://doi.org/10.1093/mnras/staa1273>
- Chandrasekhar S (1943) Dynamical Friction. I. General Considerations: the Coefficient of Dynamical Friction. *ApJ* 97:255. <https://doi.org/10.1086/144517>
- Chen WC, Liu WM (2013) Evolution of neutron star + he star binaries: an alternative evolutionary channel to intermediate-mass binary pulsars. *MNRAS* 432:L75–L79. <https://doi.org/10.1093/mnras/slt043>. [arXiv:1303.6155](https://arxiv.org/abs/1303.6155) [astro-ph.SR]
- Chen Z, Coleman MSB, Blackman EG, Frank A (2019) Solving the riemann problem for realistic astrophysical fluids. *Journal of Computational Physics* 388:490–517. <https://doi.org/10.1016/j.jcp.2019.03.016>. [arXiv:1903.04568](https://arxiv.org/abs/1903.04568) [physics.comp-ph]
- Chevalier RA (2012) Common envelope evolution leading to supernovae with dense interaction. *ApJ* 752(1):L2. <https://doi.org/10.1088/2041-8205/752/1/L2>. [arXiv:1204.3300](https://arxiv.org/abs/1204.3300) [astro-ph.HE]
- Clayton M, Podsiadlowski P, Ivanova N, Justham S (2017) Episodic mass ejections from common-envelope objects. *MNRAS* 470(2):1788–1808. <https://doi.org/10.1093/mnras/stx1290>. [arXiv:1705.08457](https://arxiv.org/abs/1705.08457) [astro-ph.SR]
- Colella P, Glaz HM (1985) Efficient solution algorithms for the riemann problem for real gases. *Journal of Computational Physics* 59:264–289
- Colella P, Woodward PR (1984) The Piecewise Parabolic Method (PPM) for gas-dynamical simulations. *Journal of Computational Physics* 54:174–201
- Corradi RLM, Schwarz HE (1995) Morphological populations of planetary nebulae: which progenitors? I. Comparative properties of bipolar nebulae. *A&A* 293:871–888

- Courant R, Friedrichs KO, Lewy H (1928) Über die partiellen Differentialgleichungen der mathematischen Physik. *Math Ann* 100:32–74
- Croft RAC, Di Matteo T, Springel V, Hernquist L (2009) Galaxy morphology, kinematics and clustering in a hydrodynamic simulation of a Λ cold dark matter universe. *MNRAS* 400(1):43–67. <https://doi.org/10.1111/j.1365-2966.2009.15446.x>. [arXiv:0803.4003](https://arxiv.org/abs/0803.4003) [astro-ph]
- Dan M, Rosswog S, Brüggen M (2009) Mass transfer dynamics in double degenerate binary systems. *Journal of Physics Conference Series* 172(1):012034–+. <https://doi.org/10.1088/1742-6596/172/1/012034>. [arXiv:0811.1517](https://arxiv.org/abs/0811.1517)
- Dan M, Rosswog S, Guillochon J, Ramirez-Ruiz E (2011) Prelude to A Double Degenerate Merger: The Onset of Mass Transfer and Its Impact on Gravitational Waves and Surface Detonations. *ApJ* 737:89. <https://doi.org/10.1088/0004-637X/737/2/89>. [arXiv:1101.5132](https://arxiv.org/abs/1101.5132) [astro-ph.HE]
- Dan M, Rosswog S, Guillochon J, Ramirez-Ruiz E (2012) How the merger of two white dwarfs depends on their mass ratio: orbital stability and detonations at contact. *MNRAS* p 2742. <https://doi.org/10.1111/j.1365-2966.2012.20794.x>. [arXiv:1201.2406](https://arxiv.org/abs/1201.2406) [astro-ph.HE]
- Darwin GH (1879) The determination of the secular effects of tidal friction by a graphical method. *Proceedings of the Royal Society of London* 29(196-199):168–181. <https://doi.org/10.1098/rspl.1879.0028>
- De S, MacLeod M, Everson RW, et al. (2020) Common Envelope Wind Tunnel: The Effects of Binary Mass Ratio and Implications for the Accretion-driven Growth of LIGO Binary Black Holes. *ApJ* 897(2):130. <https://doi.org/10.3847/1538-4357/ab9ac6>. [arXiv:1910.13333](https://arxiv.org/abs/1910.13333) [astro-ph.SR]
- De Colle F, Granot J, López-Cámara D, Ramirez-Ruiz E (2012) Gamma-ray burst dynamics and afterglow radiation from adaptive mesh refinement, special relativistic hydrodynamic simulations. *ApJ* 746(2):122. <https://doi.org/10.1088/0004-637X/746/2/122>. [arXiv:1111.6890](https://arxiv.org/abs/1111.6890) [astro-ph.HE]
- de Kool M (1987) Models of interacting binary stars. PhD thesis, University of Amsterdam
- de Kool M, van den Heuvel EPJ, Pylyser E (1987) An evolutionary scenario for the black hole binary A0620-00. *A&A* 183:47–52
- De Marco O (2009) The Origin and Shaping of Planetary Nebulae: Putting the Binary Hypothesis to the Test. *PASP* 121:316–342. <https://doi.org/10.1086/597765>. [arXiv:0902.1137](https://arxiv.org/abs/0902.1137)
- De Marco O, Izzard RG (2017) Dawes Review 6: The Impact of Companions on Stellar Evolution. *PASA*34:e001. <https://doi.org/10.1017/pasa.2016.52>. [arXiv:1611.03542](https://arxiv.org/abs/1611.03542) [astro-ph.SR]
- De Marco O, Sandquist EL, Mac Low MM, Herwig F, Taam RE (2003a) Of Wolf-Rayet Central Stars and Common Envelopes. In: Arthur J, Henney WJ (eds) *Revista Mexicana de Astronomía y Astrofísica Conference Series*. *Revista Mexicana de Astronomía y Astrofísica Conference Series*, vol 15. pp 34–37
- De Marco O, Sandquist EL, Mac Low MM, Herwig F, Taam RE (2003b) Wolf-Rayet Central Stars and the Binary Evolution Channel. In: Reyes-Ruiz M, Vázquez-Semadeni E (eds) *Revista Mexicana de Astronomía y Astrofísica Conference Series*. *Revista Mexicana de Astronomía y Astrofísica Conference Series*, vol 18. pp

24–30

- De Marco O, Passy JC, Moe M, et al. (2011) On the α formalism for the common envelope interaction. *MNRAS* 411:2277–2292. <https://doi.org/10.1111/j.1365-2966.2010.17891.x>. [arXiv:1010.4374](https://arxiv.org/abs/1010.4374) [astro-ph.SR]
- de Medeiros JR, Da Rocha C, Mayor M (1996) The distribution of rotational velocity for evolved stars. *A&A* 314:499–502
- Dehnen W (2001) Towards optimal softening in three-dimensional N-body codes - I. Minimizing the force error. *MNRAS* 324(2):273–291. <https://doi.org/10.1046/j.1365-8711.2001.04237.x>. [arXiv:astro-ph/0011568](https://arxiv.org/abs/astro-ph/0011568) [astro-ph]
- Dehnen W, Aly H (2012) Improving convergence in smoothed particle hydrodynamics simulations without pairing instability. *MNRAS* 425(2):1068–1082. <https://doi.org/10.1111/j.1365-2966.2012.21439.x>. [arXiv:1204.2471](https://arxiv.org/abs/1204.2471) [astro-ph.IM]
- Delgado AJ (1980) Evolution of a blue supergiant with a neutron star companion immersed in its envelope. *A&A* 87:343–348
- Deloye CJ, Taam RE (2010) Adiabatic mass loss and the outcome of the common envelope phase of binary evolution. *ApJ* 719(1):L28–L31. <https://doi.org/10.1088/2041-8205/719/1/L28>. [arXiv:1007.1036](https://arxiv.org/abs/1007.1036) [astro-ph.SR]
- Dennis TJ, Cunningham AJ, Frank A, et al. (2008) Proto-planetary nebulae as explosions: Bullets versus jets and nebular shaping. *ApJ* 679(2):1327–1337. <https://doi.org/10.1086/587730>. [arXiv:0707.1641](https://arxiv.org/abs/0707.1641) [astro-ph]
- Dewi JDM, Tauris TM (2000) On the energy equation and efficiency parameter of the common envelope evolution. *A&A* 360:1043–1051. [astro-ph/0007034](https://arxiv.org/abs/astro-ph/0007034)
- Dewi JDM, Podsiadlowski P, Sena A (2006) Double-core evolution and the formation of neutron star binaries with compact companions. *MNRAS* 368:1742–1748. <https://doi.org/10.1111/j.1365-2966.2006.10233.x>. [astro-ph/0602510](https://arxiv.org/abs/astro-ph/0602510)
- Dokuchaev VP (1964) Emission of magnetoacoustic waves in the motion of stars in cosmic space. *Soviet Ast.* 8:23
- Dominik M, Belczynski K, Fryer C, et al. (2012) Double Compact Objects. I. The Significance of the Common Envelope on Merger Rates. *ApJ* 759(1):52. <https://doi.org/10.1088/0004-637X/759/1/52>. [arXiv:1202.4901](https://arxiv.org/abs/1202.4901) [astro-ph.HE]
- Drake AJ, Djorgovski SG, Mahabal A, et al. (2009) First results from the catalina real-time transient survey. *ApJ* 696(1):870–884. <https://doi.org/10.1088/0004-637X/696/1/870>. [arXiv:0809.1394](https://arxiv.org/abs/0809.1394) [astro-ph]
- Eckart C (1960) Variation principles of hydrodynamics. *Physics of Fluids* 3(3):421–427. <https://doi.org/10.1063/1.1706053>
- Edelmann PVF, Röpke FK, Hirschi R, Georgy C, Jones S (2017) Testing a one-dimensional prescription of dynamical shear mixing with a two-dimensional hydrodynamic simulation. *A&A* 604:A25. <https://doi.org/10.1051/0004-6361/201629873>. [arXiv:1704.06261](https://arxiv.org/abs/1704.06261) [astro-ph.SR]
- Edelmann PVF, Horst L, Berberich JP, et al. (2021) Well-balanced treatment of gravity in astrophysical fluid dynamics simulations at low mach numbers. *A&A* 652:A53. <https://doi.org/10.1051/0004-6361/202140653>. [arXiv:2102.13111](https://arxiv.org/abs/2102.13111) [astro-ph.SR]
- Edgar R (2004) A review of bondi-hoyle-lyttleton accretion. *New Astronomy Reviews* 48(10):843–859. <https://doi.org/10.1016/j.newar.2004.06.001>. [arXiv:astro-ph/0406166](https://arxiv.org/abs/astro-ph/0406166) [astro-ph]

- Eggleton PP (1983) Approximations to the radii of Roche lobes. *ApJ* 268:368. <https://doi.org/10.1086/160960>
- Everson RW, MacLeod M, De S, Macias P, Ramirez-Ruiz E (2020) Common envelope wind tunnel: Range of applicability and self-similarity in realistic stellar envelopes. *ApJ* 899(1):77. <https://doi.org/10.3847/1538-4357/aba75c>. [arXiv:2006.07471](https://arxiv.org/abs/2006.07471) [astro-ph.SR]
- Faber JA, Rasio FA (2012) Binary neutron star mergers. *Living Reviews in Relativity* 15(1):8. <https://doi.org/10.12942/lrr-2012-8>. [arXiv:1204.3858](https://arxiv.org/abs/1204.3858) [gr-qc]
- Ferziger JH, Perić M, Street RL (2020) *Computational Methods for Fluid Dynamics*, 4th edn. Springer Nature, Switzerland
- Foglizzo T, Galletti P, Ruffert M (2005) A fresh look at the unstable simulations of Bondi-Hoyle-Lyttleton accretion. *A&A* 435(2):397–411. <https://doi.org/10.1051/0004-6361:20042201>. [arXiv:astro-ph/0502168](https://arxiv.org/abs/astro-ph/0502168) [astro-ph]
- Fragos T, Andrews JJ, Ramirez-Ruiz E, et al. (2019) The complete evolution of a neutron-star binary through a common envelope phase using 1D hydrodynamic simulations. *ApJ* 883(2):L45. <https://doi.org/10.3847/2041-8213/ab40d1>. [arXiv:1907.12573](https://arxiv.org/abs/1907.12573) [astro-ph.HE]
- Frank A, Chen Z, Reichardt T, et al. (2018) Planetary Nebulae Shaped by Common Envelope Evolution. *Galaxies* 6(4):113. <https://doi.org/10.3390/galaxies6040113>. [arXiv:1807.05925](https://arxiv.org/abs/1807.05925) [astro-ph.SR]
- Fryer CL, Woosley SE (1998) Helium star/black hole mergers: A new gamma-ray burst model. *ApJ* 502(1):L9–L12. <https://doi.org/10.1086/311493>. [arXiv:astro-ph/9804167](https://arxiv.org/abs/astro-ph/9804167) [astro-ph]
- Fryer CL, Rockefeller G, Warren MS (2006) SNSPH: A parallel three-dimensional smoothed particle radiation hydrodynamics code. *ApJ* 643(1):292–305. <https://doi.org/10.1086/501493>. [arXiv:astro-ph/0512532](https://arxiv.org/abs/astro-ph/0512532) [astro-ph]
- Fryxell B, Olson K, Ricker P, et al. (2000) FLASH: An adaptive mesh hydrodynamics code for modeling astrophysical thermonuclear flashes. *ApJS* 131:273–334. <https://doi.org/10.1086/317361>
- Fryxell BA, Taam RE (1988) Numerical Simulations of Nonaxisymmetric Adiabatic Accretion Flow. *ApJ* 335:862. <https://doi.org/10.1086/166973>
- Galaviz P, De Marco O, Passy JC, Staff JE, Iaconi R (2017) Common Envelope Light Curves. I. Grid-code Module Calibration. *ApJS* 229(2):36. <https://doi.org/10.3847/1538-4365/aa64e1>. [arXiv:1702.07872](https://arxiv.org/abs/1702.07872) [astro-ph.SR]
- García-Arredondo F, Frank A (2004) Collimated outflow formation via binary stars: Three-dimensional simulations of asymptotic giant branch wind and disk wind interactions. *ApJ* 600(2):992–1003. <https://doi.org/10.1086/379821>. [arXiv:astro-ph/0307454](https://arxiv.org/abs/astro-ph/0307454) [astro-ph]
- García-Segura G, Ricker PM, Taam RE (2018) Common Envelope Shaping of Planetary Nebulae. *ApJ* 860(1):19. <https://doi.org/10.3847/1538-4357/aac08c>. [arXiv:1804.09309](https://arxiv.org/abs/1804.09309) [astro-ph.SR]
- García-Segura G, Taam RE, Ricker PM (2020) Common Envelope Shaping of Planetary Nebulae. II. Magnetic Solutions and Self-collimated Outflows. *ApJ* 893(2):150. <https://doi.org/10.3847/1538-4357/ab8006>. [arXiv:2003.06073](https://arxiv.org/abs/2003.06073) [astro-ph.SR]

- García-Segura G, Taam RE, Ricker PM (2021) Common Envelope Shaping of Planetary Nebulae. III. The Launching of Jets in Proto-Planetary Nebulae. *ApJ* 914(2):111. <https://doi.org/10.3847/1538-4357/abfc4e>. [arXiv:2104.12831](https://arxiv.org/abs/2104.12831) [astro-ph.SR]
- Ge H, Hjellming MS, Webbink RF, Chen X, Han Z (2010) Adiabatic mass loss in binary stars. i. computational method. *ApJ* 717(2):724–738. <https://doi.org/10.1088/0004-637X/717/2/724>. [arXiv:1005.3099](https://arxiv.org/abs/1005.3099) [astro-ph.SR]
- Geier S, Classen L, Heber U (2011) The Fast-rotating, Low-gravity Subdwarf B Star EC 22081-1916: Remnant of a Common Envelope Merger Event. *ApJ* 733(1):L13. <https://doi.org/10.1088/2041-8205/733/1/L13>. [arXiv:1104.4202](https://arxiv.org/abs/1104.4202) [astro-ph.SR]
- Gilkis A, Soker N, Kashi A (2019) Common envelope jets supernova (CEJSN) impostors resulting from a neutron star companion. *MNRAS* 482(3):4233–4242. <https://doi.org/10.1093/mnras/sty3008>. [arXiv:1802.08669](https://arxiv.org/abs/1802.08669) [astro-ph.HE]
- Ginat YB, Glanz H, Perets HB, Grishin E, Desjacques V (2020) Gravitational waves from in-spirals of compact objects in binary common-envelope evolution. *MNRAS* 493(4):4861–4867. <https://doi.org/10.1093/mnras/staa465>. [arXiv:1903.11072](https://arxiv.org/abs/1903.11072) [astro-ph.SR]
- Gingold RA, Monaghan JJ (1977) Smoothed particle hydrodynamics - Theory and application to non-spherical stars. *MNRAS* 181:375–389
- Glanz H, Perets HB (2018) Efficient common-envelope ejection through dust-driven winds. *MNRAS* 478(1):L12–L17. <https://doi.org/10.1093/mnras/sly065>. [arXiv:1801.08130](https://arxiv.org/abs/1801.08130) [astro-ph.SR]
- Glanz H, Perets HB (2021a) Common envelope evolution of eccentric binaries. *MNRAS* 507(2):2659–2670. <https://doi.org/10.1093/mnras/stab2291>. [arXiv:2105.02227](https://arxiv.org/abs/2105.02227) [astro-ph.SR]
- Glanz H, Perets HB (2021b) Simulations of common envelope evolution in triple systems: circumstellar case. *MNRAS* 500(2):1921–1932. <https://doi.org/10.1093/mnras/staa3242>. [arXiv:2004.00020](https://arxiv.org/abs/2004.00020) [astro-ph.SR]
- Godunov SK (1959) Finite difference method for numerical computation of discontinuous solution of the equations of fluid dynamics. *Matematicheskii Sbornik* 47:271
- Gonzalez-Bolivar M, De Marco O, Lau MYM, Hirai R, Price DJ (2022) Common envelope binary interaction simulations between a thermally-pulsating AGB star and a low mass companion. *arXiv e-prints* [arXiv:2205.09749](https://arxiv.org/abs/2205.09749). [arXiv:2205.09749](https://arxiv.org/abs/2205.09749) [astro-ph.SR]
- Goranskij VP, Shugarov SY, Barsukova EA, Kroll P (2004) V838 Mon before and after its outburst. *Information Bulletin on Variable Stars* 5511:1
- Górski KM, Hivon E, Banday AJ, et al. (2005) HEALPix: A Framework for High-Resolution Discretization and Fast Analysis of Data Distributed on the Sphere. *ApJ* 622:759–771. <https://doi.org/10.1086/427976>. [arXiv:astro-ph/0409513](https://arxiv.org/abs/astro-ph/0409513)
- Grichener A, Sabach E, Soker N (2018) The limited role of recombination energy in common envelope removal. *MNRAS* 478(2):1818–1824. <https://doi.org/10.1093/mnras/sty1178>. [arXiv:1803.05864](https://arxiv.org/abs/1803.05864) [astro-ph.SR]
- Han Z, Podsiadlowski P, Eggleton PP (1995) The formation of bipolar planetary nebulae and close white dwarf binaries. *MNRAS* 272:800–820. <https://doi.org/10.1093/mnras/272.4.800>

- Hillel S, Schreier R, Soker N (2022) Three-dimensional simulations of the jet feedback mechanism in common envelope jets supernovae. *MNRAS* 514(3):3212–3221. <https://doi.org/10.1093/mnras/stac1341>. [arXiv:2112.01459](https://arxiv.org/abs/2112.01459) [astro-ph.HE]
- Hillwig TC, Jones D, De Marco O, et al. (2016) Observational Confirmation of a Link Between Common Envelope Binary Interaction and Planetary Nebula Shaping. *ApJ* 832(2):125. <https://doi.org/10.3847/0004-637X/832/2/125>. [arXiv:1609.02185](https://arxiv.org/abs/1609.02185) [astro-ph.SR]
- Hjellming MS, Webbink RF (1987) Thresholds for rapid mass transfer in binary system. I. polytropic models. *ApJ* 318:794. <https://doi.org/10.1086/165412>
- Holgado AM, Ricker PM, Huerta EA (2018) Gravitational waves from accreting neutron stars undergoing common-envelope inspiral. *ApJ* 857(1):38. <https://doi.org/10.3847/1538-4357/aab6a9>. [arXiv:1706.09413](https://arxiv.org/abs/1706.09413) [astro-ph.HE]
- Howitt G, Stevenson S, Vigna-Gómez Ar, et al. (2020) Luminous red novae: population models and future prospects. *MNRAS* 492(3):3229–3240. <https://doi.org/10.1093/mnras/stz3542>. [arXiv:1912.07771](https://arxiv.org/abs/1912.07771) [astro-ph.HE]
- Hoyle F, Lyttleton RA (1939) The effect of interstellar matter on climatic variation. *Proceedings of the Cambridge Philosophical Society* 35(3):405. <https://doi.org/10.1017/S0305004100021150>
- Huarte-Espinosa M, Frank A, Balick B, et al. (2012) From bipolar to elliptical: simulating the morphological evolution of planetary nebulae. *MNRAS* 424(3):2055–2068. <https://doi.org/10.1111/j.1365-2966.2012.21348.x>. [arXiv:1107.0415](https://arxiv.org/abs/1107.0415) [astro-ph.SR]
- Iaconi R, De Marco O (2019) Speaking with one voice: simulations and observations discuss the common envelope α parameter. *MNRAS* 490(2):2550–2566. <https://doi.org/10.1093/mnras/stz2756>. [arXiv:1902.02039](https://arxiv.org/abs/1902.02039) [astro-ph.SR]
- Iaconi R, Reichardt T, Staff J, et al. (2017a) Effect of initial separation on common envelope simulations: The effect of a wider initial separation on common envelope binary interaction simulations. *MNRAS* 464(4):4028–4044. <https://doi.org/10.1093/mnras/stw2377>. [arXiv:1603.01953](https://arxiv.org/abs/1603.01953) [astro-ph.SR]
- Iaconi R, Reichardt T, Staff J, et al. (2017b) Effect of initial separation on common envelope simulations: The effect of a wider initial separation on common envelope binary interaction simulations. *MNRAS* 464(4):4028–4044. <https://doi.org/10.1093/mnras/stw2377>. [arXiv:1603.01953](https://arxiv.org/abs/1603.01953) [astro-ph.SR]
- Iaconi R, De Marco O, Passy JC, Staff J (2018) The effect of binding energy and resolution in simulations of the common envelope binary interaction. *MNRAS* 477(2):2349–2365. <https://doi.org/10.1093/mnras/sty794>. [arXiv:1706.09786](https://arxiv.org/abs/1706.09786) [astro-ph.SR]
- Iaconi R, Maeda K, Nozawa T, De Marco O, Reichardt T (2020) Properties of the post in-spiral common envelope ejecta II: dust formation. *MNRAS* <https://doi.org/10.1093/mnras/staa2169>. [arXiv:2003.06151](https://arxiv.org/abs/2003.06151) [astro-ph.SR]
- Ilkov M, Soker N (2012) Type ia supernovae from very long delayed explosion of core-white dwarf merger. *MNRAS* 419:1695–1700. <https://doi.org/10.1111/j.1365-2966.2011.19833.x>. [arXiv:1106.2027](https://arxiv.org/abs/1106.2027) [astro-ph.SR]
- Ivanova N (2018) On the use of hydrogen recombination energy during common envelope events. *ApJ* 858(2):L24. <https://doi.org/10.3847/2041-8213/aac101>. [arXiv:1804.10681](https://arxiv.org/abs/1804.10681) [astro-ph.SR]

- Ivanova N, Nandez JLA (2016) Common envelope events with low-mass giants: understanding the transition to the slow spiral-in. *MNRAS* 462:362–381. <https://doi.org/10.1093/mnras/stw1676>. [arXiv:1606.04923](https://arxiv.org/abs/1606.04923) [astro-ph.SR]
- Ivanova N, Justham S, Chen X, et al. (2013) Common envelope evolution: where we stand and how we can move forward. *A&A Rev.* 21:59. <https://doi.org/10.1007/s00159-013-0059-2>. [arXiv:1209.4302](https://arxiv.org/abs/1209.4302) [astro-ph.HE]
- Ivanova N, Justham S, Podsiadlowski P (2015) On the role of recombination in common-envelope ejections. *MNRAS* 447:2181–2197. <https://doi.org/10.1093/mnras/stu2582>. [arXiv:1409.3260](https://arxiv.org/abs/1409.3260) [astro-ph.SR]
- Ivezić Ž, Kahn SM, Tyson JA, et al. (2019) LSST: From Science Drivers to Reference Design and Anticipated Data Products. *ApJ* 873(2):111. <https://doi.org/10.3847/1538-4357/ab042c>. [arXiv:0805.2366](https://arxiv.org/abs/0805.2366) [astro-ph]
- Jacoby GH, Hillwig TC, Jones D, et al. (2021) Binary central stars of planetary nebulae identified with kepler/K2. *MNRAS* 506(4):5223–5246. <https://doi.org/10.1093/mnras/stab2045>. [arXiv:2104.07934](https://arxiv.org/abs/2104.07934) [astro-ph.SR]
- Jia S, Spruit HC (2018) Disruption of a planet spiraling into its host star. *ApJ* 864(2):169. <https://doi.org/10.3847/1538-4357/aad77c>. [arXiv:1808.00467](https://arxiv.org/abs/1808.00467) [astro-ph.EP]
- Jones D (2016) The discovery and characterisation of binary central stars in planetary nebulae. In: *Journal of Physics Conference Series*. *Journal of Physics Conference Series*, vol 728. p 032014. <https://doi.org/10.1088/1742-6596/728/3/032014>. [arXiv:1602.00846](https://arxiv.org/abs/1602.00846) [astro-ph.SR]
- Kalogera V, Belczynski K, Kim C, O’Shaughnessy R, Willems B (2007) Formation of double compact objects. *Phys. Rep.* 442(1-6):75–108. <https://doi.org/10.1016/j.physrep.2007.02.008>. [arXiv:astro-ph/0612144](https://arxiv.org/abs/astro-ph/0612144) [astro-ph]
- Kamiński T, Steffen W, Bujarrabal V, et al. (2021) Molecular remnant of Nova 1670 (CK Vulpeculae). II. A three-dimensional view of the gas distribution and velocity field. *A&A* 646:A1. <https://doi.org/10.1051/0004-6361/202039634>. [arXiv:2010.05832](https://arxiv.org/abs/2010.05832) [astro-ph.SR]
- Kashi A, Soker N (2011) A circumbinary disc in the final stages of common envelope and the core-degenerate scenario for Type Ia supernovae. *MNRAS* 417:1466–1479. <https://doi.org/10.1111/j.1365-2966.2011.19361.x>. [arXiv:1105.5698](https://arxiv.org/abs/1105.5698) [astro-ph.SR]
- Kasliwal MM (2012) Systematically Bridging the Gap Between Novae and Supernovae. *PASA* 29:482–488. <https://doi.org/10.1071/AS11061>
- Kim H, Kim WT (2007) Dynamical friction of a circular-orbit perturber in a gaseous medium. *ApJ* 665(1):432–444. <https://doi.org/10.1086/519302>. [arXiv:0705.0084](https://arxiv.org/abs/0705.0084) [astro-ph]
- Kim WT (2010) Nonlinear dynamical friction of a circular-orbit perturber in a gaseous medium. *ApJ* 725(1):1069–1081. <https://doi.org/10.1088/0004-637X/725/1/1069>. [arXiv:1010.1995](https://arxiv.org/abs/1010.1995) [astro-ph.GA]
- Kippenhahn R, Weigert A, Weiss A (2012) *Stellar Structure and Evolution*. Springer-Verlag, Berlin Heidelberg. <https://doi.org/10.1007/978-3-642-30304-3>
- Kochanek CS, Adams SM, Belczynski K (2014) Stellar mergers are common. *MNRAS* 443(2):1319–1328. <https://doi.org/10.1093/mnras/stu1226>. [arXiv:1405.1042](https://arxiv.org/abs/1405.1042) [astro-ph.SR]

- Kramer M, Schneider FRN, Ohlmann ST, et al. (2020) Formation of sdB-stars via common envelope ejection by substellar companions. *A&A* 642:A97. <https://doi.org/10.1051/0004-6361/202038702>. [arXiv:2007.00019](https://arxiv.org/abs/2007.00019) [astro-ph.SR]
- Kruckow MU, Tauris TM, Langer N, et al. (2016) Common-envelope ejection in massive binary stars. Implications for the progenitors of GW150914 and GW151226. *A&A* 596:A58. <https://doi.org/10.1051/0004-6361/201629420>. [arXiv:1610.04417](https://arxiv.org/abs/1610.04417) [astro-ph.SR]
- Krumholz MR, McKee CF, Klein RI (2004) Embedding Lagrangian Sink Particles in Eulerian Grids. *ApJ* 611(1):399–412. <https://doi.org/10.1086/421935>. [arXiv:astro-ph/0312612](https://arxiv.org/abs/astro-ph/0312612) [astro-ph]
- Kuruwita RL, Staff J, De Marco O (2016) Considerations on the role of fallback discs in the final stages of the common envelope binary interaction. *MNRAS* 461(1):486–496. <https://doi.org/10.1093/mnras/stw1414>. [arXiv:1606.04635](https://arxiv.org/abs/1606.04635) [astro-ph.SR]
- Kwok S, Purton CR, Fitzgerald PM (1978) On the origin of planetary nebulae. *ApJ* 219:L125–L127. <https://doi.org/10.1086/182621>
- Lau MYM, Hirai R, González-Bolívar M, et al. (2022a) Common envelopes in massive stars: Towards the role of radiation pressure and recombination energy in ejecting red supergiant envelopes. *MNRAS* <https://doi.org/10.1093/mnras/stac049>. [arXiv:2111.00923](https://arxiv.org/abs/2111.00923) [astro-ph.SR]
- Lau MYM, Hirai R, Price DJ, Mandel I (2022b) Common envelopes in massive stars II: The distinct roles of hydrogen and helium recombination. *arXiv e-prints* [arXiv:2206.06411](https://arxiv.org/abs/2206.06411). [arXiv:2206.06411](https://arxiv.org/abs/2206.06411) [astro-ph.SR]
- Law NM, Kulkarni SR, Dekany RG, et al. (2009) The palomar transient factory: System overview, performance, and first results. *PASP* 121:1395–1408. <https://doi.org/10.1086/648598>. [arXiv:0906.5350](https://arxiv.org/abs/0906.5350)
- Law-Smith JAP, Everson RW, Ramirez-Ruiz E, et al. (2020) Successful Common Envelope Ejection and Binary Neutron Star Formation in 3D Hydrodynamics. *arXiv e-prints* [arXiv:2011.06630](https://arxiv.org/abs/2011.06630). [arXiv:2011.06630](https://arxiv.org/abs/2011.06630) [astro-ph.HE]
- Lax PD, Richtmyer RD (1956) Survey of the stability of linear finite difference equations. *Communications in Pure and Applied Mathematics* 9:267–293
- Lee CF, Sahai R (2003) Shaping proto-planetary and young planetary nebulae with collimated fast winds. *ApJ* 586(1):319–337. <https://doi.org/10.1086/346265>. [arXiv:astro-ph/0211510](https://arxiv.org/abs/astro-ph/0211510) [astro-ph]
- Lee CF, Sahai R (2004) Magnetohydrodynamic models of the bipolar knotty jet in Henize 2-90. *ApJ* 606(1):483–496. <https://doi.org/10.1086/381677>
- Liu M, Di Matteo T, Feng Y (2016) The effects of AGN feedback and SPH formulation on black hole growth in galaxies. *MNRAS* 458(2):1402–1416. <https://doi.org/10.1093/mnras/stw342>
- Livio M, Riess AG (2003) Have the elusive progenitors of type Ia supernovae been discovered? *ApJ* 594:L93–L94. <https://doi.org/10.1086/378765>. [arXiv:astro-ph/0308018](https://arxiv.org/abs/astro-ph/0308018)
- Livio M, Soker N (1984a) On the masses of the white dwarfs in cataclysmic variables. *MNRAS* 208:783–797. <https://doi.org/10.1093/mnras/208.4.783>
- Livio M, Soker N (1984b) Star-planet systems as possible progenitors of cataclysmic binaries. *MNRAS* 208:763–781. <https://doi.org/10.1093/mnras/208.4.763>

- Livio M, Soker N (1988) The common envelope phase in the evolution of binary stars. *ApJ* 329:764–779. <https://doi.org/10.1086/166419>
- Livio M, Soker N, de Kool M, Savonije GJ (1986) Accretion from an inhomogeneous medium - III. General case and observational consequences. *MNRAS* 222:235–250. <https://doi.org/10.1093/mnras/222.2.235>
- Lombardi J J C, Holtzman W, Dooley KL, et al. (2011) Twin binaries: Studies of stability, mass transfer, and coalescence. *ApJ* 737(2):49. <https://doi.org/10.1088/0004-637X/737/2/49>. [arXiv:1009.1300](https://arxiv.org/abs/1009.1300) [astro-ph.SR]
- López-Cámara D, De Colle F, Moreno Méndez E (2019) Self-regulating jets during the common-envelope phase. *MNRAS* 482(3):3646–3655. <https://doi.org/10.1093/mnras/sty2959>. [arXiv:1806.11115](https://arxiv.org/abs/1806.11115) [astro-ph.HE]
- López-Cámara D, Moreno Méndez E, De Colle F (2020) Disc formation and jet inclination effects in common envelopes. *MNRAS* 497(2):2057–2065. <https://doi.org/10.1093/mnras/staa1983>. [arXiv:2004.04158](https://arxiv.org/abs/2004.04158) [astro-ph.HE]
- López-Cámara D, De Colle F, Moreno Méndez E, Shiber S, Iaconi R (2022) Jets in common envelopes: a low-mass main-sequence star in a red giant. *MNRAS* 513(3):3634–3645. <https://doi.org/10.1093/mnras/stac932>. [arXiv:2110.02227](https://arxiv.org/abs/2110.02227) [astro-ph.HE]
- Loveridge AJ, van der Sluys MV, Kalogera V (2011) Analytical expressions for the envelope binding energy of giants as a function of basic stellar parameters. *ApJ* 743(1):49. <https://doi.org/10.1088/0004-637X/743/1/49>. [arXiv:1009.5400](https://arxiv.org/abs/1009.5400) [astro-ph.SR]
- Lucy LB (1977) A numerical approach to the testing of the fission hypothesis. *AJ* 82:1013–1024. <https://doi.org/10.1086/112164>
- MacLeod M, Ramirez-Ruiz E (2015a) Asymmetric Accretion Flows within a Common Envelope. *ApJ* 803:41. <https://doi.org/10.1088/0004-637X/803/1/41>. [arXiv:1410.3823](https://arxiv.org/abs/1410.3823) [astro-ph.SR]
- MacLeod M, Ramirez-Ruiz E (2015b) On the Accretion-fed Growth of Neutron Stars during Common Envelope. *ApJ* 798:L19. <https://doi.org/10.1088/2041-8205/798/1/L19>. [arXiv:1410.5421](https://arxiv.org/abs/1410.5421) [astro-ph.SR]
- MacLeod M, Antoni A, Murguía-Berthier A, Macías P, Ramirez-Ruiz E (2017a) Common envelope wind tunnel: Coefficients of drag and accretion in a simplified context for studying flows around objects embedded within stellar envelopes. *ApJ* 838(1):56. <https://doi.org/10.3847/1538-4357/aa6117>. [arXiv:1704.02372](https://arxiv.org/abs/1704.02372) [astro-ph.SR]
- MacLeod M, Macías P, Ramirez-Ruiz E, et al. (2017b) Lessons from the Onset of a Common Envelope Episode: the Remarkable M31 2015 Luminous Red Nova Outburst. *ApJ* 835:282. <https://doi.org/10.3847/1538-4357/835/2/282>. [arXiv:1605.01493](https://arxiv.org/abs/1605.01493) [astro-ph.SR]
- MacLeod M, Ostriker EC, Stone JM (2018a) Bound Outflows, Unbound Ejecta, and the Shaping of Bipolar Remnants during Stellar Coalescence. *ApJ* 868(2):136. <https://doi.org/10.3847/1538-4357/aae9eb>. [arXiv:1808.05950](https://arxiv.org/abs/1808.05950) [astro-ph.SR]
- MacLeod M, Ostriker EC, Stone JM (2018b) Runaway Coalescence at the Onset of Common Envelope Episodes. *ApJ* 863(1):5. <https://doi.org/10.3847/1538-4357/aacf08>. [arXiv:1803.03261](https://arxiv.org/abs/1803.03261) [astro-ph.SR]

- MacLeod M, Vick M, Loeb A (2022) Tidal wave breaking in the eccentric lead-in to mass transfer and common envelope phases. arXiv e-prints arXiv:2203.01947. [arXiv:2203.01947](https://arxiv.org/abs/2203.01947) [astro-ph.SR]
- Madappatt N, De Marco O, Villaver E (2016) The effect of tides on the population of PN from interacting binaries. MNRAS 463(1):1040–1056. <https://doi.org/10.1093/mnras/stw2025>. [arXiv:1608.03041](https://arxiv.org/abs/1608.03041) [astro-ph.SR]
- Marchant P, Pappas KMW, Gallegos-Garcia M, et al. (2021) The role of mass transfer and common envelope evolution in the formation of merging binary black holes. A&A 650:A107. <https://doi.org/10.1051/0004-6361/202039992>. [arXiv:2103.09243](https://arxiv.org/abs/2103.09243) [astro-ph.SR]
- Matsumoto T, Metzger BD (2022) Light-curve Model for Luminous Red Novae and Inferences about the Ejecta of Stellar Mergers. ApJ 938(1):5. <https://doi.org/10.3847/1538-4357/ac6269>. [arXiv:2202.10478](https://arxiv.org/abs/2202.10478) [astro-ph.SR]
- Menon H, Wesolowski L, Zheng G, et al. (2015) Adaptive techniques for clustered N-body cosmological simulations. Computational Astrophysics and Cosmology 2:1. <https://doi.org/10.1186/s40668-015-0007-9>. [arXiv:1409.1929](https://arxiv.org/abs/1409.1929) [astro-ph.IM]
- Metzger BD, Pejcha O (2017) Shock-powered light curves of luminous red novae as signatures of pre-dynamical mass-loss in stellar mergers. MNRAS 471:3200–3211. <https://doi.org/10.1093/mnras/stx1768>. [arXiv:1705.03895](https://arxiv.org/abs/1705.03895) [astro-ph.HE]
- Meyer F, Meyer-Hofmeister E (1979) Formation of cataclysmic binaries through common envelope evolution. A&A 78:167–176
- Mignone A, Zanni C, Tzeferacos P, et al. (2012) The PLUTO Code for Adaptive Mesh Computations in Astrophysical Fluid Dynamics. ApJS 198:7. <https://doi.org/10.1088/0067-0049/198/1/7>. [arXiv:1110.0740](https://arxiv.org/abs/1110.0740) [astro-ph.HE]
- Miszalski B, Acker A, Moffat AFJ, Parker QA, Udalski A (2009) Binary planetary nebulae nuclei towards the Galactic bulge. I. Sample discovery, period distribution, and binary fraction. A&A 496:813–825. <https://doi.org/10.1051/0004-6361/200811380>. [arXiv:0901.4419](https://arxiv.org/abs/0901.4419) [astro-ph.SR]
- Moe M, Di Stefano R (2017) Mind your Ps and Qs: The interrelation between period (P) and mass-ratio (Q) distributions of binary stars. ApJS 230(2):15. <https://doi.org/10.3847/1538-4365/aa6fb6>. [arXiv:1606.05347](https://arxiv.org/abs/1606.05347) [astro-ph.SR]
- Monaghan JJ (1992) Smoothed particle hydrodynamics. ARA&A 30:543–574. <https://doi.org/10.1146/annurev.aa.30.090192.002551>
- Monaghan JJ, Gingold RA (1983) Shock simulation by the particle method SPH. Journal of Computational Physics 52(2):374–389. [https://doi.org/10.1016/0021-9991\(83\)90036-0](https://doi.org/10.1016/0021-9991(83)90036-0)
- Monaghan JJ, Lattanzio JC (1985) A refined particle method for astrophysical problems. A&A 149(1):135–143
- Monaghan JJ, Price DJ (2001) Variational principles for relativistic smoothed particle hydrodynamics. MNRAS 328(2):381–392. <https://doi.org/10.1046/j.1365-8711.2001.04742.x>
- Moreno MM, Schneider FRN, Röpke FK, et al. (2021) From 3D hydrodynamic simulations of common-envelope interaction to gravitational-wave mergers. submitted to A&A [arXiv:2111.12112](https://arxiv.org/abs/2111.12112) [astro-ph.SR]
- Moreno Méndez E, López-Cámara D, De Colle F (2017) Dynamics of jets during the common-envelope phase. MNRAS 470(3):2929–2937. <https://doi.org/10.1093/>

- [mnras/stx1385](#). [arXiv:1702.03293](#) [astro-ph.HE]
- Motl PM, Frank J, Staff J, et al. (2017) A Comparison of Grid-based and SPH Binary Mass-transfer and Merger Simulations. *ApJS* 229(2):27. <https://doi.org/10.3847/1538-4365/aa5bde>. [arXiv:1702.03562](#) [astro-ph.SR]
- Munari U, Henden A, Kiyota S, et al. (2002) The mysterious eruption of V838 Mon. *A&A* 389:L51–L56. <https://doi.org/10.1051/0004-6361:20020715>. [astro-ph/0205288](#)
- Munday J, Jones D, García-Rojas J, et al. (2020) The post-common-envelope binary central star of the planetary nebula ETHOS 1. *MNRAS* 498(4):6005–6012. <https://doi.org/10.1093/mnras/staa2753>. [arXiv:2009.03577](#) [astro-ph.SR]
- Munson B, Chatzopoulos E, Frank J, et al. (2021) R Coronae Borealis Star Evolution: Simulating 3D Merger Events to 1D Stellar Evolution Including Large-scale Nucleosynthesis. *ApJ* 911(2):103. <https://doi.org/10.3847/1538-4357/abeb6c>. [arXiv:2103.01741](#) [astro-ph.SR]
- Murphy S, Keller S, Schmidt B, et al. (2009) Skymapper and the southern sky survey: A valuable resource for stellar astrophysics. In: S J Murphy & M S Bessell (ed) *Astronomical Society of the Pacific Conference Series*. Astronomical Society of the Pacific Conference Series, vol 404. pp 356–+
- Mustill AJ, Villaver E (2012) Foretellings of Ragnarök: World-engulfing Asymptotic Giants and the Inheritance of White Dwarfs. *ApJ* 761:121. <https://doi.org/10.1088/0004-637X/761/2/121>. [arXiv:1210.0328](#) [astro-ph.EP]
- Nandez JLA, Ivanova N (2016) Common envelope events with low-mass giants: understanding the energy budget. *MNRAS* 460:3992–4002. <https://doi.org/10.1093/mnras/stw1266>. [arXiv:1606.04922](#) [astro-ph.SR]
- Nandez JLA, Ivanova N, Lombardi JC Jr (2014) V1309 Sco – understanding a merger. *ApJ* 786:39. <https://doi.org/10.1088/0004-637X/786/1/39>. [arXiv:1311.6522](#) [astro-ph.SR]
- Nandez JLA, Ivanova N, Lombardi JC (2015) Recombination energy in double white dwarf formation. *MNRAS* 450:L39–L43. <https://doi.org/10.1093/mnras/slv043>. [arXiv:1503.02750](#) [astro-ph.SR]
- Nelemans G, Tauris TM (1998) Formation of undermassive single white dwarfs and the influence of planets on late stellar evolution. *A&A* 335:L85–L88. [arXiv:astro-ph/9806011](#) [astro-ph]
- Nelemans G, Tout CA (2005) Reconstructing the evolution of white dwarf binaries: further evidence for an alternative algorithm for the outcome of the common-envelope phase in close binaries. *MNRAS* 356:753–764. <https://doi.org/10.1111/j.1365-2966.2004.08496.x>. [astro-ph/0410301](#)
- Nelemans G, Verbunt F, Yungelson LR, Portegies Zwart SF (2000) Reconstructing the evolution of double helium white dwarfs: envelope loss without spiral-in. *A&A* 360:1011–1018. [arXiv:astro-ph/0006216](#)
- Nelemans G, Portegies Zwart SF, Verbunt F, Yungelson LR (2001a) Population synthesis for double white dwarfs. II. Semi-detached systems: AM CVn stars. *A&A* 368:939–949. <https://doi.org/10.1051/0004-6361:20010049>. [astro-ph/0101123](#)
- Nelemans G, Yungelson LR, Portegies Zwart SF, Verbunt F (2001b) Population synthesis for double white dwarfs. I. Close detached systems. *A&A* 365:491–507. <https://doi.org/10.1051/0004-6361:20000147>. [astro-ph/0010457](#)

- Nordhaus J, Wellons S, Spiegel DS, Metzger BD, Blackman EG (2011) Formation of high-field magnetic white dwarfs from common envelopes. *Proceedings of the National Academy of Science* 108:3135–3140. <https://doi.org/10.1073/pnas.1015005108>. [arXiv:1010.1529](https://arxiv.org/abs/1010.1529) [astro-ph.SR]
- Ohlmann ST (2016) Hydrodynamics of the common envelope phase in binary stellar evolution. Dissertation, Universität Heidelberg. <https://doi.org/10.11588/heidok.00021513>, available at <http://www.ub.uni-heidelberg.de/archiv/21513>
- Ohlmann ST, Röpke FK, Pakmor R, Springel V (2016a) Hydrodynamic moving-mesh simulations of the common envelope phase in binary stellar systems. *ApJ* 816(1):L9. <https://doi.org/10.3847/2041-8205/816/1/L9>, URL <http://stacks.iop.org/2041-8205/816/i=1/a=L9>. [arXiv:1512.04529](https://arxiv.org/abs/1512.04529) [astro-ph.SR]
- Ohlmann ST, Röpke FK, Pakmor R, Springel V, Müller E (2016b) Magnetic Field Amplification During the Common Envelope Phase. *MNRAS* 462(1):L121–L125. <https://doi.org/10.1093/mnras/144>, URL <http://mnras.oxfordjournals.org/content/462/1/L121.abstract>. [arXiv:1607.05996](https://arxiv.org/abs/1607.05996) [astro-ph.SR]
- Ohlmann ST, Röpke FK, Pakmor R, Springel V (2017) Constructing stable 3D hydrodynamical models of giant stars. *A&A* 599:A5. <https://doi.org/10.1051/0004-6361/201629692>. [arXiv:1612.00008](https://arxiv.org/abs/1612.00008) [astro-ph.SR]
- Ondratschek PA, Röpke FK, Schneider FRN, et al. (2022) Bipolar planetary nebulae from common-envelope evolution of binary stars. *A&A* 660:L8. <https://doi.org/10.1051/0004-6361/202142478>. [arXiv:2110.13177](https://arxiv.org/abs/2110.13177) [astro-ph.SR]
- Osher S, Chakravarthy S (1983) Upwind Schemes and Boundary Conditions with Applications to Euler Equations in General Geometries. *Journal of Computational Physics* 50(3):447–481. [https://doi.org/10.1016/0021-9991\(83\)90106-7](https://doi.org/10.1016/0021-9991(83)90106-7)
- Ostriker EC (1999) Dynamical friction in a gaseous medium. *ApJ* 513:252–258. <https://doi.org/10.1086/306858>. [astro-ph/9810324](https://arxiv.org/abs/astro-ph/9810324)
- Paczyński B (1976) Common Envelope Binaries. In: Eggleton P, Mitton S, Whelan J (eds) *Structure and Evolution of Close Binary Systems*. IAU Symposium, vol 73. p 75
- Pakmor R, Springel V (2013) Simulations of magnetic fields in isolated disc galaxies. *MNRAS* 432:176–193. <https://doi.org/10.1093/mnras/stt428>. [arXiv:1212.1452](https://arxiv.org/abs/1212.1452) [astro-ph.CO]
- Pakmor R, Bauer A, Springel V (2011) Magnetohydrodynamics on an unstructured moving grid. *MNRAS* 418:1392–1401. <https://doi.org/10.1111/j.1365-2966.2011.19591.x>. [arXiv:1108.1792](https://arxiv.org/abs/1108.1792) [astro-ph.IM]
- Pakmor R, Edelman P, Röpke FK, Hillebrandt W (2012) Stellar GADGET: a smoothed particle hydrodynamics code for stellar astrophysics and its application to Type Ia supernovae from white dwarf mergers. *MNRAS* 424:2222–2231. <https://doi.org/10.1111/j.1365-2966.2012.21383.x>. [arXiv:1205.5806](https://arxiv.org/abs/1205.5806) [astro-ph.HE]
- Pakmor R, Kromer M, Taubenberger S, Springel V (2013) Helium-ignited violent mergers as a unified model for normal and rapidly declining type Ia supernovae. *ApJ* 770:L8. <https://doi.org/10.1088/2041-8205/770/1/L8>. [arXiv:1302.2913](https://arxiv.org/abs/1302.2913) [astro-ph.HE]
- Pakmor R, Springel V, Bauer A, et al. (2016) Improving the convergence properties of the moving-mesh code AREPO. *MNRAS* 455(1):1134–1143. <https://doi.org/10.1093/mnras/stv2380>. [arXiv:1503.00562](https://arxiv.org/abs/1503.00562) [astro-ph.GA]

- Passy JC, Bryan GL (2014) An adaptive particle-mesh gravity solver for ENZO. *ApJS* 215(1):8. <https://doi.org/10.1088/0067-0049/215/1/8>. arXiv:1410.0010 [astro-ph.IM]
- Passy JC, De Marco O, Fryer CL, et al. (2012) Simulating the Common Envelope Phase of a Red Giant Using Smoothed-particle Hydrodynamics and Uniform-grid Codes. *ApJ* 744:52. <https://doi.org/10.1088/0004-637X/744/1/52>. arXiv:1107.5072 [astro-ph.SR]
- Pastorello A, Chen TW, Cai YZ, et al. (2019) The evolution of luminous red nova AT 2017jfs in NGC 4470. *A&A* 625:L8. <https://doi.org/10.1051/0004-6361/201935511>. arXiv:1906.00811 [astro-ph.SR]
- Paxton B, Bildsten L, Dotter A, et al. (2011) Modules for experiments in stellar astrophysics (mesa). *ApJS* 192:3. <https://doi.org/10.1088/0067-0049/192/1/3>. arXiv:1009.1622 [astro-ph.SR]
- Pejcha O (2014) Burying a Binary: Dynamical Mass Loss and a Continuous Optically thick Outflow Explain the Candidate Stellar Merger V1309 Scorpii. *ApJ* 788(1):22. <https://doi.org/10.1088/0004-637X/788/1/22>. arXiv:1307.4088 [astro-ph.SR]
- Pejcha O, Metzger BD, Tomida K (2016a) Binary stellar mergers with marginally bound ejecta: excretion discs, inflated envelopes, outflows, and their luminous transients. *MNRAS* 461:2527–2539. <https://doi.org/10.1093/mnras/stw1481>. arXiv:1604.07414 [astro-ph.SR]
- Pejcha O, Metzger BD, Tomida K (2016b) Cool and luminous transients from mass-losing binary stars. *MNRAS* 455:4351–4372. <https://doi.org/10.1093/mnras/stv2592>. arXiv:1509.02531 [astro-ph.SR]
- Pelupessy FI, Jänes J, Portegies Zwart S (2012) N-body integrators with individual time steps from hierarchical splitting. *New Astronomy* 17(8):711–719. <https://doi.org/10.1016/j.newast.2012.05.009>. arXiv:1205.5668 [astro-ph.IM]
- Podsiadlowski P (2001) Common-Envelope Evolution and Stellar Mergers. In: Podsiadlowski P, Rappaport S, King AR, D'Antona F, Burderi L (eds) *Evolution of Binary and Multiple Star Systems*. *Astronomical Society of the Pacific Conference Series*, vol 229. p 239
- Politano M, Weiler KP (2007) Population synthesis studies of close binary systems using a variable common envelope efficiency parameter. I. dependence on secondary mass. *ApJ* 665:663–679. <https://doi.org/10.1086/518997>. astro-ph/0702662
- Portegies Zwart S, McMillan S, Harfst S, et al. (2009) A multiphysics and multi-scale software environment for modeling astrophysical systems. *New Astronomy* 14(4):369–378. <https://doi.org/10.1016/j.newast.2008.10.006>. arXiv:0807.1996 [astro-ph]
- Press WH, Teukolsky SA, Vetterling WT, Flannery BP (2007) *Numerical Recipes: The Art of Scientific Computing*, vol 3. Cambridge University Press
- Price DJ (2012) Smoothed particle hydrodynamics and magnetohydrodynamics. *Journal of Computational Physics* 231(3):759–794. <https://doi.org/10.1016/j.jcp.2010.12.011>. arXiv:1012.1885 [astro-ph.IM]
- Price DJ, Monaghan JJ (2007) An energy-conserving formalism for adaptive gravitational force softening in smoothed particle hydrodynamics and N-body codes. *MNRAS* 374:1347–1358. <https://doi.org/10.1111/j.1365-2966.2006.11241>.

- x. [arXiv:astro-ph/0610872](https://arxiv.org/abs/astro-ph/0610872)
- Price DJ, Wurster J, Tricco TS, et al. (2018) Phantom: A smoothed particle hydrodynamics and magnetohydrodynamics code for astrophysics. PASA35:e031. <https://doi.org/10.1017/pasa.2018.25>. [arXiv:1702.03930](https://arxiv.org/abs/1702.03930) [astro-ph.IM]
- Prust LJ (2020) Moving and reactive boundary conditions in moving-mesh hydrodynamics. MNRAS 494(4):4616–4626. <https://doi.org/10.1093/mnras/staa1031>. [arXiv:2002.04287](https://arxiv.org/abs/2002.04287) [physics.comp-ph]
- Prust LJ, Chang P (2019) Common envelope evolution on a moving mesh. MNRAS 486(4):5809–5818. <https://doi.org/10.1093/mnras/stz1219>. [arXiv:1904.09256](https://arxiv.org/abs/1904.09256) [astro-ph.SR]
- Radice D, Bernuzzi S, Perego A (2020) The dynamics of binary neutron star mergers and GW170817. Annual Review of Nuclear and Particle Science 70:95–119. <https://doi.org/10.1146/annurev-nucl-013120-114541>. [arXiv:2002.03863](https://arxiv.org/abs/2002.03863) [astro-ph.HE]
- Rapoport I, Bear E, Soker N (2021) The future influence of six exoplanets on the envelope properties of their parent stars on the giant branches. MNRAS 506(1):468–472. <https://doi.org/10.1093/mnras/stab1774>. [arXiv:2103.14335](https://arxiv.org/abs/2103.14335) [astro-ph.SR]
- Rasio FA, Livio M (1996) On the Formation and Evolution of Common Envelope Systems. ApJ 471:366. <https://doi.org/10.1086/177975>. [astro-ph/9511054](https://arxiv.org/abs/astro-ph/9511054)
- Rasio FA, Shapiro SL (1992) Hydrodynamical evolution of coalescing binary neutron stars. ApJ 401:226. <https://doi.org/10.1086/172055>
- Regős E, Tout CA (1995) The effect of magnetic fields in common-envelope evolution on the formation of cataclysmic variables. MNRAS 273:146–156. <https://doi.org/10.1093/mnras/273.1.146>
- Reichardt TA, De Marco O, Iaconi R, Tout CA, Price DJ (2019) Extending common envelope simulations from roche lobe overflow to the nebular phase. MNRAS 484(1):631–647. <https://doi.org/10.1093/mnras/sty3485>. [arXiv:1809.02297](https://arxiv.org/abs/1809.02297) [astro-ph.SR]
- Reichardt TA, De Marco O, Iaconi R, Chamandy L, Price DJ (2020) The impact of recombination energy on simulations of the common-envelope binary interaction. MNRAS 494(4):5333–5349. <https://doi.org/10.1093/mnras/staa937>. [arXiv:1911.02759](https://arxiv.org/abs/1911.02759) [astro-ph.SR]
- Renzo M, Callister T, Chatziioannou K, et al. (2021) Prospects of gravitational wave detections from common envelope evolution with LISA. ApJ 919(2):128. <https://doi.org/10.3847/1538-4357/ac1110>. [arXiv:2102.00078](https://arxiv.org/abs/2102.00078) [astro-ph.SR]
- Rephaeli Y, Salpeter EE (1980) Flow past a massive object and the gravitational drag. ApJ 240:20–24. <https://doi.org/10.1086/158202>
- Rest A, Prieto JL, Walborn NR, et al. (2012) Light echoes reveal an unexpectedly cool η Carinae during its nineteenth-century Great Eruption. Nature 482(7385):375–378. <https://doi.org/10.1038/nature10775>. [arXiv:1112.2210](https://arxiv.org/abs/1112.2210) [astro-ph.GA]
- Ricker PM, Taam RE (2008) The Interaction of Stellar Objects within a Common Envelope. ApJ 672:L41–L44. <https://doi.org/10.1086/526343>. [arXiv:0710.3631](https://arxiv.org/abs/0710.3631)
- Ricker PM, Taam RE (2012) An AMR Study of the Common-envelope Phase of Binary Evolution. ApJ 746:74. <https://doi.org/10.1088/0004-637X/746/1/74>. [arXiv:1107.3889](https://arxiv.org/abs/1107.3889) [astro-ph.SR]
- Ricker PM, Taam RE, Webbink RF, Timmes FX, Holgado AM (2019a) Common Envelope Evolution of Massive Binaries. In: American Astronomical Society Meet-

- ing Abstracts #233. American Astronomical Society Meeting Abstracts, vol 233. p 348.11
- Ricker PM, Timmes FX, Taam RE, Webbink RF (2019b) Common envelope evolution of massive stars. In: Oskinova LM, Bozzo E, Bulik T, Gies DR (eds) IAU Symposium. IAU Symposium, vol 346. pp 449–454. <https://doi.org/10.1017/S1743921318007433>. [arXiv:1811.03656](https://arxiv.org/abs/1811.03656) [astro-ph.SR]
- Robertson BE, Kravtsov AV, Gnedin NY, Abel T, Rudd DH (2010) Computational eulerian hydrodynamics and Galilean invariance. MNRAS 401(4):2463–2476. <https://doi.org/10.1111/j.1365-2966.2009.15823.x>. [arXiv:0909.0513](https://arxiv.org/abs/0909.0513) [astro-ph.CO]
- Rogers FJ, Nayfonov A (2002) Updated and Expanded OPAL Equation-of-State Tables: Implications for Helioseismology. ApJ 576:1064–1074. <https://doi.org/10.1086/341894>
- Rogers FJ, Swenson FJ, Iglesias CA (1996) OPAL Equation-of-State Tables for Astrophysical Applications. ApJ 456:902. <https://doi.org/10.1086/176705>
- Rosswog S (2015) SPH Methods in the Modelling of Compact Objects. Living Reviews in Computational Astrophysics 1. <https://doi.org/10.1007/lrca-2015-1>. [arXiv:1406.4224](https://arxiv.org/abs/1406.4224) [astro-ph.IM]
- Rosswog S, Liebendörfer M, Thielemann FK, et al. (1999) Mass ejection in neutron star mergers. A&A 341:499–526. [arXiv:astro-ph/9811367](https://arxiv.org/abs/astro-ph/9811367) [astro-ph]
- Rosswog S, Speith R, Wynn GA (2004) Accretion dynamics in neutron star-black hole binaries. MNRAS 351:1121–1133. <https://doi.org/10.1111/j.1365-2966.2004.07865.x>. [arXiv:astro-ph/0403500](https://arxiv.org/abs/astro-ph/0403500)
- Różyczka M, Spruit HC (1989) Spiral shocks in accretion disks: a preliminary numerical study. In: Meyer F (ed) Theory of Accretion Disks. NATO Advanced Study Institute (ASI) Series C, vol 290. pp 341–354
- Ruderman MA, Spiegel EA (1971) Galactic wakes. ApJ 165:1. <https://doi.org/10.1086/150870>
- Ruffert M (1993) Collisions between a white dwarf and a main-sequence star. 3: Simulations including the white dwarf surface. A&A 280(1):141–156
- Ruffert M (1994) Three-dimensional hydrodynamic Bondi-Hoyle accretion. III. Mach 0.6, 1.4 and 10; $\gamma=5/3$. A&AS 106:505–522
- Ruffert M (1995) Three-dimensional hydrodynamic Bondi-Hoyle accretion. IV. Specific heat ratio 4/3. A&AS 113:133. [arXiv:astro-ph/9503026](https://arxiv.org/abs/astro-ph/9503026) [astro-ph]
- Ruffert M (1996) Three-dimensional hydrodynamic Bondi-Hoyle accretion. V. Specific heat ratio 1.01, nearly isothermal flow. A&A 311:817–832. [arXiv:astro-ph/9510021](https://arxiv.org/abs/astro-ph/9510021) [astro-ph]
- Ruffert M (1997) Non-axisymmetric wind-accretion simulations. I. Velocity gradients of 3% and 20% over one accretion radius. A&A 317:793–814. [arXiv:astro-ph/9605072](https://arxiv.org/abs/astro-ph/9605072) [astro-ph]
- Ruffert M (1999) Non-axisymmetric wind-accretion simulations. II. Density gradients. A&A 346:861–877. [arXiv:astro-ph/9903304](https://arxiv.org/abs/astro-ph/9903304) [astro-ph]
- Ruffert M, Janka HT, Schaefer G (1996) Coalescing neutron stars - a step towards physical models. I. hydrodynamic evolution and gravitational-wave emission. A&A 311:532–566. [arXiv:astro-ph/9509006](https://arxiv.org/abs/astro-ph/9509006) [astro-ph]
- Ruiter AJ, Belczynski K, Fryer C (2009) Rates and delay times of type ia supernovae. ApJ 699:2026–2036. <https://doi.org/10.1088/0004-637X/699/2/2026>.

- [arXiv:0904.3108](#)
- Sabach E, Soker N (2015) A formation scenario for the triple pulsar PSR J0337+1715: breaking a binary system inside a common envelope. *MNRAS* 450(2):1716–1723. <https://doi.org/10.1093/mnras/stv717>. [arXiv:1501.06787](#) [astro-ph.SR]
- Sabach E, Hillel S, Schreier R, Soker N (2017) Energy transport by convection in the common envelope evolution. *MNRAS* 472(4):4361–4367. <https://doi.org/10.1093/mnras/stx2272>. [arXiv:1706.05838](#) [astro-ph.SR]
- Sana H, de Mink SE, de Koter A, et al. (2012) Binary Interaction Dominates the Evolution of Massive Stars. *Science* 337:444. <https://doi.org/10.1126/science.1223344>. [arXiv:1207.6397](#) [astro-ph.SR]
- Sand C, Ohlmann ST, Schneider FRN, Pakmor R, Röpke FK (2020) Common-envelope evolution with an asymptotic giant branch star. *A&A* 644:A60. <https://doi.org/10.1051/0004-6361/202038992>. [arXiv:2007.11000](#) [astro-ph.SR]
- Sandquist EL, Taam RE, Chen X, Bodenheimer P, Burkert A (1998) Double Core Evolution. X. Through the Envelope Ejection Phase. *ApJ* 500:909. <https://doi.org/10.1086/305778>. [arXiv:astro-ph/9801230](#)
- Sandquist EL, Taam RE, Burkert A (2000) On the Formation of Helium Double Degenerate Stars and Pre-Cataclysmic Variables. *ApJ* 533:984–997. <https://doi.org/10.1086/308687>. [astro-ph/9912243](#)
- Schaffenroth V, Classen L, Nagel K, et al. (2014) Two candidate brown dwarf companions around core helium-burning stars. *A&A* 570:A70. <https://doi.org/10.1051/0004-6361/201424616>. [arXiv:1409.4357](#) [astro-ph.SR]
- Schaffenroth V, Barlow BN, Drechsel H, Dunlap BH (2015) An eclipsing post common-envelope system consisting of a pulsating hot subdwarf B star and a brown dwarf companion. *A&A* 576:A123. <https://doi.org/10.1051/0004-6361/201525701>. [arXiv:1502.04459](#) [astro-ph.SR]
- Schaffenroth V, Barlow BN, Geier S, et al. (2019) The EREBOS project: Investigating the effect of substellar and low-mass stellar companions on late stellar evolution. survey, target selection, and atmospheric parameters. *A&A* 630:A80. <https://doi.org/10.1051/0004-6361/201936019>. [arXiv:1907.09892](#) [astro-ph.SR]
- Schneider FRN, Ohlmann ST, Podsiadlowski P, et al. (2019) Stellar mergers as the origin of magnetic massive stars. *Nature* 574(7777):211–214. <https://doi.org/10.1038/s41586-019-1621-5>. [arXiv:1910.14058](#) [astro-ph.SR]
- Schneider FRN, Ohlmann ST, Podsiadlowski P, et al. (2020) Long-term evolution of a magnetic massive merger product. *MNRAS* 495(3):2796–2812. <https://doi.org/10.1093/mnras/staa1326>. [arXiv:2005.05335](#) [astro-ph.SR]
- Schreiber MR, Gänsicke BT (2003) The age, life expectancy, and space density of Post Common Envelope Binaries. *A&A* 406:305–321. <https://doi.org/10.1051/0004-6361:20030801>. [astro-ph/0305531](#)
- Schreier R, Hillel S, Soker N (2019) Inclined jets inside a common envelope of a triple stellar system. *MNRAS* 490(4):4748–4755. <https://doi.org/10.1093/mnras/stz2914>. [arXiv:1907.13175](#) [astro-ph.SR]
- Schreier R, Hillel S, Shiber S, Soker N (2021) Simulating highly eccentric common envelope jet supernova impostors. *MNRAS* 508(2):2386–2398. <https://doi.org/10.1093/mnras/stab2687>. [arXiv:2106.11601](#) [astro-ph.HE]

- Schreier R, Hillel S, Soker N (2022) Simulating the deposition of angular momentum by jets in common envelope evolution. arXiv e-prints arXiv:2209.13573. [arXiv:2209.13573](https://arxiv.org/abs/2209.13573) [astro-ph.HE]
- Schröder SL, MacLeod M, Loeb A, Vigna-Gómez A, Mandel I (2020) Explosions Driven by the Coalescence of a Compact Object with the Core of a Massive-star Companion inside a Common Envelope: Circumstellar Properties, Light Curves, and Population Statistics. *ApJ* 892(1):13. <https://doi.org/10.3847/1538-4357/ab7014>. [arXiv:1906.04189](https://arxiv.org/abs/1906.04189) [astro-ph.HE]
- Shibata M, Hotokezaka K (2019) Merger and mass ejection of neutron star binaries. *Annual Review of Nuclear and Particle Science* 69:41–64. <https://doi.org/10.1146/annurev-nucl-101918-023625>. [arXiv:1908.02350](https://arxiv.org/abs/1908.02350) [astro-ph.HE]
- Shiber S, Soker N (2018) Simulating a binary system that experiences the grazing envelope evolution. *MNRAS* 477(2):2584–2598. <https://doi.org/10.1093/mnras/sty843>. [arXiv:1706.00398](https://arxiv.org/abs/1706.00398) [astro-ph.SR]
- Shiber S, Kashi A, Soker N (2017) Simulating the onset of grazing envelope evolution of binary stars. *MNRAS* 465(1):L54–L58. <https://doi.org/10.1093/mnras/slw208>. [arXiv:1607.00839](https://arxiv.org/abs/1607.00839) [astro-ph.SR]
- Shiber S, Iaconi R, De Marco O, Soker N (2019) Companion-launched jets and their effect on the dynamics of common envelope interaction simulations. *MNRAS* 488(4):5615–5632. <https://doi.org/10.1093/mnras/stz2013>. [arXiv:1902.03931](https://arxiv.org/abs/1902.03931) [astro-ph.SR]
- Shima E, Matsuda T, Takeda H, Sawada K (1985) Hydrodynamic calculations of axisymmetric accretion flow. *MNRAS* 217:367–386. <https://doi.org/10.1093/mnras/217.2.367>
- Smith N, Andrews JE, Van Dyk SD, et al. (2016) Massive star mergers and the recent transient in NGC 4490: a more massive cousin of V838 Mon and V1309 Sco. *MNRAS* 458:950–962. <https://doi.org/10.1093/mnras/stw219>. [arXiv:1602.05203](https://arxiv.org/abs/1602.05203) [astro-ph.SR]
- Soker N (1994) Influences of wide binaries on the structures of planetary nebulae. *MNRAS* 270:774
- Soker N (1998a) Binary Progenitor Models for Bipolar Planetary Nebulae. *ApJ* 496(2):833–841. <https://doi.org/10.1086/305407>
- Soker N (1998b) Can planets influence the horizontal branch morphology? *AJ* 116(3):1308–1313. <https://doi.org/10.1086/300503>. [arXiv:astro-ph/9803223](https://arxiv.org/abs/astro-ph/9803223) [astro-ph]
- Soker N (1998c) Magnetic field, dust and axisymmetrical mass loss on the asymptotic giant branch. *MNRAS* 299(4):1242–1248. <https://doi.org/10.1046/j.1365-8711.1998.01884.x>. [arXiv:astro-ph/9808289](https://arxiv.org/abs/astro-ph/9808289) [astro-ph]
- Soker N (2004a) Bubbles in planetary nebulae and clusters of galaxies: Jet properties. *A&A* 414:943–947. <https://doi.org/10.1051/0004-6361:20034120>. [arXiv:astro-ph/0309095](https://arxiv.org/abs/astro-ph/0309095) [astro-ph]
- Soker N (2004b) Shaping planetary nebulae and related objects. In: Meixner M, Kastner JH, Balick B, Soker N (eds) *Asymmetrical Planetary Nebulae III: Winds, Structure and the Thunderbird*. *Astronomical Society of the Pacific Conference Series*, vol 313. p 562. [arXiv:astro-ph/0309228](https://arxiv.org/abs/astro-ph/0309228) [astro-ph]

- Soker N (2015) Close Stellar Binary Systems by Grazing Envelope Evolution. *ApJ* 800(2):114. <https://doi.org/10.1088/0004-637X/800/2/114>. arXiv:1410.5363 [astro-ph.SR]
- Soker N (2016a) Intermediate luminosity optical transients during the grazing envelope evolution (GEE). *New Astronomy* 47:16–18. <https://doi.org/10.1016/j.newast.2016.01.005>. arXiv:1601.05913 [astro-ph.SR]
- Soker N (2016b) The jet feedback mechanism (JFM) in stars, galaxies and clusters. *New Astronomy Reviews* 75:1–23. <https://doi.org/10.1016/j.newar.2016.08.002>. arXiv:1605.02672 [astro-ph.HE]
- Soker N (2017) Energizing the last phase of common-envelope removal. *MNRAS* 471(4):4839–4843. <https://doi.org/10.1093/mnras/stx1978>. arXiv:1706.03720 [astro-ph.SR]
- Soker N, Gilkis A (2018) Explaining iPTF14hls as a common-envelope jets supernova. *MNRAS* 475(1):1198–1202. <https://doi.org/10.1093/mnras/stx3287>. arXiv:1711.05180 [astro-ph.HE]
- Soker N, Tylenda R (2006) Violent stellar merger model for transient events. *MNRAS* 373:733–738. <https://doi.org/10.1111/j.1365-2966.2006.11056.x>. astro-ph/0606467
- Soker N, Livio M, Harpaz A (1984) The evolution of a star–planet system in the double core phase. *MNRAS* 210:189–195. <https://doi.org/10.1093/mnras/210.2.189>
- Soker N, Livio M, de Kool M, Savonije GJ (1986) Accretion of angular momentum from an inhomogeneous medium. II - Isothermal flow. *MNRAS* 221:445–452. <https://doi.org/10.1093/mnras/221.2.445>
- Soker N, Kashi A, García-Berro E, Torres S, Camacho J (2013) Explaining the type ia supernova ptf 11kx with a violent prompt merger scenario. *MNRAS* 431:1541–1546. <https://doi.org/10.1093/mnras/stt271>. arXiv:1207.5770 [astro-ph.SR]
- Soker N, Grichener A, Sabach E (2018) Radiating the Hydrogen Recombination Energy during Common Envelope Evolution. *ApJ* 863(1):L14. <https://doi.org/10.3847/2041-8213/aad736>. arXiv:1805.08543 [astro-ph.SR]
- Soker N, Grichener A, Gilkis A (2019) Diversity of common envelope jets supernovae and the fast transient AT2018cow. *MNRAS* 484(4):4972–4979. <https://doi.org/10.1093/mnras/stz364>. arXiv:1811.11106 [astro-ph.HE]
- Sparks WM, Stecher TP (1974) Supernova: The result of the death spiral of a white dwarf into a red giant. *ApJ* 188:149. <https://doi.org/10.1086/152697>
- Springel V (2005) The cosmological simulation code GADGET-2. *MNRAS* 364:1105–1134. <https://doi.org/10.1111/j.1365-2966.2005.09655.x>. arXiv:astro-ph/0505010
- Springel V (2010a) E pur si muove: Galilean-invariant cosmological hydrodynamical simulations on a moving mesh. *MNRAS* 401:791–851. <https://doi.org/10.1111/j.1365-2966.2009.15715.x>. arXiv:0901.4107 [astro-ph.CO]
- Springel V (2010b) Smoothed Particle Hydrodynamics in Astrophysics. *ARA&A* 48:391–430. <https://doi.org/10.1146/annurev-astro-081309-130914>
- Springel V, Hernquist L (2002) Cosmological smoothed particle hydrodynamics simulations: the entropy equation. *MNRAS* 333:649–664. <https://doi.org/10.1046/j.1365-8711.2002.05445.x>. arXiv:astro-ph/0111016

- Springel V, Yoshida N, White SDM (2001) GADGET: a code for collisionless and gasdynamical cosmological simulations. *New Astronomy* 6:79–117. [https://doi.org/10.1016/S1384-1076\(01\)00042-2](https://doi.org/10.1016/S1384-1076(01)00042-2). [arXiv:astro-ph/0003162](https://arxiv.org/abs/astro-ph/0003162)
- Springel V, Pakmor R, Zier O, Reinecke M (2021) Simulating cosmic structure formation with the GADGET-4 code. *MNRAS* 506(2):2871–2949. <https://doi.org/10.1093/mnras/stab1855>. [arXiv:2010.03567](https://arxiv.org/abs/2010.03567) [astro-ph.IM]
- Staff JE, De Marco O, Macdonald D, et al. (2016a) Hydrodynamic simulations of the interaction between an AGB star and a main-sequence companion in eccentric orbits. *MNRAS* 455:3511–3525. <https://doi.org/10.1093/mnras/stv2548>. [arXiv:1510.08429](https://arxiv.org/abs/1510.08429) [astro-ph.SR]
- Staff JE, De Marco O, Wood P, Galaviz P, Passy JC (2016b) Hydrodynamic simulations of the interaction between giant stars and planets. *MNRAS* 458:832–844. <https://doi.org/10.1093/mnras/stw331>. [arXiv:1602.03130](https://arxiv.org/abs/1602.03130) [astro-ph.SR]
- Stinson GS, Brook C, Macciò AV, et al. (2013) Making galaxies in a cosmological context: the need for early stellar feedback. *MNRAS* 428(1):129–140. <https://doi.org/10.1093/mnras/sts028>. [arXiv:1208.0002](https://arxiv.org/abs/1208.0002) [astro-ph.CO]
- Stone JM, Norman ML (1992) ZEUS-2D: A Radiation Magnetohydrodynamics Code for Astrophysical Flows in Two Space Dimensions. II. The Magnetohydrodynamic Algorithms and Tests. *ApJS* 80:791–+. <https://doi.org/10.1086/191681>
- Stone JM, Tomida K, White CJ, Felker KG (2020) The Athena++ Adaptive Mesh Refinement Framework: Design and Magnetohydrodynamic Solvers. *ApJS* 249(1):4. <https://doi.org/10.3847/1538-4365/ab929b>. [arXiv:2005.06651](https://arxiv.org/abs/2005.06651) [astro-ph.IM]
- Szölgvény Á, MacLeod M, Loeb A (2022) Eccentricity evolution in gaseous dynamical friction. *arXiv e-prints arXiv:2203.01334*. [arXiv:2203.01334](https://arxiv.org/abs/2203.01334) [astro-ph.EP]
- Taam RE (1979) Double core evolution and X-ray binaries. *Astrophys. Lett.* 20:29
- Taam RE, Bodenheimer P (1989) Double-core evolution. VIII - The evolution of a 5 solar mass red giant with a 1 solar mass companion. *ApJ* 337:849–857. <https://doi.org/10.1086/167155>
- Taam RE, Bodenheimer P (1991) Double core evolution. IV - The late stages of evolution of a 2-solar mass red giant with a 1-solar mass companion. *ApJ* 373:246–249. <https://doi.org/10.1086/170043>
- Taam RE, Ricker PM (2006) Common Envelope Evolution. *arXiv e-prints astro-ph/0611043*. [arXiv:astro-ph/0611043](https://arxiv.org/abs/astro-ph/0611043) [astro-ph]
- Taam RE, Bodenheimer P, Ostriker JP (1978) Double core evolution. I - A 16 solar mass star with a 1 solar mass neutron-star companion. *ApJ* 222:269–280. <https://doi.org/10.1086/156142>
- Taam RE, Bodenheimer P, Różyczka M (1994) Double Core Evolution. VI. Effects of Gravitational Torques. *ApJ* 431:247. <https://doi.org/10.1086/174482>
- Tauris TM, Dewi JDM (2001) Research note on the binding energy parameter of common envelope evolution. dependency on the definition of the stellar core boundary during spiral-in. *A&A* 369:170–173. <https://doi.org/10.1051/0004-6361:20010099>. [arXiv:astro-ph/0101530](https://arxiv.org/abs/astro-ph/0101530) [astro-ph]
- Tauris TM, van den Heuvel EPJ (2014) Formation of the Galactic Millisecond Pulsar Triple System PSR J0337+1715—A Neutron Star with Two Orbiting White Dwarfs. *ApJ* 781(1):L13. <https://doi.org/10.1088/2041-8205/781/1/L13>. [arXiv:1401.0941](https://arxiv.org/abs/1401.0941) [astro-ph.SR]

- Terman JL, Taam RE (1996) Double-Core Evolution. IX. The Infall of a Main-Sequence Star through the Envelope of Its Intermediate-Mass Red Giant Companion. *ApJ* 458:692. <https://doi.org/10.1086/176850>
- Terman JL, Taam RE, Hernquist L (1994) Double-core evolution. V. Three-dimensional effects in the merger of a red giant with a dwarf companion. *ApJ* 422:729–736. <https://doi.org/10.1086/173765>
- Terman JL, Taam RE, Hernquist L (1995) Double core evolution. vii. the infall of a neutron star through the envelope of its massive star companion. *ApJ* 445:367–376. <https://doi.org/10.1086/175702>
- Thorne KS, Zytkow AN (1975) Red giants and supergiants with degenerate neutron cores. *ApJ* 199:L19–L24. <https://doi.org/10.1086/181839>
- Tocknell J, De Marco O, Wardle M (2014) Constraints on common envelope magnetic fields from observations of jets in planetary nebulae. *MNRAS* 439:2014–2024. <https://doi.org/10.1093/mnras/stu079>. [arXiv:1308.5027](https://arxiv.org/abs/1308.5027) [astro-ph.SR]
- Toonen S, Nelemans G, Portegies Zwart S (2012) Supernova type ia progenitors from merging double white dwarfs. using a new population synthesis model. *A&A* 546:A70. <https://doi.org/10.1051/0004-6361/201218966>. [arXiv:1208.6446](https://arxiv.org/abs/1208.6446) [astro-ph.HE]
- Toonen S, Perets HB, Igoshev AP, Michaely E, Zenati Y (2018) The demographics of neutron star - white dwarf mergers. Rates, delay-time distributions, and progenitors. *A&A* 619:A53. <https://doi.org/10.1051/0004-6361/201833164>. [arXiv:1804.01538](https://arxiv.org/abs/1804.01538) [astro-ph.HE]
- Toro EF (2009) *Riemann Solvers and Numerical Methods for Fluid Dynamics: A Practical Introduction*. Springer, Berlin Heidelberg. URL <http://books.google.de/books?id=SqEjX0um8o0C>
- Tout CA (1991) On the relation between the mass-ratio distribution in binary stars and the mass function for single stars. *MNRAS* 250:701–706
- Tylenda R, Soker N (2006) Eruptions of the V838 Mon type: stellar merger versus nuclear outburst models. *A&A* 451(1):223–236. <https://doi.org/10.1051/0004-6361:20054201>. [arXiv:astro-ph/0509379](https://arxiv.org/abs/astro-ph/0509379) [astro-ph]
- Tylenda R, Soker N, Szczerba R (2005) On the progenitor of V838 Monocerotis. *A&A* 441(3):1099–1109. <https://doi.org/10.1051/0004-6361:20042485>. [arXiv:astro-ph/0412183](https://arxiv.org/abs/astro-ph/0412183) [astro-ph]
- Tylenda R, Hajduk M, Kamiński T, et al. (2011) V1309 Scorpii: merger of a contact binary. *A&A* 528:A114. <https://doi.org/10.1051/0004-6361/201016221>. [arXiv:1012.0163](https://arxiv.org/abs/1012.0163) [astro-ph.SR]
- van den Heuvel EPJ (1976) Late stages of close binary systems. In: Eggleton P, Mitton S, Whelan J (eds) *Structure and Evolution of Close Binary Systems*. vol 73. p 35
- Vanderburg A, Rappaport SA, Xu S, et al. (2020) A giant planet candidate transiting a white dwarf. *Nature* 585(7825):363–367. <https://doi.org/10.1038/s41586-020-2713-y>. [arXiv:2009.07282](https://arxiv.org/abs/2009.07282) [astro-ph.EP]
- Velázquez PF, Raga AC, Riera A, et al. (2012) Multipolar young planetary nebulae modelled as a precessing and orbiting jet with time-dependent ejection velocity. *MNRAS* 419(4):3529–3536. <https://doi.org/10.1111/j.1365-2966.2011.19991.x>

- Vigna-Gómez A, Neijssel CJ, Stevenson S, et al. (2018) On the formation history of Galactic double neutron stars. *MNRAS* 481(3):4009–4029. <https://doi.org/10.1093/mnras/sty2463>. arXiv:1805.07974 [astro-ph.SR]
- Vigna-Gómez A, Wassink M, Klencki J, et al. (2022) Stellar response after stripping as a model for common-envelope outcomes. *MNRAS* 511(2):2326–2338. <https://doi.org/10.1093/mnras/stac237>. arXiv:2107.14526 [astro-ph.HE]
- Vogelsberger M, Genel S, Sijacki D, et al. (2013) A model for cosmological simulations of galaxy formation physics. *MNRAS* 436:3031–3067. <https://doi.org/10.1093/mnras/stt1789>. arXiv:1305.2913
- Vogelsberger M, Genel S, Springel V, et al. (2014) Introducing the Illustris Project: simulating the coevolution of dark and visible matter in the Universe. *MNRAS* 444:1518–1547. <https://doi.org/10.1093/mnras/stu1536>. arXiv:1405.2921
- Wang B (2018) Mass-accreting white dwarfs and type Ia supernovae. *Research in Astronomy and Astrophysics* 18(5):049. <https://doi.org/10.1088/1674-4527/18/5/49>. arXiv:1801.04031 [astro-ph.SR]
- Warren MS, Salmon JK (1993) A parallel hashed oct-tree N-body algorithm. In: Proceedings of the 1993 ACM/IEEE Conference on Supercomputing. Supercomputing '93. Association for Computing Machinery, New York, NY, USA, pp 12–21. <https://doi.org/10.1145/169627.169640>, URL <https://doi.org/10.1145/169627.169640>
- Webbink RF (1984) Double white dwarfs as progenitors of R Coronae Borealis stars and Type I supernovae. *ApJ* 277:355–360. <https://doi.org/10.1086/161701>
- Webbink RF (2008) Common Envelope Evolution Redux. In: Milone EF, Leahy DA, Hobill DW (eds) *Astrophysics and Space Science Library*. Astrophysics and Space Science Library, vol 352. p 233. arXiv:0704.0280
- Wickramasinghe DT, Tout CA, Ferrario L (2014) The most magnetic stars. *MNRAS* 437:675–681. <https://doi.org/10.1093/mnras/stt1910>. arXiv:1310.2696 [astro-ph.SR]
- Wilson EC, Nordhaus J (2019) The role of convection in determining the ejection efficiency of common envelope interactions. *MNRAS* 485(4):4492–4501. <https://doi.org/10.1093/mnras/stz601>. arXiv:1811.03161 [astro-ph.SR]
- Wilson EC, Nordhaus J (2020) Convection and spin-up during common envelope evolution: the formation of short-period double white dwarfs. *MNRAS* 497(2):1895–1903. <https://doi.org/10.1093/mnras/staa2088>. arXiv:2006.09360 [astro-ph.SR]
- Xiong H, Chen X, Podsiadlowski P, Li Y, Han Z (2017) Subdwarf B stars from the common envelope ejection channel. *A&A* 599:A54. <https://doi.org/10.1051/0004-6361/201629622>. arXiv:1608.08739 [astro-ph.SR]
- Yorke HW, Bodenheimer P, Taam RE (1995) Double Core Evolution. VIII. The Spiral-in of a Main-Sequence Star through the Envelope of an Asymptotic Giant Branch Companion. *ApJ* 451:308. <https://doi.org/10.1086/176220>
- Zahn JP (1977) Tidal friction in close binary stars. *A&A* 57:383–394
- Zhang W, Fryer CL (2001) The merger of a helium star and a black hole: Gamma-ray bursts. *ApJ* 550(1):357–367. <https://doi.org/10.1086/319734>. arXiv:astro-ph/0011236 [astro-ph]

- Zhu C, Pakmor R, van Kerkwijk MH, Chang P (2015) Magnetized Moving Mesh Merger of a Carbon–Oxygen White Dwarf Binary. *ApJ* 806:L1. <https://doi.org/10.1088/2041-8205/806/1/L1>. [arXiv:1504.01732](https://arxiv.org/abs/1504.01732) [astro-ph.SR]
- Zingale M, Dursi LJ, ZuHone J, et al. (2002) Mapping initial hydrostatic models in Godunov codes. *ApJS* 143(2):539–565. <https://doi.org/10.1086/342754>. [arXiv:astro-ph/0208031](https://arxiv.org/abs/astro-ph/0208031) [astro-ph]
- Zorotovic M, Schreiber MR, Gänsicke BT, Nebot Gómez-Morán A (2010) Post-common-envelope binaries from SDSS. IX: Constraining the common-envelope efficiency. *A&A* 520:A86. <https://doi.org/10.1051/0004-6361/200913658>. [arXiv:1006.1621](https://arxiv.org/abs/1006.1621) [astro-ph.SR]
- Zou Y, Frank A, Chen Z, et al. (2020) Bipolar planetary nebulae from outflow collimation by common envelope evolution. *MNRAS* 497(3):2855–2869. <https://doi.org/10.1093/mnras/staa2145>. [arXiv:1912.01647](https://arxiv.org/abs/1912.01647) [astro-ph.SR]
- Zou Y, Chamandy L, Carroll-Nellenback J, Blackman EG, Frank A (2022) Jets from main sequence and white dwarf companions during common envelope evolution. *MNRAS* 514(2):3041–3057. <https://doi.org/10.1093/mnras/stac1529>. [arXiv:2202.05715](https://arxiv.org/abs/2202.05715) [astro-ph.SR]

Acronyms

1D one-dimensional	4
2D two-dimensional	74
3D three-dimensional	5
AGB asymptotic giant branch	6
AMR adaptive mesh refinement	40
BHL Bondi–Hoyle–Lyttleton	18
CE common envelope	4
CEE common-envelope evolution	4
CFL Courant–Friedrichs–Lewy	39
HSE hydrostatic equilibrium	24
LRN luminous red nova	
MHD magneto-hydrodynamics	33

PN planetary nebula	6
RG red giant	8
RN red nova	6
ILRT intermediate-luminosity red transient	
RGB red giant branch	
SPH smoothed particle hydrodynamics	22